MECHANISTIC INVESTIGATION OF [2+2] CYCLOADDITION REACTIONS OF KETENIMINIUM SALTS: PROBING THEIR APPLICATIONS IN SYNTHESIS

by

Beyza Horoz

B.S., Integrated BS&MS Program in Teaching Chemistry, Boğaziçi University, 2018

Submitted to the Institute for Graduate Studies in
Science and Engineering in partial fulfillment of
the requirements for the degree of
Master of Science

Graduate Program in Chemistry
Boğaziçi University
2021

ACKNOWLEDGEMENTS

Being a CCBG Lab member gave me an experience beyond my expectations. I have learned so much about questioning, looking for answers, and more importantly, the power of doing all these in a supportive environment. I am deeply grateful to my thesis supervisor Assoc. Prof. Saron Catak for her guidance, patience for my endless questions, and support in every aspect. The valuable things that I have learned from you will be with me all my life. My gratitude extends to Prof. Viktorya Aviyente for her unwavering helpfulness during my master journey.

I would like to express my special thanks to the members of my committee, Assoc. Prof. Ersin Acar and Assist. Prof. Burcu Dedeoglu for their valuable guidance and support for my thesis.

I acknowledge the TÜBİTAK and Bogazici University Research Fund (BAP-D) for financial support under grant numbers 115Z738 and 15325, respectively. TÜBİTAK ULAKBİM High Performance Computing Center and the computational resources at CCBG were used for DFT calculations.

All current and former members of CCBG and CCBU groups, you are the most amazing people, a person can meet and work with. Thank you all, for your endless support and friendship. You have made my life easier and more meaningful in every way.

Gamze Tanriver and Esma Birsen Boydas, I have learned so much from you. I want to tell you a big heartfelt thank you for being always there for me with your friendship and of course, your mentorship. Zeynep Aktas, Busenur Aslanoglu, Pelin Ulukan, Aslihan Hepguler, Oguzhan Kucur, Semiha Kevser Bali, Oykum Naz Avci, Ekin Esme Bas, Basak Findik, Ipek Munar, Evrim Arslan thank you all for laughter, coffee parties ,and incredible years that we spent together.

Busenur Aslanoglu, you have been my biggest supporter during all those years, no doubt no doubt no doubt. Busra Karadalan, even kilometers separate us, we were always together. I gratefully thank these wonderful and strong women, I am so lucky to have you. I would like to thank to Funda Gul, Melike Hacioglu, Kenan Cagdas Yilmaz, Atakan Arabaci, Tubanur Yilmaz and all my frineds at Bogazici University for their amazing friendship.

Finally, I would like to express my biggest thankfulness to my father Mustafa Horoz, my mother Zeynep Horoz ,and my little brother Basar Horoz. You have encouraged me all through my life. You always loved me, believed in me ,and did what is best for me. Therefore, I would like to dedicate my thesis to my beloved family.

ABSTRACT

MECHANISTIC INVESTIGATION OF [2+2] CYCLOADDITION REACTIONS OF KETENIMINIUM SALTS: PROBING THEIR APPLICATIONS IN SYNTHESIS

This thesis has two main parts, involving theoretical studies based on Density Functional Theory (DFT), related to [2+2] cycloaddition reactions of keteniminium salts, (KI)s, and their applications in industry.

In the first part, the [2+2] cycloaddition reactions between KIs and alkenes were modeled to examine the mechanistic aspects of the reaction with respect to varying substitution patterns of alkenes. Moreover, the reactivity of KIs toward [2+2] cycloaddition was evaluated by differing substitution on KIs. Energetic analysis and conceptual DFT methods were used to rationalize the difference in reactivity of KIs. This study aims to provide know-how to experimental studies that use keteniminium salts as key intermediates.

In the second part, DFT studies conducted in collaboration with industry were presented. First, the reaction mechanism that leads to the formation of zealactone 1a/b was modeled. Second, the reactivity of vinyl-acetylenyl ketene toward olefins was compared. Finally, geometry optimizations of KI-enamine structures were performed to analyze reactivity patterns in relation to coplanarity.

ÖZET

KETENİMİNYUM TUZLARININ [2+2] SİKLOKATILMA TEPKİMELERİNİN MEKANİSTİK İNCELEMESİ: SENTEZLERDE KULLANIMININ ARAŞTIRILMASI

Bu tez keteniminyum tuzlarının, (KI), [2+2] siklokatılma tepkimeleri ve endüstrideki uygulamaları ile ilişkili, Yoğunluk Fonksiyonel Teorisine (YFT) dayalı teorik çalışmaları içeren iki ana bölümden oluşmaktadır.

İlk bölümde, alken üzerindeki sübstitüentlerin tepkime mekanizması üzerindeki etkisini incelemek için KI'lar ve alkenler arasındaki [2+2] siklokatılma tepkimesi modellendi. Ayrıca, KI'ların [2+2] siklokatılma tepkimesindeki reaktivitesi, KI'lar üzerindeki farklı sübstitüentler ile değerlendirildi. Enerji analizi ve kavramsal YFT yöntemleri KI'ların reaktivite farkını rasyonelleştirmek için kullanıldı. Bu çalışma, temel ara ürün olarak keteniminyum tuzlarını kullanan deneysel çalışmalara bilgi sağlamayı amaçlamaktadır.

İkinci bölümde, endüstri ile işbirliğinde yürütülen YFT çalışmaları sunuldu. İlk olarak, zealakton 1a/b oluşumuna yol açan reaksiyon mekanizması modellendi. İkinci olarak, vinil-asetilenil ketenin olefinlere karşı reaktivitesi karşılaştırıldı. Son olarak, eş düzlemlilik ile ilişkili olan reaktivite analizi için KI-enamin yapılarının geometri optimizasyonları gerçekleştirilmiştir.

TABLE OF CONTENTS

ACKNOWLEDGEMENTS . . . iii
ABSTRACT . . . v
ÖZET . . . vi
LIST OF FIGURES . . . ix
LIST OF TABLES . . . xiv
LIST OF SYMBOLS . . . xvi
LIST OF ACRONYMS/ABBREVIATIONS . . . xvii
1. INTRODUCTION . . . 1
2. METHODOLOGY . . . 5
2.1. Density Functional Theory . . . 5
2.2. Functionals . . . 7
2.3. Basis Sets . . . 9
2.4. Continuum Solvation Models . . . 10
2.5. Conceptual Density Functional Theory . . . 11
2.5.1. Reactivity Descriptors: Fukui and Parr Functions . . . 12
2.6. Natural Population Analysis . . . 14
2.7. Noncovalent Interaction Analysis . . . 15
3. INTERMOLECULAR [2+2] CYCLOADDITION REACTIONS BETWEEN KETENIMINIUMS SALTS AND ALKENES . . . 16
3.1. Background . . . 16
3.1.1. Mechanistic Studies of [2+2] Cycloaddition Reactions *via* Keteniminium Salts . . . 18
3.2. Aim of the Study . . . 22
3.3. Computational Methodology . . . 23
3.4. Investigation of [2+2] Cycloaddition Reaction Mechanisms Involving KIs and Alkenes with Differing Substitution Patterns . . . 24
3.5. Computational Assessment of KI Reactivity . . . 46
3.5.1. The effect of *C*-substitution on Reactivity of KIs . . . 47
3.5.2. The effect of *N*-substitution on Reactivity of KIs . . . 53

3.6. Population Analysis, Reactivity Indices and Non-covalent Interactions . 62
3.6.1. Natural Population Analysis 62
3.6.2. Local Reactivity Indices: Parr and Fukui Functions 64
3.6.3. Non-covalent Interactions 67
3.7. Conclusions 68
4. APPLICATION AREAS OF INTERMOLECULAR [2+2] CYCLOADDITION REACTIONS OF KETENIMINIUM SALTS AND KETENES IN INDUSTRY 70
4.1. Energetic and Mechanistic Analysis of [2+2] Cycloadditions Leading to the Formation of Zealactone 1a/b 70
4.1.1. The Aim and Computational Methodology of the Study 73
4.1.2. Computational Results 73
4.2. Pyramidalization of Keteniminium-Enamines 76
4.2.1. The Aim and Computational Methodology of the Study 77
4.2.2. Computational Results 78
4.3. Conclusions 81
REFERENCES 83
APPENDIX A: ARTICLES 96
A.1. Total Synthesis and Biological Evaluation of Zealactone 1a/b 96
A.2. Synthesis of Highly Substituted Cyclobutanones by a One-Pot Keteniminium-Enamine Process 122
APPENDIX B: C_3-SUBSTITUENT EFFECT 133
APPENDIX C: N_1-SUBSTITUENT EFFECT 134
APPENDIX D: COPY-RIGHT LIST 135
D.1. The License for Figure 3.2 135
D.2. The License for Figure 3.3 140
D.3. The License for Figure 3.4 146
D.4. The License for Figure 1.3, Figure 4.1, Figure 4.2, Figure 4.3, Figure 4.4 and Figure 4.5 152
D.5. The License for Figure 1.4, Figure 4.6, Figure 4.7, Figure 4.8, Figure 4.9, Figure 4.10 and Figure 4.11 157

LIST OF FIGURES

Figure 1.1. Schematic representation of the possible regioselectivity in [2+2] cycloaddition reactions between KI and substituted alkenes studied in Part I. 2

Figure 1.2. KIs to investigate a) the effect of substituent(s) on terminal carbon atom b) the effect of substituent(s) on nitrogen atom, on the free energy of activation and reaction. 3

Figure 1.3. Chemical structure of zealactone 1a/b [1]. 3

Figure 1.4. Enamine structure and derivatives: coplanarity of the enamine [2]. 4

Figure 3.1. a) Keto, b) Aldo and c) Activated keteniminium salts. 16

Figure 3.2. Formation of KI and access to functionalized cyclobutanones *via* [2+2] cycloaddition reactions between KIs and alkenes [26]. 17

Figure 3.3. Proposed two-step mechanism for asymmetric [2+2] cycloaddition reactions between KIs and *cis*-2-butenes [65]. 19

Figure 3.4. Schematic representation of Domingo's mechanism for [2+2] cycloaddition of keteniminium salt to acetylene and propyne, MPWB1K/6-311G(d,p) [67]. 21

Figure 3.5. General structure of keteniminium salts with respect to *C*-substituents and *N*-substituents. 22

Figure 3.6. Schematic representation of possible [2+2] cycloaddition reaction mechanisms between KIs and substituted alkenes. 25

Figure 3.7. The reaction mechanism of [2+2] cycloaddition between KI and mono-substituted alkene 1a, M06-2X/6-31+G(d,p). 27

Figure 3.8. Possible attack orientations of 1a to KI and formation of enantiomer pairs of cycloadducts, M06-2X/6-31+G(d,p). 29

Figure 3.9. The reaction mechanism of [2+2] cycloaddition between KI and gem-substituted alkene 1b, M06-2X/6-31+G(d,p). 31

Figure 3.10. Possible attack orientations of 1b to KI, M06-2X/6-31+G(d,p). . . 33

Figure 3.11. The reaction mechanism of [2+2] cycloaddition between KI and *cis*-substituted alkene 1c, M06-2X/6-31+G(d,p). 35

Figure 3.12. Possible attack orientations of 1c to KI and formation of enantiomer pairs of cycloadducts, M06-2X/6-31+G(d,p). 36

Figure 3.13. The reaction mechanism of [2+2] cycloaddition between KI and *trans*-substituted alkene 1d, M06-2X/6-31+G(d,p). 38

Figure 3.14. Possible attack orientations of 1d to KI and formation of enantiomer pairs of cycloadducts, M06-2X/6-31+G(d,p). 39

Figure 3.15. The reaction mechanism of [2+2] cycloaddition between KI and tri-substituted alkene 1e, M06-2X/6-31+G(d,p). 41

Figure 3.16. Possible attack orientations of 1e to KI and formation of enantiomer pairs of cycloadducts, M06-2X/6-31+G(d,p). 42

Figure 3.17. Two possible conformers of alkene 1f, the most stable conformer on the left. 43

Figure 3.18. The reaction mechanism of [2+2] cycloaddition between KI and tetra-substituted alkene 1f, M06-2X/6-31+G(d,p). 44

Figure 3.19. Free energies of activation and reaction for [2+2] cycloaddition reaction between unsubstituted KIs and ethylene. Optimized transition states (TSs) at M06-2X/6-31+G(d,p) level in $CHCl_3$. 46

Figure 3.20. Substitution on keteniminium salts with respect to a) C_3-substituents and b) N_1-substituents. 47

Figure 3.21. Optimized structures of KI_5 and TS1-KI_5, pink color denotes CH-π interactions. 50

Figure 3.22. Optimized structures of TS1-KI_5, TS1-KI_6, TS1-KI_7 along with $\Delta G^{\ddagger}$ and ΔG_{rxn} values. 6-311++G(3df,3pd) extra basis set applied for sulfur atom, CH-π interactions in TS1-KI_5 depicted in Å. . . . 51

Figure 3.23. C_2-symmetrical and non-C_2 symmetrical chiral pyrrolidinyl groups used for asymmetric induction in [2+2] cycloaddition of KIs and olefins. 53

Figure 3.24. Optimized structure of KI_{16} and attack trajectories for ethylene in [2+2] cycloadditions. 55

Figure 3.25. $\Delta G^{\ddagger}$ and ΔG_{rxn} values and optimized structures of TS1-KI_{14}, TS1-KI_{16}, TS1-KI_{18}. 56

Figure 3.26. $\Delta G^{\ddagger}$ and ΔG_{rxn} values and optimized structures of TS1-KI_{17}, TS1-KI_{18}, TS1-KI_{19} and TS1-KI_{20}. 57

Figure 3.27. $\Delta G^{\ddagger}$ and ΔG_{rxn} values and optimized structures of TS1-KI_{9}, TS1-KI_{22} and TS1-KI_{26}. 58

Figure 3.28. Comparison of optimized structures of keteniminium salts KI_{9}, KI_{22} and KI_{26}, M06-2X/6-31+G(d,p), critical distances in Å. 59

Figure 3.29. $\Delta G^{\ddagger}$ and ΔG_{rxn} values and optimized structures of TS1-KI_{23} and TS1-KI_{24}. 59

Figure 3.30. The noncovalent interactions (NCI) plots of the KI_{5}, KI_{6}, KI_{7} and KI_{21} structures and their corresponding first transition states. Isosurface= 0.5 au using SCF densities. 67

Figure 4.1. General structure of Strigol-type canonical strigolactones [1]. . . . 71

Figure 4.2. The structures of zealactones 1a and 1b [1]. 71

Figure 4.3. Retrosynthetic analysis of zealactone 1a/b [1]. 72

Figure 4.4. General scheme of plausible intermediates and side products in the formation reaction of vinyl acetylenyl ketenes. Optimized transition state structures and relative free energies of activation ($\Delta G^{\ddagger}$) at the ωB97XD/6-31+G(d,p) level of theory, in DCM) [1]. 74

Figure 4.5. The [2+2] cycloaddition of IB and MC to ketene 13. $\Delta G^{\ddagger}_{1}$ and ΔG_{rxn} values for optimized transition states $TS1_{IB}$ and $TS1_{MC}$, free energies in kcal/mol; distances in Å[1]. 76

Figure 4.6. Synthesis of highly substituted cyclobutanones from amides *via* [2+2] cycloaddition of KIs and alkenes [2]. 77

Figure 4.7. Representation of a) pyramidalization degrees (d) and b) improper dihedral angles (φ) for cyclic enamines [2]. 78

Figure 4.8. *N*-substituent effect on pyramidalization degrees (d) and improper dihedrals (φ) [2]. 79

Figure 4.9. *C*-substituent effect on pyramidalization degrees (d) and improper dihedrals (φ) [2]. 79

Figure 4.10. Alkene substituent effect on pyramidalization degrees (d) and improper dihedrals (φ) [2]. 80

Figure 4.11. The ring size effect of cyclic enamines on pyramidalization degrees (d) and improper dihedrals (φ) [2]. 81

Figure A.1. Article 1. 96

Figure A.2. Article 2. 122

Figure B.1. C_3-substituted KIs with differing ring size with respect to piperidinyl, *N,N*-dimethyl and *N,N*-dially moieties. 133

Figure C.1. KIs bearing chiral auxiliaries as N_1-substituent. 134

LIST OF TABLES

Table 3.1. The regioselectivity in [2+2] cycloadditions of KIs to alkenes and alkynes. 23

Table 3.2. Free energy of activation ($\Delta G^{\ddagger}$) and reaction (ΔG_{rxn}) values for [2+2] cycloaddition of 1a to KI. 30

Table 3.3. Free energy of activation ($\Delta G^{\ddagger}$) and reaction (ΔG_{rxn}) values for [2+2] cycloaddition of 1b to KI. 32

Table 3.4. Free energy of activation ($\Delta G^{\ddagger}$) and reaction (ΔG_{rxn}) values for [2+2] cycloaddition of 1c to KI. 34

Table 3.5. Free energy of activation ($\Delta G^{\ddagger}$) and reaction (ΔG_{rxn}) values for [2+2] cycloaddition of 1d to KI. 37

Table 3.6. Free energy of activation ($\Delta G^{\ddagger}$) and reaction (ΔG_{rxn}) values for [2+2] cycloaddition of 1e to KI. 40

Table 3.7. Free energy of activation ($\Delta G^{\ddagger}$) and reaction (ΔG_{rxn}) values for [2+2] cycloaddition of 1f to KI. 45

Table 3.8. Effect of C_{β}-substituents on free energ of activation ($\Delta G^{\ddagger}$) and reaction (ΔG_{rxn}), M06-2X/6-31+G(d,p) in $CHCl_3$, energies in kcal/mol. 48

Table 3.9. Free energy of activation ($\Delta G^{\ddagger}$) and reaction (ΔG_{rxn}) for [2+2] cycloaddition of ethylenes with KIs of differing C-substituents, energies in kcal/mol. 52

Table 3.10. Effect of N_1-substituents on free energy of activation ($\Delta G^{\ddagger}$) and reaction (ΔG_{rxn}), M06-2X/6-31+G(d,p) in $CHCl_3$, energies in kcal/mol. 54

Table 3.11. Free energy of activation ($\Delta G^{\ddagger}$) and reaction (ΔG_{rxn}) for [2+2] cycloaddition of ethylenes with KIs of differing N-substituents, energies in kcal/mol. 61

Table 3.12. Natural Population Analysis (NPA) of C_3-substituted KIs. 62

Table 3.13. Natural Population Analysis (NPA) of N_1-substituted KIs. 63

Table 3.14. ${P_k}^+$ and ${f_k}^+$ values for C_3-substituted keteniminium salts. 65

Table 3.15. ${P_k}^+$ and ${f_k}^+$ values for N_1-substituted keteniminium salts. 66

Table B.1. Free energy of activation ($\Delta G^{\ddagger}$) and reaction (ΔG_{rxn}) for comparison of the ring size effect on reactivity of KIs when N_1-substituents are piperidinyl, *N,N*-dimethyl and *N,N*-dially, M06-2X/6-31+G(d,p) with IEFPCM in $CHCl_3$ (ϵ=4.7113); energies in kcal/mol. 133

Table C.1. Free energy of activation ($\Delta G^{\ddagger}$) and reaction (ΔG_{rxn}) for KIs bearing chiral auxiliaries, M06-2X/6-31+G(d,p) with IEFPCM in $CHCl_3$ (ϵ=4.7113); energies in kcal/mol. 134

LIST OF SYMBOLS

E_{el}	Electronic Energy
$E_c[\rho]$	Correlation Energy
$E_x[\rho]$	Exchange Energy
$f(r)$	Fukui Function
H	Hamiltonian Operator
h_{KS}	Kohn-Sham Hamiltonian Operator
$P(r)$	Parr Function
q_A	Atomic Charge
$J[\rho(r)]$	Coulomb Energy
$T[\rho(r)]$	Kinetic Energy of Interacting Electrons
$T_{ni}[\rho(r)]$	Kinetic Energy of Non-Interacting Electrons
$V_{ext}(r)$	External Potential
$V_{ee}[\rho(r)]$	Electron-Electron Interactions
Z	Atomic Number
$\Delta G^{\ddagger}$	Gibbs Free Energy of Activation
ΔG_{rxn}	Gibbs Free Energy of Reaction
ε	Dielectric Constant
$\rho(r)$	Electron Density
ϕ_s	Quantitative Topological Descriptor
$\Delta G_{solvation}$	Solvation Free Energy
k^a	Local Stretching Force Constant
$\rho(r)$	Electron Density
H(r)	Energy Density
ψ_i	Kohn-Sham Orbitals

LIST OF ACRONYMS/ABBREVIATIONS

ADF	Amsterdam Density Functional
ASD	Atomic Spin Density
B3LYP	Becke-3-Parameter Lee-Yang-Parr Functional
B2PLYP	Double Hybrid Exchange-Correlation Functional
BMK	Boese-Martin for Kinetics
DFT	Density Functional Theory
EDG	Electron Donating Group
EWG	Electron Withdrawing Group
GGA	Generalized Gradient Approximation
GTO	Gaussian Type Orbital
HF	Hartree-Fock Theory
HOMO	Highest Occupied Molecular Orbital
IEF-PCM	Integral Equation Formalism of Polarizable Continuum Model
IRC	Intrinsic Reaction Coordinate
KI	Keteniminium Salt
LDA	Local Density Approximation
LUMO	Lowest Unoccupied Molecular Orbital
M06-2X	Hybrid Meta Exchange-Correlation Functional
MPW1K	Modified Perdew-Wang 1-Parameter Model for Kinetics
NAO	Natural Atomic Orbitals
NBO	Natural Bond Orbitals
NCI	Non-Covalent Interactions
NPA	Natural Population Analysis
PES	Potential Energy Surface
PC	Product Complex
PCM	Polarizable Continuum Model
PRC	Pre-Reactive Complex
SCF	Self Consistent Field

SCRF	Self Consistent Reaction Field
TS	Transition State
ωB97xD	Long-Range Corrected Hybrid Functional with Dispersion Correction

1. INTRODUCTION

Computational chemistry is a field of chemistry that enables chemists to perform mathematical equations on computer based programs with different methods to obtain information about chemical concepts. The biggest benefit of computational chemistry is it makes possible to approximate Schrödinger equations for the many-body problem. By virtue of its field of applications, today's chemists can rationalize the reaction mechanisms, explore unknown intermediate formations during a reaction, predict and interpret the experimental data, design drug molecules based on specific interactions between targets by use of simulations and assist experimental studies *via* calculations based on quantum mechanic methods to inform about molecular structures of molecules that appear on the potential energy surface.

In the history of computational chemistry, *ab initio* calculations and machine learning based methods are broadened day by day with the development of computers. The milestones of the field are the foundation of Density Functional Theory (DFT) by Walter Kohn and development of computational methods in quantum chemistry by John Pople. These studies were awarded with the 1998 Nobel Prize in Chemistry. More recently, Martin Karplus, Michael Levitt and Arieh Warshel originated multi-scale models for complex chemical systems which brought them the 2013 Nobel Prize in Chemistry. Since then, the developments of the methods used in computational chemistry are in progress with a broader extend.

In this thesis, DFT methods are used to investigate the mechanism of organic reactions, reactivities of molecules, and energetic aspects of organic reactions. The main reason for the selection of DFT throughout this study is that the method is the most widely used quantum chemical method with high accuracy and low computational cost. Molecular modeling of organic reactions with DFT can give very realistic results. This thesis consists of mainly two parts namely, [2+2] cycloaddition reactions through highly reactive keteniminium salts (KI)s which are nitrogen analogues of ketenes and organic reactions that involve KIs or ketenes.

In the first part, [2+2] cycloaddition reactions between KIs and olefins have been examined in two aspects. As shown in Figure 1.1, the [2+2] cycloaddition reactions between KIs and substituted alkenes have been modelled to determine cyclic or acyclic intermediate formation which plays a key role for the regioselectivity of the reaction mechanism.

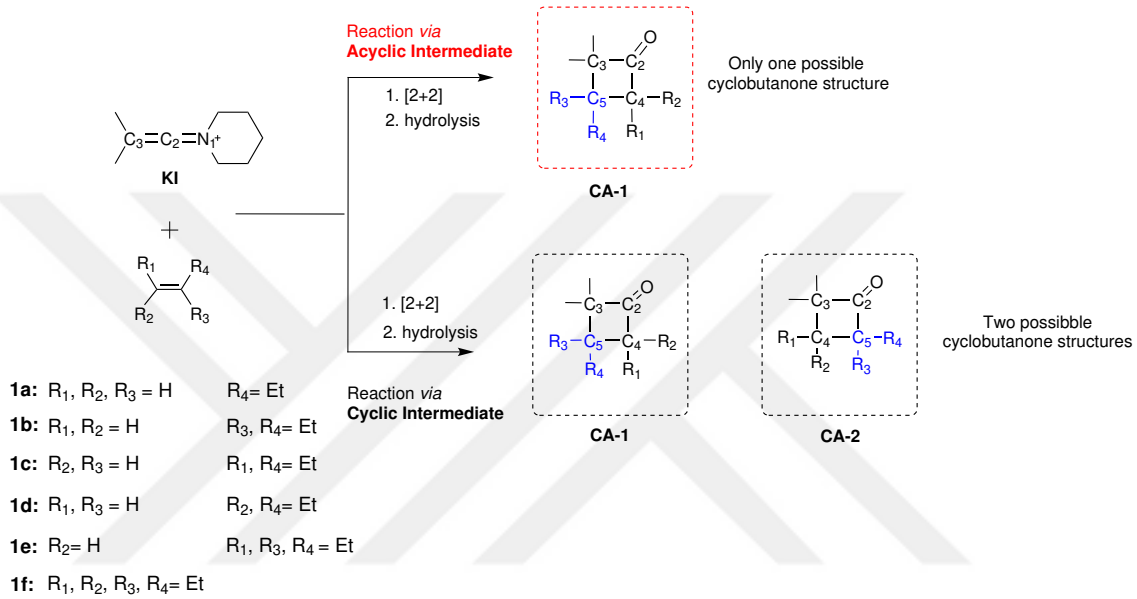

Figure 1.1. Schematic representation of the possible regioselectivity in [2+2] cycloaddition reactions between KI and substituted alkenes studied in Part I.

Furthermore, computational assessment of KI reactivity toward [2+2] cycloadditions has been conducted by means of DFT. KIs were examined with respect to substituents on terminal carbon atom and substituents on nitrogen atom as depicted in Figure 1.2. Conceptual DFT analysis has been also used to calculate reactivity indices of KIs involved in [2+2] cycloaddition reactions. This study will be submitted to The Journal of Organic Chemistry soon.

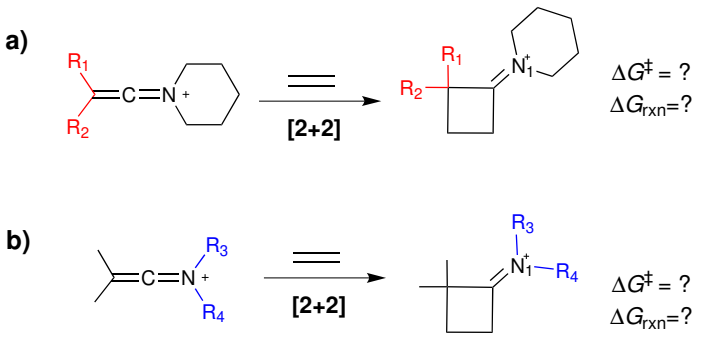

Figure 1.2. KIs to investigate a) the effect of substituent(s) on terminal carbon atom b) the effect of substituent(s) on nitrogen atom, on the free energy of activation and reaction.

The second part of the thesis consists of the studies in which the keteniminium salts or ketene molecules are the main intermediates. In more detail, in the first study, the synthesis and biological activities of zealactone 1a/b (shown in Figure 1.3) which belongs to the strigolactone family have been presented with both experimental and computational results. The study has been published in Helvetica Chimica Acta in 2020 [1]. Initially, the formation of plausible intermediates and side products in the reaction leading to the synthesis of building blocks of zealactones 1a/b have been analysed. Then, the reactivity of two different olefins toward [2+2] cycloadditions with a ketene molecule have been probed *via* computational methods.

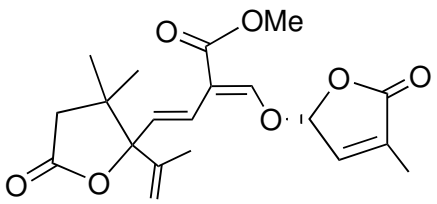

Zealactone 1a/b

Figure 1.3. Chemical structure of zealactone 1a/b [1].

In the second study, a process in which enamines react with electrophiles to produce highly substituted cyclobutanones have been established. The results of the study have been published in Helvetica Chimica Acta recently and online version of the article is available [2].

Cyclic enamines have been formed *via* [2+2] cycloadditions between keteniminium salts and an alkene. The importance of the [2+2] cycloaddition reaction is the formation of cyclobutaniminium ions that take place in a keteniminium-enamine equilibrium. A thorough analysis of structural properties of cyclic enamines (Figure 1.4) have been discussed to compare reactivities of enamines toward electrophiles.

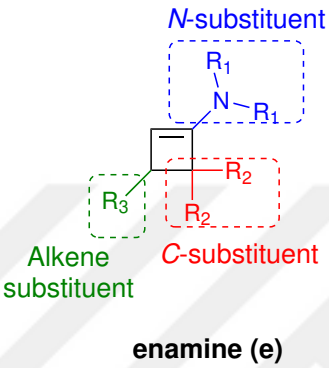

Figure 1.4. Enamine structure and derivatives: coplanarity of the enamine [2].

2. METHODOLOGY

2.1. Density Functional Theory

Density Functional Theory (DFT) [3], which enables first-principle computational calculations is pioneered by Hohenberg and Kohn [4, 5] to obtain ground state energy of molecules and atoms as a function of electron density. Even though the solution of Schrödinger equation gives all the information about a system, unfortunately solving the equation for many electron systems is highly complicated. As an important and promising advantage, three spatial coordinated electron density function enables to form Hamiltonian of a system to calculate total energy, hence makes it possible to obtain the solution for the Schrödinger equation. DFT is based on Khon-Sham equations, which basically rely on two theorems. The first theorem indicates that the external potential ($V_{ext}(r)$) is the potential caused by the nuclei and can be expressed as a function of electron density $\rho(r)$ given as

$$\rho(r) : N \int ... \int |\Psi(r_1, r_2, ...r_n)|^2 dr_1 dr_2 ... dr_n \tag{2.1}$$

in which r_i is the representation of coordinates of the electrons.

The second theorem states that if the electron density belongs to the ground state density, then the functional gives the energy of the ground state as minimum energy. The ground state energy of a system is calculated as a function of electron density and expressed as

$$E[\rho(r)] = \int V(r)\rho(r)dr + T[\rho(r)] + V_{ee}[\rho(r)] \, . \tag{2.2}$$

In the ground state electronic energy equation, while $T[\rho(r)]$ is the kinetic energy of interacting electrons, $V_{ee}[\rho(r)]$ is the interelectronic interaction energy.

According to Kohn-Sham theory, a reference system of independent and non-interacting electrons was proposed to define non-interacting density, which is equal to the density of the real, interacting system [5]. On this basis, the ground state electronic energy can be rewritten as

$$E[\rho(r)] = \int V(r)\rho(r)d(r) + T_{ni}[\rho(r)] + J[\rho(r)] + E_{XC}[\rho(r)] \tag{2.3}$$

where $T_{ni}[\rho]$ stands for the kinetic energy for non-interacting electrons, $E_{XC}[\rho]$ is the exchange-correlation energy term and $J[\rho]$ denotes the coulomb energy. The coulomb energy $J[\rho]$ caused by electron-electron Coulomb repulsion disfavors the total electronic energy. It can be defined as

$$J[\rho(r)] = -\sum_{A=1}^{M} \int \frac{Z_A}{\mid r - R_A \mid} \rho(r)dr + \int \frac{\rho(r_1)\rho(r_2)}{\mid r_1 - r_2 \mid} dr_1 dr_2 \tag{2.4}$$

where M represents the total number of nuclei. The kinetic energy of independent electrons,$T_{ni}[\rho]$ is defined as

$$T_{ni}[\rho(r)] = \sum_{i=1}^{N} \int \psi_i(r) - \frac{\nabla^2}{2}\psi_i(r)dr \tag{2.5}$$

where N represents the total number of electrons.

The exchange-correlation energy functional, $E_{XC}[\rho]$ is the sum of two functionals namely, an exchange functional $E_X[\rho]$, which is the interaction betwen electrons of same spin and a correlation functional $E_C[\rho]$, which is related to the interactions between electrons that have opposite spin. $E_{XC}[\rho]$ term is the only unknown in the ground state electronic energy and can be represented as

$$E_{XC}[\rho] = E_X[\rho] + E_C[\rho]\,. \tag{2.6}$$

Kohn-Sham theory defines independent reference orbitals, (ψ_i) and these orbitals can be obtained by solving the Kohn-Sham equations given as

$$h_{KS}\psi_i = \varepsilon_i\psi_i \tag{2.7}$$

where the Hamiltonian operator, h_{KS} can be detailed as follows

$$h_{KS} = -\frac{\nabla^2}{2} - \sum_{A=1}^{N} \frac{Z_A}{\mid r - R_A \mid} + \int \frac{\rho(r_1)\rho(r_2)}{\mid r_1 - r_2 dr_1 dr_2 \mid} + V_{XC}[\rho(r)] \,. \tag{2.8}$$

The term $\mathrm{V_{XC}}$ is the exchange-correlation potential. Also, $\mathrm{V_{XC}}$ is the functional derivative of exchange-correlation energy with respect to density as

$$V_{XC} = \frac{\delta E_{XC}}{\delta \rho} \,. \tag{2.9}$$

The electron density of a system can be expressed in terms of independent Kohn-Sham orbitals (ψ_i) as

$$\rho(r) = \sum_{i=1}^{N} |\psi_i|^2 \,. \tag{2.10}$$

At this point, if the exact form of the exchange-correlation functional is known, then generating the exact electron density will be possible. As indicated before, the exchange-correlation energy functional is an unknown term, hence with useful approximations it can be estimated.

2.2. Functionals

In order to overcome the drawback of DFT arising from the unkown exchange-correlation functional (E_{XC}), different types of approximations were developed. The local density approximation (LDA), which is derived from uniform electron gas model is one of them.

On the other hand, assuming homogeneous electron density is not suitable to estimate exchange-correlation energy due to the non-homogeneous electron density nature of molecules. To avoid this situation considering that electron density is not the same everywhere in a molecule, Generalized gradient approximation (GGA) [6] expanded the exchange-correlation energy term as the gradient of electron density,

$$E_{XC}^{GGA}[n] = \int drn(r)\epsilon_{XC}(n(r), |\nabla n(r)|) \, . \tag{2.11}$$

Hybrid density functionals are another approximation to exchange-correlation energy functionals. These functionals mix exchange-correlation energy from GGA and exact exchange from Hartree-Fock (HF) theory. One of the most popular hybrid functional is B3LYP(Becke, 3-parameter, Lee–Yang–Parr) [7, 8] shows important improvements compared to HF method. Basically, B3LYP is a DFT and HF based method, composed of LDA and GGA approximations expressed as

$$E_{XC}^{B3LYP} = (1-a)E_X^{LSDA} + aE_X^{HF} + b\Delta E_X^B + (1-c)E_C^{LSDA} + cE_C^{LYP} \tag{2.12}$$

where a=0.20, b=0.72 and c=0.81.

M06-2X functional is a hybrid meta-generalized gradient-approximation (hybrid meta-GGA) functional [9] which belongs to the Minnesota Functional Family. M06-2X functional is known to give accurate results for main group thermochemistry, kinetics and non-covalent interactions [10]. The functional can be described as

$$E_{XC}^{hyb} = \frac{X}{100}E_X^{HF} + (1 - \frac{X}{100})E_X^{DFT} + E_C^{DFT} \tag{2.13}$$

where X stands for the percentage of Hartree-Fock exchange, and for M06-2X functional its value is 54.

In Kohn-Sham density functional theory, long-range correction (LC) for exchange functional is another method that enables to model processes such as Van der Waals bonding, electron excitation and poor optical response properties [11]. The long-range corrected hybrid of a density functional approximation (LCDFA) can be formulated as

$$E_{XC}^{LCDFA} = E_X^{SR-DFA}(\omega) + E_X^{LR-HF}(\omega) + E_C^{DFA} \,. \tag{2.14}$$

One of the most widely used LC hybrid density functionals is the ωB97XD functional that includes empirical dispersion corrections [12]. Mainly, ωB97XD functional includes 100% of long-range exact exchange and 22% of short-range exact exchange.

2.3. Basis Sets

Basis sets in computational chemistry refer to a set of functions that are used to define molecular orbitals. Basis set functions can be described as a linear combinations of atomic orbitals (LCAO), and is represented as

$$\phi_i = \sum_{\mu=1}^{K} c_{\mu i} f_\mu \tag{2.15}$$

where μ_i symbolise molecular orbitals, $c_{\mu i}$ coefficients, f_μ atomic orbitals and K is the total number of atomic orbital functions.

Basis sets can be sectioned mainly into two types of orbitals: Slater-Type Orbitals (STO's) and Gaussian-Type Orbitals (GTO's). The former is a solution to the Schrödinger equation for hydrogen-like species. However, describing non-spherical orbitals with STO's is a problem. In addition, even though they have higher accuracy, STO's are more costly. On the other hand, GTO's are approximated versions of STO's and resolve these shortfalls. There is no limitation as hydrogen-like atom and much less computational cost, therefore GTO's are widely used in DFT calculations.

Split valence basis sets were developed by Pople *et al.* to treat valence and core orbitals separately. As we know, the chemical environment has more effect on electrons in the valence orbital compared to electrons in the core orbitals. Hence, valence electrons are treated with a larger basis set to get more accurate results and core electrons are treated with a minimal basis set for lower computational cost. The most well-known Pople basis sets are 3-21G, 6-21G, 6-31G*, 6-311G**and 6-31++G**. The former notation that comes before the dash represents the number of primitive Gaussian functions used to calculate core atomic orbitals and the latter one that comes after the dash indicates that the valence shell orbitals are composed of a linear combination of that many Gaussian functions. The numbers; two, three and four after the dash indicates that these basis sets are split-valence double-zeta, triple-zeta and quadruple-zeta basis sets, respectively.

Polarization and diffuse function terms should be included in the basis sets to get more reliable results for electronic energy by improving calculations. In Pople basis sets, one asterisk (*) or (d) indicates that polarization functions added to heavy atoms in the molecule. To consider polarization of both heavy and light atoms (such as hydrogen and helium) two asterisks (**) or (d,p) sign is used. A plus sign (+) denotes addition of diffuse functions to basis set for heavy atoms. Two plus sign (++) means diffuse functions are also added for light atoms as well as heavy ones.

2.4. Continuum Solvation Models

The chemical reactions taking place in the liquid phase have important role in chemistry. Therefore, modelling the solvent environment in which a reaction takes place is a primary issue for computational chemists. Solvent models were developed to define solvent effect in the reactions [13]. The models can be subdivided into two main groups as explicit and implicit solvent models. In the explicit solvent models, individual solvent molecules are included, therefore specific interactions between solvent and solute molecules can be observed. Even though explicit models are more realistic, computational cost of them is high.

On the other hand, implicit solvent (continuum solvent) models accept the solvent environment as an uniformly polarizable medium and defines the polarizability with dielectric constant (ε) that is specific to solvents. The solute molecules are modelled in a cavity embedded in the polarizable medium. Implicit solvent models can be useful because this approximation reduces the computationally cost. The value of total free energy of solvation can be calculated as

$$\Delta G_{solvation} = \Delta G_{cavity} + \Delta G_{dispersion} + \Delta G_{electrostatic} + \Delta G_{repulsion} \tag{2.16}$$

in which ΔG_{cavity} denotes the energy cost to create a cavity in the solvent for the solute. The favorable change in the energy due to dispersion interactions between solute and solvent is added as $\Delta G_{dispersion}$. The third term, $\Delta G_{electostatic}$, is the electrostatic energy and $\Delta G_{repulsion}$ is the energy caused by the exchange solute-solvent interactions, which is not included in the cavitation energy term.

Polarizable Continuum Model (PCM) is one of the most used implicit solvent models. This model defines the cavity surface through spheres defined by Van der Waals radii centered at each atom. There are varying versions of PCM which are commonly used. One is the dielectric PCM (D-PCM) that uses dielectric approach as in the original. Another method named Conducter-like PCM (C-PCM) treats the solvent environment as conductor medium. Lastly, there is an Integral Equation Formalism of PCM (IEF-PCM), which is the method used in this thesis [14].

2.5. Conceptual Density Functional Theory

As explained, density functional theory (DFT) enables to describe ground states of molecules and atoms regarding the idea that the electron density can be used as fundamental function to solve the Schrödinger equation. Conceptual DFT was introduced by Parr and coworkers to get numerical results for chemical concepts, such as electronegativity χ, chemical potential μ, hardness η, softness S, electrophilicity ω, nucleophilicity N etc. [15]. Quantitative results of chemical concepts enable chemist to predict reactivity, chemoselectivity and regioselectivity.

Conceptual DFT is based on the Hohenberg-Kohn theorem, where the ground state energy of a system with N electrons and external potential V(r) is defined as a function of electron density. The $E[N; v(r)]$ term decribes how the system is affected by a change in the number of electrons and external potential given as

$$E[\rho(r)] = E[N; v(r)] \,. \tag{2.17}$$

One of the conceptual DFT reactivity indices is electrophilicity. The electrophilicity index ω, combines electronic chemical potential μ and absolute chemical hardness η to measure the reactivity of an electrophilic reagent. The electrophilicity index ω can be presented as

$$\omega = \frac{\mu^2}{2\eta} \,. \tag{2.18}$$

The higher value of ω means a good electrophile, which is related to high μ and low η value. The relative nucleophilicity index N is the HOMO energies with respect to HOMO energy of tetracyanoethylene (TCE) having lowest HOMO energy in which the value of N(TCE) is accepted zero as reference given as

$$N = E_{HOMO(Nu)}(eV) - E_{HOMO(TCE)}(eV) \,. \tag{2.19}$$

2.5.1. Reactivity Descriptors: Fukui and Parr Functions

The Fukui function $f(r)$ was proposed by Parr and Yang [16] based on DFT method, assuming a reagent approaches others from the reactive side which has the highest value of $f(r)$, defined as

$$f(r) = \left[\frac{\partial \rho(r)}{\partial N}\right]_{v(r)} \,. \tag{2.20}$$

They assumed a frozen core [17], in which;

$$\partial\rho = \partial\rho_{valence}$$

and defined $f^{-}(r)$ for electrophilic and $f^{+}(r)$ for nucleophilic attacks as

$$f^{-}(r) \approx \rho_{HOMO}(r) \tag{2.21}$$

$$f^{+}(r) \approx \rho_{LUMO}(r)\,. \tag{2.22}$$

The condensed Fukui functions based on Mulliken charges proposed by Yang and Mortier [18] depicted as

$$f^{-} = q_k(N) - q_k(N-1) \tag{2.23}$$

$$f^{+} = q_k(N+1) - q_k(N) \tag{2.24}$$

where, N is the number of total electrons and $q_k(N)$, $q_k(N+1)$, $q_k(N-1)$ are the atomic charges in the original, anionic radical and cationic radical species, respectively. Fukui functions are used to determine local electrophilicity ω_{k} and nucleophilicity N_{k} indices allowing the detection of the most electrophilic and/or nucleophilic atom in a molecule defined by

$$\omega_k = \omega f_k^{+} \tag{2.25}$$

$$N_k = N f_k^{-}\,. \tag{2.26}$$

Domingo and coworkers [17] have studied polar reactions examining the Atomic Spin Density (ASD) Analysis and proposed Parr functions P(r) based on ASD for the radical of the original reagent and given as

$$P^{-}(r) = \rho_s^{rc}(r) \tag{2.27}$$

$$P^{+}(r) = \rho_s^{ra}(r) \tag{2.28}$$

in which the ASD of the radical cation is denoted as $\rho_s^{rc}(r)$ andASD of the radical anion is represented as $\rho_s^{ra}(r)$.

Local electrophilic, ${P_k}^+$, can be used to predict nucleophilic attacks and local nucleophilic, ${P_k}^-$, for the electrophilic attacks. These Parr functions are ASD values at each atom in a system. Local electrophilicity ω_{k} and local nucleophilicity N_{k} can also be rewritten with Parr functions to find most electrophilic and most nucleophilic atoms in a molecule,

$$\omega_k = \omega P_k^+ \tag{2.29}$$

$$N_k = N P_k^- \ . \tag{2.30}$$

2.6. Natural Population Analysis

Atomic charge distribution in a polyatomic molecule provides means for chemists to interpret chemical processes. Unfortunately, it is not possible to determine exact atomic charges quantitatively [19]. There are methods used for population analysis, such as Mulliken population analysis, based on wavefunctions and Hirsfeld analysis, based on electron density. Mulliken population is one of the well known methods for atomic charge analysis as expressed

$$q_A = Z_A - \sum_{\mu \epsilon A}^{AO} (PS)\mu\mu \tag{2.31}$$

in which for the atom A, the atomic charge and the atomic number is denoted by q_A and Z_A, respectively. The term subtracted from the atomic number is the total number of electrons (N) described as

$$N = \sum_{\mu}^{AO} (PS)\mu\mu \tag{2.32}$$

where P is the density and S is the overlap population of the localized basis sets. Mulliken population analysis is criticized because of being highly sensitive to basis set choice and giving unrealistic results in the case of ionic species.

Natural population analysis (NPA) based on Natural Bond Orbitals (NBO) is an improved method that is preferred in recent studies. Natural bond orbitals are an orthonormal set of localized orbitals that describe possible Lewis structures of bonding electrons and lone pairs. Advantages of this method over Mulliken population are the lack of dependence on the basis set and more rational electron distribution in ionic compounds.

2.7. Noncovalent Interaction Analysis

Noncovalent Interactions (NCIs) such as π-π interactions, electrostatic interactions and Van der Waals interactions play a critical role in chemical and biological systems. Noncovalent interactions can be determined *via* NCI analysis that generates an index [20] given as

$$s = \frac{1}{2(3\pi^2)^{1/3}} \frac{|\nabla\rho|}{\rho^{4/3}} \tag{2.33}$$

in which, s is the reduced density gradient and ρ is the electron density. s dramatically changes in case of the presence of a weak interaction producing density critical points on 2D plot of s and ρ. Also, 3D NCI plots are useful tools for visualization of noncovalent interactions.

3. INTERMOLECULAR [2+2] CYCLOADDITION REACTIONS BETWEEN KETENIMINIUMS SALTS AND ALKENES

3.1. Background

Within organic chemistry, reaction mechanisms can take place *via* either a concerted or a stepwise pathway. In the case of stepwise mechanism, reactive intermediates are formed at each step. The driving force of these types of reactions is to transform unstable intermediates into stable structures. Keteniminium salts (KI)s are one of the highly reactive intermediates used in synthetic organic chemistry. KI has a cationic nature and is the nitrogen analogs of ketenes [21, 22]. KIs can be sectioned in three groups with respect to its substituents as depicted in Figure 3.1.

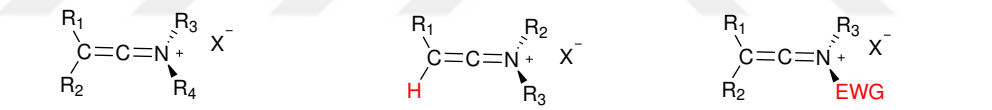

Figure 3.1. a) Keto, b) Aldo and c) Activated keteniminium salts.

The synthesis of organic compounds through reactions involving KIs was initiated by the pioneering work of Viehe and Ghosez in the 60's [23–25]. Since then, KIs have been used in a broad range of synthetic process due to their higher reacivity, electrophilicity and selectivity [21, 22, 25–27]. Besides these properties, advantages such as cheap starting materials to synthesize KIs and lack of polymerization, dimerization make KIs preferable to ketenes [28]. By reason of its high reactivity, it has been observed that KIs react with ethylene even at room temperature [28]. Importantly, using chiral KI intermediates is an effective and promising way to produce enantiopure cyclobutanones [29–33].

In the literature, different ways to synthesize keteniminium salts have been reported until today. One of the methods had been introduced by Ghosez *et al.* indicating that α-chloro enamine can be used as starting reagent to produce KI intermediates. Subsequently, these intermediates can undergo [2+2] cycloaddition reactions with alkenes, alkynes and dienes to produce cycloadducts, which become cyclobutanones after hydrolysis [28, 34, 35]. Nowadays, the most widely used procedure to synthesize KIs are the reaction of amides with triflic anhydride and base such as collidine [26] as shown in Figure 3.2.

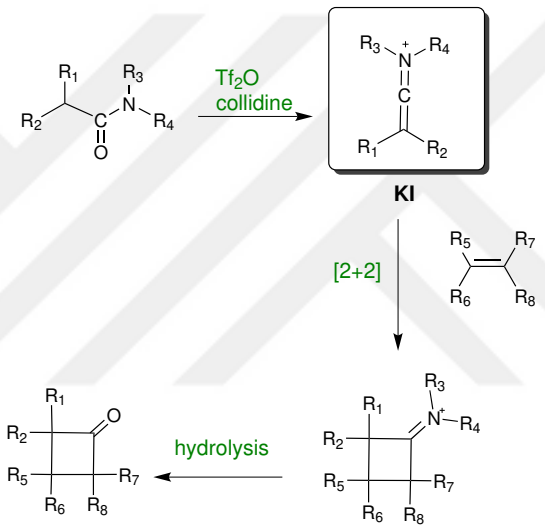

Figure 3.2. Formation of KI and access to functionalized cyclobutanones *via* [2+2] cycloaddition reactions between KIs and alkenes [26].

In synthetic organic chemistry, keteniminium salts are used as intermediates in many reactions that lead to the synthesis of highly complex structural motifs, such as $6\pi/10\pi$ electrocyclizations, [36–38] [4+2] cycloaddition reactions with dienes, [39–41] Pictet-Spengler cyclizations, [42] arene-ynamide cyclizations, [43] (1,5) hydride shifts [44,45] and nucleophilic additions followed by [3,3]-sigmatropic rearrangements [46,47].

Significantly, KIs serve as key intermediates in intermolecular [26,40,48,49] and intramolecular [2+2] cycoaddition reactions [50–52] with alkenes and alkynes to produce cyclobutaniminium and cyclobuteniminium salts, respectively. These cycloadducts can be used as reagents in Diels-Alder [53, 54], Michael addition [55] and nucleophilic addition reactions [56].

The main focus of this thesis is the [2+2] cycloaddition reactions *via* keteniminium salts. The [2+2] cycloaddition of KIs to alkenes/alkynes is one of the most substantial methods to produce functionalized cyclobutanones and cyclobutenones. These cycloadducts are used in the synthesis of many natural and biological compounds [57–60], such as GR-24 that is the synthetic analogue of natural strigolactone, [61] prostanoid scaffolds [33] and nucleosides act as HIV inhibitor [62]. The cyclic compounds cyclopentenones, furans and α, β butenolines can be obtained by [2+2] cycloaddition between KIs and alkynes. Notably, stereospecific Baeyer-Villager oxidation of cyclobutanones lead to the formation of γ-lactones [29, 32, 63].

3.1.1. Mechanistic Studies of [2+2] Cycloaddition Reactions *via* Keteniminium Salts

Along with the studies that use KIs in cycloaddition, the mechanism of the reaction had become an important question. In 1972, Ghosez and coworkers proposed a concerted [$\pi 2_s + \pi 2_a$] type of mechanism [35] based on Woodward and Hoffmann's cycloaddition mechanism [64] for the addition of dienes and olefins to KIs. The main idea was that this type of mechanism for ketene addition should be more favorable when ketenes are replaced by keteniminiums. In 1982, Ghosez and coworkers conducted another experimental study involving KIs. According to the diastereoselectivity of cycloadducts, they suggested two possible transition state structures in which cyclopentene is perpendicular to KIs bearing a chiral auxiliary [30].

In the following year, Saimoto *et al.* have conducted an experimental study and found out that the stereospecifity of [2+2] cycloaddition of KIs to olefins was determined by the *N*-substituent of KI [65]. A stepwise pathway was proposed based on the enantiomeric excess values of *cis* and *trans* cyclobutanones. The proposed mechanism is represented in Figure 3.3. In the first step, olefin attacks from a favorable attack trajectory, which is less hindered. As a result of this attack, a carbocation intermediate int-*cis* is formed. Rotation around C-N and C-C enables formation of enamine-like structure. At the second step, the bond is formed between terminal carbon of KI and carbocationic center to produce CA-*cis*.

After hydrolysis of the resulting cyclobutaniminium ion, cyclobutanone *cis*-1 is formed. Isomerization during hydrolysis enables the production of stereoisomer *trans*-2. There is also possibility for the isomerization of int-*cis* to int-*trans*, and after the second bond is formed, CA-*trans* would be produced. Hydrolysis and hydrolysis with isomerization of CA-*trans* give *cis*-3 (enantiomer of *cis*-1) and *trans*-4 (enantiomer of *trans*-2).

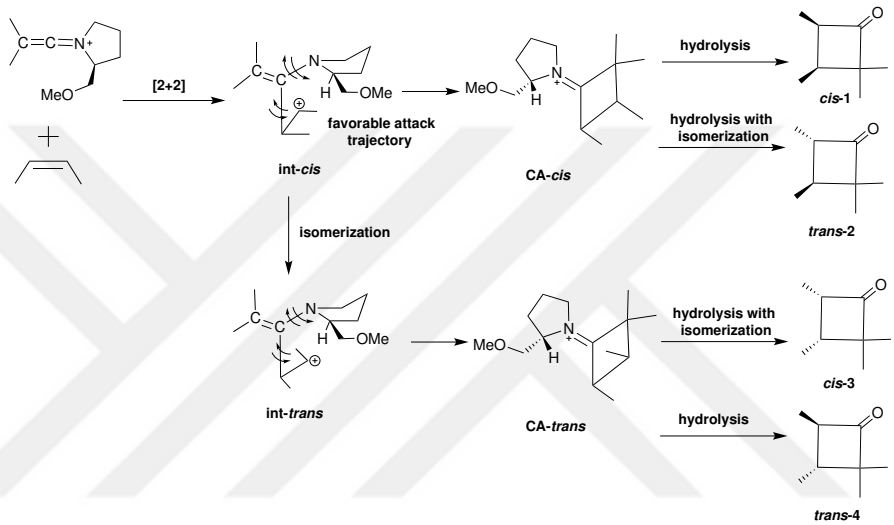

Figure 3.3. Proposed two-step mechanism for asymmetric [2+2] cycloaddition reactions between KIs and *cis*-2-butenes [65].

In 1999, a computational study to investigate the mechanism of silicon directed intramolecular [2+2] cycloaddition of KIs was performed at RHF/6-31G* and B3LYP/6-31G* level of theories [57]. Based on DFT calculations, Ghosez and Houk and coworkers have suggested a two-step mechanism in which electrophilic KI is attacked by double bond to form 7-membered ring intermediate in a bridged enamine cation form. Also, selectivity of the cycloaddition was affected by the face selection of alkene.

Afterward, in 2001, Fang and coworkers computationally explored the [2+2] cycloaddition between KIs and olefins at the BHandHLYP/6-31G* level of theory [66]. The results indicated that the reaction between tetrahydroketeniminium and ethylene has a 2x[1+1] type asynhronous concerted mechanism. On the other hand, if substituted KI or substituted olefin is the reagent, then the reaction follows a two-step mechanism.

In case of substituted KI, a cyclopropane-like intermediate is formed at the end of the first step. Turning this highly unstable cyclic molecule into more thermodynamically favorable structure is the driving force for the second step. Notably, dichloro-substituted alkene had geminal isomerization. Due to steric factors, instead of cyclopropane-like intermediate, acyclic intermediate structure was detected at saddle point. The first bond was formed between electrophilic carbon of KI and unsubstituted carbon of alkene.

More recently, Domingo *et al.* have modeled the intermolecular [2+2] cycloaddition of tetramethylketeniminium with acetylene and propyne by means of DFT [67]. As computational methodology, MPWB1K/6-311G(d,p) level of theory was used for optimizations, and conceptual DFT methods for reactivity indices were applied to explain and rationalize the reaction mechanism and electrophilic nature of KI. The mechanism of the reaction was stated as a two-step mechanism as shown in Figure 3.4. The nucleophilic attack of alkynes to the electrophilic central carbon of KI leads to formation of first activated complex.

The transition state that propyne was involved occurred in an asymmetrical two stage process. Cyclic intermediates were formed as a result of the first attack. For the second bond formation, there were two possibilities when propyne was used enabling the production of regioisomeric structures. Energetic analysis showed that the cyclobuteniminium formation where the second bond was formed between substituted carbon of alkene and terminal carbon of KI was both kinetically and thermodynamically favorable. The experimental study of De Mesmaeker *et al.* with the same reagents showed that there was a 3:1 ratio for the regioisomerism, [53] the results were supported with the computational data. In addition, free energy analysis showed that the rate determining step is the first step for the [2+2] cycloaddition reaction with KIs.

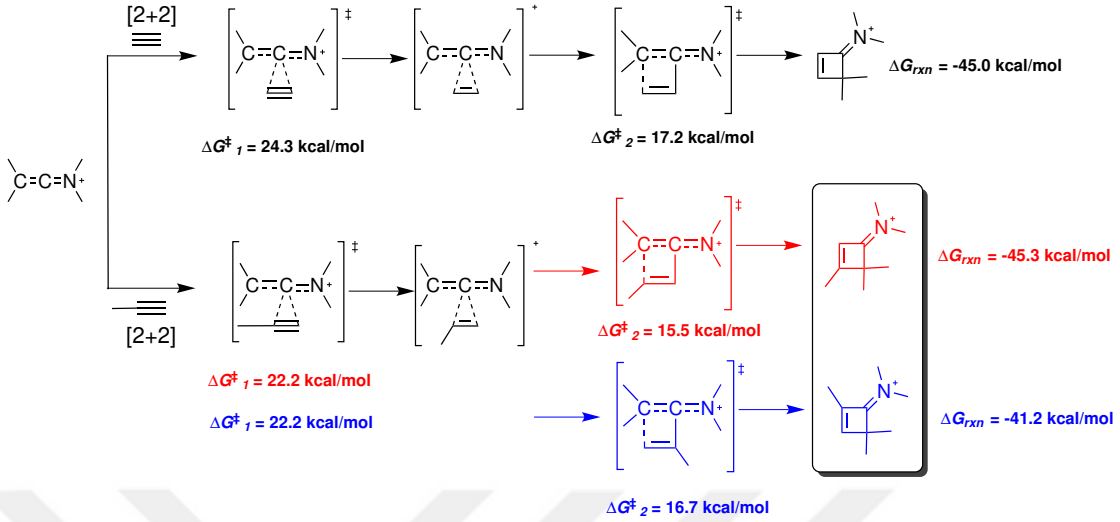

Figure 3.4. Schematic representation of Domingo's mechanism for [2+2] cycloaddition of keteniminium salt to acetylene and propyne, MPWB1K/6-311G(d,p) [67].

In their reactions with dienes, KIs can undergo [4+2] or [2+2] cycloadditions depending on the choice of diene [35, 39–41]. The C=N double bond of KIs serve as dienophile in [4+2] additions. The theoretical investigation to explain selectivity pattern with respect to diene structure was conducted by Houk and coworkers in 2020 [41]. The optimizations were done at ωB97XD level of theory in gas phase. Cyclopentadiene, cyclohexadiene, 1,3-pentadiene and 2,3-dimethylbutadiene were selected as 1,3-dienes in the cycloaddition reactions modeled with tetramethylketenimiium ion. Free energy of activation and reaction analysis showed that for the reactions with *cis*-fixed cyclic dienes, [4+2] cycloaddition was more favorable. The main difference between cyclopentadiene and cyclohexadiene was that while the reaction with the former occurs *via* a concerted mechanism, with the latter one, a stepwise pathway is preferred. On the other hand, reactions of KIs with acyclic conjugated dienes were affected by the *s-cis* or *s-trans* conformations of dienes. According to results, *s-trans* 1,3-pentadiene underwent a two-step [2+2] cycloaddition where the first step is the rate determining step. The reaction with 2,3-dimethylbutadiene had different selectivity with respect to *s-cis* and *s-trans* conformers. *S-trans* 2,3-dimethylbutadiene gave the [2+2] cycloadduct in reaction with KI through stepwise mechanism where rate determining step was again, the first step. There was a small energy difference between *s-cis* and *s-trans* conformers of 2,3-dimethylbutadiene. Hence, it was said that the diene can undergo in both concerted [4+2] (favored by 0.8 kcal/mol) and stepwise [2+2] cycloadditions.

Notably, by focusing on stepwise [2+2] cycloadditions, it can be said that the main difference from Domingo's mechanism is the formation of acyclic intermediates that have allylic stabilization.

3.2. Aim of the Study

The [2+2] cycloaddition reactions of KIs are highly regioselective. Some experimental results from the literature are given in Table 3.1. There are limited computational studies that explain the regioselectivity of reactions in which mono-substituted alkenes and terminal alkynes were used [48,67]. These studies clarified that the activation barrier of the second step and reaction free energy values provide an explanation for the determination of the major product. In addition, the calculations for the [2 + 2] cycloaddition reactions of keteniminium salts with alkynes, *cis*-alkenes and *trans*-alkenes revealed stepwise reaction mechanisms, where the rate determining step (RDS) is the formation of cyclopropane-like intermediate through the first transition state [48].

In this study, the first aim is to conduct a mechanistic study of intermolecular [2+2] cycloaddition reactions of keteniminium salts with substituted alkenes to enlighten the effect of alkene substitution on the mechanism and regioselectivity. The second aim is to examine the reactivity of a set of KIs to guide experimental studies which spread over a wide application area. The reactivity of KIs is compared with respect to its C-substituents and N-substituents as in Figure 3.5

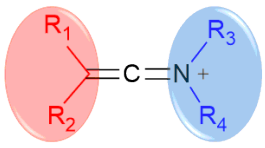

Figure 3.5. General structure of keteniminium salts with respect to C-substituents and N-substituents.

Table 3.1. The regioselectivity in [2+2] cycloadditions of KIs to alkenes and alkynes.

Entry	KI	Alkene/Alkyne	Adduct	Yield %
1 [41]		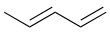	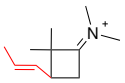	89
2 [26]			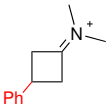	70
3 [48]	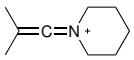	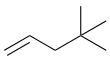	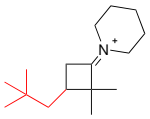	100
4 [48]	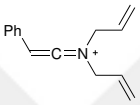		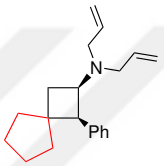	85
5 [53]			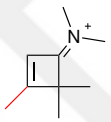	68
6 [32]	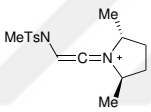		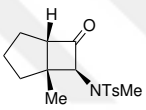	44

3.3. Computational Methodology

An extensive Density Functional Theory (DFT) study has been carried out on [2+2] cycloadditions between keteniminium salts and alkenes. The optimizations were utilized the hybrid meta-GGA exchange-correlation (M06-2X) functional with dispersion effects, which is known to give accurate results in terms of thermochemistry, kinetics and noncovalent interactions [9, 10, 68–70]. As basis set 6-31+G(d,p) was employed for all calculations. 6-311++G(3df,3pd) extra basis set was used for sulphur atoms to get more realistic energy results [71]. The solvent medium was taken into consideration with respect to self-consistent reaction field (SCRF) theory [13, 72] by applying IEF-PCM solvent model [73–76]. As the solvent, $CHCl_3$ (ϵ= 4.7113) was selected due to its prevalence in many experimental studies. For the sake of energy refinements, single point calculations were performed with long-range corrected ωB97XD, [12] hybrid-GGA MPW1K, [77] double hybrid B2PLYP [78] and the empirical dispersion corrected variation B2PLYPD in $CHCl_3$ over M06-2X/6-31+G(d,p) optimized structures.

Gaussian 16 (G16) program package [79] was used to perform calculations. A thorough conformational analysis was done for all reactants, transition states, intermediates and products. Intrinsic reaction coordinate (IRC) analysis [80–82] was applied to confirm reaction mechanism and to find intermediates formed as a result of transition state structures. Normal mode analysis was used to confirm saddle point geometries. The reactions were modeled at 298.15 K and 1 atm conditions. All free energy of activation $\Delta G^{\ddagger}$ and reaction free energy ΔG_{rxn} values are relative to the separate reactants.

Conceptual DFT methods were used to predict the effect of different substituents on reactivity of KIs toward [2+2] cycloadditions. Firstly, Domingo's [17] electrophilic Parr function ${P_k}^+$ and Yang and Mortier's [18] Fukui function $f^+(r)$ for nucleophilic attack were calculated at UM06-2X/6-31+G(d,p)//M06-2X/6-31+G(d,p) and M06-2X/6-31+G(d,p) level of theories in $CHCl_3$, respectively. To obtain population analysis, Natural Bond Orbital (NBO 6.0) calculations [83] were performed with the Amsterdam Density Functional (ADF) program package [84, 85] at the M06-2X/ATZ2P level of theory in $CHCl_3$. In order to visualize the non-covalent interactions of selected TSs and KI intermediates optimized at M06-2X/6-31+G(d,p) were investigated by using NCI-plot program [20]. The interactions in which KIs with sulphur atom were involved were attained by using 6-311++G(3df,3pd) extra basis set.

3.4. Investigation of [2+2] Cycloaddition Reaction Mechanisms Involving KIs and Alkenes with Differing Substitution Patterns

[2+2] cycloaddition of KIs with substituted alkenes is a way to synthesize cyclobutanones. Alkene susbtitution pattern may cause steric and electronic factors that is important for the mechanism preference as indicated in Figure 3.6. By detecting the intermediate formed by the nucleophilic attack of alkene to KIs, possible cycloadducts can be verified. There are two probable types of intermediates, cyclic and acyclic. If the mechanism of the reaction proceeds through an acyclic intermediate as a result of the bond formation between C_2-C_4, there is only one possibility for the second bond formation. Cycloadduct 4 is produced *via* C_3-C_5 addition followed by hydrolysis.

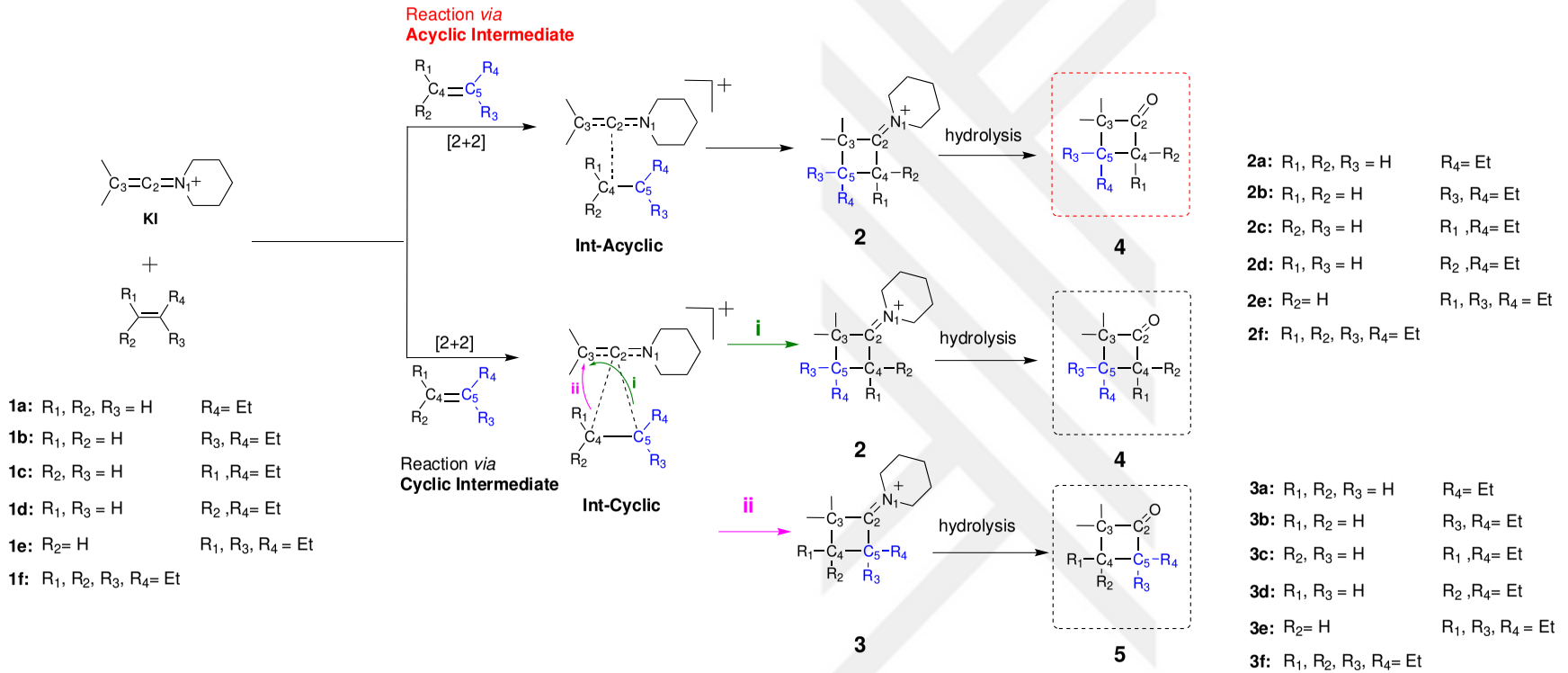

Figure 3.6. Schematic representation of possible [2+2] cycloaddition reaction mechanisms between KIs and substituted alkenes.

As the other probability, the addition of alkene to KI can end up with a cyclic intermediate structure as a minima on the PES. This highly reactive intermediate can undergo the second step *via* pathway i or pathway ii. The selection of the pathway determines which regioisomer will be the major product. In more detail, if the pathway i is more feasible kinetically and/or thermodynamically, then the cycloaddition occurs via bond formation between C_3-C_5 resulting in the substituents at positions as in cyclobutanone 4. However, if pathway ii is more feasible cyclobutanone 5 is the major product.

Initially, the [2+2] addition of KIs was modelled with mono-substituted alkene 1a and results were summarized in Figure 3.7. The computed results confirmed that the exergonic reaction proceeds in two-step in which the first step is the RDS. First transition state TS1-a is the attack of 1a to KI and shows asynchronous character based on critical distances. The IRC calculations confirmed the formation of highly strained cyclic intermediate, Int-a. Pathway i and pathway ii are two possibilities for the cycloadditions leading to the synthesis of either 2a or 3a that have ethyl groups at different positions. The pathway i is kinetically more favorable by 3.5 kcal/mol compared to pathway ii. Therefore, the bond is formed between C_3-C_5 determining the regioselectivity and giving the major product, 2a.

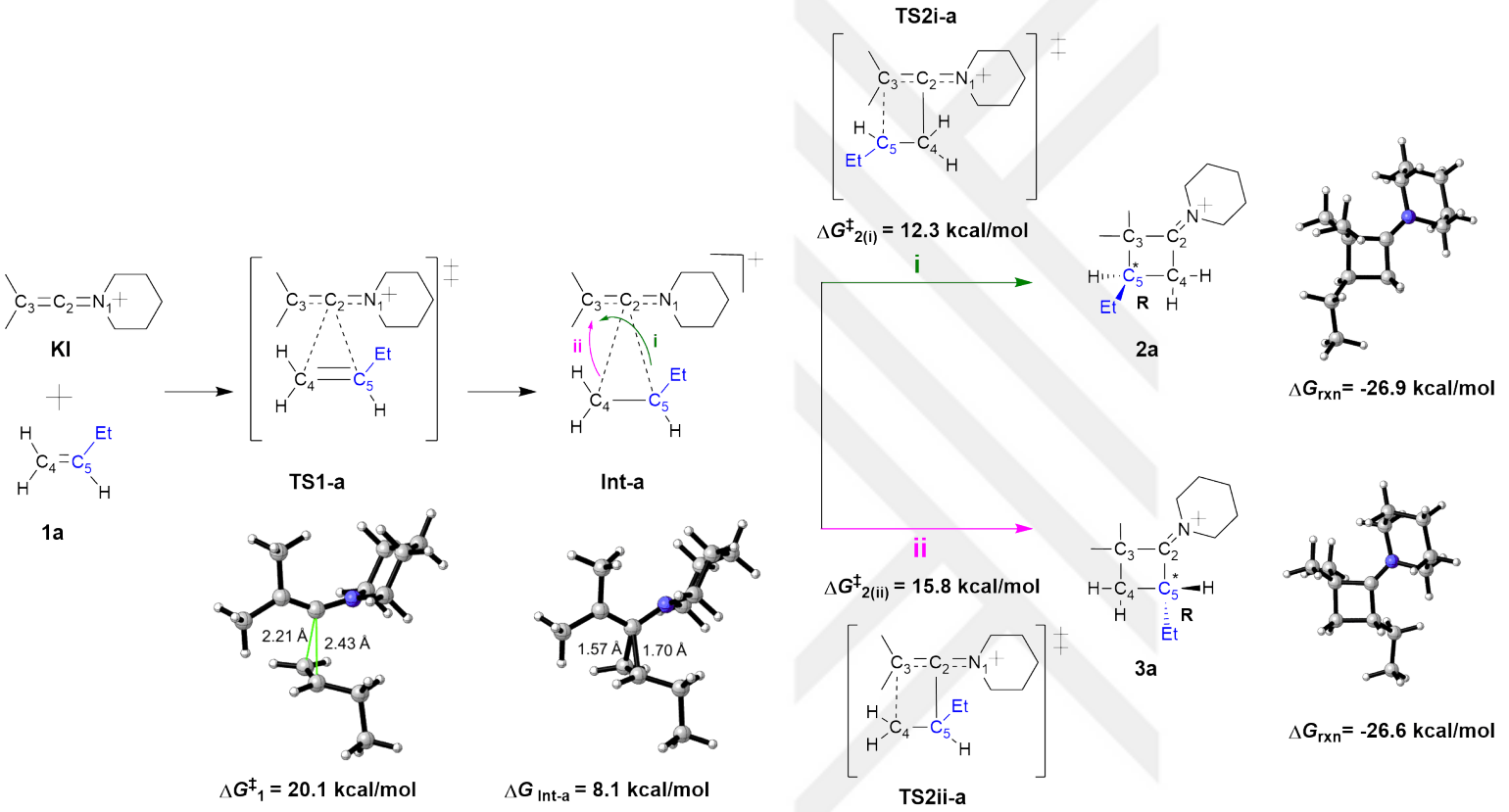

Figure 3.7. The reaction mechanism of [2+2] cycloaddition between KI and mono-substituted alkene 1a, M06-2X/6-31+G(d,p).

Furthermore, the conformational space was thoroughly investigated in order to predict the formation of other enantiomer pairs. Four possible attack orientations of 1a with respect to KI was considered and tabulated in Figure 3.8 as A, B, C and D. The approach orientation of alkene in the first step of the reaction determines the stereochemistry of the product formed and the routes for that are shown in Figure 3.8. Since both reagents, KI and alkene, are achiral molecules, there is no difference in free energy of activation and reaction values, but knowing the route which gives the desired enantiomer of the cycloadduct gives important know-how to experimental studies. By using a chiral auxilary as *N*-substituent a selective synthesis can be enabled. The first step as the RDS was confirmed by using different level of theories *via* single point energy calculations. Results are represented in Table 3.2. Another important finding is that calculations with all functionals showed the looser bond in the intermediate structure was more favorable to break and undergo cyclization (for example it is 1.70 Å in Int-a, M06-2X/6-31+G(d,p)).

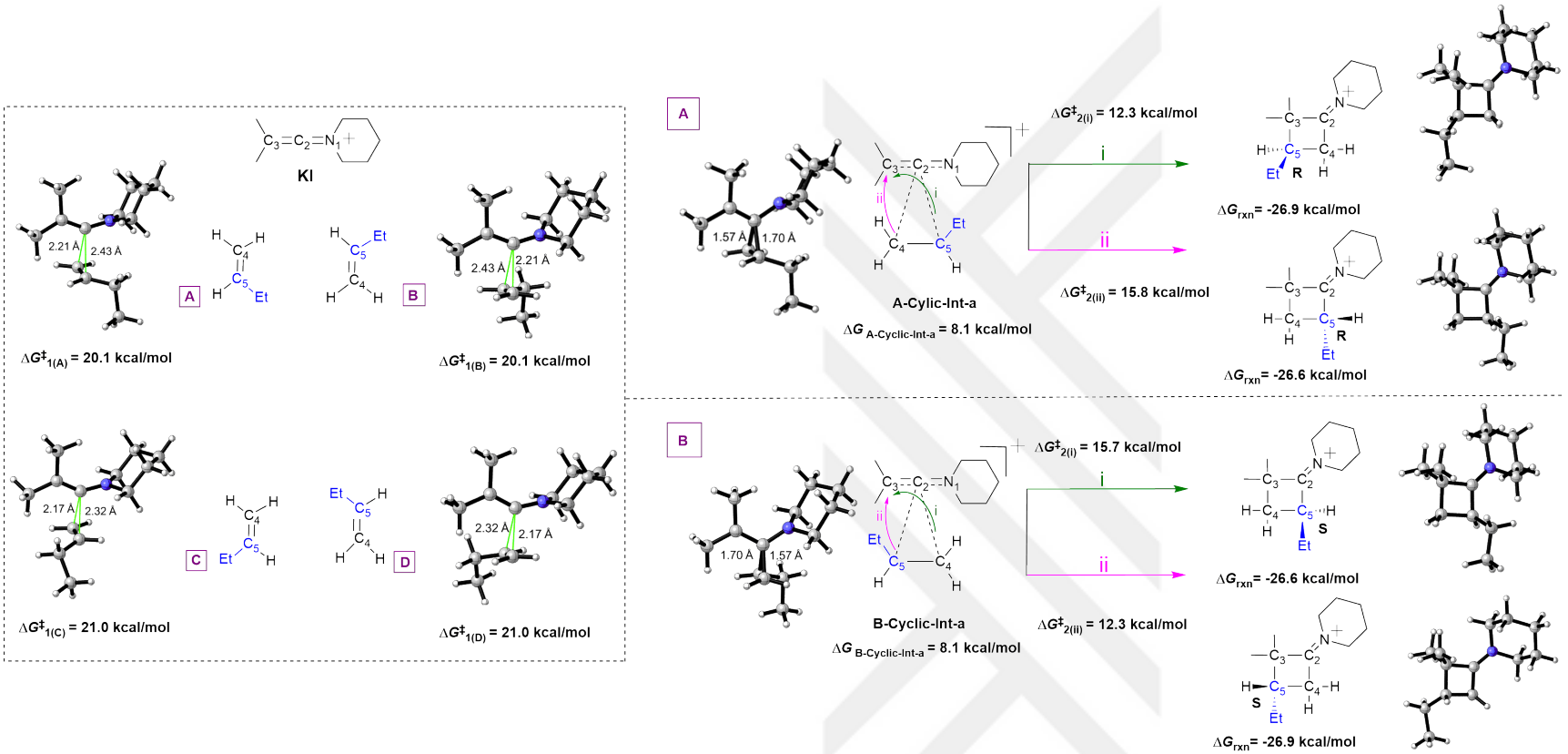

Figure 3.8. Possible attack orientations of 1a to KI and formation of enantiomer pairs of cycloadducts, M06-2X/6-31+G(d,p).

Table 3.2. Free energy of activation ($\Delta G^{\ddagger}$) and reaction (ΔG_{rxn}) values for [2+2] cycloaddition of 1a to KI.

	M06-2X					MPW1K				
	$\Delta G^{\ddagger}_1$	$\Delta G^{\ddagger}_{2(\text{i})}$	$\Delta G^{\ddagger}_{2(\text{ii})}$	$\Delta G_{\text{rxn(i)}}$	$\Delta G_{\text{rxn(ii)}}$	$\Delta G^{\ddagger}_1$	$\Delta G^{\ddagger}_{2(\text{i})}$	$\Delta G^{\ddagger}_{2(\text{ii})}$	$\Delta G_{\text{rxn(i)}}$	$\Delta G_{\text{rxn(ii)}}$
A	20.1	12.3	15.8	-26.9	-26.6	26.6	15.5	19.1	-28.0	-27.6
B	20.1	15.7	12.3	-26.6	-26.9	26.6	19.1	15.5	-27.5	-28.0
	ωB97XD					B2PLYPD				
	$\Delta G^{\ddagger}_1$	$\Delta G^{\ddagger}_{2(\text{i})}$	$\Delta G^{\ddagger}_{2(\text{ii})}$	$\Delta G_{\text{rxn(i)}}$	$\Delta G_{\text{rxn(ii)}}$	$\Delta G^{\ddagger}_1$	$\Delta G^{\ddagger}_{2(\text{i})}$	$\Delta G^{\ddagger}_{2(\text{ii})}$	$\Delta G_{\text{rxn(i)}}$	$\Delta G_{\text{rxn(ii)}}$
A	20.1	11.8	15.6	-31.2	-31.2	27.2	22.6	26.5	-21.0	-21.0
B	20.1	15.6	11.8	-31.2	-31.2	27.2	26.5	22.6	-21.0	-21.0
	B2PLYP									
	$\Delta G^{\ddagger}_1$	$\Delta G^{\ddagger}_{2(\text{i})}$	$\Delta G^{\ddagger}_{2(\text{ii})}$	$\Delta G_{\text{rxn(i)}}$	$\Delta G_{\text{rxn(ii)}}$					
A	34.3	31.5	35.5	-13.3	-13.1					
B	34.3	35.5	31.5	-13.1	-13.3					

The [2+2] cycloaddition was modeled with KI and di-substituted alkene 1b at the geminal position as depicted in Figure 3.9. Steric hindrance caused by ethyl groups increases the asynchronous character of the transition state, TS1-b. Thereby, acyclic Int-b is formed as a result of bond formation between the unsubstituted carbon atom of alkene (C_4) and central carbon of KI (C_2). This situation leaves only one possibility for the second bond formation through TS2-b structure giving only one possible cyclobutaniminium, 2b. Hence, in the case of geminal substitution, the regioselectivity of the reaction is specified by the nature of the acyclic intermediate. Energetics show that, within the stepwise mechanism, the first step is the RDS. Same reaction was also modelled with the reverse orientations of alkene for modelling the other possible attack orientation.

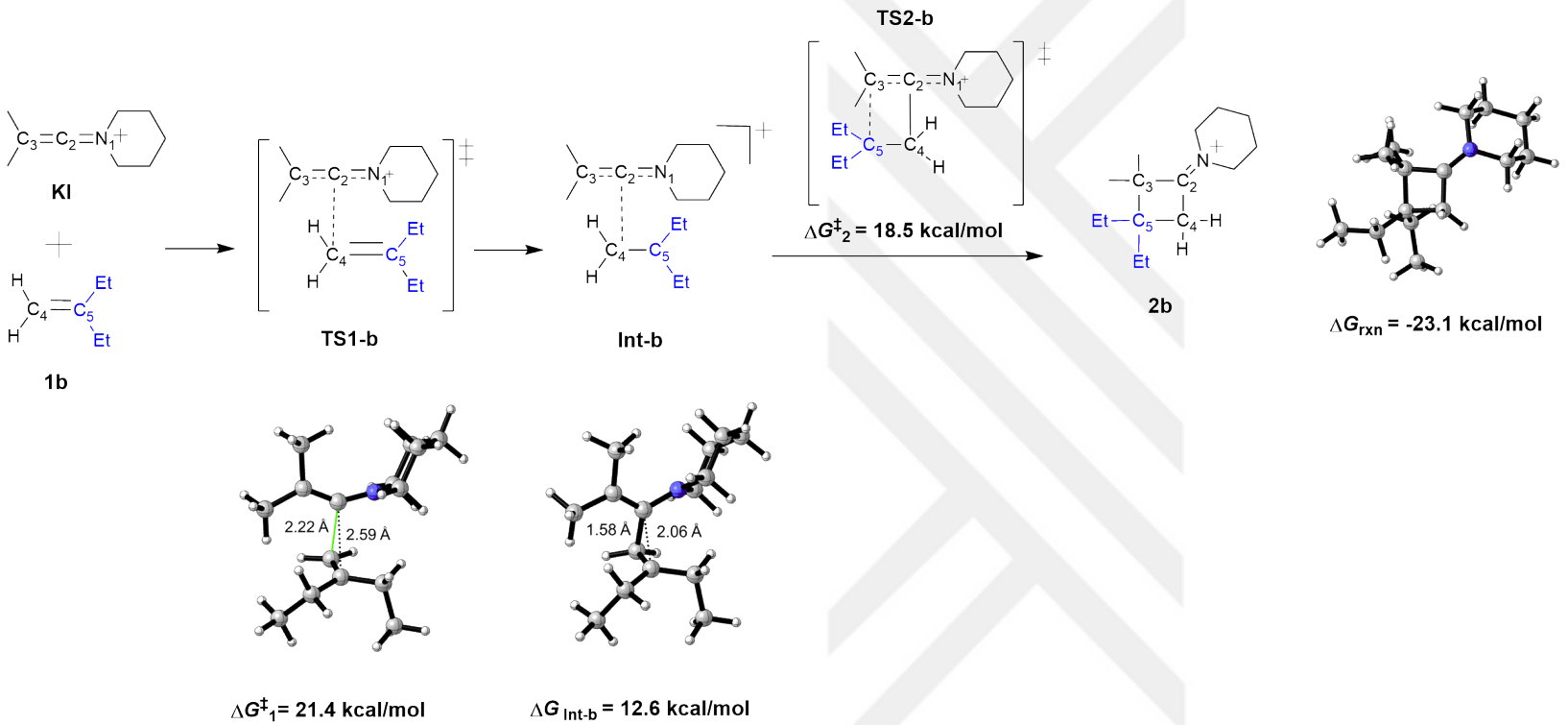

Figure 3.9. The reaction mechanism of [2+2] cycloaddition between KI and gem-substituted alkene 1b, M06-2X/6-31+G(d,p).

Table 3.3. Free energy of activation ($\Delta G^{\ddagger}$) and reaction (ΔG_{rxn}) values for [2+2] cycloaddition of 1b to KI.

	M06-2X			MPW1K			ωB97XD		
	$\Delta G^{\ddagger}_1$	$\Delta G^{\ddagger}_2$	ΔG_{rxn}	$\Delta G^{\ddagger}_1$	$\Delta G^{\ddagger}_2$	ΔG_{rxn}	$\Delta G^{\ddagger}_1$	$\Delta G^{\ddagger}_2$	ΔG_{rxn}
A	21.4	18.5	-23.1	29.4	23.5	-20.9	20.5	17.1	-27.5
	B2PLYPD			B2PLYP					
	$\Delta G^{\ddagger}_1$	$\Delta G^{\ddagger}_2$	ΔG_{rxn}	$\Delta G^{\ddagger}_1$	$\Delta G^{\ddagger}_2$	ΔG_{rxn}			
A	28.8	28.9	-15.7	37.3	39.8	-4.9			

There are two possibilities for the attack orientation of gem-substituted alkene (Figure 3.10). The energetics are the same for A and B because there is no chirality, but using a chiral auxiliary may create a difference in energetics for the choice of attack orientation either through sterics or electronics. Also, the conformer of piperidine moiety is different for products corresponding to A and B.

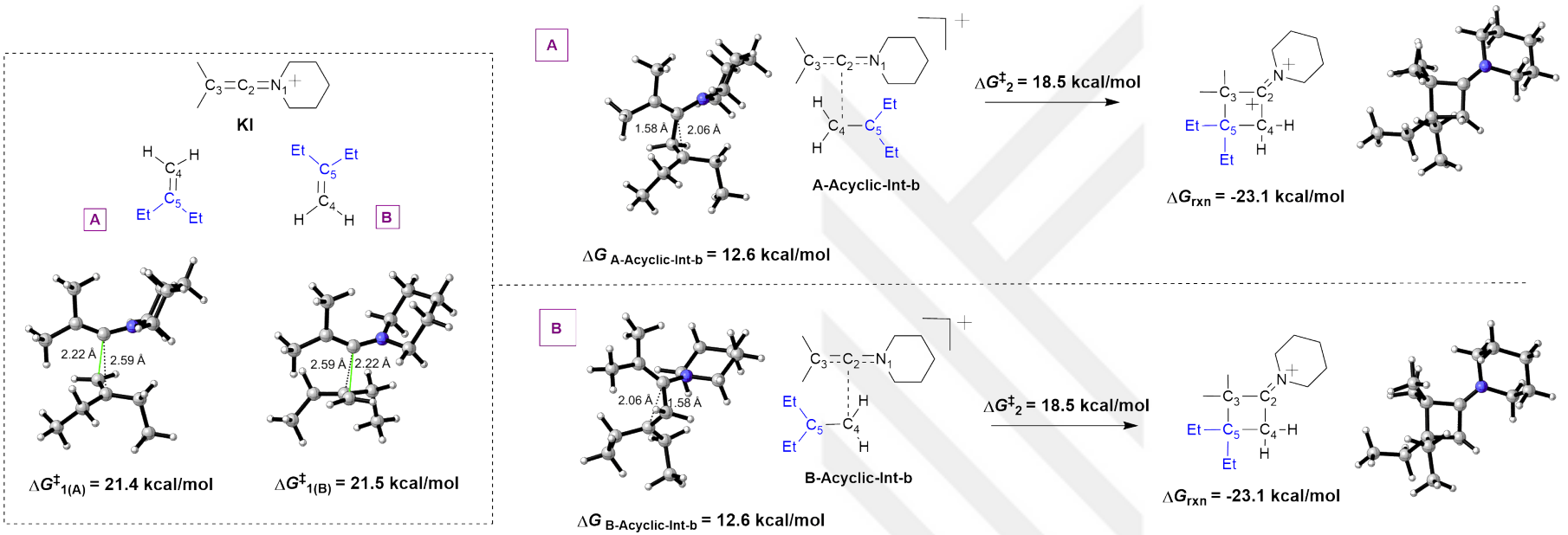

Figure 3.10. Possible attack orientations of 1b to KI, M06-2X/6-31+G(d,p).

Another di-substituted alkene was taken into consideration with *cis* substituted alkene 1c see Figure 3.11. During the approach of alkene toward KI, ethyl groups were positioned on piperidinyl side of KI due to steric factors. Free energy of activation values indicate that in the stepwise mechanism, first step is the RDS. The approach of alkene toward KI forms TS1-c complex having synchronous character. The mechanism proceeds through cyclic intermediate, Int-c. In second step, pathways i and ii results in the enantiomer pairs of cyclobutaniminiums, 2c and 3c as depicted in Figure 3.11. Having no chiral auxiliaries there is no difference in energetic values of TS2i-c and TS2ii-c, however using chiral elements would cause a difference in the stereochemistry of the major product. Energy refinements at different levels of theory confirmed that the first step is the RDS.

Table 3.4. Free energy of activation ($\Delta G^{\ddagger}$) and reaction (ΔG_{rxn}) values for [2+2] cycloaddition of 1c to KI.

	M06-2X					MPW1K				
	$\Delta G^{\ddagger}_1$	$\Delta G^{\ddagger}_{2(\text{i})}$	$\Delta G^{\ddagger}_{2(\text{ii})}$	$\Delta G_{\text{rxn(i)}}$	$\Delta G_{\text{rxn(ii)}}$	$\Delta G^{\ddagger}_1$	$\Delta G^{\ddagger}_{2(\text{i})}$	$\Delta G^{\ddagger}_{2(\text{ii})}$	$\Delta G_{\text{rxn(i)}}$	$\Delta G_{\text{rxn(ii)}}$
A	20.3	16.7	16.7	-24.1	-24.2	29.0	22.4	22.4	-22.4	-22.4
	ωB97XD					B2PLYPD				
	$\Delta G^{\ddagger}_1$	$\Delta G^{\ddagger}_{2(\text{i})}$	$\Delta G^{\ddagger}_{2(\text{ii})}$	$\Delta G_{\text{rxn(i)}}$	$\Delta G_{\text{rxn(ii)}}$	$\Delta G^{\ddagger}_1$	$\Delta G^{\ddagger}_{2(\text{i})}$	$\Delta G^{\ddagger}_{2(\text{ii})}$	$\Delta G_{\text{rxn(i)}}$	$\Delta G_{\text{rxn(ii)}}$
A	19.7	15.5	15.5	-29.2	-29.2	28.1	27.5	27.5	-17.7	-17.7
	B2PLYP									
	$\Delta G^{\ddagger}_1$	$\Delta G^{\ddagger}_{2(\text{i})}$	$\Delta G^{\ddagger}_{2(\text{ii})}$	$\Delta G_{\text{rxn(i)}}$	$\Delta G_{\text{rxn(ii)}}$					
A	37.2	39.0	39.0	-7.2	-7.3					

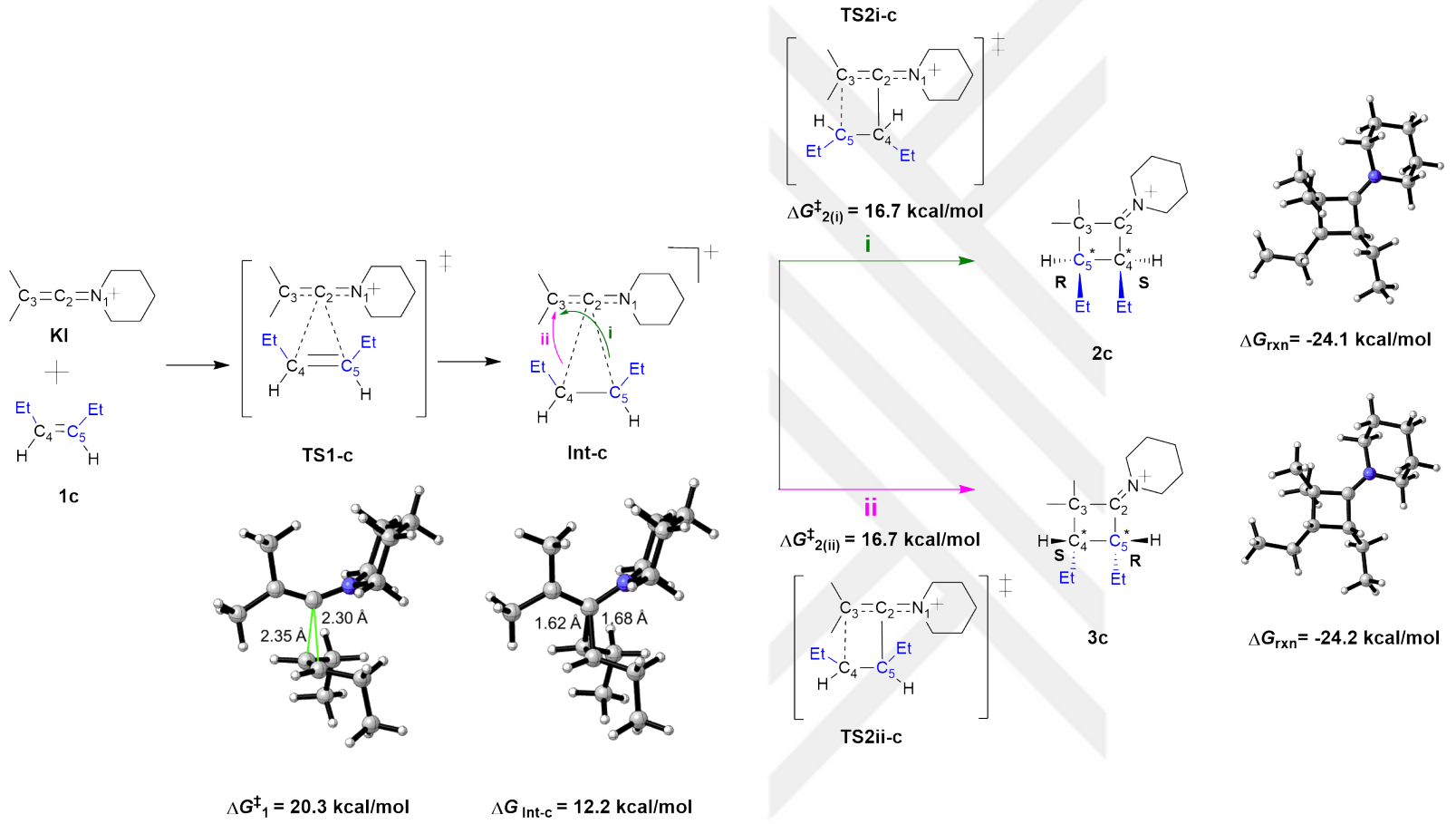

Figure 3.11. The reaction mechanism of [2+2] cycloaddition between KI and *cis*-substituted alkene 1c, M06-2X/6-31+G(d,p).

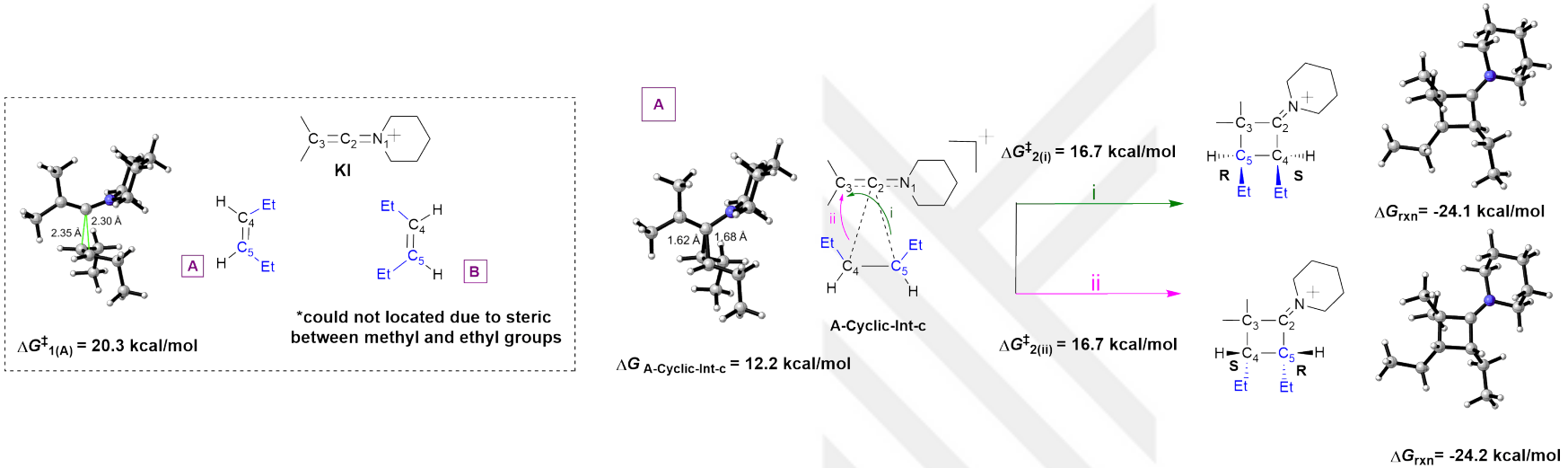

Figure 3.12. Possible attack orientations of 1c to KI and formation of enantiomer pairs of cycloadducts, M06-2X/6-31+G(d,p).

To compare the effect of substituent positions on the alkene, *trans* substituted alkene 1d was selected as a third di-substituted alkene. Similar results with *cis* substituted alkene were obtained. The mechanism consists of two steps, where RDS is still the first step. The asynchronism in critical distances increases for TS1-d compared to its *cis* counterpart. Cyclic intermediate, Int-d is observed as the corresponding minima of the first transition state structure (Figure 3.13). At the second step, bond formation for C_3-C_5 or C_3-C_4 are represented by pathways i and ii. The cyclization is more feasible for C_3-C_5 bond formation due to less hindered cyclization, causing 1.5 kcal/mol energy difference between $\Delta G^{\ddagger}_{2(i)}$ and $\Delta G^{\ddagger}_{2(ii)}$. Consequently, even though 2d and 3d are both thermodynamically favored, 2d is the kinetic product.

Table 3.5. Free energy of activation ($\Delta G^{\ddagger}$) and reaction (ΔG_{rxn}) values for [2+2] cycloaddition of 1d to KI.

	M06-2X					MPW1K				
	$\Delta G^{\ddagger}_1$	$\Delta G^{\ddagger}_{2(i)}$	$\Delta G^{\ddagger}_{2(ii)}$	$\Delta G_{rxn(i)}$	$\Delta G_{rxn(ii)}$	$\Delta G^{\ddagger}_1$	$\Delta G^{\ddagger}_{2(i)}$	$\Delta G^{\ddagger}_{2(ii)}$	$\Delta G_{rxn(i)}$	$\Delta G_{rxn(ii)}$
A	21.1	17.4	18.9	-25.5	-25.3	29.4	22.9	24.7	-23.4	-23.4
	ωB97XD					B2PLYPD				
	$\Delta G^{\ddagger}_1$	$\Delta G^{\ddagger}_{2(i)}$	$\Delta G^{\ddagger}_{2(ii)}$	$\Delta G_{rxn(i)}$	$\Delta G_{rxn(ii)}$	$\Delta G^{\ddagger}_1$	$\Delta G^{\ddagger}_{2(i)}$	$\Delta G^{\ddagger}_{2(ii)}$	$\Delta G_{rxn(i)}$	$\Delta G_{rxn(ii)}$
A	20.7	16.2	17.7	-30.6	-30.4	29.3	28.6	29.9	-18.8	-18.7
	B2PLYP									
	$\Delta G^{\ddagger}_1$	$\Delta G^{\ddagger}_{2(i)}$	$\Delta G^{\ddagger}_{2(ii)}$	$\Delta G_{rxn(i)}$	$\Delta G_{rxn(ii)}$					
A	38.4	39.6	41.4	-8.2	-8.1					

For detailed investigation, another attack orientation of alkene which is the reverse orientation of the one depicted in Figure 3.13 was modelled, enantiomer pairs of cyclobutaniminiums were obtained as shown in Figure 3.14. The rate determining step is the first step of [2+2] cycloaddition of *trans* substituted alkene with KI.

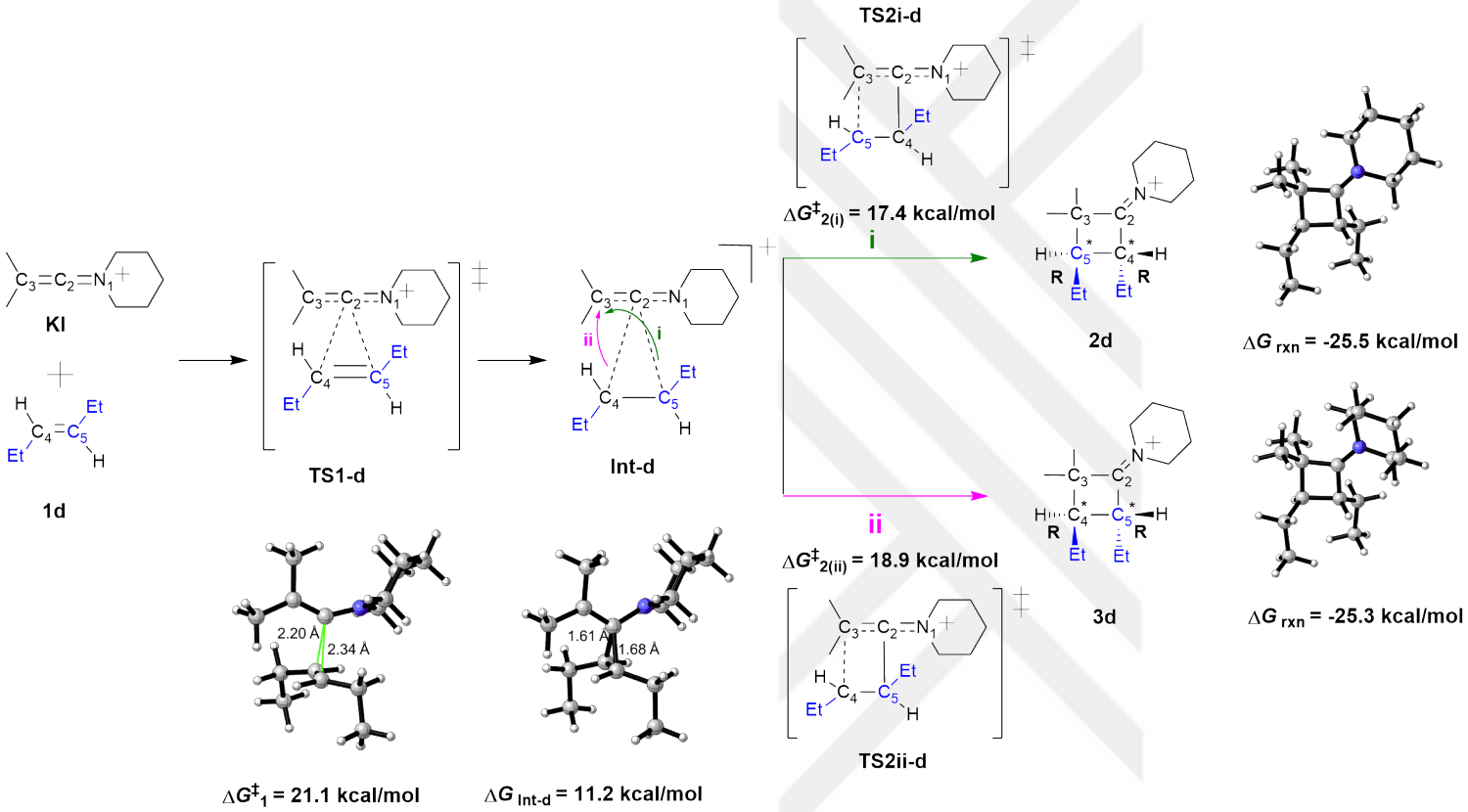

Figure 3.13. The reaction mechanism of [2+2] cycloaddition between KI and *trans*-substituted alkene 1d, M06-2X/6-31+G(d,p).

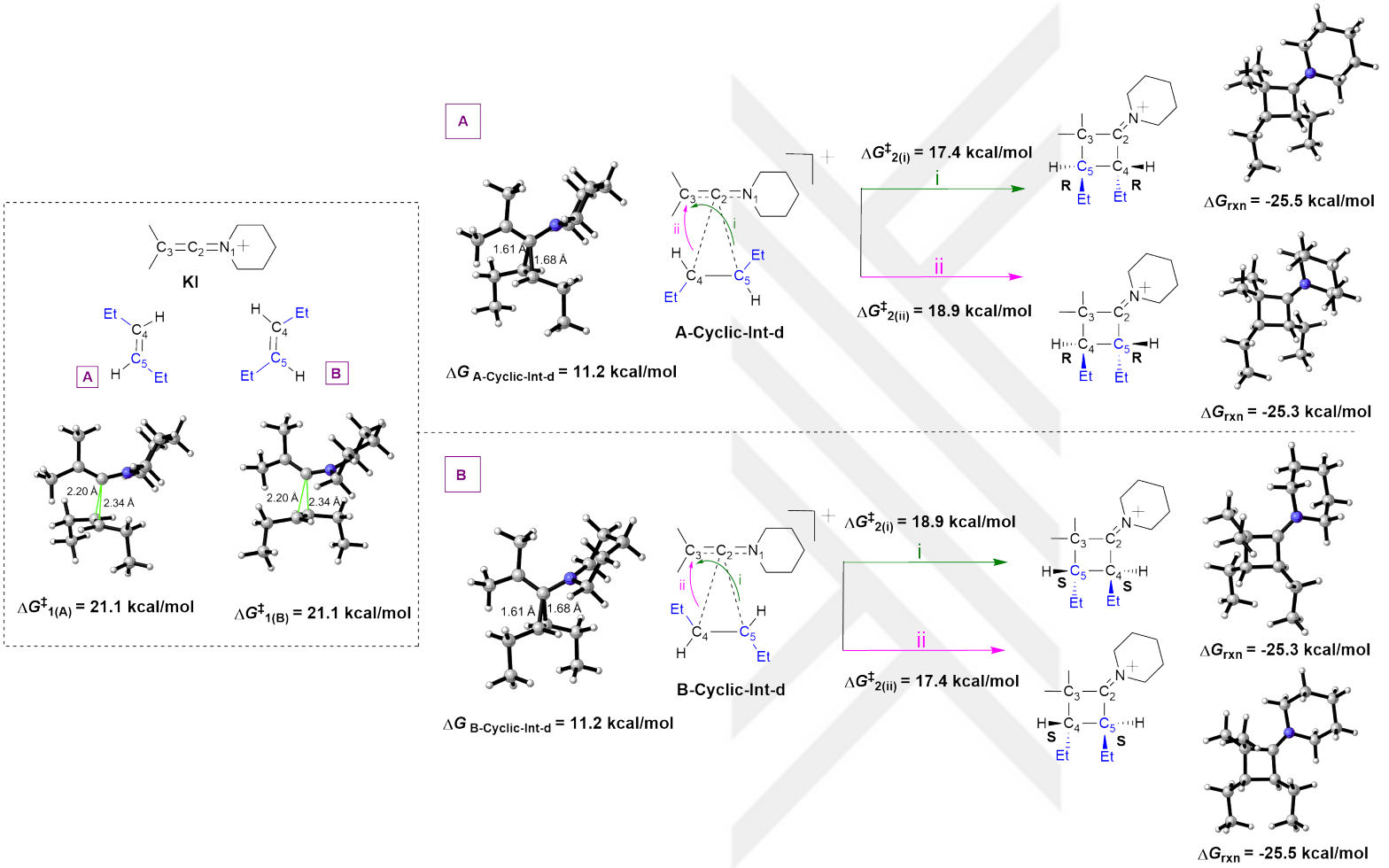

Figure 3.14. Possible attack orientations of 1d to KI and formation of enantiomer pairs of cycloadducts, M06-2X/6-31+G(d,p).

The effect of the number of ethyl groups on the mechanism and product was also evaluated with tri-substituted alkene 1e (Figure 3.15). Ethyl groups are located mostly on the piperidine side in order to minimize steric clash with the first activated complex, TS1-e. The complex shows asynchronous nature similar to TS1-a. First transition state evolves to highly energetic acyclic intermediate, Int-e. Only one possible cycloadduct 2e is produced through TS2-2e complex. Since intermediate is acyclic, C_3-C_5 bond is formed defining regioselectivity of the mechanism. The attack orientation of tri-substituted alkene determines the stereochemistry of the cycloadduct seen in Figure 3.16. Using chiral KI can create a difference in the preference of stereochemistry. Energetic values for M06-2X optimizations indicate that rate determining step becomes the second step, single point energy refinement with double hybrid functionals B2PLYP and B2PLYPD supports this outcome, see Table 3.6.

Table 3.6. Free energy of activation ($\Delta G^{\ddagger}$) and reaction (ΔG_{rxn}) values for [2+2] cycloaddition of 1e to KI.

	M06-2X			MPW1K			ωB97XD		
	$\Delta G^{\ddagger}_1$	$\Delta G^{\ddagger}_2$	ΔG_{rxn}	$\Delta G^{\ddagger}_1$	$\Delta G^{\ddagger}_2$	ΔG_{rxn}	$\Delta G^{\ddagger}_1$	$\Delta G^{\ddagger}_2$	ΔG_{rxn}
A	22.4	24.0	-22.6	32.6	32.2	-18.2	21.0	21.8	-27.6
	B2PLYPD			B2PLYP					
	$\Delta G^{\ddagger}_1$	$\Delta G^{\ddagger}_2$	ΔG_{rxn}	$\Delta G^{\ddagger}_1$	$\Delta G^{\ddagger}_2$	ΔG_{rxn}			
A	31.0	35.3	-15.1	42.0	49.2	-1.9			

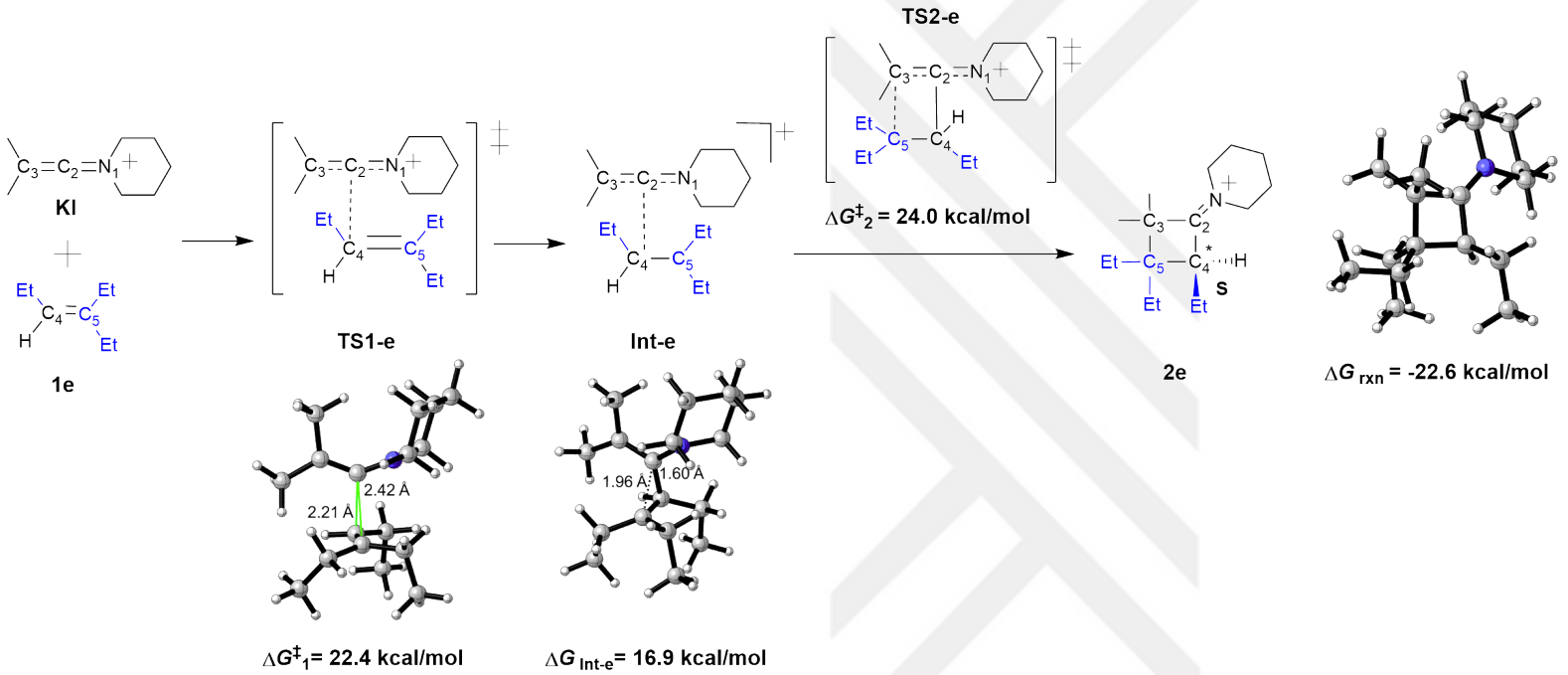

Figure 3.15. The reaction mechanism of [2+2] cycloaddition between KI and tri-substituted alkene 1e, M06-2X/6-31+G(d,p).

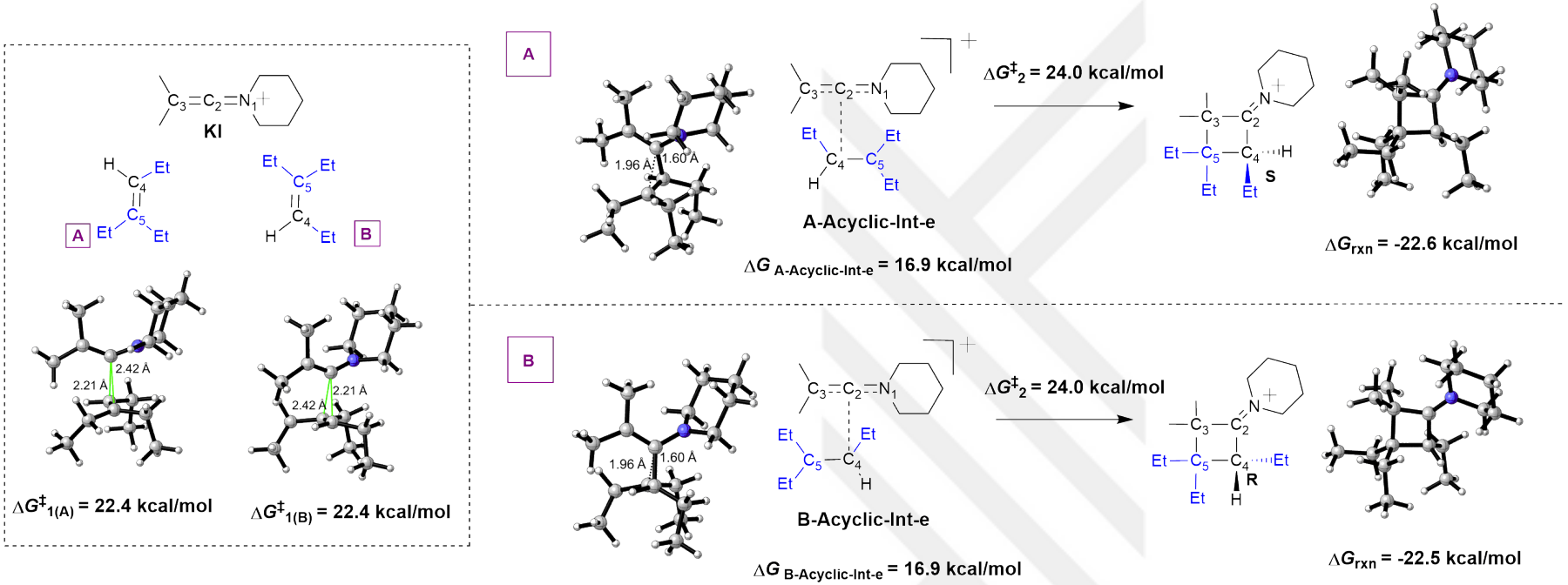

Figure 3.16. Possible attack orientations of 1e to KI and formation of enantiomer pairs of cycloadducts, M06-2X/6-31+G(d,p).

The systematic analysis of the effect of alkene substitution on mechanism preference was finalized with highly steric ally strained tetra-substituted alkene 1f. Relative free energies were reported with respect to most stable conformer of alkene, see Figure 3.17.

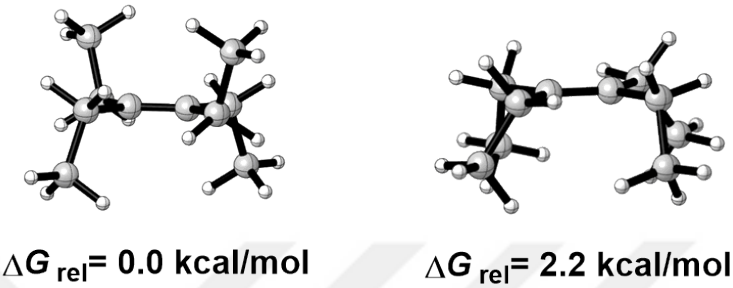

Figure 3.17. Two possible conformers of alkene 1f, the most stable conformer on the left.

Results showed that TS1-f exhibit synchronous character according to critical distances. Therefore what was expected is the formation of cyclic intermediate but IRC optimizations and trying to get cyclic minima gave the same acyclic intermediate, Int-f, despite all efforts (see Figure 3.18). If the cyclic intermediate had been optimized, the conformer energy would be higher due to the higher strain. The free energy of acyclic intermediate is very high and very close to free energy of first activated complex, causing lower persistency. There is only one possible transition sate TS2-f at the second step. Notably, for this case too, RDS becomes second step with the increase in number of ethyl groups. Compared to tri- substitution the difference between first and second free energy of activation values increases. Energy refinements with MPW1K, ωB97XD, B2PLYPD and B2PLYP level of theories are in agreement with these results, Table 3.7 .

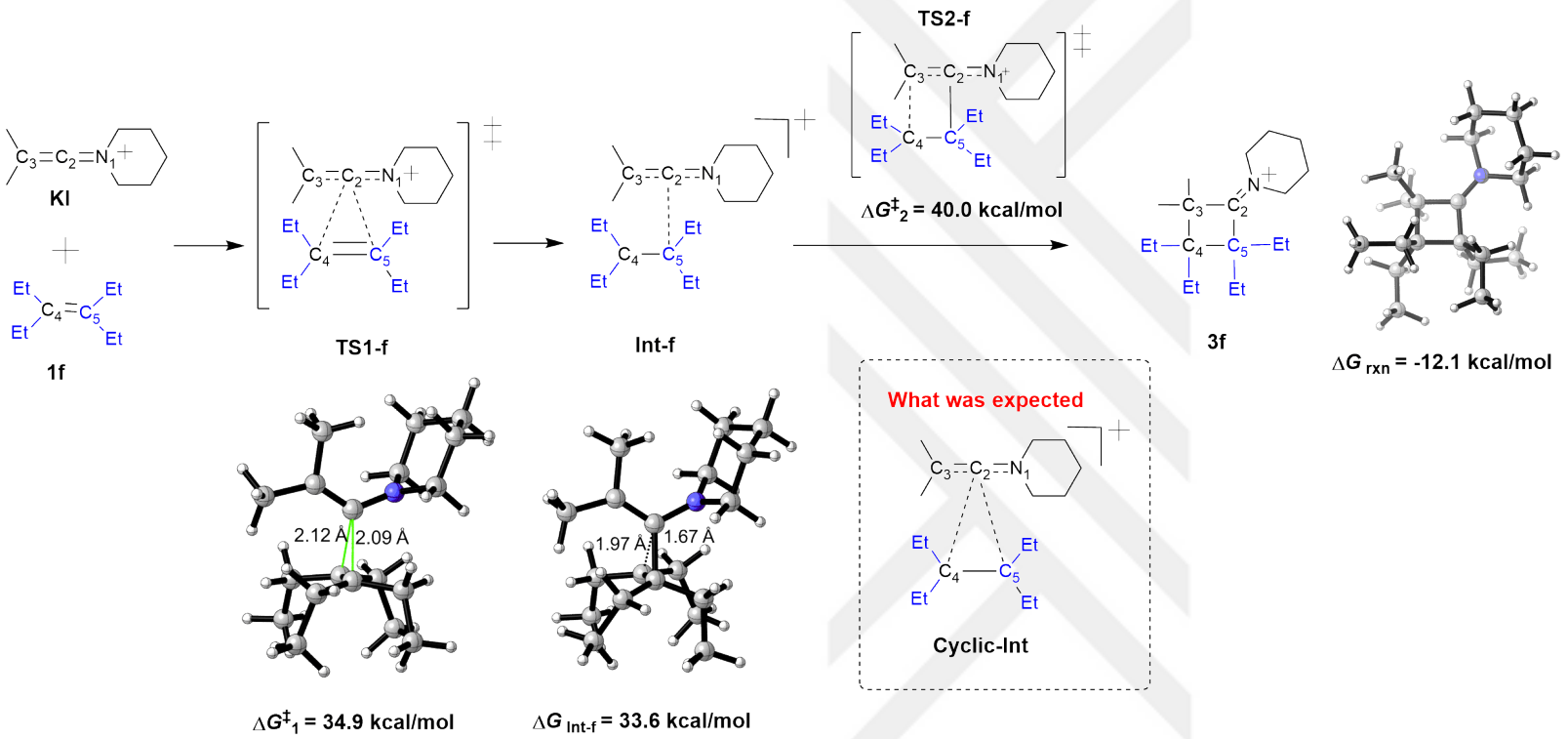

Figure 3.18. The reaction mechanism of [2+2] cycloaddition between KI and tetra-substituted alkene 1f, M06-2X/6-31+G(d,p).

Table 3.7. Free energy of activation ($\Delta G^{\ddagger}$) and reaction (ΔG_{rxn}) values for [2+2] cycloaddition of 1f to KI.

M06-2X				MPW1K			
$\Delta G^{\ddagger}_1$	ΔG_{int}	$\Delta G^{\ddagger}_2$	ΔG_{rxn}	$\Delta G^{\ddagger}_1$	ΔG_{int}	$\Delta G^{\ddagger}_2$	ΔG_{rxn}
34.9	33.6	40.0	-12.1	47.5	45.2	51.9	-4.3
ωB97XD				B2PLYPD			
$\Delta G^{\ddagger}_1$	ΔG_{int}	$\Delta G^{\ddagger}_2$	ΔG_{rxn}	$\Delta G^{\ddagger}_1$	ΔG_{int}	$\Delta G^{\ddagger}_2$	ΔG_{rxn}
33.7	31.8	38.7	-17.2	46.0	45.4	53.5	-3.1
B2PLYP							
$\Delta G^{\ddagger}_1$	ΔG_{int}	$\Delta G^{\ddagger}_2$	ΔG_{rxn}				
61.0	61.9	70.5	13.8				

The conclusions that can be drawn from this study are that high regioselectivity of [2+2] cycloaddition of KI intermediates to alkenes can be dictated by either mechanistic preference or energetic difference at the second step where the cycloadduct is formed. More specifically, at the end of the first step, if the acyclic intermediate is the saddle point due to substitution on alkene, there is only one possible cyclobutanone structure that can be synthesized. On the other hand, if cyclic intermediate is formed, the determining factor for regioselectivity is the second free energy of activation value.

Additionally, the [2+2] cycloaddition of ethylene to unsubstituted KIs (the carbon susbtituents are both hydrogen) was modeled. Piperidinyl, *N,N*-dimethyl and *N,N*-diallyl derivatives were selected as *N*-substituents. Despite efforts, cyclic intermediate and second activated complex were not located. First transition states resemble Domingo's TS1 [67] as in Figure 3.4 but IRC results give cyclobutaniminium ion as minima. This seems to point to a concerted single step mechanism as depicted in Figure 3.19 similar to Fang *et al.*'s study for [2+2] cycloadditions of KIs with unsubstituted KIs [66].

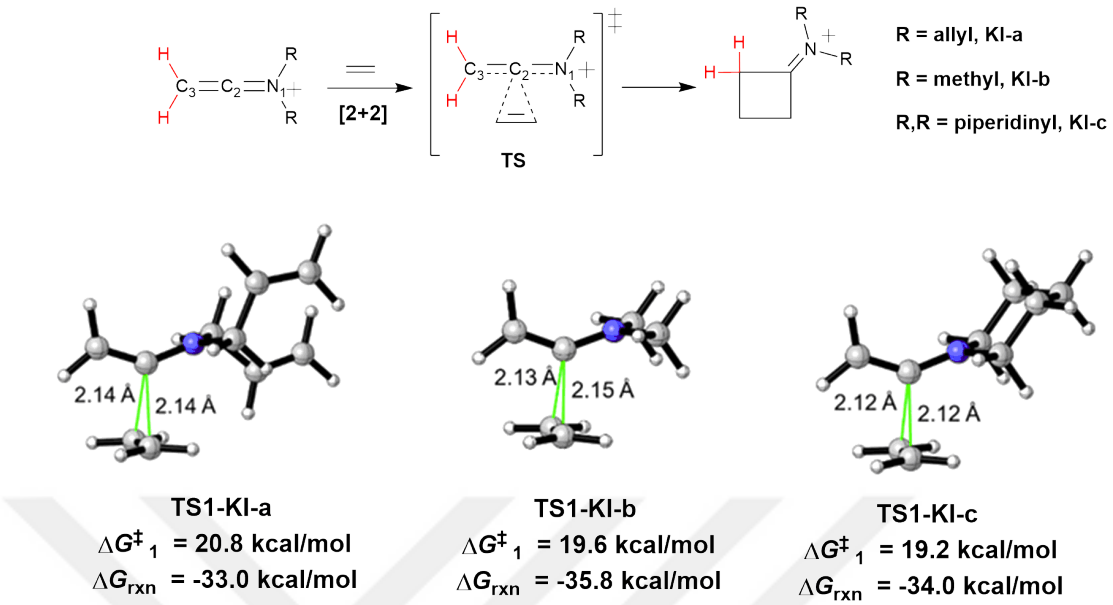

Figure 3.19. Free energies of activation and reaction for [2+2] cycloaddition reaction between unsubstituted KIs and ethylene. Optimized transition states (TSs) at M06-2X/6-31+G(d,p) level in $CHCl_3$.

In summary, the substitution patterns of alkene effectively change the mechanism determining the formation of possible cycloadducts. Also the increase in the number of alkyl groups on KIs changes the RDS of the reaction to the second step. With the unsubstituted KI and ethylene, the reaction undergoes a concerted single step mechanism. These findings may give insight to experimental studies while designing the procedure and selecting the reagents to be used.

3.5. Computational Assessment of KI Reactivity

The substituents on KIs have prior importance to synthesize the desired substituted cycloadduct which can be used as reagent in specific reactions. Moreover, the electronic and steric nature of substituents have influence on the reactivity of these reactive intermediates toward [2+2] cycloaddition. The DFT study was planned in order to conduct a systematic analysis for the reactivity comparison of selected KIs. To do that, experimentally most commonly used piperidine [52, 54, 55] and methyl [53] moieties were determined as reference groups in the investigation of the effect of *C*-substituent(s) and *N*-substituent(s) respectively, as depicted in Figure 3.20.

Competition reactions between alkenes and alkynes pointed out that the reactivity of alkenes in reaction with KIs are lower compared to alkynes [48]. Therefore, the [2+2] cycloadditions of KIs to alkenes has been modeled with ethylene in order to obtain more realistic and accurate results about reactivity of KIs.

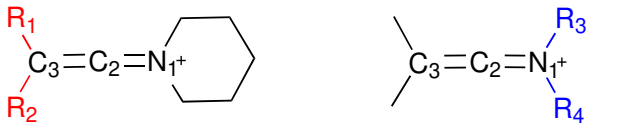

Figure 3.20. Substitution on keteniminium salts with respect to a) C_3-substituents and b) N_1-substituents.

3.5.1. The effect of *C*-substitution on Reactivity of KIs

The electronic and steric nature of substituents on keteniminium salts have an influence on mechanistic and energetics aspects of cycloaddition reactions with olefins [66]. Firstly, the energetic outcomes of the reaction with C_3-substituted KIs have been investigated. Furthermore, both keto- and aldo-keteniminium salts were covered as listed in Table 3.8. Note that, in the formation of first activated complex, ethylene reagent approaches aldo KIs from hydrogen atom side to avoid steric hinderance. The cyclic intermediate could not been detected for KI_1, probably due to flat potential energy surface (PES). The *N*-substituents on KI_8, KI_{11}, KI_{12} and KI_{13} were modified for a systematic analysis of *C*-substituent effect.

Table 3.8. Effect of C_3-substituents on free energ of activation ($\Delta G^{\ddagger}$) and reaction (ΔG_{rxn}), M06-2X/6-31+G(d,p) in $CHCl_3$, energies in kcal/mol.

Aldo KI		$\Delta G^{\ddagger}_1$	$\Delta G^{\ddagger}_2$	ΔG_{rxn}	Keto KI		$\Delta G^{\ddagger}_1$	$\Delta G^{\ddagger}_2$	ΔG_{rxn}
KI$_1$ [54]	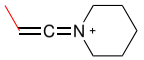	18.8	12.2	-32.2	**KI$_9$** [48, 53]	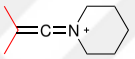	20.6	11.9	-28.8
KI$_2$ [54]	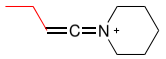	19.1	13.5	-32.3	**KI$_{10}$** [52]	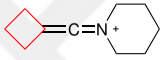	18.2	4.8	-31.2
KI$_3$ [54]	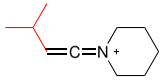	17.9	14.5	-31.2	**KI$_{11}$** [53]	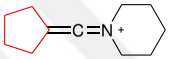	19.7	8.7	-28.7
KI$_4$ [54]	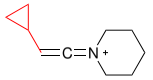	18.1	6.4	-30.7	**KI$_{12}$** [53]	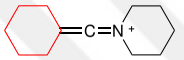	20.6	13.8	-30.0
KI$_5$ [54]	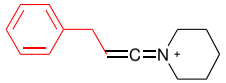	20.9	12.7	-31.2	**KI$_{13}$** [53]	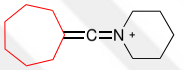	21.7	12.6	-26.0
KI$_6$ [54]	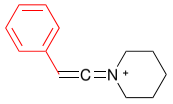	17.0	7.4	-32.7					
KI$_7$ [54]	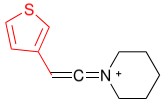	16.3	6.8	-31.5					
KI$_8$ [32]	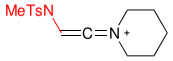	19.1	7.0	-35.1					

Computed results show that, the [2+2] cycloaddition of C_3-substituted KIs to ethylene are exergonic reactions with free energy of reaction values varying between -35.1 and -26.0 kcal/mol. Notably, the reaction with aldo-keteniminiums are slightly more exergonic than their keto-counterparts. Energetic results verify that RDS is the first step for [2+2] cycloaddition of KIs to ethylene. In comparison of aldo and keto KIs, activation barriers of aldo-keteniminium salt KI_1 is lower than that of KI_9 due to the advantage of less hindered attack for aldo KIs. The first free energy of activation values (RDS) varies in the range of 16.3¬20.9 kcal/mol for aldo-keteniminium salts and 18.2-21.7 kcal/mol for keto-keteniminium salts. Thiophene group on β-position makes KI_7 the most reactive aldo-keteniminium salt ($\Delta G^{\ddagger}_1$= 16.3 kcal/mol) among all KIs in Table 3.8 followed by phenyl substituted KI_6, which has almost equal reactivity, ($\Delta G^{\ddagger}_1$= 17.0 kcal/mol). Having less electron donating nature thiophene and phenyl group result in more positive charge on the central carbon atom, C_2 (see Table 3.12). Likewise, both thiophene and phenyl substituents give both thermodynamically stable cyclobutaniminiums with -31.5 kcal/mol and -32.7 kcal/mol reaction free energy values, respectively.

Benzyl substituted KI_5 is the most stable aldo-keteniminium salt structure with highest free energy of activation for RDS ($\Delta G^{\ddagger}_1$= 20.9 kcal/mol) toward cycloaddition reaction with ethylene. The main reason behind this was detected with non-covalent interactions. The CH-π interaction in TS1-KI_5 (CH$\cdots\pi$ distance = 2.61 Å and 3.45 Å) between delocalized electrons on benzyl group and hydrogen atoms on piperidine derivative enables extra stabilization to first transition state complex (Figure 3.21, and NCI plot in Figure 3.30). Also, this favorable interaction exists in KI_5 intermediate (CH$\cdots\pi$ distance = 3.04 Å and 3.24 Å. The presence of favorable interactions in both KI and TS structures enables stabilization to both, therefore, the resulting barrier ($\Delta G^{\ddagger}_1$ = 20.9 kcal/mol) is still higher than others (Figure 3.21).

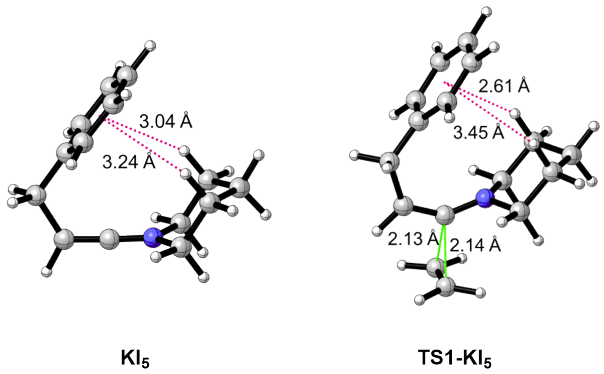

Figure 3.21. Optimized structures of KI_5 and TS1-KI_5, pink color denotes CH-π interactions.

Moreover, transition state structures of thiophene, phenyl and benzyl bearing keteniminium salts reflect the electronic effect on free energy of activation. While larger critical distances in TS1-KI_6 and TS1-KI_7 point to early transition states leading to lower barriers, smaller critical distance in TS1-KI_5 is the sign of a larger barrier (Figure 3.22).

In consideration of keto-keteniminium salts in Table 3.8, free energy of activation values for RDS varies between 18.2 and 21.7 kcal/mol. In the case of cyclic substituents, steric factors take an active role in the change in the free energy of activation, as a result of increase in ring size. Activation barriers increase from smaller ring to larger rings. De Mesmaeker and coworkers reported lower yields for seven-membered ring in the [2+2] cycloaddition between KIs and terminal alkynes, compared to smaller ring sizes [53].

Overall, the cycloaddition reactions of aldo KIs with ethylene are more reactive than those of keto KIs. The higher activation barriers are observed due to the steric hinderance and strong EDG effect. Considering keteniminium salts listed in Table 3.8, the difference in first free energies of activation values between most and least reactive KIs is significant for [2+2] cycloaddition reaction ($\Delta\Delta G^{\ddagger}_1$= 5.4 kcal/mol), as a proof of the importance of substituent effect on the reactivity of keteniminium salts.

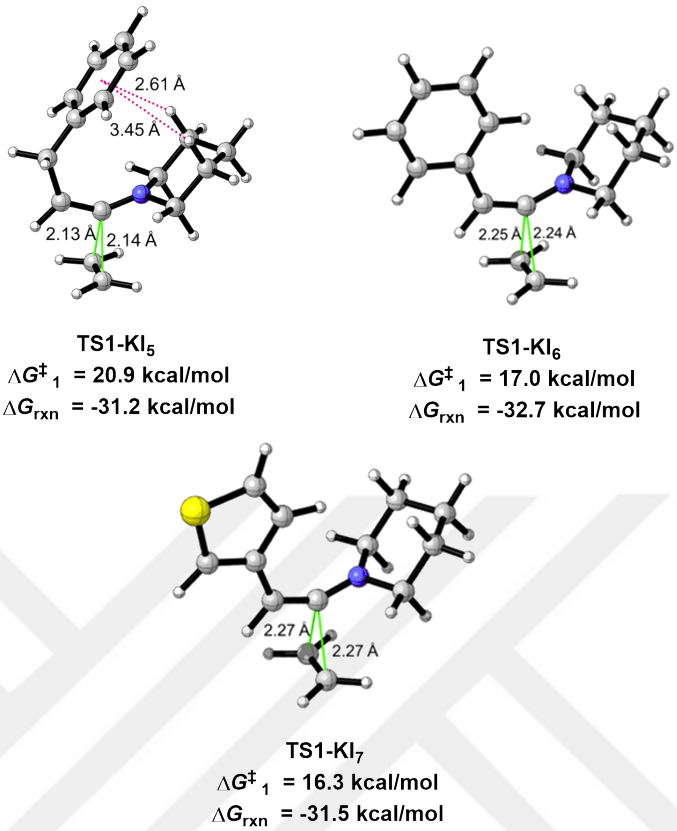

Figure 3.22. Optimized structures of TS1-KI$_5$, TS1-KI$_6$, TS1-KI$_7$ along with $\Delta G^{\ddagger}$ and ΔG_{rxn} values. 6-311++G(3df,3pd) extra basis set applied for sulfur atom, CH-π interactions in TS1-KI$_5$ depicted in Å.

Energy refinement on computed results for free energy of activation and reaction was also conducted by using different levels of theory and results are depicted in Table 3.9. Energetic analysis trends hold with MPW1K, ωB97XD, B2PLYPD, and B2PLYP functionals. The results for all functionals are in agreement that thiophene and phenyl substituents make KIs more reactive toward [2+2] cycloaddition reaction. Moreover, energy refinement supports that the increase in the ring size of cyclic substituents cause an increase in the free energy of activation values.

Table 3.9. Free energy of activation ($\Delta G^{\ddagger}$) and reaction (ΔG_{rxn}) for [2+2] cycloaddition of ethylenes with KIs of differing C-substituents, energies in kcal/mol.

	M06-2X			MPW1K			ωB97XD			B2PLYPD			B2PLYP		
KI	$\Delta G^{\ddagger}_1$	$\Delta G^{\ddagger}_2$	ΔG_{rxn}	$\Delta G^{\ddagger}_1$	$\Delta G^{\ddagger}_2$	ΔG_{rxn}	$\Delta G^{\ddagger}_1$	$\Delta G^{\ddagger}_2$	ΔG_{rxn}	$\Delta G^{\ddagger}_1$	$\Delta G^{\ddagger}_2$	ΔG_{rxn}	$\Delta G^{\ddagger}_1$	$\Delta G^{\ddagger}_2$	ΔG_{rxn}
KI$_1$	18.8	12.2	-32.2	21.9	11.9	-36.7	19.0	12.1	-36.3	24.6	20.1	-27.4	29.0	25.7	-22.8
KI$_2$	19.1	13.5	-32.3	22.5	13.3	-36.2	19.2	13.2	-36.4	25.1	21.4	-27.3	29.7	27.1	-22.1
KI$_3$	17.9	14.5	-31.2	21.2	14.9	-33.5	17.8	14.2	-35.4	23.8	22.4	-25.2	28.5	28.6	-18.6
KI$_4$	18.1	6.4	-30.7	21.3	6.8	-34.9	18.1	6.2	-35.1	23.6	15.4	-25.9	27.9	21.5	-20.8
KI$_5$	20.9	12.7	-31.2	24.5	10.1	-35.9	21.0	12.7	-34.7	27.4	18.6	-26.6	32.7	23.1	-21.7
KI$_6$	17.0	7.4	-32.7	20.5	7.7	-36.9	16.8	6.9	-37.2	22.4	15.8	-27.6	27.5	22.6	-22.5
KI$_7$	16.3	6.8	-31.5	19.8	7.4	-35.9	16.1	6.6	-36.0	21.7	16.0	-26.5	26.5	22.7	-21.6
KI$_8$	19.1	7.0	-35.1	24.3	9.6	-37.1	20.3	8.2	-38.6	25.5	18.1	-29.8	31.1	25.4	-23.0
KI$_9$	20.6	11.9	-28.8	25.1	13.3	-31.7	21.1	12.4	-32.8	27.0	22.1	-23.4	32.5	29.1	-17.5
KI$_{10}$	18.2	4.8	-31.2	21.8	5.5	-34.3	18.2	4.7	-35.8	24.0	13.6	-26.3	28.9	20.0	-20.2
KI$_{11}$	19.7	8.7	-28.7	24.2	9.8	-31.0	19.9	8.5	-32.9	25.9	17.9	-23.1	31.3	25.0	-16.5
KI$_{12}$	20.6	13.8	-30.0	25.7	15.6	-32.1	21.0	13.9	-34.2	27.3	24.4	-24.4	33.3	32.0	-17.4
KI$_{13}$	21.7	12.6	-26.0	26.9	13.8	-28.0	22.0	12.6	-30.1	28.5	22.5	-20.3	34.7	30.0	-13.3

3.5.2. The effect of *N*-substitution on Reactivity of KIs

In this part, reactivity examination has been conducted with keto KIs, and the effect of substituents on nitrogen atom has been discussed. Even though, the *N*-substituent part of KIs is eliminated after hydrolysis, it still has an important effect on reactivity and stereospecificity. Saimoto *et al.*, indicated the dependency of stereospecificity with *N*-substituent of KIs in the [2+2] cycloadditions with olefins [65]. Additionally, steric factors on nitrogen atom determines the favorable attack face for the olefin [65]. Furthermore, Fang *et al.* computationally investigated electronic effect for -H, -Cl and -CH_3 substituents on nitrogen and showed that while electron-withdrawing groups lead to an increase in reactivity, electron-donating groups make KI more stable toward [2+2] cycoaddition [66]. Using chiral *N*-substituents such as substituents shown in Figure 3.23 make asymmetric induction possible for inter [29] and intramolecular [50] [2+2] cycloadditions, which lead to cycloadducts with high enantiomeric excess [21].

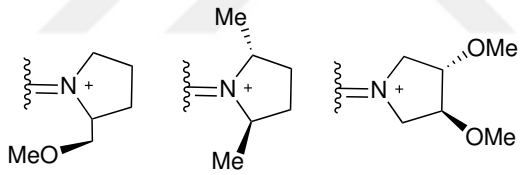

Figure 3.23. C_2-symmetrical and non-C_2 symmetrical chiral pyrrolidinyl groups used for asymmetric induction in [2+2] cycloaddition of KIs and olefins.

Chiral auxiliary, (*S*)-2-methoxymethyl pyrrolidine was used for determining selectivity when groups on terminal carbon atom are the same [30, 65]. When groups on terminal carbon are different, using C_2-symmetrical pyrollidinyl prevented the possible formation of diastereoisomers of KIs [50]. Ghosez's further studies involving aldo-KIs, in which –NMeTs functional groups were used revealed that C_2 and non-C_2 symmetrical chiral pyrrolidinyl groups can both give cyclobutanones with high enantiomeric excess in reaction with cyclohexene [32]. Considering these features, several substituents were explored and tabulated in Table 3.10. Note that, KI_{14} is a theoretical KI, not experimentally available. KI_{19}, KI_{20}, KI_{25} and KI_{26} were modified for a systematic analysis of the *N*-substituent effect.

Table 3.10. Effect of N_1-substituents on free energy of activation ($\Delta G^{\ddagger}$) and reaction (ΔG_{rxn}), M06-2X/6-31+G(d,p) in $CHCl_3$, energies in kcal/mol.

Keteniminium Salt		$\Delta G^{\ddagger}_1$	$\Delta G^{\ddagger}_2$	ΔG_{rxn}	Keteniminium Salt		$\Delta G^{\ddagger}_1$	$\Delta G^{\ddagger}_2$	ΔG_{rxn}
KI$_{14}$ [66]	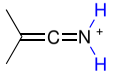	16.7	-4.2	-33.5	**KI$_{21}$** [53]	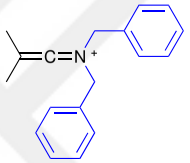	20.6	11.3	-26.5
KI$_{15}$ [26, 35]	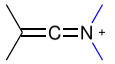	19.9	10.8	-29.8	**KI$_{22}$** [53]	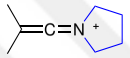	21.3	12.1	-28.7
KI$_{16}$ [53]	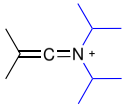	26.0	20.0	-23.9	**KI$_{23}$** [32]	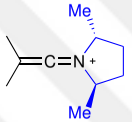	23.1	15.0	-22.5
KI$_{17}$ [48, 56]	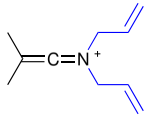	20.3	10.3	-29.0	**KI$_{24}$** [30, 32, 65]		19.9	11.4	-28.1
KI$_{18}$	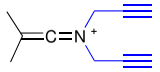	17.6	5.3	-30.2	**KI$_{9}$** [48, 53]	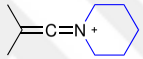	20.6	11.9	-28.8
KI$_{19}$ [48]	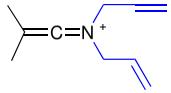	19.1	7.8	-29.3	**KI$_{25}$** [54]	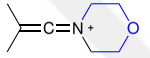	19.8	9.7	-28.7
KI$_{20}$ [56]	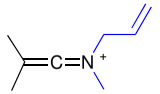	20.4	10.9	-29.3	**KI$_{26}$** [54]	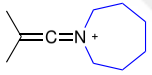	19.9	14.4	-28.7

The ΔG_{rxn} values are in the range of -33.5 to -22.5 kcal/mol indicating the reaction is highly exergonic for all *N*-substituted keteniminium salts, favoring the thermodynamic formation of cyclobutaniminium salts. Computed data presents that when the cycloaddition reaction of KI_{14} (theoretical KI) and KI_{18} with etylene have low free energies of activation values ($\Delta G^{\ddagger}_1$= 16.7 and 17.6 kcal/mol respectively), KI_{16} has the highest barrier ($\Delta G^{\ddagger}_1$= 26.0 kcal/mol) along with producing less persistent cyclobutaniminium (ΔG_{rxn}= -23.9 kcal/mol). Due to the steric hindrance caused by the bulky *N,N*-diisopropyl moiety (Figure 3.24) the attack trajectory is blocked from both sides for nucleophilic attack of ethylene to central carbon atom, C_2. The result is also consistent with the experimental results from the study of Lumbroso *et al.* saying *N,N*-diisopropyl moiety gave cycloadduct with less than 5% in the [2+2] cycloaddition with terminal alkynes [53].

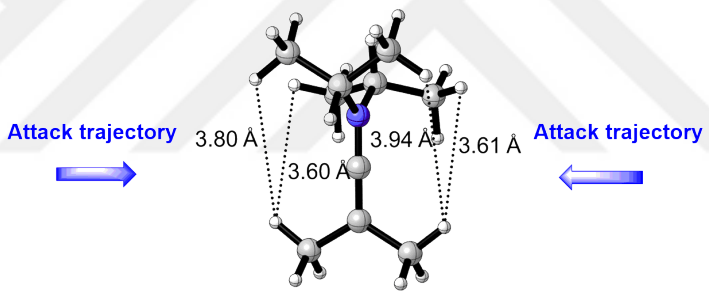

Figure 3.24. Optimized structure of KI_{16} and attack trajectories for ethylene in [2+2] cycloadditions.

Moreover, critical distances in TS1s were evaluated for the lowest and highest activation barriers (Figure 3.25). Larger critical distances of TS1-KI_{14} and TS1-KI_{18} are the sign of early transition states in line with the lower free energies of activation. On the other hand, shorter critical lengths of TS1-KI_{16} is associated with larger free energy of activation value. Another aspect is that TS1-KI_{14} and TS1-KI_{18} have synchronous character compared to asynchronous character of TS1-KI_{16}. In pursuance of these results, *N,N*-dihydrogen and *N,N*-dipropargyl groups are both kinetically and thermodynamically favorable toward the [2+2] cycloaddition reaction.

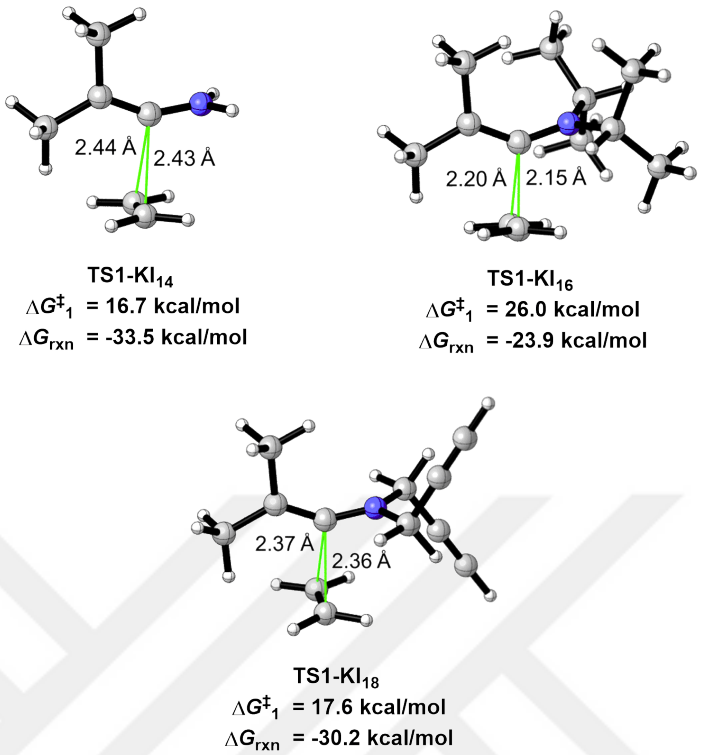

Figure 3.25. $\Delta G^{\ddagger}$ and ΔG_{rxn} values and optimized structures of TS1-KI_{14}, TS1-KI_{16}, TS1-KI_{18}.

Furthermore, dimethyl substitution on N_1 atom (TS1-KI_{15}) raise the activation barrier by 3.2 kcal/mol, compared to -H substituents on N_1 atom (TS1-KI_{14}). Electron donating nature of methyl group decreases the positive charge on C_2, which makes KI_{15} more stable keteniminium salt than KI_{14} in the [2+2] cycloaddition reaction (Table 3.13). To extend the scope of the study, the effect of *N*-ally moiety, which is one of the most used *N*-substituent and *N*-propargyl moiety on reactivity were examined [48, 56]. Among the keteniminium salts in Figure 3.26, *N,N*-dipropargyl groups on N_1 have significantly lower activation barrier. As it is known, propargyl groups have less electron pushing nature because of their higher *s* character of hybridization compared to ally group. Consequently, KIs with more propargyl groups favor the reaction. The decrease in electron donating effect results in an increase of positive charge on C_2 atom (Table 3.13). This situation contributes to decrease in free energy of activation value. The energetic analysis is also reflected by critical distances in transition states. Larger critical distances in TS1-KI_{18} and TS1-KI_{19} are the natural consequences of early transition states, which are associated with lower activation barriers.

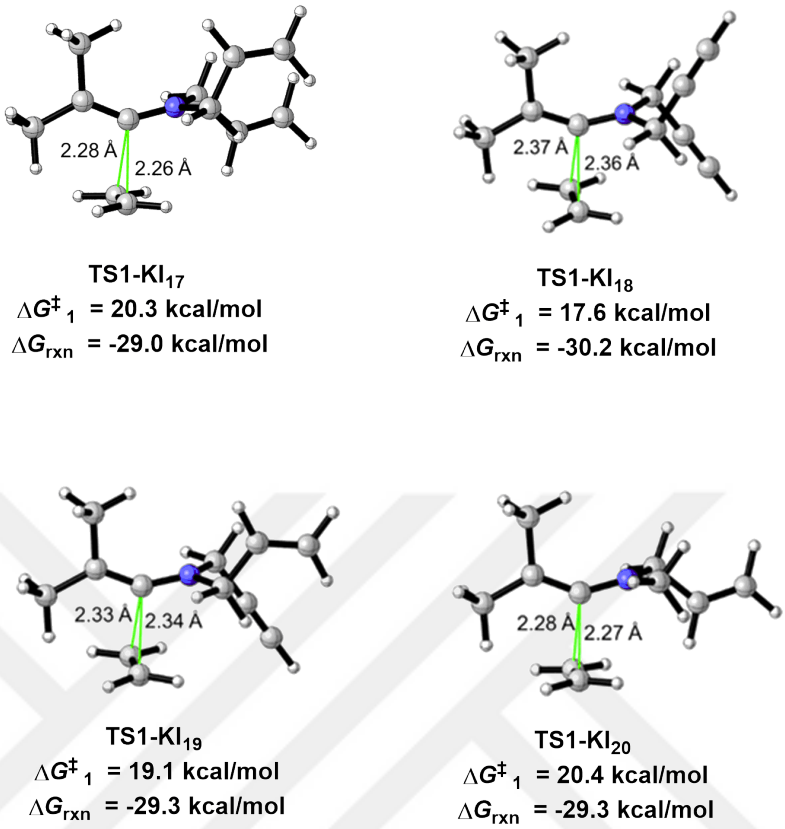

Figure 3.26. $\Delta G^{\ddagger}$ and ΔG_{rxn} values and optimized structures of TS1-KI_{17}, TS1-KI_{18}, TS1-KI_{19} and TS1-KI_{20}.

KIs may have cyclic structures as their *N*-substituent. Considering these cases, the impact of the size of cyclic groups was examined by computing five-membered ring (pyrrolidine derivative), six-membered ring (piperidine derivative) and seven-membered ring (azepane derivative). Keteniminium salts substituted with pyrrolidinyl, piperidinyl and azepanyl groups display quite similar free energy of activation values as depicted in Figure 3.27. This might seem that all three keteniminium salts give kinetically favorable cycloadducts. However, Lumbroso *et al.* found that in the reaction with terminal alkynes, while piperidinyl group gives high yield of conversion (95%), pyrrolidinyl group gives very low yield of conversion (less than 5%) [53].

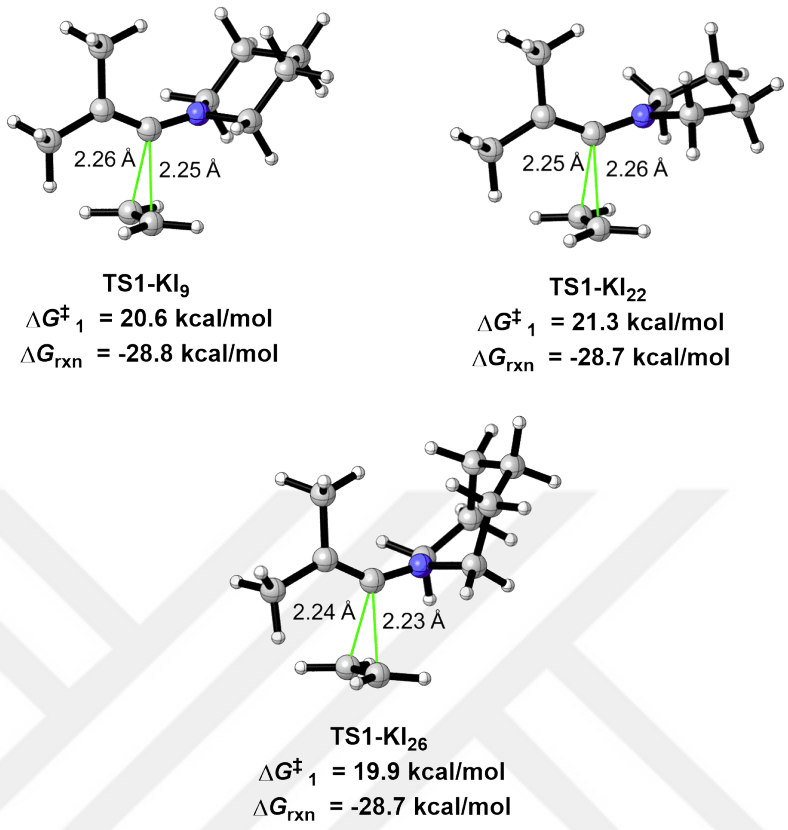

Figure 3.27. $\Delta G^{\ddagger}$ and ΔG_{rxn} values and optimized structures of TS1-KI_9, TS1-KI_{22} and TS1-KI_{26}.

A previous computational study from our group explained this situation pointing out the importance of the availability of the attack trajectory to the central carbon atom [54]. Such characteristic is owing to the position of CH_2 groups on ring which are blocking central carbon atom for the attack that leads to the first transition state TS1s (Figure 3.28). The conformation of azepanyl group shows similar structural constrains as pyrrolidinyl group. Therefore, azepanyl groups also might give only traces of cycloadduct with alkenes/alkynes because of the steric hindrance caused by hydrogen atoms on their ring, which are blocking the electrophilic carbon atom (C_2) for cycloaddition reactions.

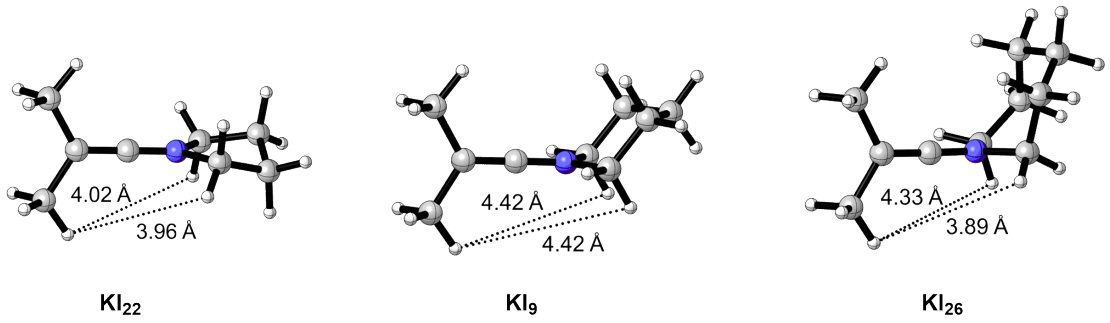

Figure 3.28. Comparison of optimized structures of keteniminium salts KI_9, KI_{22} and KI_{26}, M06-2X/6-31+G(d,p), critical distances in Å.

In additon, heteroatom effect was questioned by investigation of piperidine derivatives possessing a heteroatom (-O). By comparison of the reactivity of KI_{25} and KI_9, it can be deduced that the heteroatom makes KI as reactive as piperidinyl moiety toward cycloaddition reaction with ethylene. In 2002, Ghosez and coworkers had conducted tan experimental study [32] with the functionalized keteniminium cations bearing *N*TsMe group and hydrogen atom on the terminal carbon atom. We modified the keteniminium salts by selecting methyl groups on terminal carbon instead of *N*TsMe group and hydrogen atom to attain KI_{23} and KI_{24}.

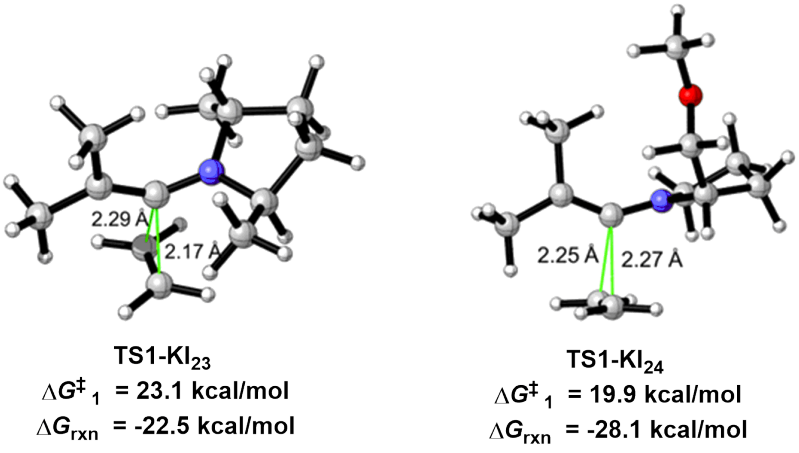

Figure 3.29. $\Delta G^{\ddagger}$ and ΔG_{rxn} values and optimized structures of TS1-KI_{23} and TS1-KI_{24}.

According to the comparison of *(S)*-2-methoxymethyl and 2,5-dimethyl bearing pyrrolidine rings, it seems that not only electronic effects, but also the steric effect caused by the groups is the dominant factor on free energy of activation values. In TS1-KI_{23} structure, the methyl group on the attack face causes steric hindrance resulting in higher free energy of activation. Charge analysis of KI_{23} and KI_{24} bearing chiral pyrrolidinyl groups is consistent with activation barriers as listed in Table 3.13. 2,5-dimethylpyrrolidine group lowers the charge on central carbon (0.447) compared to (S)-2-methoxymethyl pyrrolidine (0.458), correlated with higher energies of activation caused by lower positive charge on electrophilic carbon atom of KI. In addition, while TS1-KI_{23} shows asynchronous feature, TS1-KI_{24} have synchronous feature regarding the critical distances, see Figure 3.29.

In favor of the energetic investigation of the effect of *N*-substituents on keteniminium intermediates, the calculations have been taken into account in a wider perspective. It should be mentioned that different functionals; MPW1K, ωB97XD, B2PLYPD and B2PLYP gave similar trends with M06-2X functional as depicted in Table 3.11.

Table 3.11. Free energy of activation ($\Delta G^{\ddagger}$) and reaction (ΔG_{rxn}) for [2+2] cycloaddition of ethylenes with KIs of differing *N*-substituents, energies in kcal/mol.

	M06-2X			MPW1K			ωB97XD			B2PLYPD			B2PLYP		
KI	$\Delta G^{\ddagger}_1$	$\Delta G^{\ddagger}_2$	ΔG_{rxn}	$\Delta G^{\ddagger}_1$	$\Delta G^{\ddagger}_2$	ΔG_{rxn}	$\Delta G^{\ddagger}_1$	$\Delta G^{\ddagger}_2$	ΔG_{rxn}	$\Delta G^{\ddagger}_1$	$\Delta G^{\ddagger}_2$	ΔG_{rxn}	$\Delta G^{\ddagger}_1$	$\Delta G^{\ddagger}_2$	ΔG_{rxn}
KI$_{14}$	16.7	-4.2	-33.5	19.6	-5.6	-38.2	17.1	-4.2	-36.9	21.0	3.3	-28.8	24.8	7.8	-24.7
KI$_{15}$	19.9	10.8	-29.8	24.1	11.7	-33.2	20.6	11.4	-33.4	26.0	20.8	-24.5	31.3	27.4	-19.0
KI$_{16}$	26.0	20.0	-23.9	32.2	21.8	-26.1	26.9	20.0	-27.8	33.7	30.1	-18.4	41.2	38.1	-11.5
KI$_{17}$	20.3	10.3	-29.0	25.4	12.2	-32.0	20.9	10.8	-33.0	27.1	20.8	-23.9	32.9	28.3	-17.9
KI$_{18}$	17.6	5.3	-30.2	22.7	6.9	-33.3	18.2	6.1	-33.9	23.6	15.9	-25.1	29.3	23.1	-19.3
KI$_{19}$	19.1	7.8	-29.3	24.2	9.5	-32.5	19.6	8.4	-33.3	25.5	18.6	-24.2	31.3	26.0	-18.4
KI$_{20}$	20.4	10.9	-29.3	25.2	12.1	-32.5	21.1	11.3	-33.1	26.9	20.8	-24.0	32.5	27.8	-18.3
KI$_{21}$	20.6	11.3	-26.5	26.4	10.7	-30.5	21.1	12.2	-30.6	27.7	20.4	-22.0	34.5	26.8	-16.4
KI$_{22}$	21.3	12.1	-28.7	25.4	13.0	-32.0	21.7	12.3	-32.6	27.3	21.5	-23.4	32.7	28.3	-18.0
KI$_{23}$	23.1	15.0	-22.5	28.7	17.0	-24.4	23.7	15.0	-26.4	30.2	24.5	-17.0	36.8	32.6	-10.0
KI$_{24}$	19.9	11.4	-28.1	24.9	11.2	-31.1	20.5	11.1	-32.0	26.2	19.9	-22.9	32.4	26.3	-17.1
KI$_{9}$	20.6	11.9	-28.8	25.1	13.3	-31.7	21.1	12.4	-32.8	27.0	22.1	-23.4	32.5	29.1	-17.5
KI$_{25}$	19.8	9.7	-28.7	24.4	10.8	-31.8	20.3	10.1	-32.6	25.8	19.8	-23.3	31.2	26.7	-17.6
KI$_{26}$	19.9	14.4	-28.7	24.4	15.4	-31.7	20.3	14.7	-32.7	26.2	23.9	-23.5	32.1	31.0	-17.5

3.6. Population Analysis, Reactivity Indices and Non-covalent Interactions

In this part of the study, in order to rationalize the reactivity difference between keteniminium salts, natural bond order analysis and conceptual DFT methods were utilized. The electronic effect of substituents on electrophilicity of keteniminium salts was investigated by means of local reactivity indices and natural population analysis. Furthermore, non-covalent interactions were examined for the selected KIs.

3.6.1. Natural Population Analysis

The electrophilic nature of keteniminium salts is the major factor to elucidate its usefulness in [2+2] cycloaddition reactions. The substituents have an affect on electrophilic nature and on charge of atoms of keteniminium salts, especially on the central C_2 atom. Hence, electronic effect of substituents on reactivity of KIs was investigated *via* natural population analysis by using Amsterdam Density Functional package (ADF) to calculate NBO 6.0 at M06-2X/ATZ2P level of theory in $CHCl_3$ (ϵ= 4.7113) as tabulated in Table 3.12 and Table 3.13.

Table 3.12. Natural Population Analysis (NPA) of *C_3*-substituted KIs.

	NBO 6.0				NBO 6.0		
Aldo-KI	N_1	C_2	C_3	Keto-KI	N_1	C_2	C_3
KI_1	-0.309	0.453	-0.220	**KI_9**	-0.308	0.443	-0.023
KI_2	-0.311	0.456	-0.224	**KI_{10}**	-0.300	0.433	-0.051
KI_3	-0.311	0.456	-0.226	**KI_{11}**	-0.304	0.440	-0.033
KI_4	-0.305	0.448	-0.225	**KI_{12}**	-0.310	0.442	-0.024
KI_5	-0.314	0.466	-0.217	**KI_{13}**	-0.312	0.444	-0.021
KI_6	-0.303	0.476	-0.250				
KI_7	-0.303	0.469	-0.247				
KI_8	-0.293	0.410	-0.049				

Table 3.13. Natural Population Analysis (NPA) of *N_1*-substituted KIs.

	NBO 6.0				NBO 6.0		
Keto-KI	N_1	C_2	C_3	Keto-KI	N_1	C_2	C_3
KI_{14}	-0.633	0.473	-0.025	**KI_{21}**	-0.304	0.455	-0.020
KI_{15}	-0.294	0.443	0.019	**KI_{22}**	-0.309	0.447	-0.015
KI_{16}	-0.325	0.447	-0.032	**KI_{23}**	-0.325	0.447	-0.027
KI_{17}	-0.304	0.446	-0.017	**KI_{24}**	-0.315	0.458	-0.022
KI_{18}	-0.296	0.457	-0.003	**KI_9**	-0.308	0.443	-0.023
KI_{19}	-0.298	0.449	-0.008	**KI_{25}**	-0.311	0.441	-0.016
KI_{20}	-0.298	0.445	-0.017	**KI_{26}**	-0.312	0.446	-0.024

The electrophilic nature of KIs was reflected by highly positive charge on central sp carbon, C_2, compared to C_3 and N_1. As a result, the attack of alkenes takes place toward central carbon of KIs in TS1s. Firstly, in case of *C_3*-substituted KIs population analysis was conducted to elucidate the electronic nature on C_2 atom. The comparison of aldo KI, KI_1 and keto KI, KI_9 express the effect of electron pushing methyl group. The charge on C_2 (0.443) of keto KI is lowered by addition of one more methyl group on the β position compared to the charge on C_2 (0.453) of aldo KI. In addition, the aldo KIs, except KI_8, have more positive charge on C_2 compared to keto- KIs. Computed results in Table 3.12 indicate benzyl, thiophene and phenyl groups on terminal carbon promote more positive charge on C_2 due to less electron donating nature. The results are in line with the lower free energy of activation values for TS1-KI_6 and TS1-KI_7.

Secondly, for the *N_1*-substituted KIs, population analysis was carried out to rationalize the charges on C_2 and reported in Table 3.13. Electron donation capability of propargyl group is less than the ally group because of hybridization state difference. Therefore, *N,N*-dipropargyl bearing KI (KI_{18}) has the most positive charge on C_2 compared to KI_{19}, KI_{17} and KI_{20}. The NBO results are in aggrement with the lowest free energy of activaton energy of TS1-KI_{18}.

Moreover, examining the electron donating effect of the groups on pyrrolidine ring showed that 2,5-dimethylpyrrolidine group has lower positive charge on C_2 (0.447) compared to *(S)*-2-methoxymethyl pyrrolidine (0.458), causing higher barrier of TS1-KI_{23} in addition to the steric hindrance effect.

3.6.2. Local Reactivity Indices: Parr and Fukui Functions

In order to analyze the electrophilic nature of KIs and detect the most electrophilic atom Domingo's electrophilic Parr function P_k^+ and Yang and Mortier's Fukui function f_k^+ for nucleophilic attack were computed. The measurements of P_k^+ and f_k^+ can give insight for reactivity of KIs in relation to their energetics of the [2+2] cycloaddition reactions with ethylene.

In pursuance of f_k^+ function, NBO calculations were conducted by M06-2X functional with 6-31+G(d,p) basis set in $CHCl_3$ as single point calculations based on the structures optimized by M06-2X/6-31+G(d,p). The total population values were used for these calculations. Further, P_k^+ values were calculated by NBO atomic spin density values (UM06-2X/6-31+G(d,p)//M06-2X/6-31+G(d,p)) in $CHCl_3$. Computed results for f_k^+ and P_k^+, listed in Table 3.14 and Table 3.15, show that the most electrophilic center is C_2 atom for all keteniminium salts. In general, among C_3-substituted keteniminium salts P_k^+ results vary between 0.702 and 0.636 and f_k^+ data changes between 0.366 and 0.295 for C_2 atom (Table 3.14). Notably, thiophene and phenyl groups on terminal carbon cause dramatic changes compared to the general range, yet C_2 atom is still the most electrophilic center. In consideration of N_1-substituted keteniminium salts (Table 3.15), propargyl groups increase $P_k^+$and f_k^+ of C_2 causing higher electrophilicity. This results support the higher reactivity of KI_{18} toward [2+2] cycloadditions with alkenes.

Table 3.14. $P_k{}^+$ and $f_k{}^+$ values for C_3-substituted keteniminium salts.

	$P_k{}^+$			$f_k{}^+$				$P_k{}^+$			$f_k{}^+$		
Aldo-KI	N_1	C_2	C_3	N_1	C_2	C_3	Keto-KI	N_1	C_2	C_3	N_1	C_2	C_3
KI_1	0.241	0.677	-0.091	0.155	0.362	0.049	**KI_9**	0.238	0.702	-0.083	0.157	0.364	0.063
KI_2	0.241	0.678	-0.093	0.154	0.362	0.048	**KI_{10}**	0.245	0.636	-0.082	0.150	0.351	0.028
KI_3	0.241	0.677	-0.094	0.153	0.363	0.044	**KI_{11}**	0.242	0.682	-0.088	0.152	0.361	0.050
KI_4	0.245	0.677	-0.090	0.156	0.355	0.047	**KI_{12}**	0.239	0.702	-0.087	0.154	0.366	0.056
KI_5	0.242	0.682	-0.092	0.158	0.352	0.056	**KI_{13}**	0.239	0.701	-0.089	0.154	0.362	0.060
KI_6	-0.040	0.338	0.197	0.029	0.160	0.162							
KI_7	-0.042	0.360	0.252	0.032	0.171	0.198							
KI_8	0.232	0.657	-0.058	0.172	0.295	0.070							

Table 3.15. $P_k{}^+$ and $f_k{}^+$ values for N_1-substituted keteniminium salts.

	$P_k{}^+$			$f_k{}^+$				$P_k{}^+$			$f_k{}^+$		
Keto-KI	N_1	C_2	C_3	N_1	C_2	C_3	Keto-KI	N_1	C_2	C_3	N_1	C_2	C_3
KI$_{14}$	0.223	0.763	-0.100	0.212	0.364	0.074	**KI$_{21}$**	0.202	0.678	-0.078	0.140	0.344	0.057
KI$_{15}$	0.240	0.712	-0.085	0.158	0.368	0.066	**KI$_{22}$**	0.222	0.692	-0.080	0.148	0.366	0.059
KI$_{16}$	0.242	0.705	-0.084	0.153	0.366	0.061	**KI$_{23}$**	0.225	0.690	-0.081	0.151	0.358	0.059
KI$_{17}$	0.214	0.694	-0.083	0.146	0.353	0.059	**KI$_{24}$**	0.213	0.694	-0.081	0.150	0.355	0.060
KI$_{18}$	0.216	0.728	-0.090	0.142	0.368	0.060	**KI$_{9}$**	0.238	0.702	-0.083	0.157	0.364	0.063
KI$_{19}$	0.215	0.710	-0.086	0.145	0.362	0.058	**KI$_{25}$**	0.229	0.712	-0.086	0.153	0.365	0.062
KI$_{20}$	0.224	0.699	-0.084	0.150	0.359	0.062	**KI$_{26}$**	0.233	0.702	-0.083	0.158	0.364	0.062

3.6.3. Non-covalent Interactions

Non-covalent interactions such as CH$-\pi$, cation-π interactions could stabilize keteniminium intermediates or transition state structures by effecting the reactivity of KIs toward the [2+2] cycloaddition reactions. Therefore, non-covalent interactions were investigated with NCI-plot program for the selected KIs depicted in Figure 3.30. Non-covalent interactions exist in KI_6 and KI_7. The hydrogen atom on thiophene and phenyl interacts with the lone pair of nitrogen atom of KIs. The pull of the lone pair by positive central carbon decreases. As expected, this results in higher charge values on C_2 for KI with thiophene and phenyl group on β-position (Table 3.12) by lowering the free energy of activation for the RDS. The CH-π interaction in KI_5 and TS1-KI_5 can be directly observed in NCI plot. In order to form an activated complex, the interactions present in the KI intermediate need to be broken temporarily. This probably causes an increase in distortion energy related with the higher free energy of activation of the RDS. The T-shaped interaction in KI_{21} and TS1-KI_{21} between quadrupole of one benzyl moiety and CH on the other benzyl functional can be observed in NCI plot (Figure 3.30). The interactions in the first activated complex contribute to stabilize the transition state.

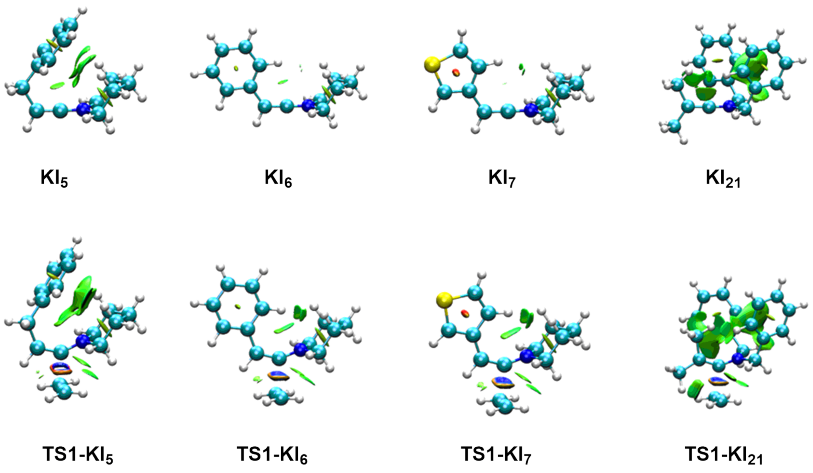

Figure 3.30. The noncovalent interactions (NCI) plots of the KI_5, KI_6, KI_7 and KI_{21} structures and their corresponding first transition states. Isosurface= 0.5 au using SCF densities.

3.7. Conclusions

In this study [2+2] cycloaddition reactions between highly reactive keteniminium salts and alkenes were elucidated with respect to the effects of substituents on alkenes and KIs. At first, the effect of alkene substitution on mechanism and product outcomes were examined. In general, the reaction mechanism consists of two steps. The reaction with mono-substituted alkene (1a) proceeds *via* a cyclic intermediate. The energetic difference between possible bond formations at the second step is the determining factor for regioselectivity of the product. Next, di-substituted alkenes gem, *cis* and *trans* isomers were evaluated. Gem-substitution (1b) results in the acyclic intermediate formation caused by steric hindrance of ethyl groups. Therefore, regioselectivity of the cycloadduct is adjusted by the nature of the intermediate. The reaction mechanism for *cis* (1c) and *trans* (1d) isomers of alkene give cyclic intermediates. For the *cis*-alkene second bond formation leads to enantiomer pairs of cyclobutaniminiums by choice of possible pathways at the second step. On the other hand, *trans*-alkene has difference in steric factors while deciding pathways at the second step, establishing the kinetic product. With the increase in number of alkyl groups on alkene, RDS becomes the second step for the reaction with tri (1e) and especially, for tetra (1f) substituted alkenes. Tri-substitution enables acyclic intermediate minima at the end of the first step. Therefore, regioselectivity of the mechanism is again affected since there is one possibility for second bond formation. Lastly, tetra-substituted alkene creates highly strained acyclic intermediate even though, first activated complex shows synchronous character. Also, RDS becomes the second step.

Furthermore, the substituents on KIs have electronic and steric effects on reactivity of KIs toward cycloaddition reactions. These effects have been investigated within two groups: C-substituent and N-substituent effect. The computed results indicate that among C-substituent effect, aldo keteniminium salts are more reactive compared to keto keteniminium salts. Considering β substituents on KI, the thiophene group makes KI the most reactive salt followed by the phenyl group. Whereas the benzyl group contributes to CH-π interactions bestowing a stable nature to the KI.

In association with *N*-substituent effect, the KI with *N,N*-diisopropyl groups shows highly persistant nature toward cycloaddition as a result of steric factors blocking the attack trajectory. KI with *N,N*-dipropargyl group has lowest free energy of activation owing to its higher *s* character in hybridization state enabling less electron donation. Therefore, propargyl moiety as *N*-substituent make KI intermediate more reactive compared to ally group. Chiral compounds were evaluated with 2,5-dimethylpyrrolidine and (*S*)-2-methoxymethyl pyrrolidine moieties. C_2-symmetric methyl groups on pyrrolidinyl generate steric effect by proximity to attack area, consequently, increasing the barrier for complex formation. In contrast, non-symmetric methoxymethyl group have lower free energy of activation. Additionally, the high electrophilicity of the central carbon atom of KIs is confirmed by population analysis and local reactivity indices. To conclude, this study is intended to explain the rationale behind the regioselectivity of [2+2] cycloaddition of keteniminium intermediates to alkenes with different substitution patterns. Another important aim was to systematically investigate the substituent effect on reactivity of KIs. It is aimed to provide know-how for highly substituted cycloadduct synthesis *via* [2+2] cycloaddition reaction of KIs. Therefore, the results of this study will be submitted to The Journal of Organic Chemistry soon.

4. APPLICATION AREAS OF INTERMOLECULAR [2+2] CYCLOADDITION REACTIONS OF KETENIMINIUM SALTS AND KETENES IN INDUSTRY

4.1. Energetic and Mechanistic Analysis of [2+2] Cycloadditions Leading to the Formation of Zealactone 1a/b

The strigolactone family consists of compounds that are classified as plant hormones, which are responsible for the regulation of some physiological processes [86]. Natural strigolactones are synthesized by plant's roots and are responsible for inhibition of branching, reinforcing leaf senescence, germination of parasitic plants such as Striga, known as witchweed and regulates symbiotic interaction with the fungus to provide nutrients from soil [87].

The importance of these plant signalling compounds relies has potential impact on agriculture and hence interest in strigolactones is increasing rapidly. Applications of natural and synthetic strigolactones in agriculture have crucial positive influence in terms of tolerance to abiotic stress such as drought, lack of nutrients etc. In addition, strigolactones enable a resistance toward various diseases and provide control over weeds. These plant hormones facilitate a symbiotic relationship between the plant and beneficial microbial communities which favors the soil stability and up taking of nutrients. If we look at the effect of strigolactones on the production and market stages of agricultural products, it has been indicated that the use of these hormones extends the shelf life of plants, increases the overall yield, regulates growing uniformly and enables efficient rooting [88].

The very first discovered strigolactone was isolated from the root of cotton and named as (+)-Strigol in 1966 [89]. Later, the structure of the Strigol compound was reported by Cook and coworkers in 1972 [90]. The general structure profile of strigolactones is classified as canonical strigolactones as shown in Figure 4.1.

The ABC-part is composed of a tricyclic lactone, which may show variety among strigolactones. The D-part is hydroxymethyl butenolide and this part is preserved in differing strigolactones. Therefore this part is considered as the moiety which is responsible for biological activity [91, 92].

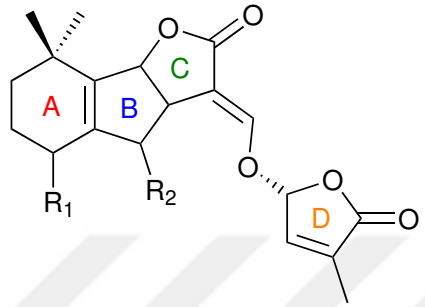

Canonical Strigolactones

Figure 4.1. General structure of Strigol-type canonical strigolactones [1].

In recent years, non-canonical strigolactones as two diastereomers named zealactone 1a/b shown in Figure 4.2 were identified from corn as the major strigolactone specie [93]. By analysing the root exudates, the structure of zealactone 1a/b was reported as having the D-ring, which is the same part in all strigolactones, bonded to γ-butyrolactone group *via* a diene chain. Notably, the diastereomerism is caused by the chiral center at C(6) and the ratio of the zealactone 1a/b mixture was found as 1:1.

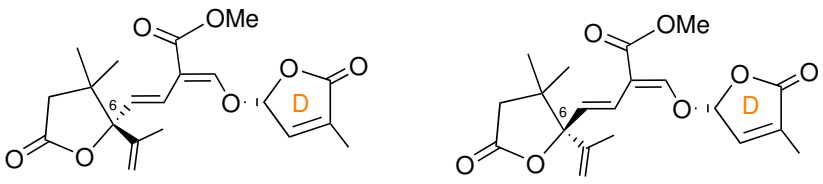

Zealactone 1a **Zealactone 1b**

Figure 4.2. The structures of zealactones 1a and 1b [1].

In Alain De Mesmaeker's work, the routes for the sythesis of racemic mixture zealactone 1a/b and its derivatives were introduced in order to improve sustainable crop production [1]. Besides that, they have conducted the research to investigate biological activity on leaf senescence and interaction with ZmD14 receptor. The use of [2+2] cycloaddition as the pivotal reaction in retrosynthetic analysis of zealactone 1a/b is a novel method. As indicated in Figure 4.3, the [2+2] cycloaddition of α, α'-vinyl-acetylenyl ketene 6 with isobutene (IB) leads to the formation of cycloadduct (7). They have used TBS as protecting group (PG). The regioselective Baeyer-Villiger oxidation and hydrostannylation of (7) enables producing vinyl stannane (8). At the last step, through a Stille coupling of vinyl stannane (8) and vinyl iodide (9), total synthesis of zealactone 1a/b is achieved. One of the important features of this study is being the first study that vinyl acetylenyl ketene and its reactivity toward olefins was reported.

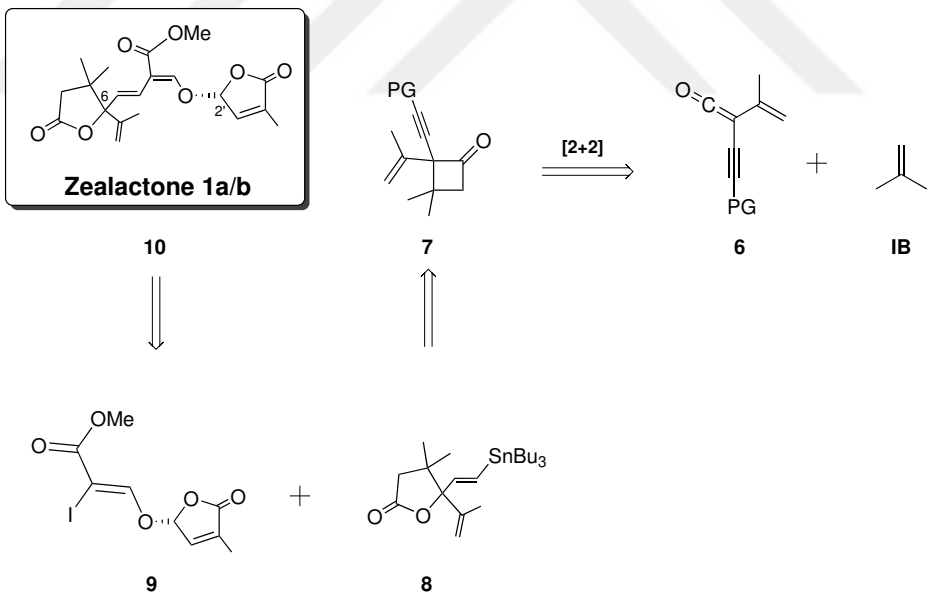

Figure 4.3. Retrosynthetic analysis of zealactone 1a/b [1].

The [2+2] cycloaddition of vinyl acetylenyl ketene and isobutene was experimentally studied. The drawback of this reaction was indicated as the lower reactivity of isobutene and this situation caused low yield of cycloadduct. So, to get the optimum reaction conditions more reactive methylenecyclopentane (MC) was used and optimum conditions determined. Triethylamine was selected as base, and $(COCl)_2$ was used as halogenating agent.

The need for an explanation based on energetic analysis was raised for the process of the formation of vinyl acetylenyl ketene from carboxylic acid to avoid possible dimer formations as side product. Moreover, when the optimum conditions were applied in the [2+2] cycloaddition between vinyl acetylenyl ketene 6 and olefins, the yield of cycloadduct is 23% for isobutene, and 95% for metylenecyclopentane.

4.1.1. The Aim and Computational Methodology of the Study

A density functional (DFT) study was performed in order to examine the mechanism in Figure 4.4. The aim is to enlighten the mechanism of the reaction that leads to the formation of ketene 13. The purpose is to bring forth the know-how to avoid from the formation of side products 16 and 17 and control the process where cyclobutanone 18 is obtained. The cycloadduct is used as a building block in the synthesis of zealactones 1a/b. Furthermore, the reactivity difference between IB and MC toward [2+2] cycloaddition reaction with ketene 13 was also investigated with the same computational method. Gaussian 16 program package Revision A.03 [79] was utilized for modeling the reactions. Long-range corrected ωB97XD density functional [12] was selected due to its high accuracy in kinetics and thermochemistry. The reaction takes place in a solvent environment. Hence, the solvent effect was considered while modeling the reaction. Dichloromethane (ϵ=8.93) was used as solvent and to evaluate the solvent effects self-consistent reaction field (SCRF) theory [13, 72] utilizing IEF-PCM [75, 76] was applied to create a continuum solvation.

4.1.2. Computational Results

According to the optimized contiditions for the experimental study, triethylamine was used as base and tert-butyldimethylsilyl (TBS) was used as protecting group. In order to reduce computational cost, trimethylamine and trimethylsilyl (TMS) was used as the base and PG respectively through out the computational study. The two possible conformations namely *s-cis* and *s-trans* of intermediates 12, 14, 15, carboxylic acid 11 and ketene 13 in Figure 4.4 were compared by means of relative energy values. The free energies of persistent intermediates were reported herein.

Interestingly, the *s-cis* conformer of ketene 13 compound is found to lack a co-planar structure with respect to the single bond that is in between the two double bonds. The computed results showed that the *s-trans* conformer of ketene 13 is lower in energy (1.6 kcal/mol) compared to its *s-cis* alternative.

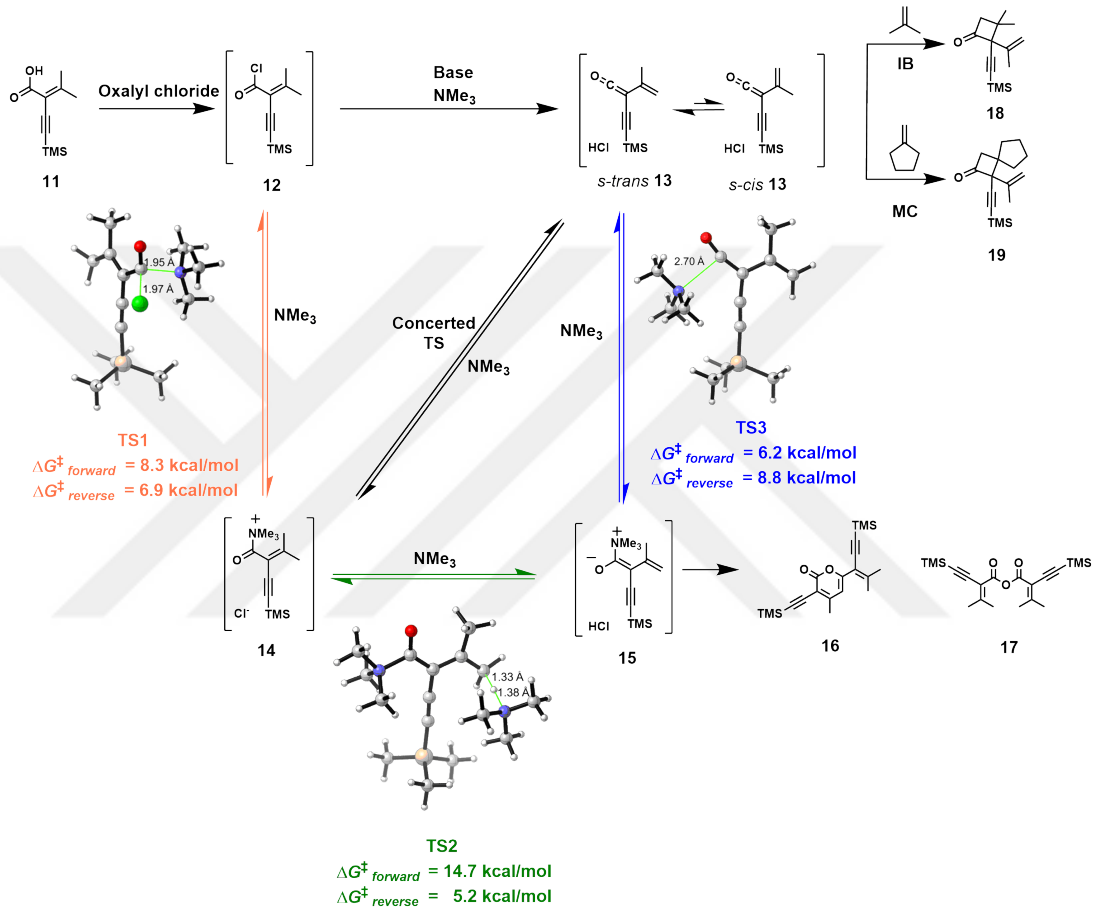

Figure 4.4. General scheme of plausible intermediates and side products in the formation reaction of vinyl acetylenyl ketenes. Optimized transition state structures and relative free energies of activation ($\Delta G^{\ddagger}$) at the ωB97XD/6-31+G(d,p) level of theory, in DCM) [1].

The reversible steps that take place in the formation of ketene 13 was modelled. Free energy of activation values for the forward and reverse reactions were reported with respect to separate reactants for TS2 and TS3. The effect of higly polarizable nature of the chloride ion on energetics was included in calculations to obtain more accurate energy barriers.

Considering this situation, free energy of activation values for TS1 were evaluated with respect to pre-reactive complex ($\Delta G^{\ddagger}_{\text{forward}}$)= 8.3 kcal/mol and product complex ($\Delta G^{\ddagger}_{\text{reverse}}$)= 6.9 kcal/mol as indicated in Figure 4.4. The formation of dimers 16 and 17 decreases the total yield of cyclobutanones 18 and 19. Energetic analysis showed that the forward barrier leading to formation of ketene 13 from ammonium enolate 15 to be 2.6 kcal/mol lower compared to reverse barrier. Experimentalists can control this step in order to increase the yield of cyclobutanones. Despite all efforts, concerted transition state structure between ketene 13 and intermediate 14 could not been located.

In order to rationalize the reactivity difference between isobutene (IB) and methylene cyclopentane (MC), the [2+2] cycloaddition reactions with ketene 13 was modeled at the same level of theory. TMS was used as protecting group for mimicking the reaction conditions. The solvent environment (DCM) was included implicitly. Relative energies were calculated with respect to separate reactants and relative to *s-trans* conformer of ketene 13. The mechanism of [2+2] cycloaddition consists of two consecutive steps. At the first step C_3 of olefin attacks C_1 of ketene resulting in the formation of a highly activated, acyclic intermediate. The second step is the cyclization where C_2-C_4 bond is formed leading to cyclobutanones 18 and 19 (Figure 4.5). Furthermore, there are two possible attack trajectories of olefins toward ketene 13 shown in Figure 4.5. The computed results showed that the favorable side is the less crowded side. The energy difference between favorable and unfavorable attack trajectories is found to be $\approx$ 5 kcal/mol.

According to experimental results, yields of cyclobutanone 18 (23%) and cyclobutanone 19 (95%) with the same experimental conditions. The reactivity difference between olefins toward [2+2] cycloaddition is seen in the difference in free energy of activations ($\Delta\Delta G^{\ddagger}_{1}$)= 2.8 kcal/mol. Figure 4.5 represents free energies of activation and reaction values for the [2+2] cycloaddition of IB and MC with ketene 13. These results can be supported with the Frontier Molecular Orbital analysis.

Highest Occupied Molecular Orbital (HOMO) energies of olefins were examined and $HOMO_{IB}$= -8.907 eV and $HOMO_{MC}$= -8.704 eV were reported. The difference between HOMO energies ($\Delta E_{HOMO} = 0.203$ eV) is in agreement with both the difference in relative free energy of activations and experimental yields. The slightly larger critical bond length in $TS1_{MC}$ also points out the early transition state, which is related to a lower barrier.

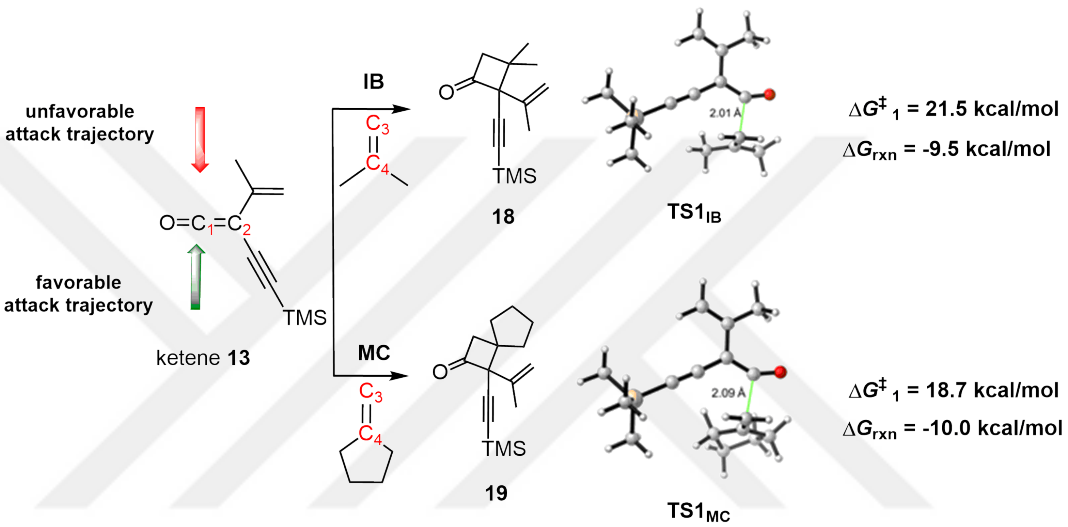

Figure 4.5. The [2+2] cycloaddition of IB and MC to ketene 13. $\Delta G^{\ddagger}_1$ and ΔG_{rxn} values for optimized transition states $TS1_{IB}$ and $TS1_{MC}$, free energies in kcal/mol; distances in Å[1].

4.2. Pyramidalization of Keteniminium-Enamines

In the first part of the thesis, the significance of [2+2] cycloaddition between keteniminium salts and alkenes in order to synthesize substituted cyclobutaniminiums has been explained. The method is highly useful to produce cyclobutanones from cyclobutaniminium intermediates as a result of hydrolysis procedure. This study proposed a novel method to synthesize higly substituted cyclobutanones by a one-pot keteniminium-enamine process. The study was conducted in collaboration with Syngenta Crop Protection AG and the results was published in Helvetica Chimica Acta recently [2].

The regioselective and stereoselective synthesis of substituted cyclobutatones consists of steps where the KI produced from amide undergoes [2+2] cycloaddition with alkene and produces cyclobutaniminium ion. Isomerization of cyclobutaniminium salt with a base enables the formation of a cyclic enamine compound. The enamine reacts with an electrophile and as a result of subsequent hydrolysis, highly substituted cyclobutanone is formed as depicted in Figure 4.6.

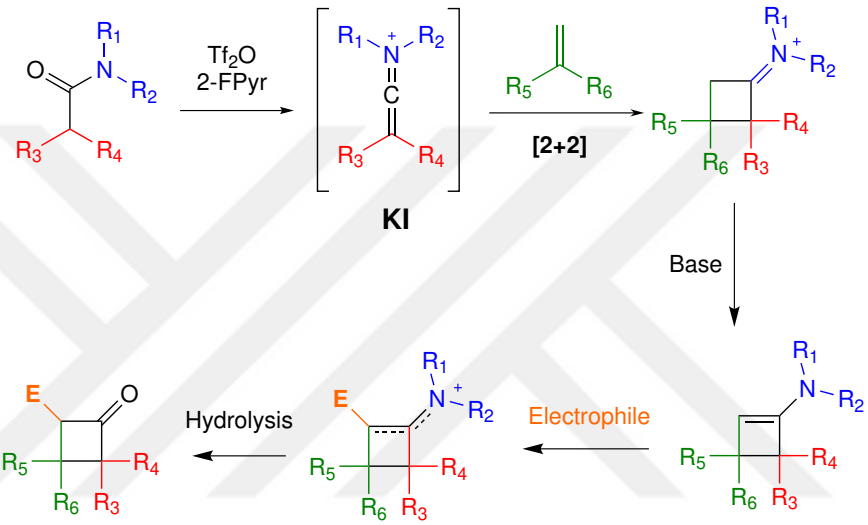

Figure 4.6. Synthesis of highly substituted cyclobutanones from amides *via* [2+2] cycloaddition of KIs and alkenes [2].

4.2.1. The Aim and Computational Methodology of the Study

The reactivity of an enamine toward electrophiles might be affected by the structural properties. If the C=C double bond and the lone pair on nitrogen atom are in optimum coplanarity, this can result with an increase in reactivity toward the electrophile. The substituents on enamine might prevent or assist to obtain coplanarity. A (DFT) study was conducted to examine coplanarity of cyclic enamines. In order to investigate structural properties, some cyclobutanones from the experimental data were selected. Geometry optimizations of all enamines were perfomed at ωB97XD level of theory, [12] by using the G16 software package [79]. The solvent was selected as DCM (ϵ=8.93), and modelled by applying the self-consistent reaction field (SCRF) theory [13] *via* IEF-PCM model [73, 76]. The conditions were 298 K and 1 atm.

4.2.2. Computational Results

In order to examine coplanarity of enamines, two descriptors were determined namely, pyramidalization degree (d) and improper dihedral angle (φ) as shown in Figure 4.7. The pyramidalization degree (d) is correlated with the hybridization degree of nitrogen atom. The lower value for (d) and (φ) illustrates closeness to sp^2 hybridization and more coplanarity.

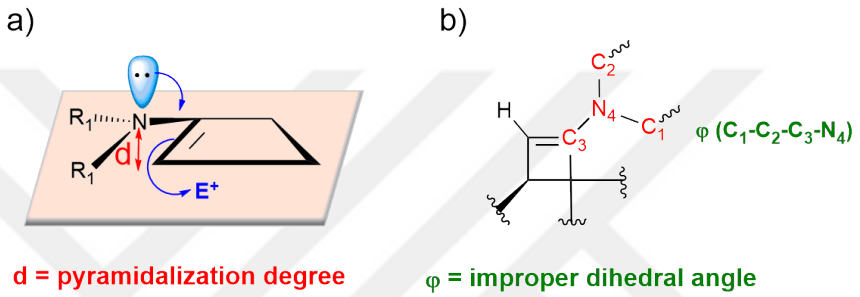

Figure 4.7. Representation of a) pyramidalization degrees (d) and b) improper dihedral angles (φ) for cyclic enamines [2].

The coplanarity of enamine structures was investigated with respect to three groups; *N*-substituent and *C*-substituent of amide part and the effect of substituent(s) on alkene part. In addition, ring size of cyclic enamines was evaluated. The effect of *N*-substituent was evaluated by comparison of e1-e4 as depicted in Figure 4.8. The change in (d) and (φ) indicated that *N*-substituent(s) have significant effect on degree of pyramidalization. Pyrrolidine moiety has the lowest pyramidalization degree and improper dihedral angle, hence the group enables to reach the most coplanar structure. *N*,*N*-dially group follows pyrrolidinyl with increasing values for (d) and (φ). Furthermore, dimethyl and piperidinyl groups decrease coplanarity and have similar (d) and (φ) values.

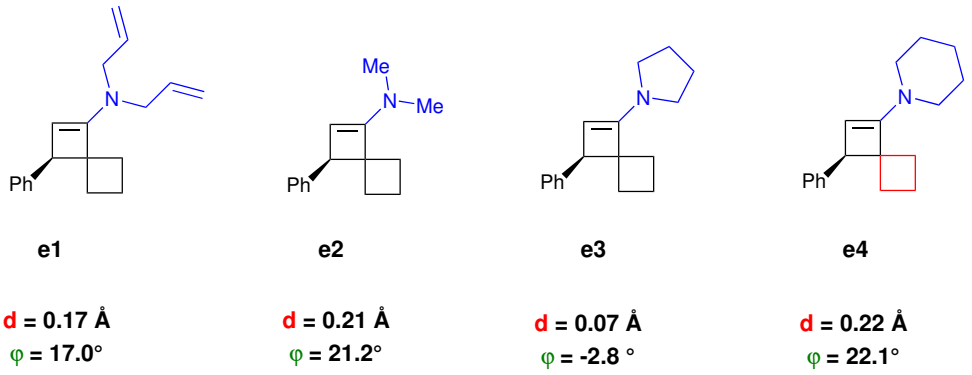

Figure 4.8. *N*-substituent effect on pyramidalization degrees (d) and improper dihedrals (φ) [2].

The effect of *C*-substituent was evaluated with cyclobutyl, cyclopentyl, cyclohexyl and dimethyl groups as shown in Figure 4.9. The comparison between e4-e6 and e1 vs e9 showed that *C*-substituent(s) do not cause a change in (d) and (φ) and hence do not effect the coplanarity of enamines.

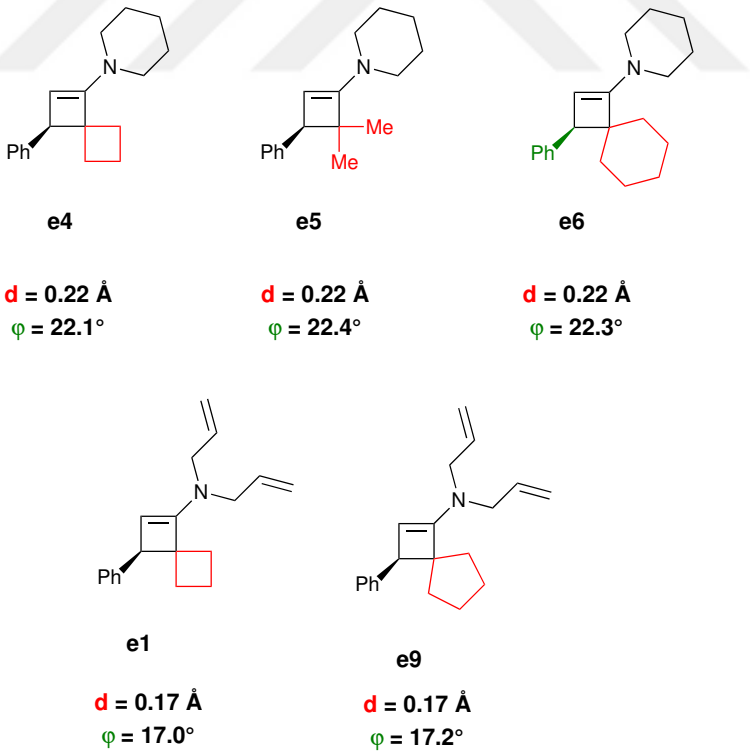

Figure 4.9. *C*-substituent effect on pyramidalization degrees (d) and improper dihedrals (φ) [2].

The substituents on alkenes in [2+2] cycloadditions might have an effect on the pyramidalization of nitrogen atom of enamines. For this reason, alkene substituent effects have also been evaluated by comparing e6 vs e7 and e8 vs e9. Computed results for (d) and (φ) indicated, like C-substituent(s), using different alkenes does not create any difference in coplanarity of enamines (see Figure 4.10).

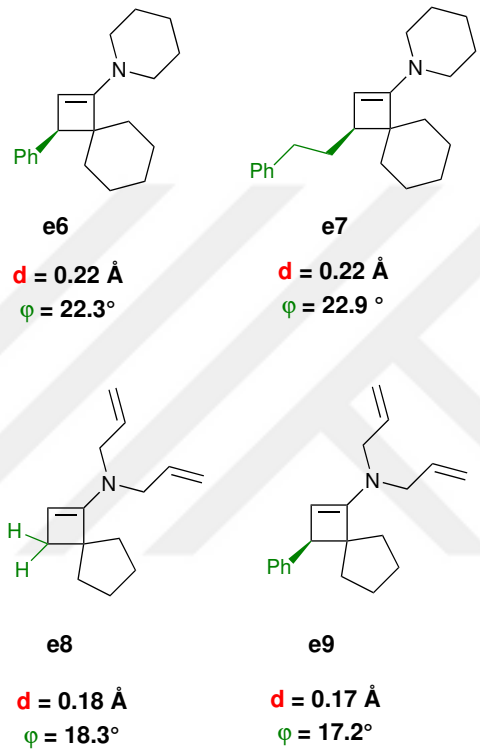

Figure 4.10. Alkene substituent effect on pyramidalization degrees (d) and improper dihedrals (φ) [2].

Furthermore, cyclopentenamine and cyclohexenamine structures were also considered in addition to cyclobutenamines, as listed in Figure 4.11. Comparison among e10-e15 gave similar results with Wennemers and coworkers‘ study [94]. By evaluating (d) and (φ) values it can be deduced that pyrrolidine moiety increases the coplanarity compared to piperidine group due to lower pyramidalization of the enamine nitrogen. Notably, among e10-e12, six-membered ring size of enamine results in decrease in coplanarity when pyrrolidinyl is used.

Moreover, the bond lengths of all enamines modelled were evaluated. It is found that C=C bond length is ≈ 1.35 Å and C-N bond lenght is in range of 1.35 Å (e3) and 1.41 Å (e15, e14). The results was compared with ideal C=C (1.33 Å), C-N (1.46 Å) and C=N (1.28 Å) bond lengths [95]. The conjugation in enamines makes C-N bond shorter and C=C bond slightly longer than the ideal.

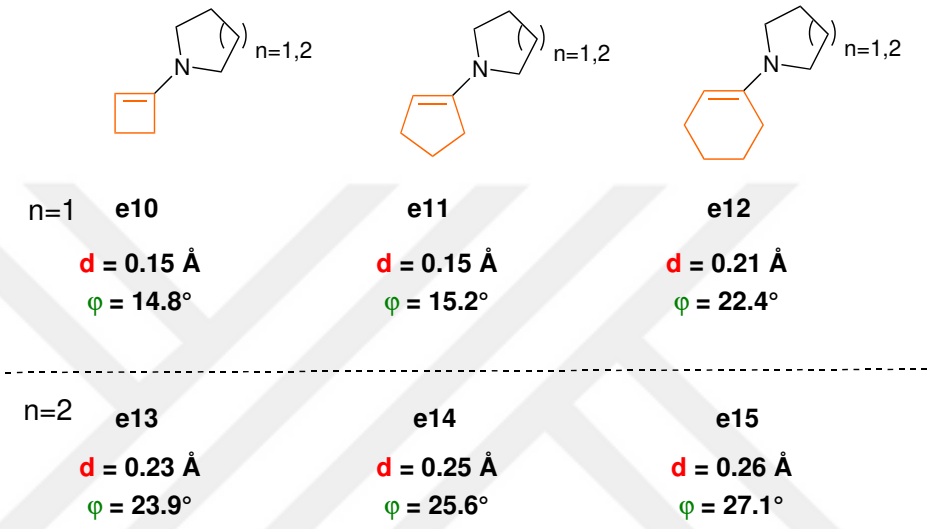

Figure 4.11. The ring size effect of cyclic enamines on pyramidalization degrees (d) and improper dihedrals (φ) [2].

4.3. Conclusions

Strigolactones are plant hormones that play a crucial role in the plant's development by enabling some responses to abiotic stresses. Therefore, the production of synthetic strigolactone derivatives is becoming increasingly important for sustainable agriculture. A procedure for the total synthesis of zealactone 1a/b, which is a non-canonical strigolactone, was presented. The [2+2] cycloaddition of α,α'-vinyl-acetylenyl ketene to olefins strategy leads to the formation of building blocks for further steps. Energetic analysis for the procedure of synthesizing vinyl-acetylenyl ketene gave insight to avoid dimer formation. Also, [2+2] cycloaddition between vinyl-acetylenyl ketene and methylenecyclopentane is more feasible than the reaction with isobutene due to the difference between HOMO energies of olefins.

Moreover, a procedure based on keteniminium-enamine process followed by the reaction between electrophile and enamine reagents to synthesize substituted cyclobutanones was introduced. Enamine structures were optimized to examine substituent's effect on coplanarity, which is related with the reactivity towards electrophiles. It was seen that while the N-substituents have a significant effect, C-substituents and alkene substitutions do not have an impact on coplanarity of enamines.

REFERENCES

1. Yoshimura, M., M. Dieckmann, P.-Y. Dakas, R. Fonné-Pfister, C. Screpanti, K. Hermann, S. Rendine, P. Quinodoz, B. Horoz, S. Catak *et al.*, "Total Synthesis and Biological Evaluation of Zealactone 1a/b", *Helvetica Chimica Acta*, Vol. 103, No. 4, p. e2000017, 2020.

2. Dagoneau, D., A. Kolleth, P. Quinodoz, B. Horoz, S. Catak, A. Lumbroso, S. Sulzer-Mossé and A. De Mesmaeker, "Synthesis of Highly Substituted Cyclobutanones by a One-Pot Keteniminium-Enamine Process", *Helvetica Chimica Acta*, Vol. 104, No. 5, p. e2100022, 2021.

3. Seminario, J. M., *Recent Developments and Applications of Modern Density Functional Theory*, Elsevier, 1996.

4. Becke, A. D., "Density-Functional Exchange-Energy Approximation with Correct Asymptotic Behavior", *Physical Review A*, Vol. 38, pp. 3098–3100, 1988.

5. Becke, A. D., "A New Mixing of Hartree–Fock and Local Density-Functional Theories", *The Journal of Chemical Physics*, Vol. 98, No. 2, pp. 1372–1377, 1993.

6. Perdew, J. P., K. Burke and M. Ernzerhof, "Generalized Gradient Approximation Made Simple.", *Physical Review Letters*, Vol. 77, pp. 3865–3868, 1996.

7. Lee, C., W. Yang and G. Parr, "Development of the Colic-Salvetti Correlation-Energy Formula into a Functional of the Electron Density", *Physical Review B*, Vol. 37, No. 2, pp. 785–789, 1988.

8. Becke, A. D., "B3LYP", *The Journal of Chemical Physics*, Vol. 98, pp. 5648–5652, 1993.

9. Zhao, Y. and D. G. Truhlar, "The M06 Suite of Density Functionals for Main Group

Thermochemistry, Thermochemical Kinetics, Noncovalent Interactions, Excited States, and Transition Elements: Two New Functionals and Systematic Testing of Four M06-class Functionals and 12 Other Functionals", *Theoretical Chemistry Accounts*, Vol. 120, pp. 215–241, 2008.

10. Zhao, Y. and D. G. Truhlar, "Density Functionals with Broad Applicability in Chemistry", *Accounts of Chemical Research*, Vol. 41, No. 2, pp. 157–167, 2008.

11. Tsuneda, T. and K. Hirao, "Long-Range Correction for Density Functional Theory", *Wiley Interdisciplinary Reviews: Computational Molecular Science*, Vol. 4, pp. 375–390, 2014.

12. Chai, J.-D. and M. Head-Gordon, "Long-Range Corrected Hybrid Density Functionals with Damped Atom–Atom Dispersion Corrections", *Physical Chemistry Chemical Physics*, Vol. 10, No. 44, pp. 6615–6620, 2008.

13. Tomasi, J., B. Mennucci and R. Cammi, "Quantum Mechanical Continuum Solvation Models", *Chemical Reviews*, Vol. 105, No. 8, pp. 2999–3094, 2005.

14. Cancès, E., B. Mennucci and J. Tomasi, "A New Integral Equation Formalism for the Polarizable Continuum Model: Theoretical Background and Applications to Isotropic and Anisotropic Dielectrics", *The Journal of Chemical Physics*, Vol. 107, No. 8, pp. 3032–3041, 1997.

15. Geerlings, P., F. De Proft and W. Langenaeker, "Conceptual Density Functional Theory", *Chemical Reviews*, Vol. 103, No. 5, pp. 1793–1873, 2003.

16. Parr, R. G. and W. Yang, "Density Functional Approach to the Frontier-Electron Theory of Chemical Reactivity", *Journal of the American Chemical Society*, Vol. 106, No. 14, pp. 4049–4050, 1984.

17. Domingo, L. R., P. Pérez and J. A. Sáez, "Understanding the Local Reactivity in Polar Organic Reactions through Electrophilic and Nucleophilic Parr Functions",

RSC Advances, Vol. 3, pp. 1486–1494, 2013.

18. Yang, W. and W. J. Mortier, "The Use of Global and Local Molecular Parameters for the Analysis of the Gas-Phase Basicity of Amines", *Journal of the American Chemical Society*, Vol. 108, No. 19, pp. 5708–5711, 1986.

19. Reed, A. E., R. B. Weinstock and F. Weinhold, "Natural Population Analysis", *The Journal of Chemical Physics*, Vol. 83, No. 2, pp. 735–746, 1985.

20. Contreras-García, J., E. R. Johnson, S. Keinan, R. Chaudret, J. P. Piquemal, D. N. Beratan and W. Yang, "NCIPLOT: A Program for Plotting Noncovalent Interaction Regions", *Journal of Chemical Theory and Computation*, Vol. 7, pp. 625–632, 2011.

21. Madelaine, C., V. Valerio and N. Maulide, "Revisiting Keteniminium Salts: More than the Nitrogen Analogs of Ketenes", *Chemistry-An Asian Journal*, Vol. 6, No. 9, pp. 2224–2239, 2011.

22. Evano, G., M. Lecomte, P. Thilmany and C. Theunissen, "Keteniminium Ions: Unique and Versatile Reactive Intermediates for Chemical Synthesis", *Synthesis*, Vol. 49, No. 15, pp. 3183–3214, 2017.

23. Viehe, H., R. Buijle, R. Fuks, R. Merenyi and J. Oth, "Acylation, Alkylation, and Protonation of Alkynylamines", *Angewandte Chemie International Edition in English*, Vol. 6, No. 1, pp. 77–78, 1967.

24. Viehe, H., "Synthesis and Reactions of the Alkynylamines", *Angewandte Chemie International Edition in English*, Vol. 6, No. 9, pp. 767–778, 1967.

25. Ghosez, L., B. Haveuaux and H. G. Viehe, "Alkyl and Aryl α-Chloro Enamines", *Angewandte Chemie International Edition in English*, Vol. 8, No. 6, pp. 454–455, 1969.

26. Falmagne, J.-B., J. Escudero, S. Taleb-Sahraoui and L. Ghosez, "Cyclobutanone and Cyclobutenone Derivatives by Reaction of Tertiary Amides with Alkenes or Alkynes", *Angewandte Chemie International Edition in English*, Vol. 20, No. 10, pp. 879–880, 1981.

27. Snider, B. B., "Intramolecular Cycloaddition Reactions of Ketenes and Keteniminium Salts with Alkenes", *Chemical Reviews*, Vol. 88, No. 5, pp. 793–811, 1988.

28. Sidani, A., J. Marchand-Brynaert and L. Ghosez, "A Convenient Procedure for the Synthesis of Cyclobutanones", *Angewandte Chemie International Edition in English*, Vol. 13, No. 4, p. 267, 1974.

29. Genicot, C. and L. Ghosez, "Asymmetric Vicinal Acylation of Olefins: A New Approach to Enantiomerically Pure γ-Lactones.", *Tetrahedron Letters*, Vol. 33, No. 48, pp. 7357–7360, 1992.

30. Houge, C., A. M. Frisque-Hesbain, A. Mockel, L. Ghosez, J. P. Declercq, G. Germain and M. Van Meerssche, "Models for Asymmetric [2+2] Cycloadditions", *Journal of the American Chemical Society*, Vol. 104, pp. 2920–2921, 1982.

31. Ghosez, L., S. Bogdan, M. Cérésiat, C. Frydrych, J. Marchand-Brynaert, M. M. Portuguez and I. Huber, "Synthesis and Uses of Azetidiniminium Salts", *Pure and Applied Chemistry*, Vol. 59, No. 3, pp. 393–398, 1987.

32. Ghosez, L., F. Mahuteau-Betzer, C. Genicot, A. Vallribera and J.-F. Cordier, "Enantioselective Vicinal Bis-Acylation of Olefins", *Chemistry–A European Journal*, Vol. 8, No. 15, pp. 3411–3422, 2002.

33. Depré, D., L.-Y. Chen and L. Ghosez, "A Short Multigram Asymmetric Synthesis of Prostanoid Scaffolds", *Tetrahedron*, Vol. 59, pp. 6797–6812, 2003.

34. Ghosez, L., "α-Chloroenamines: New Reagents for Organic Synthesis", *Angewandte Chemie International Edition in English*, Vol. 11, No. 9, pp. 852–853,

1972.

35. Marchand-Brynaert, J. and L. Ghosez, "Cycloadditions of Keteneimmonium Cations to Olefins and Dienes. A New Synthesis of Four-Membered Rings", *Journal of the American Chemical Society*, Vol. 94, No. 8, pp. 2870–2872, 1972.

36. Villedieu-Percheron, E., S. Catak, D. Zurwerra, R. Staiger, M. Lachia and A. De Mesmaeker, "$6\pi/10\pi$-Electrocyclization of Keteneiminium Salts for the Synthesis of Substituted Naphthylamines", *Tetrahedron Letters*, Vol. 55, No. 15, pp. 2446–2449, 2014.

37. Dagoneau, D., A. Kolleth, A. Lumbroso, G. Tanriver, S. Catak, S. Sulzer-Mossé and A. De Mesmaeker, "Straightforward Synthesis of 3-Aminothiophenes Using Activated Amides", *Helvetica Chimica Acta*, Vol. 102, No. 4, p. e1900031, 2019.

38. Tanriver, G., D. Dagoneau, U. Karadeniz, A. Kolleth, A. Lumbroso, S. Sulzer-Mossé, A. De Mesmaeker and S. Catak, "Keteniminium Salts: Reactivity and Propensity toward Electrocyclization Reactions", *The Journal of Organic Chemistry*, Vol. 85, No. 2, pp. 449–463, 2020.

39. Marchand-Brynaert, J. and L. Ghosez, "(2+4) Cycloadditions of Tetramethylketeneimmonium Ion to Cis-fixed Dienes", *Tetrahedron Letters*, Vol. 15, No. 4, pp. 377–380, 1974.

40. Mahuteau-Betzer, F., P.-Y. Ding and L. Ghosez, "First [4+2] Cycloadditions Involving the Olefinic Bond of an 'Aldoketeniminium Salt'(= N-Alk-1-enylideneaminium Salt)", *Helvetica Chimica Acta*, Vol. 88, No. 7, pp. 2022–2031, 2005.

41. Ramirez, M., W. Li, Y.-h. Lam, L. Ghosez and K. Houk, "Mechanisms and Conformational Control of (4+2) and (2+2) Cycloadditions of Dienes to Keteniminium Cations", *The Journal of Organic Chemistry*, Vol. 85, No. 4, pp. 2597–2606, 2020.

42. Theunissen, C., B. Métayer, M. Lecomte, N. Henry, H.-C. Chan, G. Compain, P. Gérard, C. Bachmann, N. Mokhtari, J. Marrot *et al.*, "Cationic Polycyclization of Ynamides: Building Up Molecular Complexity", *Organic and Biomolecular Chemistry*, Vol. 15, No. 20, pp. 4399–4416, 2017.

43. Yamaoka, Y., T. Yoshida, M. Shinozaki, K.-i. Yamada and K. Takasu, "Development of a Brønsted Acid-Promoted Arene–Ynamide Cyclization toward the Total Syntheses of Marinoquinolines A and C and Aplidiopsamine A", *The Journal of Organic Chemistry*, Vol. 80, No. 2, pp. 957–964, 2015.

44. Lecomte, M. and G. Evano, "Harnessing the Electrophilicity of Keteniminium Ions: A Simple and Straightforward Entry to Tetrahydropyridines and Piperidines from Ynamides", *Angewandte Chemie*, Vol. 128, No. 14, pp. 4623–4627, 2016.

45. Xu, L., P. Yang and L. Wang, "Direct Functionalization of Benzylic and Non-benzylic C (sp3)–H Bonds via Keteniminium Ion Initiated Cascade [1,5]-Hydrogen Transfer/Cyclization", *Organic Chemistry Frontiers*, Vol. 5, No. 11, pp. 1854–1858, 2018.

46. Padmanaban, M., L. C. Carvalho, D. Petkova, J.-W. Lee, A. S. Santos, M. M. B. Marques and N. Maulide, "Investigation of Cationic Claisen-Type Electrophilic Rearrangements of Amides", *Tetrahedron*, Vol. 71, No. 35, pp. 5994–6005, 2015.

47. Kaiser, D. and N. Maulide, "Making the Least Reactive Electrophile the First in Class: Domino Electrophilic Activation of Amides", *The Journal of Organic Chemistry*, Vol. 81, No. 11, pp. 4421–4428, 2016.

48. Kolleth, A., A. Lumbroso, G. Tanriver, S. Catak, S. Sulzer-Mossé and A. De Mesmaeker, "Synthesis of Amino-Cyclobutanes via [2+2] Cycloadditions Involving Keteniminium Intermediates", *Tetrahedron Letters*, Vol. 57, No. 25, pp. 2697–2702, 2016.

49. Dowd, P. and W. Zhang, "Free-Radical Ring Expansion of Fused Cyclobutanones:

Stereospecific Construction of 5, 7-, 6, 7-, 7, 7-, 8, 7-, and 5, 8-Cis-Fused Bicyclic Systems", *The Journal of Organic Chemistry*, Vol. 57, No. 26, pp. 7163–7171, 1992.

50. Chen, L.-y. and L. Ghosez, "Study of Chiral Auxiliaries for the Intramolecular [2+2] Cycloaddition of a Keteniminium Salt to an Olefinic Double Bond. A New Asymmetric Synthesis of Cyclobutanones.", *Tetrahedron Letters*, Vol. 31, No. 31, pp. 4467–4470, 1990.

51. Brady, W. T., Y. S. F. Giang, L. Weng and M. M. Dad, "Intramolecular [2+2] Cycloadditions of Keteneiminium Salts to Carbon-Carbon Double Bonds", *The Journal of Organic Chemistry*, Vol. 52, No. 11, pp. 2216–2220, 1987.

52. Kolleth, A., A. Lumbroso, G. Tanriver, S. Catak, S. Sulzer-Mossé and A. De Mesmaeker, "Synthesis of 4-membered Ring Alkaloid Analogues via Intramolecular [2+2] Cycloaddition Involving Keteniminium Salt Intermediates", *Tetrahedron Letters*, Vol. 58, No. 30, pp. 2904–2909, 2017.

53. Lumbroso, A., S. Catak, S. Sulzer-Mossé and A. De Mesmaeker, "Cycloaddition of Keteniminium with Terminal Alkynes toward Cyclobuteniminium and Their Use in Diels–Alder Reactions", *Tetrahedron Letters*, Vol. 55, No. 37, pp. 5147–5150, 2014.

54. Lumbroso, A., S. Catak, S. Sulzer-Mossé and A. De Mesmaeker, "Synthesis of Cyclobuteniminium Salts Derived from Aldo-keteniminium Salts and Study of Their Reactivity in Diels–Alder Reaction", *Tetrahedron Letters*, Vol. 55, No. 49, pp. 6721–6725, 2014.

55. Lumbroso, A., S. Catak, S. Sulzer-Mossé and A. De Mesmaeker, "Efficient Access to Functionalized Cyclobutanone Derivatives Using Cyclobuteniminium Salts as Highly Reactive Michael Acceptors", *Tetrahedron Letters*, Vol. 56, No. 19, pp. 2397–2401, 2015.

56. Kolleth, A., A. Lumbroso, G. Tanriver, S. Catak, S. Sulzer-Mossé and A. De Mes-

maeker, "New Access to Quaternary Aminocyclobutanes via Nucleophilic Addition on Cyclobutaniminium Salts", *Tetrahedron Letters*, Vol. 57, No. 31, pp. 3510–3514, 2016.

57. Adam, J.-M., L. Ghosez and K. N. Houk, "A Convergent Strategy for the Asymmetric Synthesis of Enantiomerically Pure Bicyclic Compounds by Using a Silicon-Directed Cycloaddition Reaction: The Synthesis of Enantiomerically Pure Bicyclo [3.2. 0] Hept-2-en-6-one", *Angewandte Chemie International Edition*, Vol. 38, No. 18, pp. 2728–2730, 1999.

58. Brown, R. C., J. Keily and R. Karim, "Solid-phase Synthesis of γ-Lactams, γ-Lactones and Cyclobutane Derivatives from Common Resin-Bound Intermediates", *Tetrahedron Letters*, Vol. 41, No. 17, pp. 3247–3251, 2000.

59. Delle Monache, G., D. Misiti, P. Salvatore, G. Zappia and M. Pierini, "Stereoselective Synthesis of 2-Substituted 3-Azabicyclo [3.2. 0] Heptan-2-ones by [2+2]-Cycloaddition of N-allyl-β-N-Keteniminium Salts Derived from (R)-Vinylglycinol", *Tetrahedron: Asymmetry*, Vol. 11, No. 13, pp. 2653–2659, 2000.

60. Schmid, M., A. S. Grossmann, K. Wurst and T. Magauer, "Total Synthesis of Salimabromide: A Tetracyclic Polyketide from a Marine Myxobacterium", *Journal of the American Chemical Society*, Vol. 140, No. 27, pp. 8444–8447, 2018.

61. Lachia, M., P. M. Jung and A. De Mesmaeker, "A Novel Approach toward the Synthesis of Strigolactones through Intramolecular [2+2] Cycloaddition of Ketenes and Ketene-iminiums to Olefins. Application to the Asymmetric Synthesis of GR-24", *Tetrahedron Letters*, Vol. 53, No. 34, pp. 4514–4517, 2012.

62. Lee-Ruff, E., M. Ostrowski, A. Ladha, D. V. Stynes, I. Vernik, J.-L. Jiang, W.-Q. Wan, S.-F. Ding and S. Joshi, "Synthesis and HIV Inhibition Activity of 2 ', 3 '-Dideoxy-3 '-C-Hydroxymethyl Nucleosides", *Journal of Medicinal Chemistry*, Vol. 39, No. 26, pp. 5276–5280, 1996.

63. Genicot, C., B. Gobeaux and L. Ghosez, "An Efficient Method for the Vicinal Acylation of Unactivated Olefins Using Keteniminium Salts Derived from Protected α-Hydroxy-or α-Aminoacids.", *Tetrahedron Letters*, Vol. 32, No. 31, pp. 3827–3830, 1991.

64. Woodward, R. B. and R. Hoffmann, "The Conservation of Orbital Symmetry", *Angewandte Chemie International Edition in English*, Vol. 8, No. 11, pp. 781–853, 1969.

65. Saimoto, H., C. Houge, A.-M. Hesbain-Frisque, A. Mockel and L. Ghosez, "Non-stereospecificity in the Cycloadditions of Keteneiminium Salts to Olefins. Evidence for a Stepwise Mechanism.", *Tetrahedron Letters*, Vol. 24, No. 22, pp. 2251–2254, 1983.

66. Ding, W.-J. and D.-C. Fang, "Theoretical Studies on Cycloaddition Reactions Between Keteniminium Cations and Olefins", *The Journal of Organic Chemistry*, Vol. 66, No. 20, pp. 6673–6678, 2001.

67. Domingo, L. R., M. Ríos-Gutiérrez and P. Pérez, "A DFT Study of the Ionic [2+2] Cycloaddition Reactions of Keteniminium Cations with Terminal Acetylenes", *Tetrahedron*, Vol. 71, No. 16, pp. 2421–2427, 2015.

68. Catak, S., K. Hemelsoet, L. Hermosilla, M. Waroquier and V. Van Speybroeck, "Competitive Reactions of Organophosphorus Radicals on Coke Surfaces", *Chemistry-A European Journal*, Vol. 17, No. 43, pp. 12027–12036, 2011.

69. Mollet, K., S. Catak, M. Waroquier, V. Van Speybroeck, M. D'hooghe and N. De Kimpe, "Stereoselective Synthesis of Cis-3,4-disubstituted Piperidines through Ring Transformation of 2-(2-Mesyloxyethyl) Azetidines", *The Journal of Organic Chemistry*, Vol. 76, No. 20, pp. 8364–8375, 2011.

70. Goossens, H., J. M. Winne, S. Wouters, L. Hermosilla, P. J. De Clercq, M. Waroquier, V. Van Speybroeck and S. Catak, "Possibility of [1, 5] Sigmatropic Shifts in

Bicyclo [4.2.0] octa-2,4-dienes", *The Journal of Organic Chemistry*, Vol. 80, No. 5, pp. 2609–2620, 2015.

71. Schuchardt, K. L., B. T. Didier, T. Elsethagen, L. Sun, V. Gurumoorthi, J. Chase, J. Li and T. L. Windus, "Basis Set Exchange: A Community Database for Computational Sciences", *Journal of Chemical Information and Modeling*, Vol. 47, No. 3, pp. 1045–1052, 2007.

72. Chen, J. L., L. Noodleman, D. A. Case and D. Bashford, "Incorporating Solvation Effects into Density Functional Electronic Structure Calculations", *The Journal of Physical Chemistry*, Vol. 98, No. 43, pp. 11059–11068, 1994.

73. Mennucci, B., E. Cances and J. Tomasi, "Evaluation of Solvent Effects in Isotropic and Anisotropic Dielectrics and in Ionic Solutions with a Unified Integral Equation Method: Theoretical Bases, Computational Implementation, and Numerical Applications", *The Journal of Physical Chemistry B*, Vol. 101, No. 49, pp. 10506–10517, 1997.

74. Cances, E., B. Mennucci and J. Tomasi, "A New Integral Equation Formalism for the Polarizable Continuum Model: Theoretical Background and Applications to Isotropic and Anisotropic Dielectrics", *The Journal of Chemical Physics*, Vol. 107, No. 8, pp. 3032–3041, 1997.

75. Mennucci, B. and J. Tomasi, "Continuum Solvation Models: A New Approach to the Problem of Solute's Charge Distribution and Cavity Boundaries", *The Journal of Chemical Physics*, Vol. 106, No. 12, pp. 5151–5158, 1997.

76. Tomasi, J., B. Mennucci and E. Cancès, "The IEF Version of the PCM Solvation Method: An Overview of a New Method Addressed to Study Molecular Solutes at the QM Ab Initio Level", *Journal of Molecular Structure: THEOCHEM*, Vol. 464, No. 1-3, pp. 211–226, 1999.

77. Lynch, B. J., P. L. Fast, M. Harris and D. G. Truhlar, "Adiabatic Connection for

Kinetics", *The Journal of Physical Chemistry A*, Vol. 104, No. 21, pp. 4811–4815, 2000.

78. Grimme, S., "Semiempirical Hybrid Density Functional with Perturbative Second-Order Correlation", *The Journal of Chemical Physics*, Vol. 124, No. 3, p. 034108, 2006.

79. Frisch, M. J., G. W. Trucks, H. B. Schlegel, G. E. Scuseria, M. A. Robb, J. R. Cheeseman, G. Scalmani, V. Barone, G. A. Petersson, H. Nakatsuji, X. Li, M. Caricato, A. V. Marenich, J. Bloino, B. G. Janesko, R. Gomperts, B. Mennucci, H. P. Hratchian, J. V. Ortiz, A. F. Izmaylov, J. L. Sonnenberg, D. Williams-Young, F. Ding, F. Lipparini, F. Egidi, J. Goings, B. Peng, A. Petrone, T. Henderson, D. Ranasinghe, V. G. Zakrzewski, J. Gao, N. Rega, G. Zheng, W. Liang, M. Hada, M. Ehara, K. Toyota, R. Fukuda, J. Hasegawa, M. Ishida, T. Nakajima, Y. Honda, O. Kitao, H. Nakai, T. Vreven, K. Throssell, J. A. Montgomery, Jr., J. E. Peralta, F. Ogliaro, M. J. Bearpark, J. J. Heyd, E. N. Brothers, K. N. Kudin, V. N. Staroverov, T. A. Keith, R. Kobayashi, J. Normand, K. Raghavachari, A. P. Rendell, J. C. Burant, S. S. Iyengar, J. Tomasi, M. Cossi, J. M. Millam, M. Klene, C. Adamo, R. Cammi, J. W. Ochterski, R. L. Martin, K. Morokuma, O. Farkas, J. B. Foresman and D. J. Fox, "Gaussian 16, Revision A.03", *Gaussian Inc., Wallingford, CT*, 2016.

80. Fukui, K., "The Path of Chemical Reactions-the IRC Approach", *Accounts of Chemical Research*, Vol. 14, No. 12, pp. 363–368, 1981.

81. Hratchian, H. P. and H. B. Schlegel, "Accurate Reaction Paths Using a Hessian Based Predictor–Corrector Integrator", *The Journal of Chemical Physics*, Vol. 120, No. 21, pp. 9918–9924, 2004.

82. Hratchian, H. and H. Schlegel, "Using Hessian Updating to Increase the Efficiency of a Hessian Based Predictor-Corrector Reaction Path Following Method", *Journal of Chemical Theory and Computation*, Vol. 1, No. 1, pp. 61–69, 2005.

83. Glendening, E., J. Badenhoop, A. Reed, J. Carpenter, J. Bohmann, C. Morales, C. Landis and F. Weinhold, "NBO 6.0", *Theoretical Chemistry Institute, University of Wisconsin Madison, WI*, 2013.

84. Te Velde, G. t., F. M. Bickelhaupt, E. J. Baerends, C. Fonseca Guerra, S. J. van Gisbergen, J. G. Snijders and T. Ziegler, "Chemistry with ADF", *Journal of Computational Chemistry*, Vol. 22, No. 9, pp. 931–967, 2001.

85. Guerra, C. F., J. Snijders, G. t. te Velde and E. J. Baerends, "Towards an Order-N DFT Method", *Theoretical Chemistry Accounts*, Vol. 99, No. 6, pp. 391–403, 1998.

86. Zwanenburg, B. and D. Blanco-Ania, "Strigolactones: New Plant Hormones in the Spotlight", *Journal of Experimental Botany*, Vol. 69, No. 9, pp. 2205–2218, 2018.

87. Al-Babili, S. and H. J. Bouwmeester, "Strigolactones, a Novel Carotenoid-Derived Plant Hormone", *Annual Review of Plant Biology*, Vol. 66, pp. 161–186, 2015.

88. Aliche, E. B., C. Screpanti, A. De Mesmaeker, T. Munnik and H. J. Bouwmeester, "Science and Application of Strigolactones", *New Phytologist*, Vol. 227, No. 4, pp. 1001–1011, 2020.

89. Cook, C., L. P. Whichard, B. Turner, M. E. Wall and G. H. Egley, "Germination of Witchweed (Striga Lutea Lour.): Isolation and Properties of a Potent Stimulant", *Science*, Vol. 154, No. 3753, pp. 1189–1190, 1966.

90. Cook, C., L. P. Whichard, M. Wall, G. H. Egley, P. Coggon, P. A. Luhan and A. McPhail, "Germination Stimulants. II. Structure of Strigol, A Potent Seed Germination Stimulant for Witchweed (Striga Lutea)", *Journal of the American Chemical Society*, Vol. 94, No. 17, pp. 6198–6199, 1972.

91. Umehara, M., M. Cao, K. Akiyama, T. Akatsu, Y. Seto, A. Hanada, W. Li, N. Takeda-Kamiya, Y. Morimoto and S. Yamaguchi, "Structural Requirements of Strigolactones for Shoot Branching Inhibition in Rice and Arabidopsis", *Plant*

and Cell Physiology, Vol. 56, No. 6, pp. 1059–1072, 2015.

92. Wang, Y. and H. J. Bouwmeester, "Structural Diversity in the Strigolactones", *Journal of Experimental Botany*, Vol. 69, No. 9, pp. 2219–2230, 2018.

93. Charnikhova, T. V., K. Gaus, A. Lumbroso, M. Sanders, J.-P. Vincken, A. De Mesmaeker, C. P. Ruyter-Spira, C. Screpanti and H. J. Bouwmeester, "Zealactones. Novel Natural Strigolactones from Maize", *Phytochemistry*, Vol. 137, pp. 123–131, 2017.

94. Schnitzer, T., J. S. Möhler and H. Wennemers, "Effect of the Enamine Pyramidalization Direction on the Reactivity of Secondary Amine Organocatalysts", *Chemical Science*, Vol. 11, No. 7, pp. 1943–1947, 2020.

95. Nikolaienko, T. Y., V. S. Chuiko and L. A. Bulavin, "The Dataset of Covalent Bond Lengths Resulting from the First-Principle Calculations", *Computational and Theoretical Chemistry*, Vol. 1163, p. 112508, 2019.

APPENDIX A: ARTICLES

A.1. Total Synthesis and Biological Evaluation of Zealactone 1a/b

A full-text version of the first article regarding part II is given in this section.

Check for updates

DOI: 10.1002/hlca.202000017 FULL PAPER HELVETICA

Total Synthesis and Biological Evaluation of Zealactone 1a/b

Masahiko Yoshimura,[a] Michael Dieckmann,[b] Pierre-Yves Dakas,[b] Raymonde Fonné-Pfister,[b] Claudio Screpanti,[b] Katrin Hermann,[b] Stefano Rendine,[b] Pierre Quinodoz,[b] Beyza Horoz,[c] Saron Catak,[c] and Alain De Mesmaeker*[b]

[a] Laboratorium für Organische Chemie, Department of Chemistry and Applied Biosciences, ETH Zürich, CH-8093 Zürich, Switzerland
[b] Syngenta Crop Protection AG, Chemical Research, Schaffhauserstrasse 101, CH-4332 Stein, Switzerland, e-mail: alain.de_mesmaeker@syngenta.com
[c] Bogazici University, Department of Chemistry, Bebek, TR-34342 Istanbul, Turkey

Dedicated to Professor *Jacques Lebreton* (University of Nantes, France) for his 60th birthday

Strigolactones are plant hormones, which play pivotal roles in plant growth and development with potential application in sustainable agriculture. Recently, zealactone 1a/b has been identified as the major strigolactone from the root exudates of corn. Although zealactone is a promising molecule affecting signaling in the rhizosphere as well as *in planta*, evaluating its biological activities has been hampered by its low natural abundance and its relative chemical instability. Herein, we present the total synthesis of zealactone 1a/b based on our studies employing a [2 + 2]-cycloaddition strategy and a chemoselective *Baeyer-Villiger* oxidation to forge the γ-butyrolactone fragment. Furthermore, we disclose the biological activities of zealactone 1a/b on corn and in soil in comparison with related synthetic analogues.

Keywords: strigolactone, hormones, total synthesis, ketene addition, soil stability, crop enhancement, sustainable agriculture.

Introduction

Strigolactones are terpenoid-derived natural products acting as plant-signaling molecules, which control several physiological and developmental processes in crops.[1–3] Many of these processes are related to productivity, nutrient assimilation efficiency and resilience to a range of abiotic stresses, like drought or cold. All these positive effects play a pivotal role in the promotion of sustainable agriculture.[4–7] Therefore, strigolactones represent a promising starting point to develop innovative technologies with potential applications for a more sustainable crop production. In nature, several plant species synthesize specific strigolactones. In many cases, they are structurally similar and belong to a class of canonical strigolactones that are composed of tricyclic lactone (*ABC*-rings) with a biologically essential butenolide ring (*D*-ring) (*Figure 1*).[8] Intriguingly, corn seems to produce a completely different type of strigolactones, which are called non-canonical. This suggests that perception and signaling of strigolactones in corn may differ in great

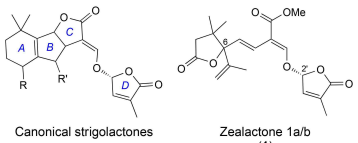

Figure 1. Chemical structure of canonical strigolactones and zealactone 1a/b (**1**).

Supporting information for this article is available on the WWW under https://doi.org/10.1002/hlca.202000017

 © 2020 Wiley-VHCA AG, Zurich, Switzerland

Figure A.1. Article 1.

Helv. Chim. Acta **2020**, *103*, e2000017

extent from other species. Previously, we have identified zealactone 1a/b (**1**) as the most abundant species of corn-derived strigolactones (*Figure 1*).[9] Zealactone 1a/b (**1**) consists of a γ-butyrolactone containing two adjacent quaternary sp^3-carbons, connected to the *D*-ring through a diene-chain. Zealactone has been isolated as 1 : 1-mixture of diastereomers (1a/b) at C(6).

Recently, *Ravazzolo et al.* reported the potential activities of zealactone on seed germination of parasitic weed, *Phelipanche ramosa*, and root development in corn.[10] However, low natural abundance, relative chemical instability and lack of synthetic accessibility of zealactone have hampered in-depth biochemical investigation and a thorough evaluation of potential agronomical applications of this molecule. Herein, we describe the first total synthesis of zealactone 1a/b (**1**) and some related analogues, and disclose data confirming that the mixture of C(6) epimers is formed during its biosynthesis and does not result from an epimerization during its isolation/purification from corn roots. Furthermore, we unveil their bioavailability in soil and biological activity on leaf senescence and seed germination of corn, as well as their affinity for corn strigolactone receptor ZmD14 through *in vitro* assays.

Our retrosynthetic plan consisted of C(3)–C(4)-disconnection of zealactone 1a/b (**1**) leading to vinyl stannane **9** and vinyl iodide **6** by a *Stille* coupling, following our previous work on the synthesis of carlactonic acid (**2**), methyl carlactonoate (**3**) and heliolactone (**7**; *Scheme 1*).[11,12] Vinyl stannane **9** was envis-

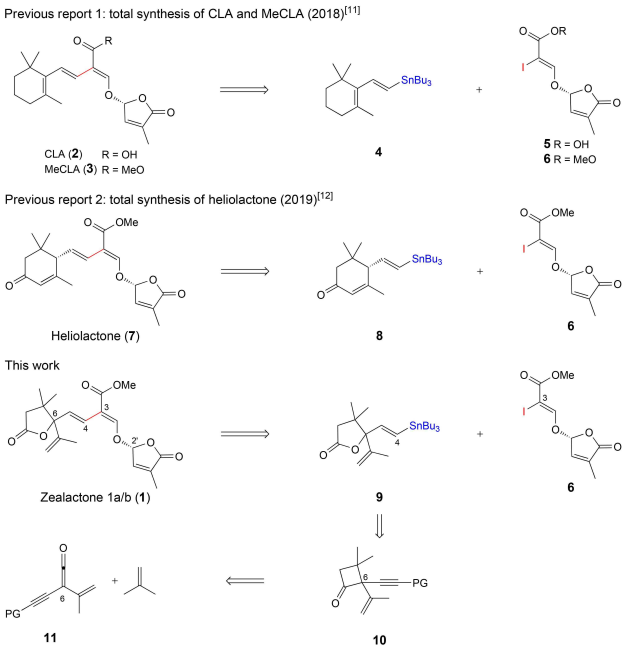

Scheme 1. Retrosynthesis of zealactone 1a/b (**1**).

 © 2020 Wiley-VHCA AG, Zurich, Switzerland

Figure A.1. Article 1. (cont.)

Helv. Chim. Acta 2020, 103, e2000017

aged to arise from hydrostannylation and chemoselective *Baeyer–Villiger* oxidation of cyclobutanone **10** that in turn was planned to be accessible by [2+2] cycloaddition of novel ketene **11** with isobutene as coupling partner. Indeed, **11** would be the first example of vinylacetylenyl ketene and its reactivity towards olefins had to be assessed.

Results and Discussion

Synthesis of ketene precursor, carboxylic acid **16**, started with α-bromination of methyl ester **12** (*Scheme 2*).[13] Subsequent *Sonogashira* coupling of vinyl bromide **13a** with mono-TBS-acetylene resulted in poor yield of the desired enyne **15** employing a variety of conditions[1].[14,15] Fortunately, the analogous vinyl iodide **13b** could be synthesized by carbocupration-iodination of **14** in excellent yield and provided high reactivity in the subsequent *Sonogashira* coupling. Saponification of methyl ester **15** was achieved by using aqueous lithium hydroxide in *tert*-butanol. Concomitant TBS-cleavage could be mostly suppressed if the saponification was stopped after 50–60% conversion, and the recovered starting material was submitted to a second cycle[2].

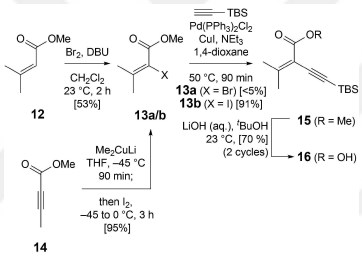

Scheme 2. Synthesis of ketene precursor **16**.

[1]The catalytic systems $PdCl_2(PPh_3)_2$/CuI/piperidine, $PdCl_2(NCPh)_2$/CuI/piperidine and $PdCl_2(PPh_3)_2$/CuI/$BuNH_2$ were tested.

[2]Other tested systems of solvent/water/MOH (solvent: MeOH, THF; base: Li/Na/KH, $Ba(OH)_2$) provided significant amounts of TBS-cleavage and/or 1,4-addition of hydroxide and subsequent *retro*-aldol reaction giving TBS-CC–CH_2CO_2H.

Initial experiments employing highly reactive keteneiminium intermediates with isobutene in [2+2]-cycloadditions revealed incompatibility of keteniminium species with α-alkenyl-substituent as well as α-alkynyl-substituent.

With ketene precursor **16** in hand, we investigated the key [2+2]-cycloaddition, to synthesize the highly functionalized strained cyclobutanone. Inspired by results from *Dreiding* and coworkers[16] using α-vinyl ketene species and olefins in [2+2]-cycloadditions, we attempted the cycloaddition of unprecedented α,α'-vinylacetylenyl ketene **19** with isobutene, a moderately reactive olefinic substrate.[3] Unfortunately, the preliminary results obtained on this reaction led to very low yield of the desired cyclobutanone **25** (*Scheme 3*). The dimers **22** and **23** were isolated as major products, and the reproducibility of the reaction was not optimal.

To optimize the reaction conditions, a liquid and more reactive substrate, methylenecyclopentane, was used as a model coupling partner (*Table 1*).[16] Carboxylic acid **16** was converted to the corresponding acid chloride *in situ* using oxalyl chloride and a catalytic amount of *N,N*-dimethylformamide (DMF), then cycloaddition with methylenecyclopentane was performed by slow addition of the base. The base could trigger the formation of the reactive ketene **19** as well as ammonium enolate **21** depending on the base used (*Scheme 3*). Since ammonium enolate **21** might react with ketene species **19** to form the undesired dimer products **22** and **23**, we investigated the effect of the base on the [2+2]-cycloaddition.[16] At first, to avoid the formation of ammonium enolate, we attempted less nucleophilic bases such as proton sponge, collidine derivative and *Hünig*'s base. Whereas proton sponge and collidine gave the undesired dimer product and no conversion of starting material, respectively, *Hünig*'s base provided the desired product in a moderate yield (*Table 1*, *Entries 1–3*). Recent flow analysis reported that ketene would be formed from the corresponding acyl halide through the corresponding ammonium enolate species.[17] The rate of ketene formation and its potential reaction with the nucleophilic ammonium enolate could profoundly affect the outcome of the desired [2+2] ketene addition on an olefin (*Scheme 3*). Thus, by fine-tuning the nucleophilicity and basicity of trialkylamine, we tried to control the equilibrium between ketene **19** and ammonium enolate **21**. Amongst the trialkylamines we tested, triethylamine showed excellent conversion of carboxylic acid **16** into the desired cyclobutanone **24** in 95% overall yield (*Entry 4*). We also assessed the effect of acyl halide reagents on our [2+2]-cycloadditions. Although the combination of *Ghosez*'s reagent and

© 2020 Wiley-VHCA AG, Zurich, Switzerland

Figure A.1. Article 1. (cont.)

Helv. Chim. Acta **2020**, *103*, e2000017

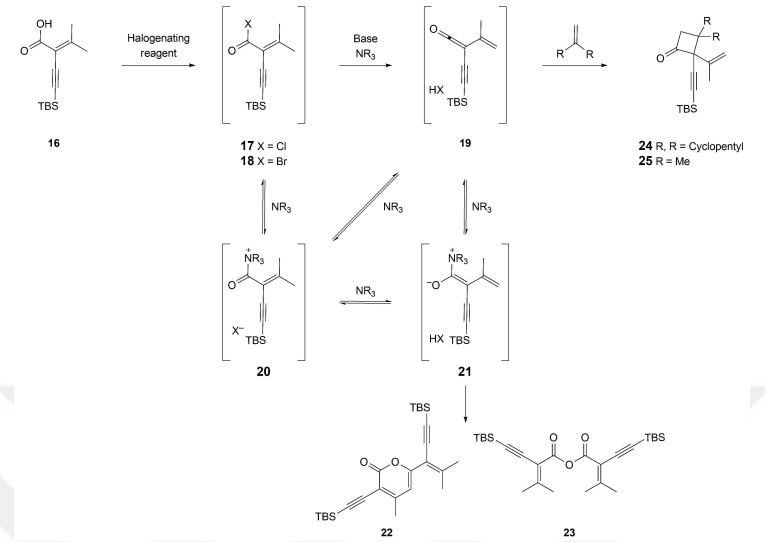

Scheme 3. Plausible intermediates and side products in the [2 + 2] cycloaddition.

triethylamine produced the desired cyclobutanone **24** in 78% overall yield, the reproducibility of these conditions depended on the quality of *Ghosez's* reagent (*Entry 10*). Use of oxalyl bromide also provided the corresponding cyclobutanone **24** through the formation of the corresponding acyl bromide intermediate, but several by-products were observed, which decreased the overall yield (*Entry 11*).

Optimal conditions were then applied to [2 + 2]-cycloaddition with isobutene, which resulted in 23% yield of the desired product due to the lower reactivity of isobutene (*Scheme 4*, Condition: *Table 1*, *Entry 4*). Thus,

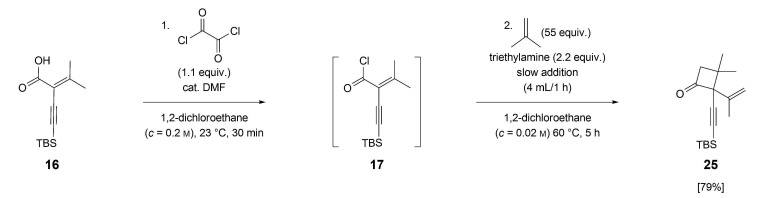

Scheme 4. Optimal conditions of [2 + 2]-cycloaddition with isobutene.

 © 2020 Wiley-VHCA AG, Zurich, Switzerland

Figure A.1. Article 1. (cont.)

Helv. Chim. Acta **2020**, *103*, e2000017

Table 1. Effect of the nature of the acyl halide and of the base.

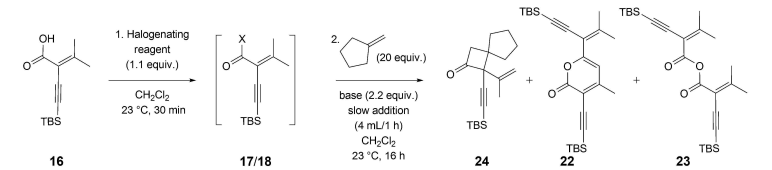

16 **17/18** **24** **22** **23**

Entry	Halogenating reagent[a]	Base	Yield: 24/22/23
1	$(COCl)_2$	proton sponge	trace/major/–
2	$(COCl)_2$	2,6-di-*tert*-butyl-4-methylpyridine	–/–/–
3	$(COCl)_2$	*N*,*N*-diisopropylethylamine	67%/–/–
4	**$(COCl)_2$**	**triethylamine**	**95%**/–/–
5	$(COCl)_2$	*N*-methylmorpholine	56%/–/26%
6	$(COCl)_2$	*N*-methylpiperidine	79%/–/–
7	$(COCl)_2$	*N*-methylpyrrolidine	46%/10%/–
8	$(COCl)_2$	quinuclidine	–/–/–
9	$(COCl)_2$	*N*-ethylpiperidine	88%/–/–
10	*Ghosez*'s reagent	triethylamine	78%/–/–
11	$(COBr)_2$	triethylamine	67%/–/–

[a] Catalytic amount of DMF was used except for *Entry 10*. Proton sponge: 1,8-bis(dimethylamino)naphthalene.

we had to optimize again the conditions and ultimately, we achieved 78% overall yield under diluted conditions at higher temperature (*Scheme 4*). The dilution enabled dissolution of up to 55 equivalents of isobutene into the reaction solution which hampered the undesired dimerization reaction between ketene **19** and ammonium enolate **21**. We reasoned that in addition to the rate acceleration of [2+2]-cycloaddition, higher temperature might speed up the decomposition of ammonium enolate species **21** into ketene **19**. To our delight, these optimal conditions are applicable to the gram scale synthesis of the desired cyclobutanone **25**. Details of the reaction conditions optimization and its application to the large scale synthesis are described in the *Supporting Information* (*Table S1* and *Figure S5*).

A computational study based on density functional theory (DFT) was conducted to elucidate the mechanism in *Scheme 3* by which cyclobutanone **25** is obtained leading to the synthesis of zealactones 1a/b. Moreover, the [2+2] cycloaddition reaction was also modelled to gain insight into the reactivity difference between olefins isobutene (**IB**) and methylenecyclopentane (**MC**) with ketene **19**. All reactions were modelled with the Gaussian 16 program package (G16, Revision A.03).[18] ω-B97X–D long-range corrected density functional, known to give accurate results in kinetics and thermochemistry, was employed.[19] The solvent environment was modeled employing the self-consistent reaction field (SCRF) theory[20] with IEF-PCM[21,22] in dichloromethane (ε= 8.93).

In favor of mimicking the experimental conditions, trimethylamine and trimethylsilyl were used as base and protecting group, respectively. Relative free energies for possible *s-cis* and *s-trans* conformers of carboxylic acid **16′**, intermediate **17′**, **20′**, **21′** and ketene **19′** were calculated and persistent intermediates were reported. Relative free energies for ketene **19′** showed the *s-trans* conformer to be 1.6 kcal mol^{-1} lower in energy than the *s-cis*, which lacks a co-planar structure with respect to its single bond. Free energy of activations for the forward and reverse reactions were reported regarding separate reactants for **TS2** and **TS3**. Due to high polarizability of the chloride ion, free energy of activation for **TS1** was calculated with respect to the pre-reactive ($\Delta G^{\ddagger}_{forward}$= 8.3 kcal mol^{-1}) and product complexes ($\Delta G^{\ddagger}_{reverse}$= 6.9 kcal mol^{-1}) to ensure more accurate energy barriers (*Scheme 5*). Computed free energy of activations show the forward barrier leading to ketene **19′** from ammonium enolate **21′** to be 2.6 kcal mol^{-1} lower than the reverse barrier, hence by controlling this step, the yield of cyclobutanones **24′** and **25′** may be enhanced, hindering the formation of dimers **22′** and **23′**. Note that a concerted mechanism, between ketene **19′** and intermediate **20′**, could not be observed.

 © 2020 Wiley-VHCA AG, Zurich, Switzerland

Figure A.1. Article 1. (cont.)

Helv. Chim. Acta **2020**, *103*, e2000017

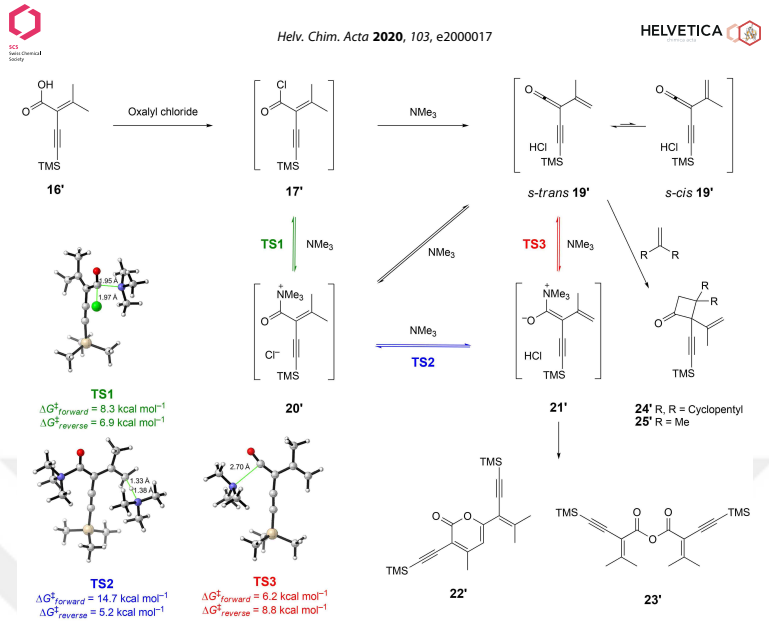

Scheme 5. Plausible intermediates and side products in the [2+2] cycloaddition. Solvent-optimized (IEF-PCM, CH_2Cl_2) transition state structures and relative free energies of activation ($\Delta G^{\ddagger}$) at the ω-B97X-D/6-31+G(d,p) level of theory; free energies in kcal mol^{-1}; critical distances in Å.

The [2+2] cycloaddition reactions of ketene **19′** with olefins isobutene (**IB**) and methylenecyclopentane (**MC**) were modeled at the same level of theory in CH_2Cl_2. Two possible attack faces to ketene **19′** were investigated, the activation free energy for the preferred (less crowded side) attack face, was found to be *ca.* 5 kcal mol^{-1} less than that of the unfavorable attack face (*Figure 2*). There are two consecutive steps in the [2+2] cycloaddition of ketenes, the initial attack of C_3 to C_1 results in the formation of a highly activated intermediate. This step was previously shown to be the rate-determining step for [2+2] cycloadditions,[23] as is the case for the systems studied herein. Subsequently, the C_2–C_4 bond formation generates the desired cyclobutanones **24′** and **25′** (*Figure 2*).

Figure 2 shows free energies of activation and reaction for the [2+2] cycloaddition of **IB** and **MC** with ketene **19′**. Computed results show a notable difference in activation free energies between **IB** and **MC**, $\Delta\Delta G^{\ddagger}_1 =$ 2.8 kcal mol^{-1}. These results agree with the experimental yields of cyclobutanone **25** (23%) and cyclobutanone **24** (95%, *Table 1*). The main difference between the reactivity of the two olefins lies in their HOMO energies ($HOMO_{IB} = -8.907$ eV, $HOMO_{MC} = -8.704$ eV, $\Delta E_{HOMO} =$ 0.203 eV), this is also reflected in the slightly larger critical bond length in $TS1_{MC}$, indicating the earlier nature of the transition state, which leads to a lower barrier (*Figure 2*).

We next investigated the anticipated *Baeyer-Villiger* oxidation using cyclobutanone **24** as model substrate (*Table 2*). Several conditions reported to selectively oxidize ketones to esters in presence of olefins either gave no conversion or full decomposition (*Table 2, Entries 1–3*).[24,25] H_2O_2 in acidic conditions reacted slowly giving desired γ-butyrolactone **26** in low yield after 36 hours (*Entry 4*). Basic conditions using NaOH/H_2O_2 in

 © 2020 Wiley-VHCA AG, Zurich, Switzerland

Figure A.1. Article 1. (cont.)

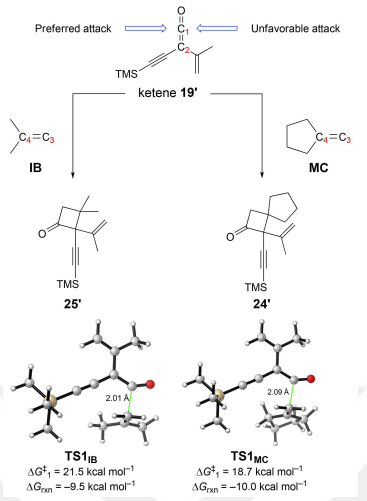

Figure 2. Relative activation ($\Delta G^{\ddagger}$) and reaction free energies (ΔG_{rxn}) for transition state structures of the first step, **TS1$_{IB}$**, **TS1$_{MC}$**, in the [2+2] cycloaddition of isobutene (**IB**) and methylenecyclopentane (**MC**) with ketene **19'**. (ω-B97X-D/6-31+G(d,p) with IEF-PCM in CH_2Cl_2; critical distances in Å; Free energies with respect to separate reactants; all energies relative to *s-trans* ketene **19'**).

ethanol gave **26** in 29% within 30 minutes at room temperature (*Entry 5*). *m*CPBA was found to give different chemoselectivity depending on the base employed (*Entries 6–9*). Whereas without base or in the presence of $NaHCO_3$, the epoxides **27**, **28** were formed in significant amounts besides the desired lactone **26**, NBu_4OH provided high selectivity for lactone formation in 76% isolated yield and only traces of **27** and **28** were formed (*Entry 9*).

The optimized oxidation protocol for cyclobutanone **24** could be applied successfully to cyclobutanone **25** giving γ-butyrolactone **29** in 61% yield, again with high selectivity for lactone formation (*Scheme 6*). TBS-Deprotection using tetrabutylammonium fluoride provided terminal alkyne **30** which was hydrostannylated with $HSnBu_3$ and catalytic amount of AIBN to give the corresponding stannane **9** in high isolated yield and as a single trans isomer. Robust *Stille* coupling conditions with vinyl iodide **6** have been developed previously[11,12] and could also successfully be applied to synthesize zealactone 1a/b (**1**) and its related derivatives. Catalytic system Pd_2dba_3/P(furyl)$_3$ in dioxane at 120 C provided the racemic mixture of **1** in 80% yield (*Scheme 6*). ^{1}H-, ^{13}C-NMR and HR-MS data of our synthetic molecule were in full accordance with natural zealactone 1a/b (*Supporting Information*; *Figures S3* and *S4*).[9] The present synthetic route starting from **14** provided racemic zealactone (**1**) in eight steps (longest linear sequence) with an overall yield of 21%. Since vinyl iodide (*R*)-**6** is readily accessible as enantiomeric pure compound, zealactone 1a/b (**1**) could be synthesized as the naturally occurring C(6)-diastereomeric material (*Scheme 7*, *Supporting Information*; *Figure S7*).[11] Furthermore, vinyl iodide (*S*)-**6** having opposite absolute configuration provided the corresponding C(2') epimer of zealactone (*Scheme 7*, *Supporting Information*; *Figure S10*).

Having this route established, the related analogue **35** could be synthesized adapting the procedure developed for the total synthesis of zealactone 1a/b (**1**). The cyclopentyl lactone **26** could be transformed to the corresponding stannane **34** in excellent yield (*Scheme 8*). Furthermore, *Stille* coupling with vinyl iodide **31** provided the analogues **32** and **36**, the latter having an additional methyl group on the *D*-ring improving its soil stability.

Fortunately, zealactone 1a/b (**1**) could be separated by HPLC on a chiral stationary phase (chiral HPLC) (*Supporting Information*; *Figures S8* and *S9*). ^{1}H- and ^{13}C-NMR analysis prove that the fast moving isomer should be zealactone **1a** and the other is zealactone **1b** (*Supporting Information*; *Figures S3* and *S4*). Stereochemistry of optically pure building blocks **9** and of the corresponding vinyl iodides **47** (*Supporting Information*; *Scheme S1*) could be assigned by the measurement of circular dichroism (CD) spectra coupled with computational simulation, which allowed the determination of the C(6)-configuration of zealactone **1a** and **1b** (*Supporting Information*; *Figures S17–S27*).

The C(6) stereogenic center of zealactone 1a/b (**1**) could undergo epimerization through heterolytic cleavage of the lactone bond leading to the formation of the corresponding carboxylate and the carbocation intermediate **37** highly stabilized by delocalization on the two adjacent allylic moieties. To clarify whether the natural mixture of C(6)-isomers is created in the biosynthetic pathway or during the isolation/purification process, we analyzed the racemization reaction of zealactone **1a** that was purified by chiral HPLC in the aqueous conditions that are used for isolation/purifica-

 © 2020 Wiley-VHCA AG, Zurich, Switzerland

Figure A.1. Article 1. (cont.)

Helv. Chim. Acta **2020**, *103*, e2000017

Table 2. Chemoselective *Baeyer-Villiger* oxidation of **24**.

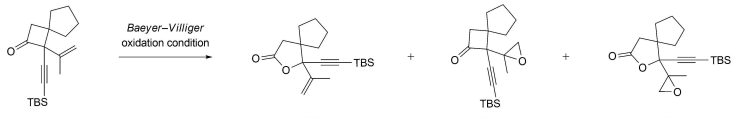

24 **26** **27** **28**

Entry	Conditions	Yield: **26/27/28**
1	$Mg(monoperoxyphthalate)_2$, $MeOH/H_2O$, 50 °C, 24 h	decomp.
2	Oxone, DMF, 23 °C or 50 °C, 36 h	no conversion
3	H_2O_2 (aq.), cat. $Li^+B(C_6F_5)_4^-$, DCE, 23 °C, 24 h	decomp.
4	H_2O_2 (aq.), AcOH, 23 °C, 36 h	20 %/–/–
5	H_2O_2 (aq.), NaOH, EtOH, 23 °C, 30 min	29 %/–/–
6	*m*CPBA, CH_2Cl_2, 23 °C, 24 h	–/15 %/45 %
7	*m*CPBA, $NaHCO_3$, CH_2Cl_2, 23 °C, 24 h	15 %/13 %/16 %
8	*m*CPBA (1.5 equiv.), NBu_4OH (2.0 equiv.), CH_2Cl_2/MeOH, 23 °C, 1 h	65 %/–/–
9	*m*CPBA (4.0 equiv.), NBu_4OH (5.0 equiv.), CH_2Cl_2/H_2O, 23 °C, 1 h	76 %/–/–

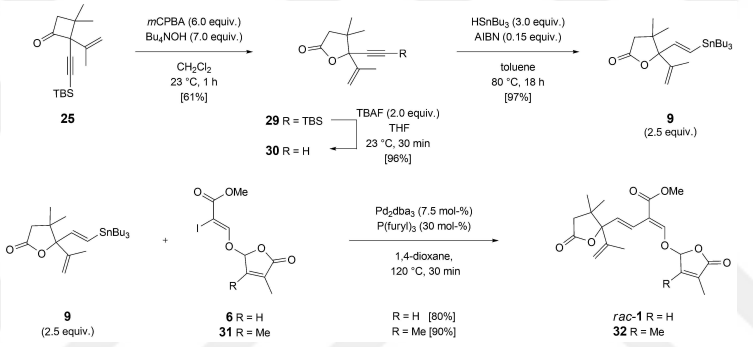

Scheme 6. Synthesis of a mixture of all four stereoisomers of zealactone 1a/b (**1**).

tion of natural zealactone. Zealactone **1a** did not epimerize in organic solvents within seven days at room temperature and can be stored without alteration for biological testing (*Table 3*, *Entries 1* and *2*). Some degradation of zealactone **1a** was observed under aqueous conditions. However, no racemization was detected for at least seven days under the buffered conditions used for the isolation of zealactone from corn roots (*Entries 3–5*, *Supporting Information*; *Figures S13–S16*).[9] In addition, no epimerization at C(6) was detected in the presence of 1 % formic acid in H_2O/MeCN, the conditions used for zealactone HPLC purification after root extraction.[9] These findings suggest that both C(6)-isomers are synthesized *in planta*. A plausible biosynthetic pathway depicting how the mixture of C(6)-isomers could be generated is described in *Scheme 9*.[9] Unselective epoxidation of compound **41** followed by fragmentation or epimerization of compound **43*** generated after asym-

 © 2020 Wiley-VHCA AG, Zurich, Switzerland

Figure A.1. Article 1. (cont.)

Helv. Chim. Acta **2020**, *103*, e2000017 HELVETICA

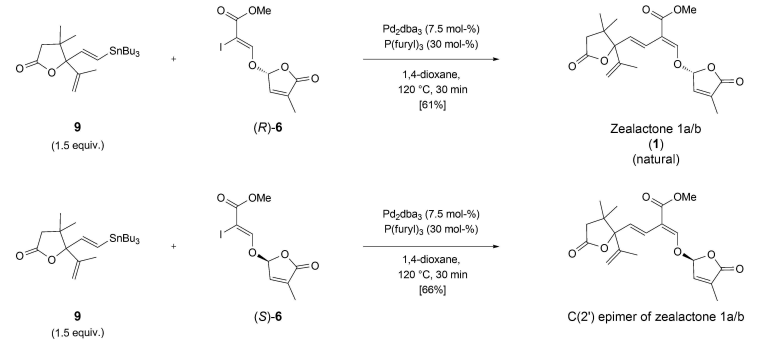

Scheme 7. Synthesis of natural zealactone 1a/b (**1**) and C(2') epimer of zealactone.

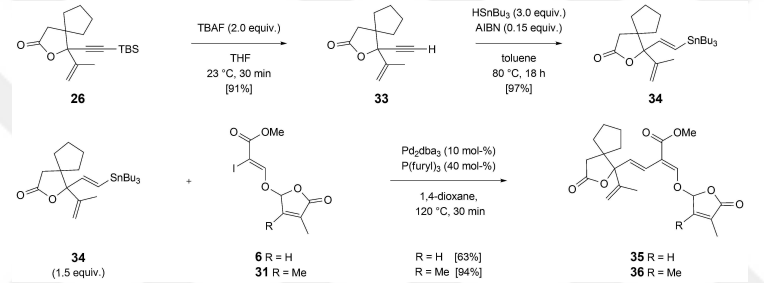

Scheme 8. Synthesis of zealactone analogues.

metric epoxidation could provide the epimeric mixture **43**, leading to zealactone **1a** and **1b**.

With the series of zealactone analogues in hand, we evaluated their biological activity against corn and their stability in soil.

In *Arabidopsis thaliana*, the mechanism of action of strigolactone has been well studied, and two essential genes *DWARF14* (*D14*) and *MORE AXILLARY GROWTH2* (*MAX2*) play a significant role in the strigolactone-dependent plant responses.[26,27] These genes encode a family of α/β-hydrolase fold proteins and a F-box protein of ubiquitin E3 ligase, respectively. The plausible molecular mechanism of strigolactone signaling is depicted in *Figure 3,A*. Binding of strigolactone to the receptor protein D14 initiates the strigolactone signaling.[28] Conformational change of D14 after strigolactone binding facilitates formation of the complex with MAX2 protein, which triggers the ubiquitination of specific repressors followed by their proteasomal degradation.[29,30] This promotes the strigolactone-responsive genes affecting plant growth and development.[31–33]

Since the strigolactone perception by D14 protein triggers the activation of strigolactone signaling *in planta*, we assessed the binding affinity of synthetic compounds to ZmD14 (D14 orthologue in corn). Several

 © 2020 Wiley-VHCA AG, Zurich, Switzerland

Figure A.1. Article 1. (cont.)

Helv. Chim. Acta 2020, 103, e2000017

Table 3. Potential epimerization of zealactone **1a**.

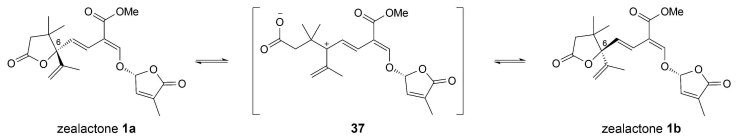

Entry	Conditions	pH	$t_{1/2}$	Epimerization
1	CH_2Cl_2	–	No decomp.	No
2	CH_3CN	–	No decomp.	No
3	H_2O/CH_3CN (9/1)	7.0	5 days	No
4	$^1/_2$ strength *Hoaland* solution with 10% MeCN (extraction cond.)	5.8	>1 week	No
5	H_2O/MeCN (9:1) with 1% formic acid (purification cond.)	2.3	22 h	No

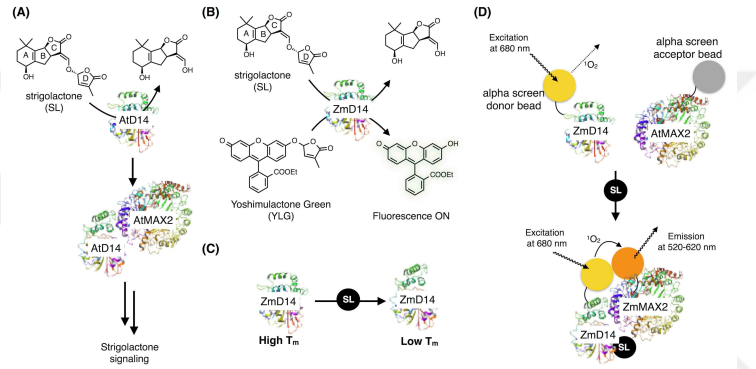

Figure 3. Molecular mechanism of strigolactone signaling and our *in vitro* assays. A) Molecular mechanism of strigolactone signaling in *Arabidopsis thaliana*. B) YLG displacement assay. The binding affinity of small molecules can be evaluated by the decrease of the YLG-dependent fluorescence. C) DSF assay. The strigolactone-induced conformational change of ZmD14 can be measured by the thermal shift of ZmD14 denaturation temperature. D) Alpha screen assay. The strigolactone-induced association of ZmD14 and ZmMAX2 can be detected by the emission at 520–620 nm. At and Zm mean *Arabidopsis thaliana* and *Zea maize*, respectively.

technologies for assessing the binding activity of small molecules to D14 have recently been developed. Yoshimulactone Green (YLG) is a useful molecular tool that can generate a strong fluorescent product upon the hydrolysis by ZmD14.[34] The competitive inhibition of YLG-hydrolysis allows the evaluation of the binding affinity of our synthetic molecules to ZmD14 (*Figure 3,B*).[12,35]

The racemic mixture of zealactone 1a/b (**1**) has comparable activity to heliolactone (**7**) and methyl carlactonoate (MeCLA) (**3**) (*Table 4*). Interestingly, spirocyclopentyl substituted analogue of zealactone **35** shows the better binding affinity to ZmD14 in comparison to zealactone. Introduction of additional methyl group on the butenolide moiety reduces the binding activity to the receptor protein as previously observed.[12] Although the configuration at C(2′) in zealactone 1a/b (**1**) was still

 © 2020 Wiley-VHCA AG, Zurich, Switzerland

Figure A.1. Article 1. (cont.)

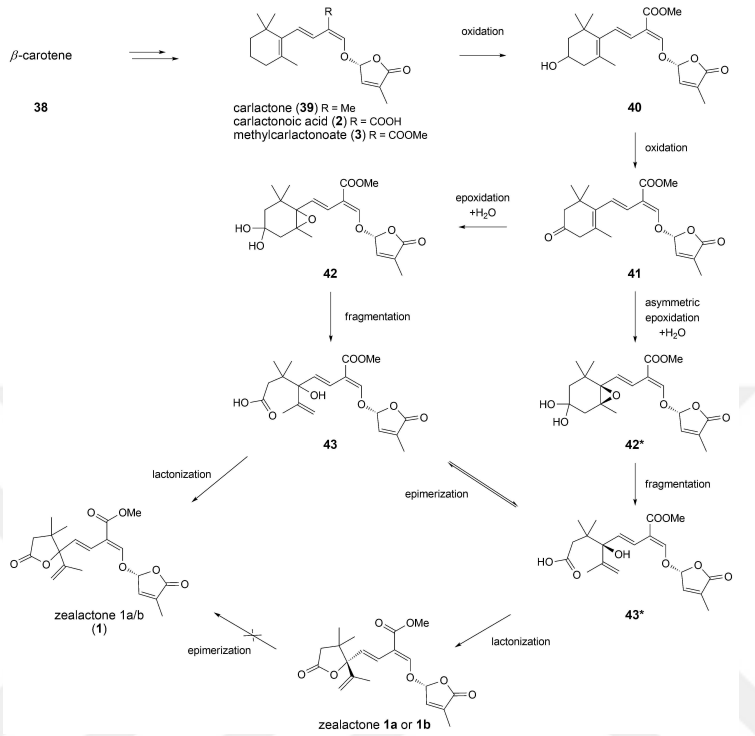

Scheme 9. Plausible biosynthetic pathway of zealactone 1a/b (**1**).

ambiguous, it was assumed to be (*R*)-configured in analogy with typical C(2′)-configuration of natural strigolactones.[9] The YLG displacement assay showed that (*R*)-C(2′) diastereoisomers of zealactone (**1**) is much more active than the others, which confirms that (*R*)-C(2′) isomers are the natural ones of zealactone 1a/b (**1**). These findings are supported by another analysis, differential scanning fluorometry (DSF) (*Figure 3,C*).[36] We also evaluated small molecule induced ZmD14 to ZmMAX2 interaction by alpha screen analysis (*Figure 3,D*). The obtained results are well consistent with the binding affinity to the receptor protein supported by the YLG displacement assay and the DSF. Altogether, our synthetic zealactone and its analogues can induce the conformational change of ZmD14 upon their binding then promote the association of ZmD14 with ZmMAX2, which might effectively activate the signal transduction *in planta*.

The putative binding mode of zealactone **1a** and **35** to ZmD14 was assessed through molecular modelling

 © 2020 Wiley-VHCA AG, Zurich, Switzerland

Figure A.1. Article 1. (cont.)

Helv. Chim. Acta **2020**, *103*, e2000017

Table 4. The half inhibition concentration (IC_{50}) of compounds against the ZmD14 dependent YLG hydrolysis, the compound-induced thermal shift of ZmD14 denaturation temperature in DSF assay and the relative value of compound-induced association of ZmD14 and ZmMAX2 in alpha screen assay.

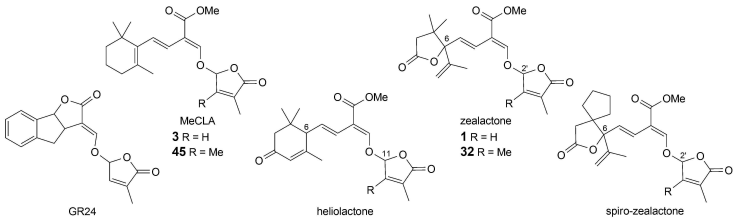

Structures	R	Configuration	Compound[a]	YLG displacement assay [IC_{50}/μM][b]	DSF analysis [ΔT_m/ C][c]	Alpha screen[d]
GR24[e]	–	mixture of all four stereoisomers	**44**	1.76	−4.4	4.54
MeCLA	H	*racemic*	**3**	1.10	–	4.01
	Me	*racemic*	**45**	4.81	–	2.26
heliolactone	H	mixture of all four stereoisomers	**7**	1.35	–	5.60
	H	**(6*S*,11*R*)**	**7**	**0.30**	**−8.0**	**5.14**
	H	(6*R*,11*R*)	**7**	0.29	−8.0	4.91
	H	mixture of (*S*)-*C*(11) diastereomers	**7**	3.35	−0.5	0.90
	Me	mixture of all four stereoisomers	**46**	2.53	–	3.52
zealactone	H	mixture of all four stereoisomers	**1**	1.30	−3.7	4.88
	H	**mixture of (*R*)-C(2′) diastereomers**	**1**	**0.59**	**−3.9**	**6.13**
	H	mixture of (*S*)-*C*(2′) diastereomers	**1**	32.42	−0.2	0.93
	Me	mixture of all four stereoisomers	**32**	2.14	−3.9	5.30
spiro-zealactone	H	mixture of all four stereoisomers	**35**	0.72	−1.4	5.69
	H	mixture of (*R*)-*C*(2′) diastereomers	**35**	0.39	−4.6	5.13
	Me	mixture of all four stereoisomers	**36**	1.99	−3.7	5.45

[a] The analytic data of **44**, **3**, **45**, **7** and **46** were referenced from our previous report[12]. [b] 1 μM of YLG was used for the YLG displacement assay. [c] 50 μM of each compound were used for the DSF analysis. [d] The values mean relative activity score (higher value means stronger interaction). [e] GR24 is a most commonly used synthetic strigolactone. Natural isomers of heliolactone and zealactone were highlighted by bold fonts.

studies. A homology model for ZmD14 (Uniprot accession number A0 A317YGV1) was built with MODELLER,[37] using the crystal structure of rice D14 (PDB 3 W04) as template. Zealactone **1a** was docked into the active site using the software GOLD.[38] The butenolide ring of zealactone **1a** establishes a hydrogen bond with the backbone of Phe26, located next to the catalytic Ser95 at the bottom of the active site (*Figure 4,A*). The (*R*)-C(2′) diastereoisomer orients the rest of the molecule in a way to establish a hydrogen bond network with surrounding

 © 2020 Wiley-VHCA AG, Zurich, Switzerland

Figure A.1. Article 1. (cont.)

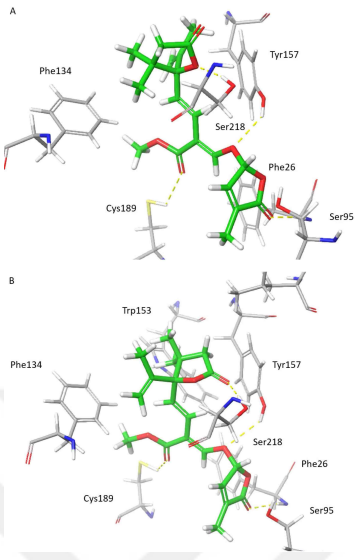

Figure 4. Docking pose of zealactone 1a/b in the active site of corn ZmD14 receptor. Hydrogen bonds are represented in dotted yellow lines. A) Docking pose of zealactone **1a**. B) Docking pose of zealactone **1b**.

amino acids. In this binding conformation, the carbonyl ester interacts with Cys189, whereas the oxygens of the vinyl ester and the γ-butyrolactone (*A*-ring) interact with the sidechains of Tyr157 and Ser218, respectively. This specific hydrogen bond pattern is only found for the (*R*)-C(2′) diastereoisomers, possibly explaining the affinity difference between (*R*)-C(2′) and (*S*)-C(2′) diastereomers observed in our *in vitro* analysis. The *gem*-dimethyl group of zealactone **1a** extends at the edge of the active site in a hydrophobic environment, leaving additional room for the spiro-cyclopentyl analogue. Such structural modification allows the spiro-cyclopentyl moiety of zealactone **35** to establish further *van der Waals* contacts with Phe134, leading to a slight improvement in binding affinity, consistently with YLG displacement assay. The docking of zealactone **1b** (*Figure 4,B*) shows a binding mode in line with that of zealactone **1a**, with a similar hydrogen bond network with Phe26, Cys189 and Tyr157. The change in configuration at the *A* ring leads to a different orientation of the γ-butyrolactone at the wide entrance of the binding cavity but doesn't affect its overall binding. In this case, Ser218 interacts with the carbonyl oxygen of the γ-butyrolactone, whereas the gem-dimethyl faces Trp153, leaving additional room for the spiro-cyclopentyl derivative to bind.

We next assessed our synthetic zealactone derivatives for impact on promotion of corn leaf senescence and stimulation of corn seed germination.

Leaf senescence is self-attrition system to relocate nutrients from aging leaves that are no longer required to newly developing plant tissues. Since leaf senescence is associated with crop productivity, chemical controlling leaf senescence enables accelerating nutrients relocation, which leads to optimization of grain quality and quantity.[39] Leaf senescence is regulated by several plant hormones and it has recently been reported that strigolactones can also accelerate leaf senescence through the D14-dependent pathway.[40–42] Herein, we assessed synthetic non-canonical strigolactones induced leaf senescence of corn by following the previously developed protocol.[12] As shown in *Table 5*, corn leaf senescence was activated by the treatment of our synthetic zealactone derivatives except for (*S*)-C(2′) diastereoisomers of zealactone (**1**). Their activities are well correlated with the binding affinity to ZmD14. The *A*-ring structure of non-canonical strigolactones affects the promotion of leaf senescence in corn. Zealactone scaffolds have a better activity on leaf senescence than heliolactone and MeCLA, and the spiro-cyclopentyl substituted zealactone showed the highest activity among non-canonical strigolactones. Since precisely chemical control of nutrients remobilization enables the optimization of grain productivity, senescence control with our developed molecules would be an innovative technology towards sustainable agriculture.

Controlling seed germination and plant growth in early stage largely contributes to the improvement of crop production. Breaking the seed dormancy is triggered by several phytohormones and environmental factors.[43] Strigolactones are well known as a germination stimulant of parasitic weeds,[44] and can also activate the seed germination of various species and even of crops.[43,45–47] Next we investigated our synthetic zealactones on the germination of corn at 15 C which is a mimic temperature of an agronomically relevant soil. Two different kinetic parameters, the speed (T_{50}) and uniformity (slope), were extracted from the kinetic curve of seed population germination. In addition to rates of

 © 2020 Wiley-VHCA AG, Zurich, Switzerland

Figure A.1. Article 1. (cont.)

Helv. Chim. Acta **2020**, *103*, e2000017

Table 5. The half maximal senescence acceleration concentration (SC_{50} in μM) measured for corn leaf discs treated with our synthetic molecules.

Structures	R	Configuration	Compound[a]	Leaf senescence (SC_{50} [μM])
GR24	–	mixture of all four stereoisomers	**44**	0.1
MeCLA	H	*racemic*	**3**	1.8
	Me	*racemic*	**45**	7
heliolactone	H	mixture of all four stereoisomers	**7**	0.8
	Me	mixture of all four stereoisomers	**46**	0.09
zealactone	H	mixture of all four stereoisomers	**1**	0.14
	H	**mixture of (*R*)-C(2′) diastereomers**	**1**	**0.17**
	H	mixture of (*S*)-C(2′) diastereomers	**1**	7.1
	Me	mixture of all four stereoisomers	**32**	0.15
spiro-zealactone	H	mixture of all four stereoisomers	**35**	0.04
	H	mixture of (*R*)-C(2′) diastereomers	**35**	0.058
	Me	mixture of all four stereoisomers	**36**	0.43

[a] The data of **3**, **45**, **7** and **46** were referenced from the previous reported manuscript.[12] Natural isomer of zealactone was highlighted by bold fonts.

seed germination, the speed of primary root growth after emergence was studied (*Figure 5*).

As shown in *Table 6*, all strigolactones we tested accelerated the seed germination of corn in comparison with untreated control. Regarding the speed and uniformity in the corn seed germination, non-canonical type strigolactones are much more active than GR24 (**44**). Interestingly, the series of zealactone analogues effectively shortened the time required for the seed population germination compared to MeCLA and heliolactone analogues. In addition, the zealactone analogues have a comparable activity to MeCLA on the parameter of germination homogeneity. Amongst non-canonical strigolactones tested, analogues that have an additional methyl group on *D*-ring showed the better accelerating activity on both factors of corn germination compared with the corresponding mono methyl *D*-ring molecules, which might be due to their improved stability. As we mentioned above, the binding affinity of (*S*)-C(2′) diastereomers of zealactone (**1**) to ZmD14 is quite low. Nevertheless, (*S*)-C(2′) diastereomers of zealactone (**1**) can also stimulate the seed germination of corn at the same level of (*R*)-C(2′) diastereomers of zealactone (**1**), which suggests that (*S*)-C(2′) diastereomers of zealactone (**1**) activates the corn seed germination through non-ZmD14 signaling pathway and might indicate that strigolactone-dependent seed germination of corn is not only regulated by the ZmD14-dependent pathway.

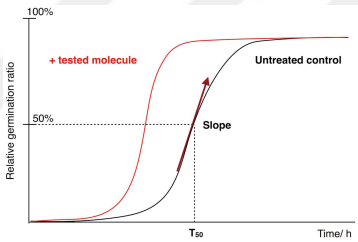

Figure 5. Kinetic curves of seed germination in the presence (red line) or absence (black) of small molecule. T_{50} value means the time point at the 50% seed population germination and was calculated from the logistic germination curve. The slope value was determined at the point of T_{50} in the logistic germination curve. All the values in *Table 6* are expressed as percentages compared to an untreated control.

Whereas natural isomers of strigolactones, which have (*R*)-C(2′) configuration at the *D*-ring, do not regulate the primary root growth after emergence, the opposite epimer showed significant effect on the primary root growth. (*S*)-C(2′) epimer of zealactone (**1**) and (*S*)-C(11) epimer of heliolactone (**7**) have the strongest primary corn root growth enhancing and suppressing activity, respectively. Apparently, the structure–activity relationship of our synthetic molecules on the primary root growth is not correlated with the *in vitro* binding affinity to ZmD14, the leaf senescence activity and the seed germination activity. These findings might suggest that the primary root growth after emergence is regulated on a separate way from the signaling of seed germination and ZmD14-dependent signaling. Interestingly, our

 © 2020 Wiley-VHCA AG, Zurich, Switzerland

Figure A.1. Article 1. (cont.)

Table 6. Effect of non-canonical strigolactones on the germination and on the root growth kinetic parameters of corn at various concentrations and 15 C.

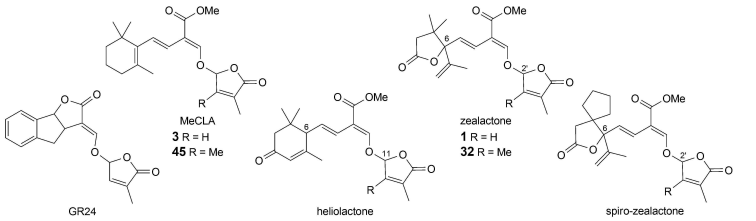

Structures	R	Chirality	Compound[a]	Germination T_{50} (% compared to control)[c]		Germination slope (% compared to control)[b]		Primary root growth slope (% compared to control)	
				50	250	50	250	50	250
GR24	–	mixture of all four stereoisomers	**44**	–	−3.4	–	50.4	–	–
MeCLA	H	*racemic*	**3**	−1.0	**−7.6**	10.9	**158.4**	3.8	**3.9**
	Me	*racemic*	**45**	**−2.8**	**−7.1**	**36.5**	**135.3**	**7.5**	**6.6**
heliolactone	H	mixture of all four stereoisomers	**7**	**−2.7**	**−8.6**	23.8	**101.5**	−0.2	−2.2
	H	**(6*S*,11*R*)**	**7**	−2.9	**−8.7**	**25.5**	**96.1**	1.3	−5.0
	H	(6*R*,11*R*)	**7**	−2.7	**−9.0**	**34.6**	**11.2**	−5.3	−3.7
	H	mixture of (*S*)-C(11) diastereomers	**7**	**−4.7**	**−9.1**	**23.9**	**118.3**	−5.7	**−13.4**
	Me	mixture of all four stereoisomers	**46**	**−4.2**	**−7.9**	**38.0**	**132.9**	5.7	−5.1
zealactone	H	mixture of all four stereoisomers	**1**	**−3.0**	**−12.0**	11.9	**116.8**	4.4	8.6
	H	**mixture of (*R*)-C(2′) diastereomers**	**1**	**−4.3**	**−12.0**	**39.8**	**119.0**	−0.2	7.3
	H	mixture of (*S*)-C(2′) diastereomers	**1**	**−5.3**	**−13.0**	9.5	**120.8**	**12.2**	**15.2**
	Me	mixture of all four stereoisomers	**32**	**−6.6**	**−13.5**	**31.7**	**149.3**	5.8	−1.9
spiro-zealactone	H	mixture of all four stereoisomers	**35**	**−8.0**	**−10.3**	17.4	**63.4**	0.1	1.4
	H	mixture of (*R*)-C(2′) diastereomers	**35**	**−7.2**	**−11.6**	**29.9**	**101.4**	1.8	−2.8
	Me	mixture of all four stereoisomers	**36**	**−8.4**	**−9.8**	**27.2**	**114.3**	4.8	−9.1

[a] The data of **44**, **3**, **45**, **7** and **46** were referenced from the previous reported article.[12,48] [b] Positive values mean a more homogeneous germination and *vice versa* for negative values. [c] Positive values mean a slower germination and *vice versa* for negative values. Data in bold are statistically validated.

synthetic molecules (*S*)-C(2′) diastereomers of zealactone (**1**) and (*S*)-C(11) diastereomers of heliolactone (**7**) work as an agonist and antagonist of this signaling pathway, respectively, which could be useful molecular tools for elucidating the signaling pathway of the primary root growth. In addition, (*S*)-C(2′) diastereomers of zealactone (**1**) showed the effective stimulation on the seed germination and the acceleration of the plant growth in early stage, which can be a promising lead molecule enhancing crop productivity.

In our previous work, we demonstrated that natural and close synthetic analogs of strigolactones can have a short half-life in soil, as short as a few hours.[12,49] Soil half-life is an important chemodynamic property of the molecule and provides indication whether compounds are stable enough and sufficiently long bioavailable in soil to deliver a given desirable biological activity. This represents an important technical attribute for practical application. In previous investigations, we showed also that specific structural changes/substitutions in various parts of the core scaffold of a natural strigolactone like heliolactone can improve their stability.[12] These findings suggested that we could optimize by structural modification the soil persistence of strigolactones. Due to the interesting *in vivo* and *in vitro* activities of zealactone, we were strongly interested to evaluate whether this specific

 © 2020 Wiley-VHCA AG, Zurich, Switzerland

Figure A.1. Article 1. (cont.)

corn strigolactone and other close derivatives were sufficiently stable in soil under laboratory conditions.

The *Table 7* reports the soil half-life of a series of non-canonical strigolactones. An estimated value of Log *P* is reported as well. Log *P* is an intrinsic property of the molecules which provides some indirect indications regarding how strongly the molecule can be bound to soil particles, especially to the organic matter fraction. For comparison purposes, alongside the zealactone (**1**) and its derivatives we also reported the soil half-life of heliolactone (**7**), MeCLA (**3**) and others close analogs disclosed in a previous study.[12] A soil stability ratio has been defined to compare the soil stability of all these compounds with GR24 (**44**). These results confirm the short soil persistence of strigolactones. All tested compounds showed a soil half-life shorter than ten hours. In this study we observed a low recovery of zealactone (**1**) already at the timing zero where we were able to extract less than one fourth of the initial treated amount. For this reason, we were not able to calculate reliably the soil half-life of zealactone. Thus, this experimental data suggests that zealactone (**1**) degrades quickly. Interestingly, the zealactone derivatives **32**, **35**, **36** displayed slightly higher stability in soil. As already observed for the heliolactone (**7**) and its derivative **46**, an additional methyl group on the *D*-ring led to a substantial increase of the soil half-life by a factor six or more. Similarly, the spiro-zealactone derivative **35**, **36** with a cyclopentyl substitution increased the soil half-life. It is noteworthy that the combined substitutions of both cyclopentyl group and additional methyl on the *D*-ring did not result in further improvement of the soil stability. Most likely other parts of the core scaffold can be still prone to metabolism, like for instance the methyl ester which might undergo hydrolysis.

All together, these results confirm the labile nature of strigolactones in soil. This can have implications for the practicability of using strigolactones in agriculture. Despite the highly intrinsic biological activity of strigolactones, for agronomical applications the improvement

Table 7. Log *P* and soil half-life of non-canonical strigolactones in a non-sterile soil.

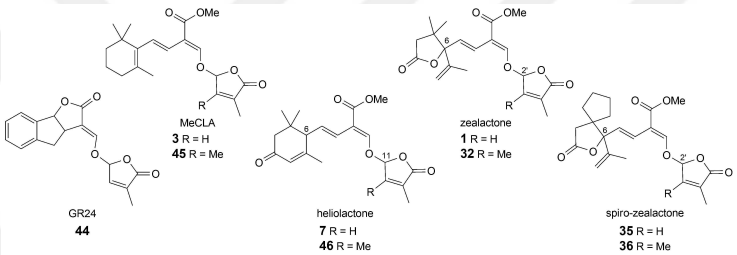

Structures	R	Compound[a]	Log *P*[b]	$t_{1/2}$ [h]	r^2	Soil Stability Ratio[c]	Remarks
MeCLA	H	**3**	4.48	10.5	0.88	3.1	Data from a previous study[12]
	Me	**45**	4.57	27.0	0.62	7.9	Data from a previous study[12]
heliolactone	H	**7**	3.23	2.5	0.99	0.7	Data from a previous study[12]
	Me	**46**	3.38	9.7	0.99	1.0	Data from a previous study[12]
zealactone	H	**1**	2.8	–	–	–	Very low recovery at T_0 (*i.e.*, 23%) did not allow to estimate the $t_{1/2}$, suggesting the compounds is highly unstable
	Me	**32**	3.0	7.56	0.85	5.9	–
spiro-zealactone	H	**35**	3.3	6.47	0.97	5.1	–
	Me	**36**	3.5	7.81	0.85	6.1	–

[a] All tested compounds are racemic mixture. [b] The log *P* values were calculated. [c] Soil stability ratio is the quotient of the measured soil half-life of the non-canonical strigolactone divided by the $t_{1/2}$ of the GR24 (**44**) measured in the same study, 3.4 h in a previous study[12] and 1.3 h in the present study.

 © 2020 Wiley-VHCA AG, Zurich, Switzerland

Figure A.1. Article 1. (cont.)

Helv. Chim. Acta **2020**, *103*, e2000017 HELVETICA

of soil stability remains critical. More stable compounds would allow the use of very low doses in the field and keep the synthetic costs per hectare sufficiently low to make this technology affordable for growers.

Conclusions

In conclusion, a total synthesis of zealactone 1a/b (**1**) has been developed providing this most abundant strigolactone from the root exudates of corn in eight steps (longest linear sequence) and an overall yield of 21%. As key-transformations a [2+2]-cycloaddition strategy using an unprecedented type of ketene could be employed followed by a chemoselective *Baeyer–Villiger* oxidation to synthesize the challenging γ-butyrolactone fragment. Our novel procedure also allowed the synthesis of closely related analogues.

Taking all these results together, we could confirm that strigolactones represent a promising area with many potential applications in agriculture. As we expected, the unique structure of zealactone 1a/b (**1**) as non-canonical strigolactones gave some specificity to the perception and signaling in corn, compared with other non-canonical type strigolactones studied in the past. The *in vitro* results showed that zealactone and its close derivatives were as active as or even more active than GR24 (**44**). Consequently, zealactone could be a lead candidate for optimization. For instance, we have demonstrated that slight changes/substitutions in the core chemotype led to an increase of *in vitro* and *in vivo* activity in relevant assays and a general improvement of soil stability. In the optic of a more sustainable crop production, synthetic derivatives closely inspired by natural corn strigolactones like zealactone could play a critical role.

Experimental Section

General Experimental Procedures

All chemicals and solvents were purchased from common suppliers and used as received. Chromatographic purifications were done on an R_f-machine *CombiFlash Rf 200i Teledyne ISCO* equipped with standard silica columns (silica gel *60*, 0.040–0.063 mm: *CHROMABOND®* Flash from *MACHEREY-NAGEL* or silica gel *60*, 0.015–0.040 mm: *RediSep®Rf GOLD* from *Teledyne ISCO*). Thin-layer chromatography was performed on precoated TLC glass plates *SIL G-254* or precoated TLC sheets *ALUGRAM SIL G-UV254* with fluorescence indicator UV_{254}. Staining agents were either $KMnO_4$ (40 g of K_2CO_3+6 g of $KMnO_4$ in 600 mL of water, then 5 mL of 10% NaOH added) or CAM (2 g $Ce(SO_4)_2$+60 g $(NH_4)_6Mo_7O_{24}\cdot 4\,H_2O$ in 360 mL of water, then 40 mL of H_2SO_4 conc added) and subsequent heating of TLC plates treated with these staining solutions. ^{1}H- and ^{13}C-NMR spectra were recorded on a *Bruker* spectrometer operating at 600 or 400 and 150 or 100 MHz, respectively, unless otherwise stated. Chemical shifts are given in ppm. The following abbreviations describe the *multiplets*: *s*, *singlet*; *d*, *doublet*; *dd*, *doublet* of *doublets*; *t*, *triplet*; *q*, *quadruplet*; *quint*, *quintet*; *sext*, *sextet*; *m*, *multiplet*. Mass spectra were recorded on a High Resolution Mass Spectrometer (*Q-Exactive*, *Orbitrap* analyzer) from *Thermofischer* equipped with an electrospray source, (Polarity: positive mode, Capillary: 3.8 kV, Capillary temperature: 320 C, S-lens RF level: 55, Sheath gas flow rate: 40, Mass range: 100 to 1000 *m/z*) coupled to a 1200 *Infinity* series UPLC from *Agilent*: Solvent degasser, binary pump, heated column compartment and diode-array detector (DAD). DAD Wavelength range [nm]: 190 to 400. Column: Waters Acquity UPLC BEH C18, 1.7 µm, 50×2.1 mm, Temp: 60 C. Solvent Gradient: *A*=water+5% MeOH+0.05% HCOOH, *B*=Acetonitrile+0.05% HCOOH. Infrared spectra were recorded on a *Perkin Elmer UATR two* FI-TR spectrometer. Melting points were measured on a *Büchi Melting Point B-540* apparatus. The CD measurements were performed on a *JASCO J-1500* CD Spectrophotometer in MeCN at 20 C in a *1115F-QS Hellma* cuvette (10 mm light path) with a scan rate of 50 nm/min. All solutions were prepared and measured under air saturated conditions if not otherwise stated. ZmD14 (Zm00001d048146), a maize orthologue of the Arabidopsis strigolactone receptor D14, was expressed as a *N*-terminal 6x His-SUMO fusion protein by cloning into the pET-SUMO vector (*Thermo Scientific*) which was used to transform *E. coli* One Shot BL21(DE3) cells (*Thermo Fisher Scientific*). For expression of ZmMAX2 (Zm00001d045313), the full-length sequence was codon-optimized for *E. coli* and gene synthesized as an *N*-terminal maltose binding protein (MBP)-TEV fusion which was inserted into a pET-DUET expression vector. Expression was carried out in *E. coli* BL21 Star (DE3) using auto-induction media. For purification, cells were lysed using a cell disruptor and the clarified lysate was applied to a 1 mL *MBPTrap* column (*GE Healthcare*) equilibrated in 5 mL PBS, 150 mM NaCl, 0.5 mM TCEP, pH 7.4. The column was washed with 20 ml of the same buffer and bound protein was eluted using PBS pH 7.4, 150 mM NaCl, 0.5 mM TCEP, 10 mM D-maltose monohydrate. Elution fractions were analyzed by SDS-PAGE and those containing the

 © 2020 Wiley-VHCA AG, Zurich, Switzerland

Figure A.1. Article 1. (cont.)

protein of interest were pooled and loaded onto a *Superdex 200 16/60* column equilibrated in PBS, 150 mM NaCl, 0.5 mM TCEP, pH 7.4. Fractions containing the target protein were re-applied to the MBPTrap column equilibrated in PBS, 150 mM NaCl, 0.5 mM TCEP, pH 7.4 and eluted with a linear gradient over 10 mL of the same buffer containing 10 mM D-maltose monohydrate. Samples were stored at −80 C until use.

Methyl 2-Iodo-3-methylbut-2-enoate (**13b**). To a suspension of copper iodide (388 mg, 2.04 mmol, 2.00 equiv.) in THF (5.00 mL) under argon atmosphere at 0 C was added methyl lithium (1.6 M in Et_2O, 2.50 mL, 4.08 mmol, 4.00 equiv.). The obtained clear colorless solution was cooled to −45 C and a solution of methyl but-2-ynoate (100 mg, 1.02 mmol, 1.00 equiv.) in THF (5.00 mL) was slowly added. The opaque white solution was stirred for 90 min at −45 C, molecular iodine (776 mg, 3.06 mmol, 3.00 equiv.) as a solution in THF (3.00 mL) was slowly added and the clear yellowish solution was stirred for 1 h at −45 C, afterwards 2 h at 0 C. Aqueous saturated solutions of NH_4Cl (10.0 mL) and $Na_2S_2O_3$ (10.0 mL) were added, and diethyl ether (20.0 mL) was added. The mixture was extracted with diethyl ether (3×25 mL), combined organic layers were dried over $MgSO_4$, filtered and concentrated *in vacuo*. Purification by flash column chromatography (SiO_2, cyclohexane/ethyl acetate 19:1) gave the title compound as colorless oil (233 mg, 969 mmol, 95%). R_f 0.57 (cyclohexane/ethyl acetate 19:1). IR: 2997, 2950, 2916, 1710, 1600, 1433, 1367, 1236, 1212, 1090, 1010, 856, 769. ^{1}H-NMR (400 MHz, $CDCl_3$): 3.78 (*s*, 3 H); 2.13 (*s*, 3 H); 2.09 (*s*, 3 H). ^{13}C-NMR (100 MHz, $CDCl_3$): 165.9; 152.3; 83.8; 52.7; 31.8; 22.0. HR-MS: 240.9719 ($C_6H_{10}IO_2^+$, $[M+H]^+$; calc. 240.9725).

Methyl 2-{[*tert*-Butyl(dimethyl)silyl]ethynyl}-3-methylbut-2-enoate (**15**). To a suspension of copper iodide (60.3 mg, 317 mmol, 0.20 equiv.) in dioxane (16.0 mL) and triethyl amine (8.00 mL) under argon atmosphere at room temperature was added vinyl iodide **13b** (380 mg, 1.58 mmol, 1.00 equiv.) obtained from above and *tert*-Butyl(ethynyl)dimethylsilane (888 mg, 6.33 mmol, 4.00 equiv.). The clear colorless mixture was degassed by bubbling argon through the solution for 15 min. $PdCl_2(PPh_3)_2$ (111 mg, 158 mmol, 0.10 equiv.) was added, and the mixture was stirred and heated to 50 C for 90 min. The mixture was allowed to cool to room temperature and was filtered over a plug of *Celite* (wash with cyclohexane/ethyl acetate 19:1, 40 mL). The solvent was removed *in vacuo* and the crude was purified by flash column chromatography over silica gel (cyclohexane/ethyl acetate 80:1 to 19:1) gave the title compound as yellowish oil (360 mg, 1.43 mmol, 91%). R_f 0.15 (cyclohexane/ethyl acetate 80:1). IR: 2953, 2930, 2857, 2149, 1725, 1605, 1435, 1284, 1229, 1156, 1086, 827, 775. ^{1}H-NMR (400 MHz, $CDCl_3$): 3.76 (*s*, 3 H); 2.23 (*s*, 3 H); 2.16 (*s*, 3 H); 0.97 (*s*, 9 H); 0.15 (*s*, 6 H). ^{13}C-NMR (100 MHz, $CDCl_3$): 165.8; 161.2; 112.6; 101.4; 97.7; 51.8; 26.1; 26.0; 22.4; 16.7; −4.6. HR-MS: 253.1620 ($C_{14}H_{25}O_2Si^+$, $[M+H]^+$; calc. 253.1624).

2-{[*tert*-Butyl(dimethyl)silyl]ethynyl}-3-methylbut-2-enoic Acid (**16**). To a solution of methyl ester **15** (200 mg, 792 mmol, 1.00 equiv.) obtained from above dissolved in *tert*-butanol (20.0 mL) was added an aqueous solution of lithium hydroxide (1.0 M, 5.00 mL, 6.30 equiv.) at room temperature. The mixture was stirred for 22 h at room temperature. An aqueous saturated solution of NH_4Cl (30 mL), acetic acid (2.0 mL) and dichloromethane (50 mL) were added, the aqueous layer was extracted with dichloromethane (4×50 mL), the combined organic layers were dried over $MgSO_4$, filtered and concentrated *in vacuo*. Purification by flash column chromatography over silica gel (cyclohexane/ethyl acetate 6:1+1%AcOH) gave the title compound (95.0 mg, R_f 0.20, cyclohexane/ethyl acetate 6:1+1%AcOH) besides recovered starting material (59.0 mg, R_f 0.59, cyclohexane/ethyl acetate 6:1+1%AcOH) that was resubmitted to the same reaction conditions as described. Two cycles gave desired acid **16** (133 mg, 558 mmol, 70%) in total as colorless crystalline solid. R_f 0.20 (cyclohexane/ethyl acetate 6:1+1%AcOH). M.p. 131–132 C. IR: 3077, 2951, 2928, 2893, 2857, 2150, 1695, 1584, 1408, 1285, 1249, 910, 839, 828, 774, 734, 666. ^{1}H-NMR (400 MHz, $CDCl_3$): 2.28 (*s*, 3 H); 2.20 (*s*, 3 H); 0.98 (*s*, 9 H); 0.17 (*s*, 6 H). ^{13}C-NMR (100 MHz, $CDCl_3$): 169.3; 164.3; 162.2; 112.1; 101.0; 98.5; 26.7; 26.1; 22.8; 16.9; −4.6. HR-MS: 239.1462 ($C_{13}H_{23}O_2Si^+$, $[M+H]^+$; calc. 239.1467).

(*rac*)-1-{[*tert*-Butyl(dimethyl)silyl]ethynyl}-1-(prop-1-en-2-yl)spiro[3.4]octan-2-one (**24**). To a solution of acid **16** (2.50 g, 10.5 mmol, 1.00 equiv.) dissolved in dichloromethane (200 mL) was added a solution of oxalyl chloride (1.0 mL, 11.5 mmol, 1.10 equiv.) and *N*,*N*-dimethylformamide (40 µL, 0.52 mmol, 0.05 equiv.) under argon at room temperature. The mixture was stirred for 30 min at room temperature. The progress of the reaction was moni-

 © 2020 Wiley-VHCA AG, Zurich, Switzerland

Figure A.1. Article 1. (cont.)

Helv. Chim. Acta 2020, 103, e2000017 HELVETICA

tored by TLC. After completion, the reaction was quenched with methanol to form the methyl ester. Methylenecyclopentane (22 mL, 210 mmol, 20.0 equiv.) was added, and then triethylamine (3.2 mL, 23.1 mmol, 2.20 equiv.) was slowly added by a syringe pump (rate of addition; 4 mL/h). The resulting solution was stirred for 16 h at room temperature. An aqueous saturated solution of NH_4Cl and dichloromethane were added, the aqueous layer was extracted with dichloromethane three times, combined organic layers were dried over Na_2SO_4, filtered and concentrated *in vacuo*. Purification by flash column chromatography over silica gel (cyclohexane/ethyl acetate 40:1) gave the title compound **24** (3.01 g, 9.95 mmol, 95%) as yellowish oil. R_f 0.30 (cyclohexane/ethyl acetate 40:1). IR: 2954, 2930, 2857, 2150, 1789, 1723, 1250, 1224, 1007, 838, 826, 812, 775. ^{1}H-NMR (400 MHz, $CDCl_3$): 5.03 (*s*, 1 H); 4.99 (*s*, 1 H); 3.12 (*d*, *J*=17.6, 1 H); 2.89 (*d*, *J*=17.6, 1 H); 2.25–2.18 (*m*, 1 H); 1.82–1.68 (*m*, 6 H); 1.81 (*s*, 3 H); 1.55–1.51 (*m*, 1 H); 0.94 (*s*, 9 H); 0.10 (*s*, 6 H). ^{13}C-NMR (100 MHz, $CDCl_3$): 203.2; 140.2; 113.7; 102.1; 90.6; 71.2; 57.7; 47.3; 37.2; 34.6; 26.1; 24.4; 24.0; 20.9; 16.7; −4.6. HR-MS: 303.2144 ($C_{19}H_{31}OSi^+$, $[M+H]^+$; calc. 303.2144).

(*rac*)-1-{[*tert*-Butyl(dimethyl)silyl]ethynyl}-1-(prop-1-en-2-yl)-2-oxaspiro[4.4]nonan-3-one (**26**). Premix solution of *m*CPBA (<77%; 246 mg, 1.32 mmol, 2.00 equiv.) and tetrabutylammonium hydroxide (56% *w/w* solution in H_2O, 760 mg, 1.65 mmol, 2.50 equiv.) was added to a clear yellowish solution of cyclobutanone **24** (200 mg, 0.66 mmol, 1.00 equiv.) dissolved in dichloromethane (16 mL) under argon at room temperature. After addition of the premix solutions described above to the reaction solution, the resulting mixture was stirred for 1 h at room temperature. After quenching with 10% $Na_2S_2O_3$ solution, the aqueous layer was extracted with dichloromethane three times. The combined organic layers were dried over Na_2SO_4, filtered and concentrated *in vacuo*. Purification by flash column chromatography over silica gel (cyclohexane/ethyl acetate 19:1) gave the title compound **26** (160 mg, 0.50 mmol, 76%) as colorless oil. R_f 0.13 (cyclohexane/ethyl acetate 40:1). IR: 2953, 2929, 2857, 2150, 1793, 1718, 1471, 1250, 1218, 1198, 948, 912, 839, 826, 813, 777. ^{1}H-NMR (400 MHz, $CDCl_3$): 5.32 (*s*, 1 H); 5.09 (*s*, 1 H); 2.72 (*d*, *J*=16.9, 1 H); 2.48 (*d*, *J*=16.9, 1 H); 2.10–2.03 (*m*, 1 H); 1.89 (*s*, 3 H); 1.80–1.74 (*m*, 2 H); 1.70–1.63 (*m*, 3 H); 1.57–1.51 (*m*, 1 H); 1.39–1.34 (*m*, 1 H); 0.94 (*s*, 9 H); 0.12 (*s*, 6 H). ^{13}C-NMR (100 MHz, $CDCl_3$): 175.0; 140.3; 114.3; 102.9; 91.4; 78.9; 55.6; 43.2; 35.2; 33.0; 26.0; 24.4; 23.4; 20.2; 16.6; −4.8. HR-MS: 319.2084 ($C_{19}H_{31}O_2Si^+$, $[M+H]^+$; calc. 319.2093).

(*rac*)-1-Ethynyl-1-(prop-1-en-2-yl)-2-oxaspiro-4.4]nonan-3-one (**33**). To a solution of TBS-protected alkyne **26** (1.20 g, 3.80 mmol, 1.00 equiv.) in THF (40 mL) was added a solution of TBAF (1.0 M in THF; 7.5 mL, 7.5 mmol, 2.00 equiv.) under argon at room temperature. The mixture was stirred for 30 min at room temperature. An aqueous saturated solution of NH_4Cl and dichloromethane were added, the aqueous layer was extracted with dichloromethane three times, combined organic layers were dried over Na_2SO_4, filtered and concentrated *in vacuo*. Purification by flash column chromatography over silica gel (cyclohexane/ethyl acetate 19:1) gave the title compound **33** (697 mg, 3.41 mmol, 91%) as colorless oil. R_f 0.20 (cyclohexane/ethyl acetate 19:1). IR: 3266, 2962, 2877, 1789, 1213, 948, 913, 676. ^{1}H-NMR (400 MHz, $CDCl_3$): 5.34 (*s*, 1 H); 5.11 (*s*, 1 H); 2.74 (*d*, *J*=16.9, 1 H); 2.68 (*s*, 1 H); 2.49 (*d*, *J*=16.9, 1 H); 2.08–2.03 (*m*, 1 H); 1.91 (*s*, 3 H); 1.84–1.77 (*m*, 2 H); 1.73–1.60 (*m*, 3 H); 1.59–1.54 (*m*, 1 H); 1.42–1.36 (*m*, 1 H). ^{13}C-NMR (100 MHz, $CDCl_3$): 174.7; 140.2; 114.6; 87.2; 81.3; 75.8; 55.5; 42.8; 35.0; 33.0; 24.2; 23.2; 20.1. HR-MS: 205.1225 ($C_{13}H_{17}O_2^+$, $[M+H]^+$; calc. 205.1228).

(*rac*)-1-(Prop-1-en-2-yl)-1-[(*E*)-2-(tributylstannyl)-ethenyl]-2-oxaspiro[4.4]nonan-3-one (**34**). To a solution of alkyne **33** (650 mg, 3.18 mmol, 1.00 equiv.) in toluene (30 mL), tributylstannane (2.5 mL, 9.5 mmol, 3.0 equiv.) and AIBN (80 mg, 0.47 mmol, 0.15 equiv.) were added under argon at room temperature. The mixture was stirred and heated to 80 C for 18 h under argon. Purification by flash column chromatography over silica gel (cyclohexane/ethyl acetate 80:1 to 19:1) gave the title compound **34** (1.53 g, 0.97 mmol, 97%) as colorless oil. R_f 0.25 (cyclohexane/ethyl acetate 40:1). IR: 2956, 2925, 2872, 2853, 1787, 1457, 1216, 1185, 997, 958. ^{1}H-NMR (400 MHz, CD_2Cl_2): 6.38–6.20 (*m*, 2 H); 5.05 (*s*, 1 H); 4.95 (*t*, *J*=1.5, 1 H); 2.35–2.28 (*m*, 2 H); 1.98–1.91 (*m*, 1 H); 1.84 (*s*, 3 H); 1.74–1.70 (*m*, 2 H); 1.69–1.59 (*m*, 3 H); 1.54–1.46 (*m*, 6 H); 1.44–1.40 (*m*, 2 H); 1.30 (*sext*, *J*=7.0, 6 H); 0.95–0.91 (*m*, 6 H); 0.88 (*t*, *J*=7.3, 9 H). ^{13}C-NMR (100 MHz, CD_2Cl_2): 175.9; 145.4; 144.1; 128.3; 112.3; 93.5; 55.0; 42.5; 34.4; 34.0; 29.7; 27.8; 24.0; 23.6; 21.3; 14.1; 10.1. HR-MS: 497.2447 ($C_{25}H_{45}O_2Sn^+$, $[M+H]^+$; calc. 497.2442).

(*rac*)-/(*R*)-C(2′)-Diastereomers of Methyl (2*E*,3*E*)-2-{[(4-Methyl-5-oxo-2,5-dihydrofuran-2-yl)oxy]-

 © 2020 Wiley-VHCA AG, Zurich, Switzerland

Figure A.1. Article 1. (cont.)

ethylidene}-4-[3-oxo-1-(prop-1-en-2-yl)-2-oxaspiro-[4.4]nonan-1-yl]but-3-enoate (**35**). To a solution of vinyl iodide 6 (25 mg, 0.077 mmol, 1.00 equiv.), tri(furan-2-yl)phosphane (7.1 mg, 0.031 mmol, 0.40 equiv.) in 1,4-dioxane (0.8 mL) was added vinylstannane 34 (57 mg, 0.12 mmol, 1.50 equiv.) under argon atmosphere. The solution was degassed by bubbling argon through the solution for 10 min. Pd_2dba_3 (7.0 mg, 7.7 µmol, 0.10 equiv.) was added, the reaction vial was sealed and heated to 120 C for 30 min. The clear yellow mixture was allowed to cool to r.t. and was filtered over *Celite* (wash with cyclohexane/ethyl acetate 2:1, 15 mL). The solvent was removed *in vacuo*, and the crude was purified by flash column chromatography (SiO_2, cyclohexane/ethyl acetate 2:1). The corresponding coupling product was obtained as colorless oil (63 mg, 0.049 mmol, 63%). The coupling with (*R*)-6 produced (*R*)-C(2′) diastereomers of compound 35. HPLC Analyses of them are described in the *Supporting Information*. R_f 0.17 (cyclohexane/ethyl acetate 2:1). IR: 2954, 1782, 1716, 1650, 1437, 1190, 1012, 953. Both diastereomers give very similar signals in ^{1}H- and ^{13}C-NMR and are reported as one compound: ^{1}H-NMR (400 MHz, CD_2Cl_2): 7.56 (*s*, 1 H); 6.99–6.97 (*m*, 1 H); 6.89 (*d*, *J*= 16.1, 1 H); 6.34 (*m*, 1 H); 6.17–6.16 (*m*, 1 H); 5.06 (*s*, 1 H); 4.95 (*s*, 1 H); 3.73 (*s*, 3 H); 2.35 s, 2 H); 1.99–1.98 (*m*, 3 H); 1.92–1.88 (*m*, 1 H); 1.82 (*s*, 3 H); 1.76–1.69 (*m*, 2 H); 1.68–1.58 (*m*, 4 H); 1.42–1.40 (*m*, 1 H). ^{13}C-NMR (100 MHz, CD_2Cl_2): 175.7; 170.9; 166.9; 153.7; 144.2; 141.8; 136.2; 133.2; 117.8; 112.7; 112.0; 101.1; 92.5; 55.3; 52.1; 42.5; 34.5; 34.0; 23.8; 23.7; 21.3; 17.1; 11.0. HR-MS: 403.1752 ($C_{22}H_{27}O_7^+$, $[M+H]^+$; calc. 403.1756). Chiral HPLC analyses are described in the *Supporting Information*.

(*rac*)-Methyl (2*E*,3*E*)-2-{[(3,4-Dimethyl-5-oxo-2,5-dihydrofuran-2-yl)oxy]methylidene}-4-[3-oxo-1-(prop-1-en-2-yl)-2-oxaspiro[4.4]nonan-1-yl]but-3-enoate (**36**). To a solution of vinyl iodide 31 (25 mg, 0.074 mmol, 1.00 equiv.), tri(furan-2-yl)phosphane (6.8 mg, 0.029 mmol, 0.40 equiv.) in 1,4-dioxane (0.8 mL) was added vinylstannane 34 (55 mg, 0.11 mmol, 1.50 equiv.) under argon atmosphere. The solution was degassed by bubbling argon through the solution for 10 min. Pd_2dba_3 (6.7 mg, 7.4 µmol, 0.10 equiv.) was added, the reaction vial was sealed and heated to 120 C for 30 min. The clear yellow mixture was allowed to cool to r.t. and was filtered over *Celite* (wash with cyclohexane/ethyl acetate 2:1, 15 mL). The solvent was removed *in vacuo* and the crude was purified by flash column chromatography (SiO_2, cyclohexane/ethyl acetate 2:1). The title compound 36 was obtained as colorless oil (29 mg, 0.069 mmol, 94%). R_f 0.17 (cyclohexane/ethyl acetate 2:1). IR: 2955, 2926, 2876, 1779, 1716, 1640, 1610, 1437, 1357, 1315, 1254, 1193, 1121, 1085, 983, 749. Both diastereomers give very similar signals in ^{1}H- and ^{13}C-NMR and are reported as one compound: ^{1}H-NMR (400 MHz, CD_2Cl_2): 7.56 (*s*, 1 H); 6.85 (*dd*, *J*=1.1, 16.1, 1 H); 6.35 (*dd*, *J*=4.4, 16.1, 1 H); 5.97 (*s*, 1 H); 5.38–5.26 (*m*, 1 H); 5.16–5.05 (*m*, 1 H); 4.94 (*d*, *J*=1.5, 1 H); 3.73 (*s*, 3 H); 2.43 (*d*, *J*=16.9, 1 H); 2.21 (*dd*, *J*=2.0, 16.7, 1 H); 2.00 (*d*, *J*=0.7, 3 H); 1.89–1.86 (*m*, 1 H); 1.87–1.79 (*m*, 5 H); 1.23 (*s*, 3 H); 1.06 (*s*, 3 H). ^{13}C-NMR (100 MHz, CD_2Cl_2): 175.62; 175.59; 171.32; 171.30; 166.91; 166.89; 153.73; 153.69; 153.35; 153.27; 144.12; 144.09; 133.07; 133.02; 128.61; 128.55; 117.96; 117.91; 102.78; 102.64; 92.5; 55.28; 55.25; 52.1; 42.4; 34.49; 34.44; 34.0; 23.8; 23.6; 11.75; 11.73; 8.9. HR-MS: 417.1905 ($C_{23}H_{29}O_7^+$, $[M+H]^+$; calc. 417.1913).

(*rac*)-2-{[*tert*-Butyl(dimethyl)silyl]ethynyl}-3,3-dimethyl-2-(prop-1-en-2-yl)cyclobutan-1-one (**25**). To a solution of acid **16** (4.00 g, 16.8 mmol, 1.00 equiv.) dissolved in dichloromethane (40 mL) was added a solution of oxalyl chloride (1.6 mL, 18.5 mmol, 1.10 equiv.) and *N*,*N*-dimethylformamide (70 µL, 0.84 mmol, 0.05 equiv.) under argon at room temperature. The mixture was stirred for 30 min at room temperature. The reaction was monitored by TLC and after completion of the reaction, quenched with methanol to form methyl ester. The mixture was diluted with 760 mL of dichloromethane. After cooling to −78 C, isobutene gas (b.p. −6.9 C; 83 mL, 922 mmol, 55.0 equiv.) through a dry column with $MgSO_4$ and $CaCl_2$ as drying reagents was dissolved into the mixture. In order not to get isobutene away, a cooling condenser (−78 C) was installed, and then the mixture solution was heated to 60 C. Triethylamine (5.2 mL, 36.9 mmol, 2.20 equiv.) was slowly added by a syringe pump (rate of addition; 4 mL/h), followed by the stirring for 5 h at 60 C. The clear yellow solution was allowed to cool to r.t., and the solvent was removed *in vacuo*. An aqueous saturated solution of NH_4Cl and dichloromethane were added, the aqueous layer was extracted with dichloromethane three times, combined organic layers were dried over Na_2SO_4, filtered and concentrated *in vacuo*. Purification by flash column chromatography over silica gel (cyclohexane/ethyl acetate 40:1) gave the title compound **25** (3.65 g, 13.2 mmol, 79%) as yellowish oil. R_f 0.27 (cyclohexane/ethyl acetate 40:1). IR: 2954, 2929, 2857, 2149, 1787, 1717, 1471, 1463, 1368, 1287, 1249, 1171,

 © 2020 Wiley-VHCA AG, Zurich, Switzerland

Figure A.1. Article 1. (cont.)

1086, 1007, 826, 812, 775. ^{1}H-NMR (400 MHz, CD_2Cl_2): 4.98 (*s*, 1 H); 4.96–4.95 (*m*, 1 H); 3.03 (*d*, *J*=17.1, 1 H); 2.71 (*d*, *J*=17.1, 1 H); 1.78 (*s*, 3 H); 1.49 (*s*, 3 H); 1.19 (*s*, 3 H); 0.94 (*s*, 9 H); 0.11 (*s*, 6 H). ^{13}C-NMR (100 MHz, CD_2Cl_2): 203.3; 141.1; 113.6; 103.0; 91.4; 72.4; 58.0; 36.1; 26.41; 26.39; 24.7; 20.7; 17.1; −4.4. HR-MS: 277.1986 ($C_{17}H_{29}OSi^+$, $[M+H]^+$; calc. 277.1987).

(*rac*)-5-{[*tert*-Butyl(dimethyl)silyl]ethynyl}-4,4-dimethyl-5-(prop-1-en-2-yl)oxolan-2-one (**29**). Premix solution of *m*CPBA (<70%; 89 mg, 0.36 mmol, 2.00 equiv.) and tetrabutylammonium hydroxide (40% *w/w* solution in H_2O, 275 mg, 0.42 mmol, 2.33 equiv.) was added to a clear yellowish solution of cyclobutanone **25** (50 mg, 0.18 mmol, 1.00 equiv.) dissolved in dichloromethane (2.0 mL) under argon at room temperature. After premix solutions descried above were additionally added to the reaction solution twice, the resulting mixture was stirred for 1 h at room temperature. Then, the reaction was quenched with 10% $Na_2S_2O_3$ aqueous solution, the aqueous layer was extracted with dichloromethane three times. The combined organic layers were dried over Na_2SO_4, filtered and concentrated *in vacuo*. Purification by flash column chromatography over silica gel (cyclohexane/ethyl acetate 19:1) gave the title compound **29** (32 mg, 0.11 mmol, 61%) as colorless oil. R_f 0.29 (cyclohexane/ethyl acetate 19:1). IR: 2955, 2930, 2858, 1795, 1471, 1464, 1251, 1232, 1198, 1119, 1099, 1042, 979, 915, 827, 778. ^{1}H-NMR (400 MHz, CD_2Cl_2): 5.23 (*s*, 1 H); 5.05 (*s*, 1 H); 2.72 (*d*, *J*=16.7, 1 H); 2.28 (*d*, *J*=16.7, 1 H); 1.90 (*s*, 3 H); 1.40 (*s*, 3 H); 0.98 (*s*, 3 H); 0.95 (*s*, 9 H); 0.14 (*s*, 6 H). ^{13}C-NMR (100 MHz, CD_2Cl_2): 174.9; 140.5; 113.6; 102.7; 93.3; 89.1; 44.8; 44.2; 26.4; 24.7; 23.4; 20.6; 17.0; −4.6. HR-MS: 293.1928 ($C_{17}H_{29}O_2Si^+$, $[M+H]^+$; calc. 293.1936).

(*rac*)-5-Ethynyl-4,4-dimethyl-5-(prop-1-en-2-yl)-oxolan-2-one (**30**). To a solution of TBS-protected alkyne **29** (220 mg, 0.75 mmol, 1.00 equiv.) in THF (7.5 mL) was added a solution of TBAF (1.0 M in THF; 1.5 mL, 1.5 mmol, 2.00 equiv.) under argon at room temperature. The mixture was stirred for 30 min at room temperature. An aqueous saturated solution of NH_4Cl and dichloromethane were added, the aqueous layer was extracted with dichloromethane three times, combined organic layers were dried over Na_2SO_4, filtered and concentrated *in vacuo*. Purification by flash column chromatography over silica gel (cyclohexane/ethyl acetate 19:1) gave the title compound **30** (125 mg, 0.70 mmol, 93%) as colorless oil. R_f 0.15 (cyclohexane/ethyl acetate 19:1). IR: 3263, 2977, 2933, 1788, 1232, 1199, 1120, 1085, 1042, 978, 959, 916, 665. ^{1}H-NMR (400 MHz, CD_2Cl_2): 5.25 (*s*, 1 H); 5.08–5.07 (*m*, 1 H); 2.80 (*s*, 1 H); 2.74 (*d*, *J*=16.7, 1 H); 2.30 (*d*, *J*=16.7, 1 H); 1.90–1.89 (*m*, 3 H); 1.41 (*s*, 3 H); 0.99 (*m*, 3 H). ^{13}C-NMR (100 MHz, CD_2Cl_2): 174.7; 140.3; 113.9; 88.6; 80.9; 77.7; 44.7; 44.1; 24.5; 23.4; 20.4. HR-MS: 179.1070 ($C_{11}H_{15}O_2^+$, $[M+H]^+$; calc. 179.1072).

(*rac*)-4,4-Dimethyl-5-(prop-1-en-2-yl)-5-[(*E*)-2-(tributylstannyl)ethenyl]oxolan-2-one (**9**). *Protocol A*: To a solution of alkyne **30** (120 mg, 0.67 mmol, 1.00 equiv.) in toluene (7 mL), tributylstannane (0.27 mL, 1.00 mmol, 3.0 equiv.) and AIBN (17 mg, 0.10 mmol, 0.15 equiv.) under argon at room temperature. The mixture was stirred and heated to 80 C for 18 h under argon. Purification by flash column chromatography over silica gel (cyclohexane/ethyl acetate 80:1 to 19:1) gave the title compound **9** (302 mg, 0.64 mmol, 96%) as colorless oil. R_f 0.24 (cyclohexane/ethyl acetate 40:1).

Protocol B: To a solution of vinyl iodide **47** (5.0 mg, 0.016 mmol, 1.0 equiv.) in *N*-methylpyrrolidone (0.15 mL), bis(tributyltin) (23.8 mg, 0.041 mmol, 2.5 equiv.) and $Pd(PPh_3)_4$ (1.0 mg, 0.81 µmol, 0.05 equiv.) were added under argon. The mixture was stirred and heated to 50 C for 1 h. The solution was allowed to cool to room temperature and was filtered over *Celite*, the filter cake was washed with dichloromethane. The resulting solvent was washed with a 10% LiCl aqueous solution three times. The organic phase was dried over anhydrous Na_2SO_4, filtrated and concentrated. The crude was purified by flash column chromatography (SiO_2, cyclohexane) to give the corresponding stannane compound **9** (4.7 mg, 0.010 mmol, 61%) as a colorless oil. IR: 2958, 2927, 2872, 2853, 1790, 1465, 1235, 1200, 1090, 1000,989, 905, 667. ^{1}H-NMR (400 MHz, CD_2Cl_2): 6.35–6.15 (*m*, 2 H); 5.08 (*s*, 1 H); 4.94 (virtual *t*, *J*=1.5, 1 H); 2.41 (*d*, *J*=16.5, 1 H); 2.16 (*d*, *J*=16.5, 1 H); 1.86–1.85 (*m*, 3 H); 1.54–1.46 (*m*, 6 H); 1.30 (*sext*, *J*=7.5, 6 H); 1.25 (*s*, 3 H); 1.05 (*s*, 3 H); 0.95–0.91 (*m*, 6 H); 0.88 (*t*, *J*=7.3, 9 H). ^{13}C-NMR (100 MHz, CD_2Cl_2): 175.4; 144.0; 142.9; 128.0; 111.4; 93.6; 43.5; 42.6; 29.1; 27.2; 24.3; 23.4; 20.6; 13.5; 9.5. HR-MS: 471.2290 ($C_{23}H_{43}O_2Sn^+$, $[M+H]^+$; calc. 471.2285).

(*rac*)-Zealactone (**1**)**, (*S*)-C(2′) Zealactone** (**1**) **and Zealactone 1a/b**. To a solution of vinyl iodide **6** (28 mg, 0.086 mmol, 1.00 equiv.), tri(furan-2-yl)phosphane (8.0 mg, 0.034 mmol, 0.40 equiv.) in 1,4-dioxane (0.9 mL) was added vinylstannane **9** (101 mg, 0.21 mmol, 2.50 equiv.) under argon atmosphere. The

 © 2020 Wiley-VHCA AG, Zurich, Switzerland

Figure A.1. Article 1. (cont.)

Helv. Chim. Acta 2020, 103, e2000017 HELVETICA

solution was degassed by bubbling argon through the solution for 10 min. Pd_2dba_3 (7.9 mg, 8.6 μmol, 0.10 equiv.) was added, the reaction vial was sealed and heated to 120 C for 30 min. The clear yellow mixture was allowed to cool to r.t. and was filtered over *Celite* (wash with cyclohexane/ethyl acetate 2:1, 15 mL). The solvent was removed *in vacuo* and the crude was purified by flash column chromatography (SiO_2, cyclohexane/ethyl acetate 2:1). The corresponding coupling product was obtained as colorless oil (25.9 mg, 0.069 mmol, 80%). The coupling with (*R*)-**6** or (*S*)-**6** produced (*R*)-C(2′) or (*S*)-C(2′) diastereomers of zealactone (**1**), respectively. HPLC Analyses of them are described in the *Supporting Information*. Chiral separation of (6*S*,2′*R*) and (6*R*,2′*R*) of zealactone (**1**) and CD spectrum of them are also given in the *Supporting Information*. R_f 0.14 (cyclohexane/ethyl acetate 2:1). IR: 2960, 2929, 1783, 1716, 1611, 1354, 1255, 1237, 1198, 1125, 1093, 1045, 1015, 990, 951. Both diastereomers give similar signals in ^{1}H- and ^{13}C-NMR. ^{1}H-NMR (600 MHz, CD_2Cl_2): 7.56 (*s*, 1 H); 6.98 (virtual *t*, *J*=1.6, 1 H); 6.97 (virtual *t*, *J*=1.6, 1 H); 6.87 (*d*, *J*=16.1, 1 H); 6.34 (*d*, *J*=16.1, 1 H); 6.33 (*d*, *J*=16.1, 1 H); 6.17–6.16 (*m*, 1 H); 5.08 (*s*, 1 H); 5.07 (*s*, 1 H); 4.94 (*s*, 1 H); 3.73 (*s*, 3 H); 2.44 (*d*, *J*=16.8, 1 H); 2.43 (*d*, *J*=16.8, 1 H); 2.22 (*d*, *J*=16.8, 1 H); 2.21 (*d*, *J*=16.8, 1 H); 1.99–1.98 (*m*, 3 H); 1.85–1.83 (br. *s*, 3 H); 1.24 (*s*, 3 H); 1.06 (*s*, 3 H). ^{13}C-NMR (150 MHz, CD_2Cl_2): 175.46; 170.92; 166.86; 153.71; 143.47; 143.43; 141.78; 141.75; 136.25; 136.21; 132.32; 117.72; 117.64; 112.29; 111.91; 101.10; 101.07; 93.19; 93.17; 52.06; 44.22; 44.21; 43.44; 43.41; 24.73; 24.14; 24.12; 21.19; 11.03; 11.02. The NMR comparison of (6*S*,2′*R*) and (6*R*,2′*R*) of zealactone (**1**) are described in the *Supporting Information*. HR-MS: 377.1593 ($C_{20}H_{25}O_7^+$, $[M+H]^+$; calc. 377.1600).

(*rac*)-Methyl (2*E*,3*E*)-2-{[(3,4-Dimethyl-5-oxo-2,5-dihydrofuran-2-yl)oxy]methylidene}-4-[3,3-dimethyl-5-oxo-2-(prop-1-en-2-yl)oxolan-2-yl]but-3-enoate (**32**). To a solution of vinyl iodide 31 (25 mg, 0.074 mmol, 1.00 equiv.), tri(furan-2-yl)phosphane (6.8 mg, 0.029 mmol, 0.40 equiv.) in 1,4-dioxane (0.75 mL) was added vinylstannane 9 (52 mg, 0.11 mmol, 1.50 equiv.) under argon atmosphere. The solution was degassed by bubbling argon through the solution for 10 min. Pd_2dba_3 (6.7 mg, 7.3 μmol, 0.10 equiv.) was added, the reaction vial was sealed and heated to 120 C for 30 min. The clear yellow mixture was allowed to cool to r.t. and was filtered over *Celite* (wash with cyclohexane/ethyl acetate 2:1, 15 mL). The solvent was removed *in vacuo* and the crude was purified by flash column chromatography (SiO_2, cyclohexane/ethyl acetate 2:1). The title compound 32 was obtained as colorless oil (26 mg, 0.66 mmol, 90%). R_f 0.14 (cyclohexane/ethyl acetate 2:1). IR: 2961, 2927, 1779, 1716, 1641, 1610, 1437, 1358, 1254, 1237, 1196, 1122, 1085, 1044, 982, 748. Both diastereomers give very similar signals in ^{1}H- and ^{13}C-NMR and are reported as one compound: ^{1}H-NMR (400 MHz, CD_2Cl_2): 7.55 (*s*, 1 H); 6.86 (*dd*, *J*=2.0, 16.0, 1 H); 6.36 (*dd*, *J*=5.0, 16.0, 1 H); 5.97 (br. *s*, 1 H); 5.08–5.03 (*m*, 1 H); 4.95 (br. *s*, 1 H); 3.72 (*s*, 3 H); 2.35 (*s*, 2 H); 2.00 (*d*, *J*=0.7, 3 H); 1.92–1.87 (*m*, 1 H); 1.86 (*s*, 3 H); 1.82 (*s*, 3 H); 1.77–1.49 (*m*, 7 H). ^{13}C-NMR (100 MHz, CD_2Cl_2): 175.45; 175.43; 171.3; 166.92; 166.89; 153.74; 153.69; 153.33; 153.26; 143.39; 143.35; 132.24; 132.21; 128.63; 128.58; 117.88; 117.84; 112.34; 112.29; 112.0; 102.8; 102.6; 93.1; 92.5; 52.1; 44.2; 24.7; 24.1; 24.0; 21.19; 21.16; 17.74; 11.71; 8.9. HR-MS: 391.1752 ($C_{21}H_{27}O_7^+$, $[M+H]^+$; calc. 391.1757).

5-[(*E*)-2-Iodoethenyl]-4,4-dimethyl-5-(prop-1-en-2-yl)oxolan-2-one (**47**). To a solution of stannane **9** (250 mg, 0.53 mmol, 1.0 equiv.) in dichloromethane (10 mL), iodine (150 mg, 0.59 mmol, 1.1 equiv.) was added. The mixture was stirred at room temperature for 5 min and then diluted with dichloromethane and water, and the layers were separated. The aqueous layer was extracted with dichloromethane three times, and the combined organic layers were dried over anhydrous Na_2SO_4, filtrated and concentrated. The crude was purified by flash column chromatography (SiO_2, cyclohexane/ethyl acetate 3:1) to give the title compound (120 mg, 0.39 mmol, 74%) as a clear oil. R_f 0.60 (cyclohexane/ethyl acetate 3:1). IR: 2971, 1789, 1772, 1643, 1605, 1466, 1418, 1376, 1291, 1234, 1200, 1123, 1094, 1044, 989, 954, 917, 799, 619, 543. ^{1}H-NMR (400 MHz, $CDCl_3$): 6.86 (*d*, *J*=14.3, 1 H); 6.92–6.80 (*m*, 1 H); 6.48 (*d*, *J*=14.7, 1 H); 5.12 (*s*, 1 H); 5.00 (*s*, 1 H); 2.46 (*d*, *J*=16.0, 1 H); 2.29 (*d*, *J*=16.0, 1H, 1.81–1.74 (*m*, 1 H); 1.70 (*s*, 3 H); 1.85 (*s*, 3 H); 1.27 (*s*, 3 H); 1.07 (*s*, 3H). ^{13}C-NMR (100 MHz, $CDCl_3$): 174.7; 143.0; 141.2; 113.1; 94.6; 77.5; 43.5; 43.0; 24.4; 23.84; 20.8. HR-MS: 307.01911 ($C_{11}H_{15}O_2I^+$, $[M+H]^+$; calc. 307.01950).

Soil Stability Analysis

Soil stability assay was carried out following the procedures as described in *Lumbroso et al.* in 2016.[49] Briefly, a loam soil (pH in H_2O 8, % OM 4.5) was collected from a field near Stein Research Center in Switzerland and was sieved 0–3 mm. Prior the experiment, the soil was mixed with sand in a ratio of 1:2,

 © 2020 Wiley-VHCA AG, Zurich, Switzerland

Figure A.1. Article 1. (cont.)

Helv. Chim. Acta **2020**, *103*, e2000017

and humidity was adjusted to the 13% *w/w*. Soil was pre-incubated for 1 week at 20 C in the dark prior the chemical treatments. Ten grams of dried soil-sand mix were transferred in 50 mL polypropylene tubes and treated with a solution of the test compounds to reach a final concentration of 3.5 μg per g^{-1} dry soil. Treated samples were incubated in the dark at 20 ± 0.5 C 80% RH. The following incubation timings were considered to study the kinetic of disappearance of parent compounds: 0, 0.5, 1, 1.5, 2, 3, 4, 6, 8 and 25 h after treatment. Compound extraction was carried out by using acetonitrile 30 mL and shake for 1 h at room temperature using a vertical mechanical shaker. Each timing point for each compound was tested in triplicate. Analyses were carried out by using an UPLC-MS/MS (*Waters Acquity UPLC-MS/MS I–Class* System). A *C18* UPLC column (*ACQUITY UPLC®* column *HSS T3* 2.1 × 30 mm, 1.8 μm particle size; *Waters*) was used.

The mobile phase was as follows: H_2O/MeOH (95:5) + 0.1% HCOOH (solvent *A*) and MeCN + 0.1% HCOOH (solvent *B*); 20–100% of solvent *B* for 1.2 min, then 100% of solvent *B* for 0.20 min and then down to 20% solvent *B* up to 1.5 min; average flow rate 0.75 mL min^{-1}. The injection volume was 2 μl. A tested selective ion recording method (SIR) depending on molecular mass of each compound was set up by MS detector. The level of the compound was determined by comparing chromatogram area counts of sample extracts *versus* area counts of the standard solution of the corresponding compound. The half-lives were calculated by an exponential regression analysis (single first-order kinetic model) plotting the percentage of recovered compound in soil against time.

Yoshimulactone Green (YLG) *Displacement Assay*

Yoshimulactone Green (YLG) is a fluorogenic agonist for the strigolactone receptor D14 and was used in competition assays to assess the binding affinity of test compounds as previously described with minor modifications. ZmD14 (1 μg) was incubated in the presence and absence of test compounds in buffer (PBS, 0.1% BSA) for 5 min at room temperature followed by the addition of YLG to 1 μM. The final reaction volume was 150 μL and all wells contained 1% DMSO. The extent of YLG hydrolysis by D14 was assessed by measuring the fluorescence intensity (excitation: 480 nm, emission: 520 nm) in a *Mithras LB 940* plate reader (*Berthold Technologies*) at a single time-point during the linear phase of the reaction. The half-maximal inhibitory concentration (IC_{50}) values were determined from the normalized fluorescence intensities relative to DMSO controls for test compounds over an 8-point dilution curve (30 μM top concentration, 3-fold dilution).

ALPHA Screen Luminescence Proximity Assay

AlphaScreen technology (Amplified Luminescent Proximity Homogenous Assay) was used to assess the ability of compounds to promote interaction between ZmD14 and ZmMAX2. ZmD14 (75 nM) was incubated in assay buffer (PBS, 0.1% BSA) in the presence and absence of test compound (5 μM) for 5 min at room temperature followed by the addition of ZmMAX2 (75 nM) and *Triton X100* to 0.02% (*w/v*). After 15 min incubation at room temperature, 416 μg/mL anti-maltose-binding protein acceptor beads in assay buffer were then added followed 5 min later by 416 μg/mL nickel chelate donor beads. Plates were incubated for 1 h at room temperature protected from light and then measured in a *Mithras LB 940* plate reader (*Berthold Technologies*) equipped with an AlphaScreen module for laser excitation at 680 nm.

Differential Scanning Fluorimetry (DSF)

DSF was performed using a *Bio-Rad CFX96 qPCR* machine with *SyproOrange* as the reporter dye. Two μg of purified ZmD14 was combined with 1 μL of test compound in DMSO and *SyproOrange* dye at 5× final concentration) in PBS to final volume of 25 μL. After 1 min incubation at 20 C samples were heat denatured using a linear 20–96 C gradient, at a rate of 1 C per min. Compounds were tested in duplicate at a concentration of 50 μM (5% DMSO final concentration). Melting temperatures were determined from the peak of the first derivatives of the melting curves.

Dark Induced Corn Leaf Senescence Assay

The effect of compounds was evaluated for their ability to promote senescence of untreated corn leaves as follows. Corn Multitop seeds were supplied by *Syngenta Seeds SAS* (Saint-Sauveur France) with Batch 11876872. Plants were raised up to V6 stage following,[50] in greenhouse at 25/22 C (day/night), humidity 80%, light intensity between 100–150 μmol m^{-2} s^{-1}, photoperiod 14 h day/10 h dark in pots. Compounds were solubilized in DMSO/water (0.5% (*v/v*)). Compounds were tested at 100, 10, 1, 0.1, 0.01, 0.001 μM and 1 mL of each solution was distributed into 24-well microtiter plates. Twelve replicates were used for each treatment character-

© 2020 Wiley-VHCA AG, Zurich, Switzerland

Figure A.1. Article 1. (cont.)

ization. Ten mm leaf discs were cut from the sixth leaf and placed axial side on the surface of each well. Plates were sealed using seal foil (*Polyolefin Art. Nr. 900360*) from *HJ-BIOANALYTIK*. Foils were immediately pierced, one hole per well using syringe needles. All plates were placed horizontally on trolleys in a climatic chamber and placed in the dark at 22 C with 80% relative humidity. Senescence was followed over time by taking photographs at different time points using an *EOS Canon 70D* camera plate. Image analysis was performed automatically with a macro which was developed using Image J software. Changes in the grey scale pixel intensity were analyzed and transformed to data points corresponding the senescence development in leaf tissue. A dynamic analysis of senescence was carried out by fitting a logistic curve. S_{50} parameter was calculated from the logistic curve.

Corn Seed Germination and Root Growth Assays

The effect of compounds was evaluated on the germination of untreated corn seeds under cold stress as follows. *Corn NK Falkone* seeds were supplied by *Syngenta Seeds SAS* (Saint-Sauveur France) with Batch 12345408. Seeds were placed in 24 well plates (each plate was considered as one experimental unit or replicate). Germination was initiated by the addition of 250 μL for corn seeds, of DMSO/water (0.5% (*v/v*)) for the check and solution at 2, 10, 50 and 250 μM of each molecules. Eight replicates (*i.e.*, eight plates) were used for each treatment characterization. Plates were sealed using seal foil (*Polyolefin Art. Nr. 900360*) from *HJ-BIOANALYTIK*. All plates were placed horizontally on trolleys in a climatic chamber at 15 C. The experiment was laid out in a completely randomized design with 75% relative humidity under complete darkness. Foils were pierced, one hole per well using syringes after 72 hours. Germination was followed over time by taking photographs at different time points using an *EOS Canon 70D* camera. Image analysis was performed automatically with a macro which was developed using the Image J software. A dynamic analysis of germination was carried out by fitting a logistic curve. Three parameters were calculated from the logistic curve: T_{50}, the slope and the plateau. All the values are expressed as percentages compared to an untreated control. Data in bold indicate statistically significant differences between treated seeds and untreated control ($p < 0.05$).

Supplementary Material

Spectral data and NMR spectra for all new compounds; HPLC analysis for *rac*-zealactone, zealactone 1a/b, (*S*)-C(2′) diastereomers of zealactone (**1**), *rac*-**35**, (*R*)-C(2′) diastereomers of **35**, **47** and CD studies for zealactone (**1a**), zealactone (**1b**), (*R*)-/(*S*)-**9**, (*R*)-/(*S*)-**47** available as a pdf file.

Acknowledgements

We thank Prof. *Jeffrey W. Bode* for fruitful discussions and for hosting Dr. *Masahiko Yoshimura* in his laboratory. We acknowledge Prof. *Christof Sparr*, Mr. *Frederic Bourgeois* (Basel University) for CD measurements and Dr. *Daniel Emery* for simulation of CD spectra. We would like to thank Ms. *Kristin Hoefer*, Ms. *Miesja Yogo* and Mr. *Gabriel Schmied* for their support for the soil stability studies. Dr. *David Brocklehurst* and *Pauline Heinimann* are acknowledged for assistance with enzymatic assays and *Maud Simonin* for corn germination assays. We further thank Dr. *Peter Renold*, Mr. *Alexander Schuschkowski* and Ms. *Juliane Vogt* for HPLC separations and measurement of HR-MS spectra. Mr. *Roman Staiger*, Dr. *Dylan Dagoneau*, Dr. *Amandine Kolleth Krieger*, Dr. *Mathilde Lachia* and Dr. *Alexandre Lumbroso* are acknowledged for the fruitful discussions. We also thank Prof. *Harro Bouwmeester* (Amsterdam University) for the initial development of the leaf senescence assay and for highly valuable collaboration.

Author Contribution Statement

M. Y. and *M. D.* contributed equally to the synthesis of zealactone 1a/b and its derivatives. The project and experiments were designed by *M. Y.*, *M. D.*, *P.-Y. D.*, *R. F.-P.*, *C. S.*, *P. Q.*, *S. C.* and *A. De M.* The experimental work was performed by *M. Y.*, *M. D.*, *P.-Y. D.*, *C. S.*, *K. H.*, *S. R.*, *P. Q.*, *B. H.* All authors contributed to the manuscript writing and review process.

References

[1] S. Al-Babili, H. J. Bouwmeester, 'Strigolactones, a Novel Carotenoid-Derived Plant Hormone', *Annu. Rev. Plant Biol.* **2015**, *66*, 161–186.
[2] B. Zwanenburg, D. Blanco-Ania, 'Strigolactones: new plant hormones in the spotlight', *J. Exp. Bot.* **2018**, *69*, 2205–2218.

 © 2020 Wiley-VHCA AG, Zurich, Switzerland

Figure A.1. Article 1. (cont.)

[3] C. De Cuyper, S. Struk, L. Bream, K. Gevaert, G. De Jaeger, S. Goormachtig, 'Strigolactones, karrikins and beyond', *Plant Cell Environ.* **2017**, *40*, 1691–1703.

[4] H. J. Bouwmeester, R. Fonne-Pfister, C. Screpanti, A. De Mesmaeker, 'Strigolactones. Plant Hormones with Promising Features', *Angew. Chem. Int. Ed.* **2019**, *55*, 12778–12786.

[5] C. Screpanti, R. Fonné-Pfister, A. Lumbroso, S. Rendine, M. Lachia, A. De Mesmaeker, 'Strigolactone derivatives for potential crop enhancement applications', *Bioorg. Med. Chem. Lett.* **2016**, *26*, 2392–2400.

[6] A. De Mesmaeker, C. Screpanti, R. Fonné-Pfister, M. Lachia, A. Lumbroso, H. J. Bouwmeester, 'Design, Synthesis and Biological Evaluation of Strigolactone and Strigolactam Derivatives for Potential Crop Enhancement Applications in Modern Agriculture', *Chimia* **2019**, *73*, 549–560.

[7] M. G. Mostofa, W. Li, K. H. Nguyen, M. Fujita, L.-S. P. Tran, 'Strigolactones in plant adaptation to abiotic stresses: An emerging avenue of plant research', *Plant Cell Environ.* **2018**, *41*, 2227–2243.

[8] Y. Wang, H. J. Bouwmeester, 'Structural diversity in the strigolactones', *J. Exp. Bot.* **2018**, *69*, 2219–2230.

[9] T. V. Charnikhova, K. Gaus, A. Lumbroso, M. Sanders, J.-P. Vincken, A. De Mesmaeker, C. P. Ruyter-Spira, C. Screpanti, H. J. Bouwmeester, 'Zealactones. Novel natural strigolactones from maize', *Phytochemistry* **2017**,*137*, 123–131.

[10] L. Ravazzolo, S. Trevisan, A. Manoli, S. Boutet-Mercey, F. Perreau, S. Quaggiotti, 'The Control of Zealactone Biosynthesis and Exudation is Involved in the Response to Nitrogen in Maize Root', *Plant Cell Physiol.* **2019**, *60*, 2100–2112.

[11] M. C. Dieckmann, P.-Y. Dakas, A. De Mesmaeker, 'Synthetic Access to Noncanonical Strigolactones: Syntheses of Carlactonic Acid and Methyl Carlactonate', *J. Org. Chem.* **2018**, *83*, 125–135.

[12] M. Yoshimura, R. Fonné-Pfister, C. Screpanti, K. Hermann, S. Rendine, M. Dieckmann, P. Quinodoz, A. De Mesmaeker, 'Total Synthesis and Biological Evaluation of Heliolactone', *Helv. Chim. Acta* **2019**, *102*, e1900211.

[13] M. Lloveras, I. Ramos, E. Molins, A. Messeguer, 'Improved Synthesis of Three Brominated Analogues of the Potent Environmental Mutagen 3-Chloro-4-(dichloromethyl)-5-hydroxy-2(5*H*)-furanone (MX)', *Tetrahedron* **2000**, *56*, 3391–3397.

[14] D. Guillerm, G. Linstrumelle, 'The facile synthesis of a large ring lactone by acid-catalysed cyclisation of an z-ene-diyne hydroxy acid precursor', *Tetrahedron Lett.* **1985**, *26*, 3811–3812.

[15] M. Alami, G. Linstrumelle, 'An efficient palladium-catalyzed reaction of vinyl chlorides with terminal acetylenes', *Tetrahedron Lett.* **1991**, *32*, 6109–6112.

[16] D. A. Jackson, M. Rey, A. S. Dreiding, '2-Vinylcyclobutanones by Cycloaddition of Vinylketenes to Simple Olefins', *Helv. Chim. Acta* **1983**, *66*, 2330–2341.

[17] A. J. Oosthoek-De Vries, P. J. Nieuwland, J. Bart, K. Koch, J. W. G. Janssen, P. J. M. Van Bentum, F. P. J. T. Rutjes, H. J. G. E. Gardeniers, A. P. M. Kentgens, 'Inline Reaction Monitoring of Amine-Catalyzed Acetylation of Benzyl Alcohol Using a Microfluidic Stripline Nuclear Magnetic Resonance Setup', *J. Am. Chem. Soc.* **2019**, *141*, 5369–5380.

[18] Gaussian 16, Revision A.03, M. J. Frisch, G. W. Trucks, H. B. Schlegel, G. E. Scuseria, M. A. Robb, J. R. Cheeseman, G. Scalmani, V. Barone, G. A. Petersson, H. Nakatsuji, X. Li, M. Caricato, A. V. Marenich, J. Bloino, B. G. Janesko, R. Gomperts, B. Mennucci, H. P. Hratchian, J. V. Ortiz, A. F. Izmaylov, J. L. Sonnenberg, D. Williams-Young, F. Ding, F. Lipparini, F. Egidi, J. Goings, B. Peng, A. Petrone, T. Henderson, D. Ranasinghe, V. G. Zakrzewski, J. Gao, N. Rega, G. Zheng, W. Liang, M. Hada, M. Ehara, K. Toyota, R. Fukuda, J. Hasegawa, M. Ishida, T. Nakajima, Y. Honda, O. Kitao, H. Nakai, T. Vreven, K. Throssell, J. A. Montgomery Jr., J. E. Peralta, F. Ogliaro, M. J. Bearpark, J. J. Heyd, E. N. Brothers, K. N. Kudin, V. N. Staroverov, T. A. Keith, R. Kobayashi, J. Normand, K. Raghavachari, A. P. Rendell, J. C. Burant, S. S. Iyengar, J. Tomasi, M. Cossi, J. M. Millam, M. Klene, C. Adamo, R. Cammi, J. W. Ochterski, R. L. Martin, K. Morokuma, O. Farkas, J. B. Foresman, D. J. Fox, Gaussian, Inc., Wallingford CT, 2016.

[19] J.-D. Chai, M. Head-Gordon, 'Long-range corrected hybrid density functionals with damped atom-atom dispersion corrections', *Phys. Chem. Chem. Phys.* **2008**, *10*, 6615–6620.

[20] J. Tomasi, B. Mennucci, R. Cammi, 'Quantum Mechanical Continuum Solvation Models', *Chem. Rev.* **2005**, *105*, 2999–3093.

[21] B. Mennucci, E. Cancès, J. Tomasi, 'Evaluation of Solvent Effects in Isotropic and Anisotropic Dielectrics and in Ionic Solutions with a Unified Integral Equation Method: Theoretical Bases, Computational Implementation, and Numerical Applications', *J. Phys. Chem. B* **1997**, *101*, 10506–10517.

[22] J. Tomasi, B. Mennucci, E. Cancès, 'The IEF version of the PCM solvation method: an overview of a new method addressed to study molecular solutes at the QM ab initio level', *J. Mol. Struct.* **1999**, 464, 211–226.

[23] A. Kolleth, A. Lumbroso, G. Tanriver, S. Catak, S. Sulzer-Mossé, A. De Mesmaeker, 'Synthesis of amino-cyclobutanes via [2+2] cycloadditions involving keteniminium intermediates', *Tetrahedron Lett.* **2016**, *57*, 2697–2702.

[24] S. Zarrabi, N. O. Mahmoodi, K. Tabatabaeian, M. A. Zanjanchi, 'Baeyer–Villiger oxidation of cyclic ketones utilizing potassium peroxydisulfate ($K_2S_2O_8$) or sodium perborate ($NaBO_3$) in acidic media', *Chin. Chem. Lett.* **2009**, *20*, 1400–1404.

[25] M. Uyanik, D. Nakashima, K. Ishihara, 'Baeyer–Villiger Oxidation and Oxidative Cascade Reactions with Aqueous Hydrogen Peroxide Catalyzed by Lipophilic $Li[B(C_6F_5)_4]$ and $Ca[B(C_6F_5)_4]_2$', *Angew. Chem. Int. Ed.* **2012**, *51*, 9093–9096; *Angew. Chem.* **2012**, *124*, 9227–9230.

[26] T. Arite, M. Umehara, S. Ishikawa, A. Hanada, M. Maekawa, S. Yamaguchi, J. Kyozuka, '*d14*, a Strigolactone-Insensitive Mutant of Rice, Shows an Accelerated Outgrowth of Tillers', *Plant Cell Physiol.* **2009**, *50*, 1416–1424.

[27] D. C. Nelson, A. Scaffidi, E. A. Dun, M. T. Waters, G. R. Flematti, K. W. Dixon, C. A. Beveridge, E. L. Ghisalberti, S. M. Smith, 'F-box protein MAX2 has dual roles in karrikin and strigolactone signaling in *Arabidopsis thaliana*', *Proc. Natl. Acad. Sci. USA* **2011**, *108*, 8897–8902.

[28] C. Hamiaux, R. S. M. Drummond, B. J. Janssen, S. E. Ledger, J. M. Cooney, R. D. Newcomb, K. C. Snowden, 'DAD2 Is an α/β Hydrolase Likely to Be Involved in the Perception of

 © 2020 Wiley-VHCA AG, Zurich, Switzerland

Figure A.1. Article 1. (cont.)

the Plant Branching Hormone, Strigolactone', *Curr. Biol.* **2012**, *22*, 2032–2036.
[29] R. Yao, Z. Ming, L. Yan, S. Li, F. Wang, S. Ma, C. Yu, M. Yang, L. Chen, L. Chen, Y. Li, C. Yan, D. Miao, Z. Sun, J. Yan, Y. Sun, L. Wang, J. Chu, S. Fan, W. He, H. Deng, F. Nan, J. Li, Z. Rao, Z. Lou, D. Xie, 'DWARF14 is a non-canonical hormone receptor for strigolactone', *Nature* **2016**, *536*, 469–473.
[30] A. de Saint Germain, G. Clavé, M.-A. Badet-Denisot, J.-P. Pillot, D. Cornu, J.-P. Le Caer, M. Burger, F. Pelissier, P. Retailleau, C. Turnbull, S. Bonhomme, J. Chory, C. Rameau, F.-D. Boyer, 'An histidine covalent receptor and butenolide complex mediates strigolactone perception', *Nat. Chem. Biol.* **2016**, *12*, 787–794.
[31] F. Zhou, Q. Lin, L. Zhu, Y. Ren, K. Zhou, N. Shabek, F. Wu, H. Mao, W. Dong, L. Gan, W. Ma, H. Gao, J. Chen, C. Yang, D. Wang, J. Tan, X. Zhang, X. Guo, J. Wang, L. Jiang, X. Liu, W. Chen, J. Chu, C. Yan, K. Ueno, S. Ito, T. Asami, Z. Cheng, J. Wang, C. Lei, H. Zhai, C. Wu, H. Wang, N. Zheng, J. Wan, 'D14–SCF^{D3}-dependent degradation of D53 regulates strigolactone signalling', *Nature* **2013**, *504*, 406–410.
[32] L. Jiang, X. Liu, G. Xiong, H. Liu, F. Chen, L. Wang, X. Meng, G. Liu, H. Yu, Y. Yuan, W. Yi, L. Zhao, H. Ma, Y. He, Z. Wu, K. Melcher, Q. Qian, H. E. Xu, Y. Wang, J. Li, 'DWARF 53 acts as a repressor of strigolactone signalling in rice', *Nature* **2013**, *504*, 401–405.
[33] L. Wang, B. Wang, L. Jiang, X. Liu, X. Li, Z. Lu, X. Meng, Y. Wang, S. M. Smith, J. Li, 'Strigolactone signaling in Arabidopsis regulates shoot development by targeting D53-Like SMXL repressor proteins for ubiquitination and degradation', *Plant Cell* **2015**, *27*, 3128–3142.
[34] Y. Tsuchiya, M. Yoshimura, Y. Sato, K. Kuwata, S. Toh, D. Holbrook-Smith, H. Zhang, P. McCourt, K. Itami, T. Kinoshita, S. Hagihara, 'Probing strigolactone receptors in *Striga hermonthica* with fluorescence', *Science* **2015**, *349*, 864–868.
[35] M. Yoshimura, A. Sato, K. Kuwata, Y. Inukai, T. Kinoshita, K. Itami, Y. Tsuchiya, S. Hagihara, 'Discovery of Shoot Branching Regulator Targeting Strigolactone Receptor DWARF14', *ACS Cent. Sci.* **2018**, *4*, 230–234.
[36] L.-H. Zhao, X. E. Zhou, W. Yi, Z. Wu, Y. Liu, Y. Kang, L. Hou, P. W. de Waal, S. Li, Y. Jiang, A. Scaffidi, G. R. Flematti, S. M. Smith, V. Q. Lam, P. R. Griffin, Y. Wang, J. Li, K. Melcher, H. E. Xu, 'Destabilization of strigolactone receptor DWARF14 by binding of ligand and E3-ligase signaling effector DWARF3', *Cell Res.* **2015**, *25*, 1219–1236.
[37] A. Šali, T. L. Blundell, 'Comparative Protein Modelling by Satisfaction of Spatial Restraints', *J. Mol. Biol.* **1993**, *234*, 779–815.
[38] G. Jones, P. Willett, R. C. Glen, A. R. Leach, R. Taylor, 'Development and validation of a genetic algorithm for flexible docking', *J. Mol. Biol.* **1997**, *267*, 727–748.
[39] K. S. V. Jagadish, P. B. Kavi Kishor, R. N. Bahuguna, N. von Wirén, N. Sreenivasulu, 'Staying Alive or Going to Die During Terminal Senescence – An Enigma Surrounding Yield Stability', *Front. Plant Sci.* **2015**, *6*, 1–14.
[40] Y. Yamada, M. Umehara, 'Possible Roles of Strigolactones during Leaf Senescence', *Plants* **2015**, *4*, 664–677.
[41] Y. Yamada, S. Furusawa, S. Nagasaka, K. Shimomura, S. Yamaguchi, M. Umehara, 'Strigolactone signaling regulates rice leaf senescence in response to a phosphate deficiency', *Planta* **2014**, *240*, 399–408.
[42] H. Ueda, M. Kusaba, 'Strigolactone Regulates Leaf Senescence in Concert with Ethylene in Arabidopsis', *Plant Physiol.* **2015**, *169*, 138–147.
[43] J. M. Bradow, W. J. Connick Jr., A. B. Pepperman, 'Comparison of the seed germination effects of synthetic analogs of strigol, gibberellic acid, cytokinins, and other plant growth regulators', *J. Plant Growth Regul.* **1988**, *7*, 227–239.
[44] C. E. Cook, L. P. Whichard, B. Turner, M. E. Wall, G. H. Egley, 'Germination of Witchweed (Striga lutea Lour.): Isolation and Properties of a Potent Stimulant', *Science* **1966**,*154*, 1189–1190.
[45] J. M. Bradow, W. J. Connick Jr., A. B. Pepperman, L. H. Wartelle, 'Germination stimulation in wild oats (*Avena fatua* L.) by synthetic strigol analogs and gibberellic acid', *J. Plant Growth Regul.* **1990**, *9*, 35–41.
[46] E. Villedieu-Percheron, M. Lachia, P. M. J. Jung, C. Screpanti, R. Fonné-Pfister, S. Wendeborn, D. Zurwerra, A. De Mesmaeker, 'Chemicals Inducing Seed Germination and Early Seedling Development', *Chimia* **2014**, *68*, 654–663.
[47] M. Lachia, R. Fonné-Pfister, C. Screpanti, S. Rendine, P. Renold, D. Witmer, A. Lumbroso, E. Godineau, D. Hueber, A. De Mesmaeker, 'New and Scalable Access to Karrikin (KAR_1) and Evaluation of Its Potential Application on Corn Germination', *Helv. Chem. Acta* **2018**, *101*, e201800081.
[48] A. De Mesmaeker, A. Lumbroso, C. Screpanti, K. Hermann, M. Lachia, R. Fonné-Pfister, 'Design, synthesis and biological evaluation of strigolactones derivatives for Crop Enhancement', in 'Recent Highlights in the Discovery and Optimization of Crop Protection Products', Eds. P. Maienfisch, I. S. Mangelinckx, Elsevier, 2020, in press.
[49] A. Lumbroso, E. Villedieu-Percheron, D. Zurwerra, C. Screpanti, M. Lachia, P. Y. Dakas, L. Castelli, V. Paul, H. C. Wolf, D. Sayer, A. Beck, S. Rendine, R. Fonné-Pfister, A. De Mesmaeker, 'Simplified strigolactams as potent analogues of strigolactones for the seed germination induction of Orobanche cumana Wallr', *Pest Manage. Sci.* **2016**, *72*, 2054–2068.
[50] 'Growth stages of mono- and dicotyledonous plants: BBCH Monograph', Ed. U. Meier, Julius Kühn-Institute (JKI), Quedlinburg, 2018.

Received January 23, 2020
Accepted February 25, 2020

 © 2020 Wiley-VHCA AG, Zurich, Switzerland

Figure A.1. Article 1. (cont.)

A.2. Synthesis of Highly Substituted Cyclobutanones by a One-Pot Keteniminium-Enamine Process

A full-text version of the second article regarding part II is given in this section.

Check for updates

DOI: 10.1002/hlca.202100022

FULL PAPER

HELVETICA chimica acta

Synthesis of Highly Substituted Cyclobutanones by a One-Pot Keteniminium-Enamine Process

Dylan Dagoneau,[a,1] Amandine Kolleth,[a,1] Pierre Quinodoz,[a] Beyza Horoz,[b] Saron Catak,[b] Alexandre Lumbroso,[a] Sarah Sulzer-Mossé,[a] and Alain De Mesmaeker*[a]

[a] Syngenta Crop Protection AG, Crop Protection Research, Research Chemistry, Schaffhauserstrasse 101, CH-4332, Stein, Switzerland, e-mail: alaindidier.demesmaeker@gmail.com
[b] Bogazici University, Department of Chemistry, Bebek, TR-34342 Istanbul, Turkey

Dedicated to Professor *E. Peter Kündig* at the occasion of his 75th birthday, in recognition of his outstanding scientific contributions and of his great leadership in the Swiss Chemistry community.

Herein, we describe an effective one-pot sequence for the regio- and stereoselective synthesis of highly substituted cyclobutanones. This process relies on first a [2+2] cycloaddition involving a keteniminium salt intermediate with an alkene followed by isomerization of the resulting cyclobutaniminium salt into its cyclic enamine form and then reaction of the latter with an electrophile. The adduct can be either hydrolyzed or reduced to give the corresponding cyclobutanone or cyclobutanamine, respectively, with excellent diastereocontrol. A variety of electrophiles was tolerated allowing the incorporation of diverse substituents and functionalities onto the cyclobutyl ring. Additionally, the coplanarity of diverse cyclic enamines was investigated through a DFT study.

Keywords: cycloaddition, cyclobutanones, diastereoselectivity, enamines, keteniminium salts.

Introduction

The very reactive and electrophilic keteniminium salts are involved in a variety of chemical processes such as [2+2] cycloadditions,[1–3] electrocyclization,[4–9] *Friedel–Crafts*,[10,11] [1,5]-hydride shift[12] and in amide umpolung,[13] among other examples.[14–16] The [2+2] cycloaddition between a keteniminium and an alkene partner is a very reliable method to generate four-membered ring cycles, the resulting cyclobutaniminium salt being usually hydrolyzed into the cyclobutanone (*Scheme 1*). More recently, we showed that the cyclobutaniminium intermediate could be transformed into the corresponding cyclobutanamine by either reduction or addition of organometallics, thus retaining the nitrogen atom in the final structure.[17–19]

In the case of acetylene, the resulting cyclobuteniminium salt could be used as activated dienophile in *Diels–Alder* reaction[20,21] or as efficient *Michael* acceptor.[22]

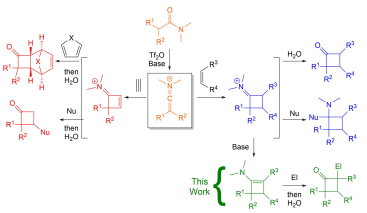

Scheme 1. Synthesis of highly substituted cyclobutanones and cyclobutylamines from the addition of keteniminium to acetylene and to olefins.

[1] These authors contributed equally to this work.
Supporting information for this article is available on the WWW under https://doi.org/10.1002/hlca.202100022

© 2021 Wiley-VHCA AG, Zurich, Switzerland

Figure A.2. Article 2.

In order to further expand the versatility of this approach, we investigated the *in situ* transformation of the initially formed cyclobutaniminium into the corresponding cyclobutenamine, which could be then reacted with electrophiles (*Scheme 1*). The resulting adduct could be hydrolyzed to afford densely substituted cyclobutanones in a highly regio- and stereoselective fashion. Cyclobutenamines have been previously synthesized from the corresponding cyclobutanones or more frequently by [2+2] cycloaddition between an ynamine and a C=C bond.[23–30] However, the ynamine usually carries stabilizing electron withdrawing substituents on the nitrogen and/or at the terminal carbon, which significantly decreases the reactivity of the corresponding enamine. Consequently, only limited examples of cyclobutenamine reactions with electrophiles have been described.[31–35]

Results and Discussion

Our strategy for the regio- and stereoselective synthesis of highly substituted cyclobutanones relies on a novel one-pot procedure involving a [2+2] cycloaddition of a keteniminium to an olefin, followed by the conversion of the resulting cyclobutaniminium into the corresponding enamine, by treatment with a base, and its reaction with an electrophile. Finally, addition of acidic water would hydrolyze the enamine/iminium intermediate to generate the desired substituted cyclobutanone after a single work-up and purification.

The efficient [2+2] cycloaddition between cyclobutyl(piperidin-1-yl)methanone **2a** and styrene **1a**, using triflic anhydride and 2-fluoropyridine, has been chosen to identify the base which would efficiently convert the cyclobutaniminium intermediate into the desired enamine (*Scheme 2*). The screening of various bases at room temperature, in the presence of phenyl isocyanate, revealed that using 3.5 equivalents of DBU together with 2.2 equivalents of electrophile led, after hydrolysis, to the resulting 1,3-ketoamide **3a** in 47% yield with complete *trans* diastereoselectivity. One equivalent of DBU was required to deprotonate the 2-fluoropyridinium formed in the [2+2] step and a second equivalent to form the enamine. As the yield decreases by roughly a factor two when only 2.2 equivalents of DBU were used (22%), it confirmed that the resulting 1,3-iminium-amide was deprotonated by either DBU or unreacted enamine and thus, requiring a third equivalent for the reaction to proceed to completion. Neither increasing the amount of base nor replacing DBU by DBN was beneficial (45% and 37%, resp.) and the use of weaker bases such as *Hünig* base produced the desired product also in lower yield (28%). No ketoamide **3a** was detected when the stronger base LiHMDS was employed.

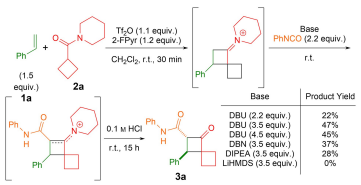

Scheme 2. Screening of bases for the formation and reaction of cyclobutenamine.

With the optimized conditions in hand, other electrophiles were evaluated (*Scheme 3*). Thioisocyanate, a representative alkyl isocyanate and ethyl chloroformate gave the expected carbonylated adducts **3b**–**3d** in good overall yields (41–68%). A variety of functionalities were introduced in moderate to good yields (**3e** to **3k**, 43–74%) by using various *Michael* acceptors with again exclusive trans stereoselectivity, although these reactions required higher temperatures to proceed. The solvent dichloromethane could be replaced easily by 1,2-dichloroethane, but we found that the sequence proceeds also effectively with the less toxic acetonitrile. Interestingly, when the reaction was performed in deuterated chloroform, we observed fully mono-deuteration at the alpha position of ester **3g**. More sterically hindered acceptors such as phenyl maleimide or beta-nitrostyrene led to the desired trans adducts **3e** and **3k**, respectively, with decent diastereocontrol of the third stereogenic center.

Incorporation of heteroatoms were also successfully carried out by using *S*-phenyl benzenethiosulfonate in the case of sulfur (**3l**, 81%) and NCS/NBS for chlorine/bromine (**3m**/**3n**, 51–52%). For the two latter examples, it was important to perform the reaction at low temperature (−20 C) and to use a stoichiometric amount of electrophile in order to cleanly produce the desired halogenated cyclobutanones **3m** and **3n**. Indeed, the use of an excess of reagent at room temperature triggered the bis halogenation which was followed by halide elimination to give the corresponding cyclic enone **3o**. Reaction of the enamine with an

 © 2021 Wiley-VHCA AG, Zurich, Switzerland

Figure A.2. Article 2. (cont.)

Helv. Chim. Acta **2021**, *104*, e2100022

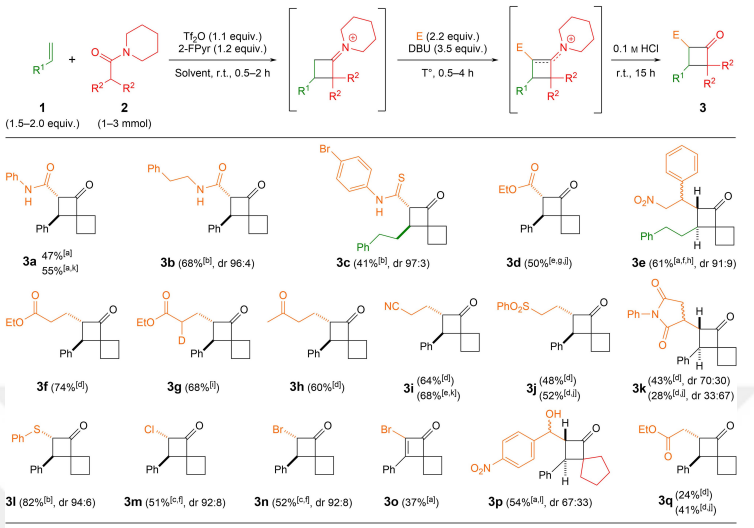

[a] Solvent: CH_2Cl_2, T°: r.t. [b] Solvent: CH_2Cl_2, T°: 40 °C. [c] Solvent: CH_2Cl_2, T°: −20 °C. [d] Solvent: MeCN, T°: 80 °C. [e] Solvent: 1,2-DCE, T°: 80 °C. [f] 1.1 equiv. of E was used instead of 2.2. [g] 4.4 equiv. of E was used instead of 2.2. [h] 2.3 equiv. of DBU was used instead of 3.5. [i] Solvent: $CDCl_3$, T°: 70 °C [j] Proton Sponge was used instead of DBU. [k] Pyrrolidinyl amide was used instead of piperidinyl. [l] *N,N*-Diallyl amide was used instead of piperidinyl.

Scheme 3. Access to highly substituted cyclobutanones through variation of the electrophile partners.

activated 4-nitrobenzaldehyde furnished the desired aldol product **3p** in 54% yield.

C-alkylation of the enamine with ethyl iodoacetate proved difficult with DBU and the desired 1,4-ketoester **3q** was isolated in poor yield which is not surprising as the fairly easy reaction of the DBU with alkylating reagents is reported.[36,37] After an additional screening of bases, the less nucleophilic proton sponge gave significant improvement in the isolation of **3q** (41% *vs.* 24%). Proton sponge was also used in other cases, for example with ethyl chloroformate (**3d**) as reaction of DBU with this electrophile at room temperature is also described.[38] When phenyl vinylsulfone was used, complete consumption of this reagent was observed with DBU whilst with proton sponge the excess of vinylsulfone did not decompose, giving a slight increase in yield for **3j**. Proton sponge was however not always beneficial as a lower yield was obtained in the case of phenylmaleimide **3k**.

In general, the order of addition of the base and electrophile was not important but can be critical in few cases, as in the monohalogenation examples **3m** and **3n**. Indeed, initial addition of NBS followed by DBU would favor the bishalogenation and elimination leading to cyclobutenone **3o**. Moreover, rapid decomposition of beta-nitrostyrene through polymerization was observed if DBU is added last. Thus, addition first of only 2.3 equivalents of DBU followed by nitrostyrene was decisive to efficiently get the desired product **3e** (61%).

Although most of the scope was carried out using amide **2a** and styrene **1a** for the [2+2] step due to the effectiveness and rapidness of the reaction, this methodology is not limited to those as shown in *Scheme 4*. Other alkenes bearing a benzyl (**3r**), alkyl

 © 2021 Wiley-VHCA AG, Zurich, Switzerland

Figure A.2. Article 2. (cont.)

Helv. Chim. Acta 2021, 104, e2100022

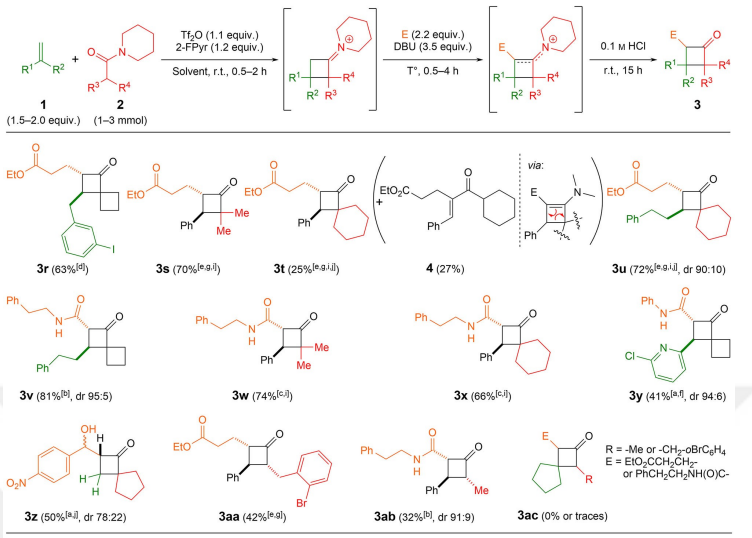

[a] Solvent: CH_2Cl_2, T°: r.t. [b] Solvent: CH_2Cl_2, T°: 40 °C. [c] Solvent: 1,2-DCE, T°: 60 °C. [d] Solvent: MeCN, T°: 80 °C. [e] Solvent: 1,2-DCE, T°: 80 °C.
[f] 1.1 equiv. of E was used instead of 2.2. [g] 4.4 equiv. of E was used instead of 2.2. [h] *N,N*-Diallyl amide was used instead of piperidinyl.
[i] [2+2] Cycloaddition performed at 60 °C. [j] Final hydrolysis performed at 70 °C.

Scheme 4. Access to highly substituted cyclobutanones through variation of the alkenes and the substituents in α-position to the amide.

(**3v**) or 2-chloropyridine (**3y**) substituents were tolerated as well as simply ethylene (**3z**). Despite giving the desired [2+2] cycloadduct, gem-disubstituted alkene like methylenecyclopentane generated too much steric bulk in the cyclobutenamine to react efficiently with an electrophile (**3ac**).

On the amide side, the cyclobutyl could be replaced by cyclopentyl (**3z**), cyclohexyl (**3t**, **3u** and **3x**) and also acyclic substituents like dimethyl (**3s** and **3w**). In the cases of the cyclohexyl and dimethyl groups, the [2+2] cycloadditions were performed at 60 C instead of room temperature due to the partial insolubility in 1,2-DCE of the initially formed iminium salts resulting from the reaction of the amide with Tf_2O (incomplete conversion was also observed in MeCN at room temperature). In addition, larger amount of electrophile was required to force the conversion to completion suggesting that the corresponding enamines were less reactive. This could arise from the steric bulk generated by the gem-dimethyl or spirocyclohexyl substituents, compared to spirocyclobutyl, and/or by the interference with the piperidine moiety which might not be able to reach the optimal coplanar orientation of the nitrogen lone pair with the C=C bond required for high nucleophilic reactivity of the enamine.

A DFT study was conducted in order to examine coplanarity of cyclic enamines preceding some of the cyclobutanones reported in *Scheme 3* and *Scheme 4*. Enamine structures were modelled at ωB97XD[39] level of theory, as implemented in the G16 software package.[40] Geometry optimizations were performed in DCM (ε = 8.93), utilizing the self-consistent reaction

 © 2021 Wiley-VHCA AG, Zurich, Switzerland

Figure A.2. Article 2. (cont.)

Helv. Chim. Acta **2021**, *104*, e2100022 HELVETICA

field (SCRF) theory[41] through the IEF-PCM[42,43] model, at 298 K and 1 atm.

Coplanarity of enamines were evaluated by using two descriptors, namely, the pyramidalization degree (d) and the improper dihedral angle (φ), as depicted in *Figure 1*.

Enamines were selected to investigate both the effect of *N*- and *C*-substituents on the amide, as well as the effect of alkene substituent(s) involved in the [2+2] cycloaddition. Moreover, the ring size of several cyclic enamines were evaluated and listed in *Figure 2*.

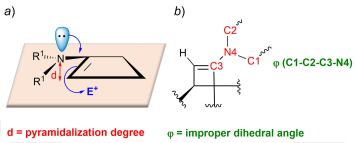

Figure 1. Depiction of pyramidalization degree (d) and improper dihedral angle (φ).

Comparison of enamines **e1**–**e4** shows that the identity of the *N*-substituent(s) has a significant effect on the degree of pyramidalization. Improper dihedral angles (φ) and degree of pyramidalization values (d) show that the pyrrolidyl moiety enables more planarity than *N,N*-diallyl, followed by dimethyl and piperidinyl moieties. On the other hand, enamines **e4**–**e6** and **e1** *vs.* **e9** show that *C*-substituent(s) adjacent to the enamine do not have a significant impact on (d) and (φ).

The effect of the alkene substituent on pyramidalization of the enamine nitrogen was investigated by comparing enamines **e6** *vs.* **e7** and **e8** *vs.* **e9**. Results show that, similar to *C*-substituent(s) on amides, using alkenes with differing substituents does not create any substantial difference in (d) and (φ) values.

Along with cyclobutenamines, cyclopentenamines and cyclohexenamines were also examined. Comparison among enamines **e10**–**e15** show similar results with *Wennemers* and coworker's[44] recent study. The pyrrolidine group lowers the degree of pyramidalization, therefore, increases the coplanarity compared to the piperidinyl moiety. Also (d) and (φ) values for

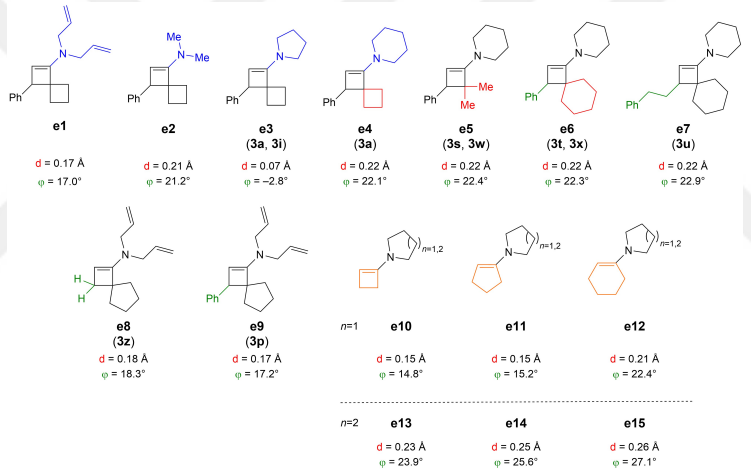

Figure 2. Enamine structures and corresponding pyramidalization degree (d) and improper dihedral angle φ (C1-C2-C3-N4) values. Corresponding cyclobutanones indicated in parenthesis, when applicable. ωB97XD/6-31+G(d,p), 298 K, 1 atm in CH_2Cl_2.

 © 2021 Wiley-VHCA AG, Zurich, Switzerland

Figure A.2. Article 2. (cont.)

Helv. Chim. Acta 2021, 104, e2100022

enamines **e10**–**e12** show a decrease in coplanarity for the cyclohexenamine **e12** even when pyrrolidinyl is used.

Moreover, for enamines listed in *Figure 2*, C=C bond lengths were shown to be around *ca.* 1.35 Å, whereas the C–N bond lengths are in the range of 1.35 Å (**e3**)–1.41 Å (**e15**, **e14**). Comparison with ideal C=C (*ca.* 1.33 Å), C–N (*ca.* 1.46 Å) and C=N (*ca.* 1.28 Å) bond lengths[45] indicate a somewhat shorter C–N bond when pyramidalization is low (**e3**), consistent with conjugation in enamines.

According to the DFT study, higher reactivity and chemoselectivity might be reached with pyrrolidinyl amides as starting material compared to the corresponding piperidinyl amides mainly used in the present work. Nevertheless, the overall yield of such multistep processes might be influenced by several factors beyond the intrinsic reactivity of the enamine intermediate (*vide infra*).

The increase of substituent's bulk also made the hydrolysis step more difficult in the case of the spirocyclohexyl derivatives, thus requiring higher temperatures, and gave additional strain into the cyclobutyl ring which triggered in the case of **3t** the formation of the retro [2 + 2] cycloadduct **4** (*Scheme 4*). This side reaction was observed prior to the hydrolysis step and occurred most probably onto the enamine intermediate level (post reaction with ethyl acrylate) and was favored by the phenyl substituent which weakens the central bond cleaved during this process. Indeed, when the aromatic ring was replaced by an alkyl substituent, the desired compound **3u** was obtained in high yield without ring cleavage. Moreover, by using an alkyl isocyanate (for **3x**) instead of ethyl acrylate (for **3t**), the resulting push-pull stabilized enamine did not undergo ring cleavage despite the presence of the phenyl and spirocyclohexyl substituents.

Alpha monosubstituted acetamides underwent, as expected, [2 + 2] cycloaddition with styrene and the resulting cyclobutaniminium could be transformed regioselectively into the less substituted enamine. The latter reacted stereoselectively with ethyl acrylate and an alkyl isocyanate leading to desired cyclobutanones **3aa** and **3ab** in encouraging overall yield. This process starting from monosubstituted amides would benefit from further optimization of the reaction.

Finally, we investigated the substituents on the nitrogen of the amide. Most of the scope was performed with a piperidinyl group as it is one of the most effective amides in the keteniminium chemistry.[6,21] It is literature known that the pyrrolidinyl would be preferred for the enamine chemistry (*cf. Stork* enamine),[46] but this moiety was previously rather inferior in the keteniminium step,[4,5,20] therefore it would be interesting to compare both in the overall process. Using either acrylonitrile or phenyl isocyanate as an electrophile, the pyrrolidinyl substrate gave a slightly improved yields in these two cases (**3a** and **3i**, *Scheme 3*). These results are in good agreement with our present DFT study. It is worth noting that the less reactive *N,N*-diallylenamine was sufficiently nucleophilic to afford the desired substituted cyclobutanones with good overall yield (**3p** in *Scheme 3* and **3z** in *Scheme 4*).

In an attempt to further extend our method to the reaction with acyl chloride as electrophile, we observed that treating a cyclobutaniminium with DBU (3.5 equiv.) and benzoyl chloride (2.2 equiv.) led to a complex mixture of adducts. When DBU was replaced by proton sponge, only traces of desired 1,3-diketone **3ad** was detected after hydrolysis but three other products could be isolated and identified: 42% of enaminone **5** and 29% of a mixture of two enol esters **6**, resulting from the reaction of **5** with a second equivalent of acyl chloride (*Scheme 5*). This mixture highlights that the process indeed goes through an enamine intermediate. These three adducts could be potentially converted into the desired product **3ad** but those proved to be reluctant towards hydrolysis, even when treated with a 2 M aqueous solution of HCl at 70 C. By reducing the amount of benzoyl chloride to 1.1 equiv., we could favor the formation of the enaminone **5** in 72% together with a small amount of **6**. On the contrary, increasing to 4.4 equiv. of electrophile, complete conversion of **5** into enol esters **6** was achieved with an isolation yield of 75%. Treating a THF solution of crude **6** with aqueous 1 M NaOH triggered the enol ester hydrolysis towards the diketone **3ad** but under these conditions, ring opening of the latter occurred readily to furnished in 67% the corresponding 1,5-ketoacid **7**. However, treating the same crude **6** with TMSOK (2.0 equiv.) afforded the desired but rather unstable diketone **3ad** in 54% yield with only traces of the over hydrolyzed product **7**. We assumed that with TMSOK the corresponding silyl enol ether of **3ad** is formed *in situ*, thus protected from the ring opening, and lead to the diketone under aqueous work-up.

The rather modest yield obtained by reaction of cyclobutenamine with an alkylating reagent as ethyl iodoacetate (**3q** in *Scheme 3*) stimulated us to investigate a more reactive electrophile as bromo(methoxy) methane which led us to another interesting reaction.

© 2021 Wiley-VHCA AG, Zurich, Switzerland

Figure A.2. Article 2. (cont.)

Helv. Chim. Acta **2021**, *104*, e2100022

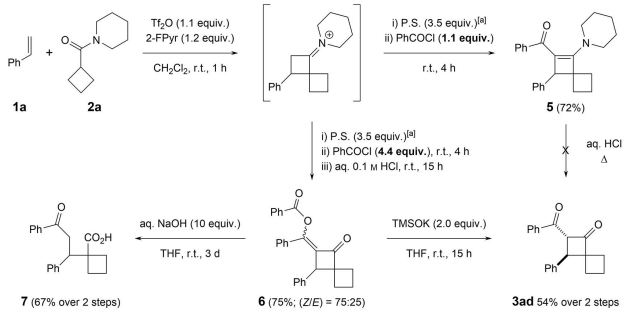

Scheme 5. Reaction of cyclobutenamine with benzoyl chloride and isolation of the resulting enamine intermediate.[a] P.S. stand for proton sponge.

As depicted in *Scheme 6*, the desired C-alkylation of the enamine **8** occurred and further elimination of methanol was triggered by the excess of base and the resulting methylene cyclobutaniminium, a highly reactive *Michael* acceptor, was trapped by a second equivalent of enamine **8** to afford after hydrolysis dicyclobutanones **9** in 62% yield.

We designed additional substrates in order to incorporate an intramolecular step into the sequence, either at the [2+2] step which gave functionalized tricyclic structure **11**, or at the enamine level (through C-alkylation) which afford in very good yields (70–75%) strain tetracyclic scaffolds (*Scheme 7*). These tetracycles **13** and **15** could potentially be obtained directly through an intermolecular [2+2] cycloaddition involving a keteniminium salt with indene or 1,4-dihydronaphthalene derivatives, thus not requiring the use of an enamine intermediate. However, such approach with unsymmetrical alkene (as the methyl group on the aromatic ring of **15**) would lead to a mixture of regioisomers of cycloadducts that we could avoid with the enamine methodology.

The use of *N,N*-diallylamide permitted to retain the amine functionality in the final product by stereoselective reduction of the final intermediate with $LiAlH(O^tBu)_3$ instead of hydrolysis. It was necessary to

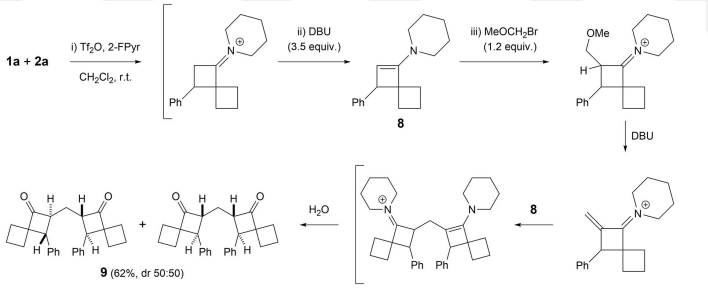

Scheme 6. Trapping of *in situ* formed methylene cyclobutaniminium salt by cyclobutenamine.

 © 2021 Wiley-VHCA AG, Zurich, Switzerland

Figure A.2. Article 2. (cont.)

Helv. Chim. Acta **2021**, *104*, e2100022

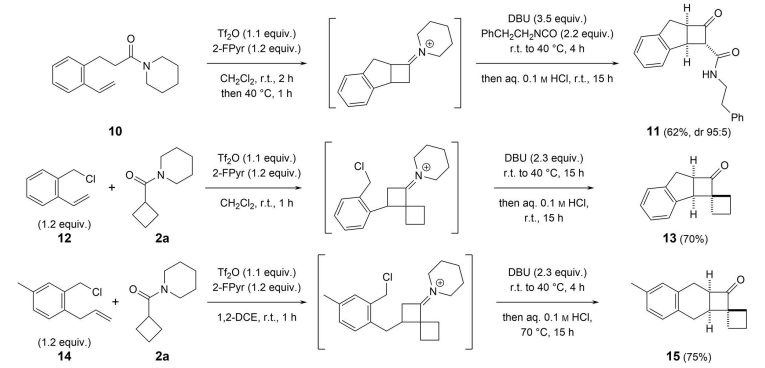

Scheme 7. Incorporation of an intramolecular step into the one-pot process to access polycyclic skeletons.

acidify the reaction medium with methanesulfonic acid prior to the reduction step to ensure that the intermediate is fully in its iminium form, and not in the enamine one. Under these conditions, the desired *N,N*-diallylcyclobutanamines were isolated with good overall yield (42–53%, *Scheme 8*). It is worth noting that the *N,N*-diallyl substituents can be readily removed under mild conditions (palladium catalyst in the presence of dimethylbarbituric acid) and the resulting free amine can be further functionalized.[17–19]

As shown in *Scheme 9*, the reaction of the cyclobutaniminium intermediate with an excess of *Bredereck's* reagent, which acts as base and electrophile, triggered the formation of a mixture of two vinamidinium salts **18** and **19**, the latter resulting from a simple piperidine/dimethylamine exchange. These species which are stable towards aqueous work-up proved to be excellent candidates for condensations with 1,3-dinucleophiles. For example, treatment of **18** and **19** with benzamidine afforded the corresponding pyrimidine *ortho*-quinodimethane **20** in 45% yield over two steps. Its structure has been confirmed by X-rays diffraction and displayed an elongated central cyclobutyl C–C bond between the phenyl and the spirocyclobutyl substituents (1.60 Å, see the *Supporting Information*).

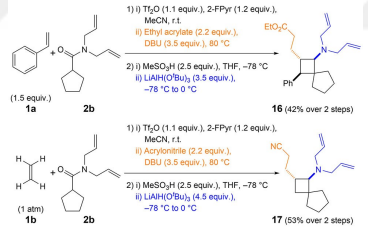

Scheme 8. Synthesis of cyclobutanamines through reduction instead of final hydrolysis.

Conclusions

In summary, we report a novel regio- and stereoselective one-pot process for the synthesis of highly substituted cyclobutanones and cyclobutanamines. This sequence relies on [2+2] cycloaddition of keteniminium with a double bond, iminium-enamine isomerization and enamine reaction with electrophiles followed by hydrolysis or reduction in high overall yield. A DFT study on various enamine intermediates was conducted to highlight the influence of the substituents on the enamine coplanarity. Structural modifications at the level of the olefin, the amide and the electrophile are very well tolerated and makes this

 © 2021 Wiley-VHCA AG, Zurich, Switzerland

Figure A.2. Article 2. (cont.)

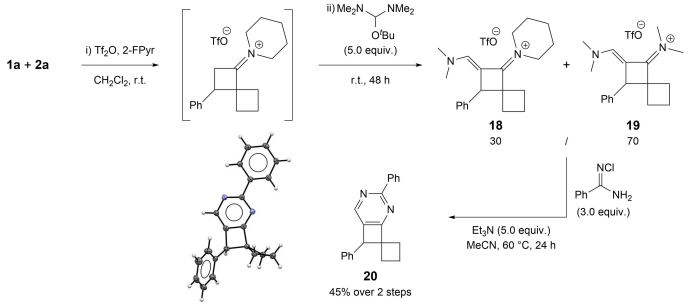

Scheme 9. Formation of vinamidiniums with *Bredereck*'s reagent and their reaction with 1,3-dinucleophile.

approach very flexible for the synthesis of functionalized cyclobutanones. The latter are key intermediates for further transformations into, for example, the corresponding cyclobutanamines, γ-lactones, γ-lactams, cyclopentanones and cyclohexanones.

Experimental Section

See the *Supporting Information* for all the experimental procedures.

Representative Procedure

In a dried flask under argon charged with a solution of cyclobutyl(piperidin-1-yl)methanone **2a** (300 mg, 1.79 mmol, 1.00 equiv.) and 2-fluoropyridine (0.185 mL, 2.15 mmol, 1.20 equiv.) in dichloromethane (14.9 mL) was added dropwise at r.t. styrene **1a** (0.309 mL, 2.69 mmol, 1.50 equiv.) and then triflic anhydride (0.332 mL, 1.97 mmol, 1.10 equiv.). The resulting mixture was stirred at r.t. for 1 h. Then benzenesulfonylsulfanylbenzene (0.988 g, 3.95 mmol, 2.20 equiv.) followed by DBU (0.938 mL, 6.28 mmol, 3.50 equiv.) were added portionwise/dropwise at r.t. and the mixture was stirred at 40 C for 4 h. The reaction was cooled to r.t. and a 0.1 M aqueous solution of HCl was added dropwise until acidic pH and the resulting biphasic mixture was stirred vigorously at r.t. for 15 h. The two layers were separated, and the aqueous phase was extracted with dichloromethane (×2). The combined organic layers were dried over Na_2SO_4, filtered and concentrated under reduced pressure. Purification of the crude by flash column chromatography (cyclohexane/AcOEt 95:5 to 85:15) afforded 435 mg (82% yield) of cyclobutanone **3l** as a light yellow oil.

Acknowledgements

We thank all the NMR experts, *Leonhard Hagmann*, *Katharina Gaus* and *Marie-Madeleine Stempien* for their help in determining the relative configurations. *B. H.* and *S. C.* acknowledge TUBITAK for financial support under grant number 115Z738.

Author Contribution Statement

The project and experiments were designed by *D. D.*, *A. K.*, *P. Q.*, *A. L.*, *S. S.-M.* and *A. De M.* The experimental work was performed by *D. D.*, *A. K.* and *P. Q.* and the computational work was conducted by *B. H.* and *S. C.* All authors contributed to the manuscript writing and review process.

References

[1] J. Marchand-Brynaert, L. Ghosez, 'Cycloadditions of Keteneimmonium Cations to Olefins and Dienes. New Synthesis

 © 2021 Wiley-VHCA AG, Zurich, Switzerland

Figure A.2. Article 2. (cont.)

of Four-Membered Rings', *J. Am. Chem. Soc.* **1972**, *94*, 2870–2872.
[2] J.-B. Falmagne, J. Escudero, S. Taleb-Sahraoui, L. Ghosez, 'Cyclobutanone and Cyclobutenone Derivatives by Reaction of Tertiary Amides with Alkenes or Alkynes', *Angew. Chem. Int. Ed.* **1981**, *20*, 879–880.
[3] M. Lachia, P. M. J. Jung, A. De Mesmaeker, 'A novel approach toward the synthesis of strigolactones through intramolecular [2+2] cycloaddition of ketenes and keteneiminiums to olefins. Application to the asymmetric synthesis of GR-24', *Tetrahedron Lett.* **2012**, *53*, 4514–4517.
[4] E. Villedieu-Percheron, S. Catak, D. Zurwerra, R. Staiger, M. Lachia, A. De Mesmaeker, '6π/10π-Electrocyclization of ketene-iminium salts for the synthesis of substituted naphthylamines', *Tetrahedron Lett.* **2014**, *55*, 2446–2449.
[5] A. Lumbroso, J. Behra, A. Kolleth, P.-Y. Dakas, U. Karadeniz, S. Catak, S. Sulzer-Mossé, A. De Mesmaeker, 'Access to functionalized 3-amino-benzothiophenes using ketenimininium intermediates', *Tetrahedron Lett.* **2015**, *56*, 6541–6545.
[6] A. Kolleth, S. Müller, A. Lumbroso, G. Tanriver, S. Catak, S. Sulzer-Mossé, A. De Mesmaeker, 'Access to 3-aminobenzothiophenes and 3-aminothiophenes fused to 5-membered heteroaromatic rings through 6π-electrocyclization reaction of keteniminium salts', *Tetrahedron Lett.* **2018**, *59*, 3242–3248.
[7] D. Dagoneau, A. Kolleth, A. Lumbroso, G. Tanriver, S. Catak, S. Sulzer-Mossé, A. De Mesmaeker, 'Straightforward Synthesis of 3-Aminothiophenes Using Activated Amides', *Helv. Chim. Acta* **2019**, *102*, e1900031.
[8] D. Dagoneau, A. Kolleth, P. Quinodoz, G. Tanriver, S. Catak, A. Lumbroso, S. Sulzer-Mossé, A. De Mesmaeker, 'Ketenimininium Salts as Key Intermediates for the Efficient Synthesis of 3-AminoIndoles and -Benzofurans', *Helv. Chim. Acta* **2019**, *102*, e1900217.
[9] G. Tanriver, D. Dagoneau, U. Karadeniz, A. Kolleth, A. Lumbroso, S. Sulzer-Mossé, A. De Mesmaeker, S. Catak, 'Ketenimininium Salts: Reactivity and Propensity toward Electrocyclization Reactions', *J. Org. Chem.* **2020**, *85*, 449–463.
[10] A. Kolleth, D. Dagoneau, P. Quinodoz, A. Lumbroso, M. Avanthay, S. Catak, S. Sulzer-Mossé, A. De Mesmaeker, 'Synthesis of Benzazepinones *via* Intramolecular Cyclization Involving Ketene Iminium Intermediates', *Helv. Chim. Acta* **2019**, *102*, e1900168.
[11] B. R. Brutiu, W. A. Bubeneck, O. Cvetkovic, L. Jing, N. Maulide, 'On the formation of seven-membered rings by arene-ynamide cyclization', *Monatsh. Chem.* **2019**, *150*, 3–10.
[12] M. Lecomte, G. Evano, 'Harnessing the Electrophilicity of Ketenimininium Ions: A Simple and Straightforward Entry to Tetrahydropyridines and Piperidines from Ynamides', *Angew. Chem. Int. Ed.* **2016**, *55*, 4547–4551.
[13] D. Kaiser, A. de la Torre, S. Shaaban, N. Maulide, 'Metal-Free Formal Oxidative C–C Coupling by In Situ Generation of an Enolonium Species', *Angew. Chem. Int. Ed.* **2017**, *56*, 5921–5925.
[14] F. Mahuteau-Betzer, P.-Y. Ding, L. Ghosez, 'First [4+2] Cycloadditions Involving the Olefinic Bond of an 'Aldoketeniminium Salt' (=*N*-Alk-1-enylideneaminium Salt)', *Helv. Chim. Acta* **2005**, *88*, 2022–2031.
[15] C. Madelaine, V. Valerio, N. Maulide, 'Revisiting Ketenimininium Salts: More than the Nitrogen Analogs of Ketenes', *Chem. Asian J.* **2011**, *6*, 2224–2239.
[16] G. Evano, M. Lecomte, P. Thilmany, C. Theunissen, 'Keteniminium Ions: Unique and Versatile Reactive Intermediates for Chemical Synthesis', *Synthesis* **2017**, *49*, 3183–3214.
[17] A. Kolleth, A. Lumbroso, G. Tanriver, S. Catak, S. Sulzer-Mossé, A. De Mesmaeker, 'Synthesis of amino-cyclobutanes via [2+2] cycloadditions involving keteniminium intermediates', *Tetrahedron Lett.* **2016**, *57*, 2697–2702.
[18] A. Kolleth, A. Lumbroso, G. Tanriver, S. Catak, S. Sulzer-Mossé, A. De Mesmaeker, 'New access to quaternary aminocyclobutanes via nucleophilic addition on cyclobutaniminium salts', *Tetrahedron Lett.* **2016**, *57*, 3510–3514.
[19] A. Kolleth, A. Lumbroso, G. Tanriver, S. Catak, S. Sulzer-Mossé, A. De Mesmaeker, 'Synthesis of 4-membered ring alkaloid analogues *via* intramolecular [2+2] cycloaddition involving keteniminium salt intermediates', *Tetrahedron Lett.* **2017**, *58*, 2904–2909.
[20] A. Lumbroso, S. Catak, S. Sulzer-Mossé, A. De Mesmaeker, 'Cycloaddition of keteniminium with terminal alkynes toward cyclobuteniminium and their use in Diels–Alder reactions', *Tetrahedron Lett.* **2014**, *55*, 5147–5150.
[21] A. Lumbroso, S. Catak, S. Sulzer-Mossé, A. De Mesmaeker, 'Synthesis of cyclobuteniminium salts derived from aldoketeniminium salts and study of their reactivity in Diels–Alder reaction', *Tetrahedron Lett.* **2014**, *55*, 6721–6725.
[22] A. Lumbroso, S. Catak, S. Sulzer-Mossé, A. De Mesmaeker, 'Efficient access to functionalized cyclobutanone derivatives using cyclobuteniminium salts as highly reactive Michael acceptors', *Tetrahedron Lett.* **2015**, *56*, 2397–2401.
[23] L. Tenud, M. Weilenmann, E. Dallwigk, '1,3-Cyclobutandionderivate aus Keten', *Helv. Chim. Acta* **1977**, *60*, 975–977.
[24] J. Ficini, A. Guingant, J. J'Angelo, G. Stork, 'Synthese stereoselective des barcis et bartrans carboxy-4', *Tetrahedron Lett.* **1983**, *24*, 907–910.
[25] S. Ghose, T. L. Gilchrist, '[2+2] Cycloadditions of lithium alkynamides produced by fragmentation of 5-lithio-1-phenyl-1,2,3-triazoles', *J. Chem. Soc. Perkin Trans. 1* **1991**, 775–779.
[26] N. Riddell, K. Villeneuve, W. Tam, 'Ruthenium-Catalyzed [2+2] Cycloadditions of Ynamides', *Org. Lett.* **2005**, *7*, 3681–3684.
[27] A. de Meijere, M. Limbach, A. Janssen, A. Lygin, V. S. Korotkov, 'Versatile Access to 2-Aminocyclobutene-1-carboxylic Acid Derivatives and Their Incorporation into Small Peptides', *Eur. J. Org. Chem.* **2010**, 3665–3671.
[28] A. B. Koldobskii, E. V. Solodova, I. A. Godovikov, P. V. Verteletskii, V. N. Kalinin, '1-Bromo-2-trifluoroacetylcyclobutenes as novel building blocks for the construction of trifluoromethyl substituted heterocycles. Part 3: Synthesis of trifluoromethylsubstituted pyridines, condensed with cyclobutene moieties', *J. Fluorine Chem.* **2010**, *131*, 873–878.
[29] H. Li, R. P. Hsung, K. A. DeKorver, Y. Wei, 'Copper-Catalyzed Ficini [2+2] Cycloaddition of Ynamides', *Org. Lett.* **2010**, *12*, 3780–3783.
[30] C. Peng, J. Zhang, J. Xue, S. Li, X.-N. Wang, J. Chang, 'Lewis Acids Catalyzed Annulations of Ynamides with Acyl

 © 2021 Wiley-VHCA AG, Zurich, Switzerland

Figure A.2. Article 2. (cont.)

Chlorides for Constructing 4-Amino-2-naphthol Derivatives and 3-Aminocyclobutenones', *J. Org. Chem.* **2018**, *83*, 9256–9266.
[31] K. T. Wanner, A. Kärtner, 'Cyclobutanone-Enamine: Synthese und Reaktionen des N-(1-Cyclobutenyl)-piperidins', *Arch. Pharm.* **1985**, *318*, 655–658.
[32] D. Hazelard, A. Fadel, 'Synthesis of optically active (+)-2-benzyl-, (+)-2-octyl-, and (+)-2-tetradec-5'-enylcyclobutanones via metallated chiral imines or hydrazones', *Tetrahedron: Asymmetry* **2005**, *16*, 2067–2070.
[33] D. J. Aitken, A. M. Bernard, F. Capitta, A. Frongia, R. Guillot, J. Ollivier, P. P. Piras, F. Secci, M. Spiga, 'Very high stereoselectivity in organocatalyzed desymmetrizing aldol reactions of 3-substituted cyclobutanones', *Org. Biomol. Chem.* **2012**, *10*, 5045–5048.
[34] F. Capitta, A. Frongia, J. Ollivier, D. J. Aitken, F. Secci, P. P. Piras, R. Guillot, 'Enantioselective Organocatalyzed Desymmetrization of 3-Substituted Cyclobutanones through Michael Addition to Nitroalkenes', *Synlett* **2015**, *26*, 123–126.
[35] M. Wang, J. Chen, Z. Chen, C. Zhong, P. Lu, 'Enantioselective Desymmetrization of Cyclobutanones Enabled by Synergistic Palladium/Enamine Catalysis', *Angew. Chem. Int. Ed.* **2018**, *57*, 2707–2711.
[36] A. Gholamipour-Shirazi, C. Rolando, 'Kinetics screening of the *N*-alkylation of organic superbases using a continuous flow microfluidic device: basicity *versus* nucleophilicity', *Org. Biomol. Chem.* **2012**, *10*, 8059–8063.
[37] M. Liu, L. Liang, T. Liang, X. Lin, L. Shi, F. Wang, 'Cycloaddition of CO_2 and epoxides catalyzed by dicationic ionic liquids mediated metal halide: Influence of the dication on catalytic activity', *J. Mol. Catal. A* **2015**, *408*, 242–249.
[38] M. Carafa, E. Mesto, E. Quaranta, 'DBU-Promoted Nucleophilic Activation of Carbonic Acid Diesters', *Eur. J. Org. Chem.* **2011**, 2458–2465.
[39] J.-D. Chai, M. Head-Gordon, 'Long-range corrected hybrid density functionals with damped atom–atom dispersion corrections', *Phys. Chem. Chem. Phys.* **2008**, *10*, 6615–6620.
[40] M. J. Frisch, G. W. Trucks, H. B. Schlegel, G. E. Scuseria, M. A. Robb, J. R. Cheeseman, G. Scalmani, V. Barone, G. A. Petersson, H. Nakatsuji, X. Li, M. Caricato, A. V. Marenich, J. Bloino, B. G. Janesko, R. Gomperts, B. Mennucci, H. P. Hratchian, J. V. Ortiz, A. F. Izmaylov, J. L. Sonnenberg, D. Williams-Young, F. Ding, F. Lipparini, F. Egidi, J. Goings, B. Peng, A. Petrone, T. Henderson, D. Ranasinghe, V. G. Zakrzewski, J. Gao, N. Rega, G. Zheng, W. Liang, M. Hada, M. Ehara, K. Toyota, R. Fukuda, J. Hasegawa, M. Ishida, T. Nakajima, Y. Honda, O. Kitao, H. Nakai, T. Vreven, K. Throssell, J. A. Montgomery Jr., J. E. Peralta, F. Ogliaro, M. J. Bearpark, J. J. Heyd, E. N. Brothers, K. N. Kudin, V. N. Staroverov, T. A. Keith, R. Kobayashi, J. Normand, K. Raghavachari, A. P. Rendell, J. C. Burant, S. S. Iyengar, J. Tomasi, M. Cossi, J. M. Millam, M. Klene, C. Adamo, R. Cammi, J. W. Ochterski, R. L. Martin, K. Morokuma, O. Farkas, J. B. Foresman, D. J. Fox, Gaussian 16, Revision A.03, Gaussian, Inc., Wallingford CT, 2016.
[41] J. Tomasi, B. Mennucci, R. Cammi, 'Quantum Mechanical Continuum Solvation Models', *Chem. Rev.* **2005**, *105*, 2999–3094.
[42] B. Mennucci, E. Cancès, J. Tomasi, 'Evaluation of Solvent Effects in Isotropic and Anisotropic Dielectrics and in Ionic Solutions with a Unified Integral Equation Method: Theoretical Bases, Computational Implementation, and Numerical Applications', *J. Phys. Chem. B.* **1997**, *101*, 10506–10517.
[43] J. Tomasi, B. Mennucci, E. Cancès, 'The IEF version of the PCM solvation method: an overview of a new method addressed to study molecular solutes at the QM ab initio level', *J. Mol. Struct.* **1999**, *464*, 211–226.
[44] T. Schnitzer, J. S. Möhler, H. Wennemers, 'Effect of the enamine pyramidalization direction on the reactivity of secondary amine organocatalysts', *Chem. Sci.* **2020**, *11*, 1943–1947.
[45] T. Y. Nikolaienko, V. S. Chuiko, L. A. Bulavin, 'The dataset of covalent bond lengths resulting from the first-principle calculations', *Comput. Theor. Chem.* **2019**, *1163*, 112508.
[46] G. Stork, A. Brizzolara, H. Landesman, J. Szmuszkovicz, R. Terrell, 'The Enamine Alkylation and Acylation of Carbonyl Compounds', *J. Am. Chem. Soc.* **1963**, *85*, 207–222.

Received February 3, 2021
Accepted March 18, 2021

 © 2021 Wiley-VHCA AG, Zurich, Switzerland

Figure A.2. Article 2. (cont.)

APPENDIX B: C_3-SUBSTITUENT EFFECT

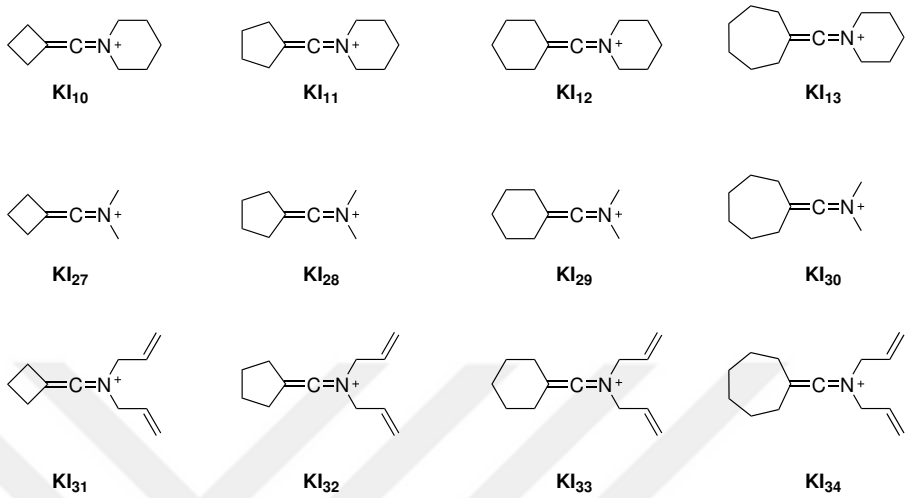

Figure B.1. C_3-substituted KIs with differing ring size with respect to piperidinyl, *N,N*-dimethyl and *N,N*-dially moieties.

Table B.1. Free energy of activation ($\Delta G^{\ddagger}$) and reaction (ΔG_{rxn}) for comparison of the ring size effect on reactivity of KIs when N_1-substituents are piperidinyl, *N,N*-dimethyl and *N,N*-dially, M06-2X/6-31+G(d,p) with IEFPCM in $CHCl_3$ (ϵ=4.7113); energies in kcal/mol.

KI	$\Delta G^{\ddagger}_1$	$\Delta G^{\ddagger}_2$	ΔG_{rxn}	**KI**	$\Delta G^{\ddagger}_1$	$\Delta G^{\ddagger}_2$	ΔG_{rxn}	**KI**	$\Delta G^{\ddagger}_1$	$\Delta G^{\ddagger}_2$	ΔG_{rxn}
KI$_{10}$	18.2	4.8	-31.2	**KI$_{27}$**	17.4	4.8	-31.9	**KI$_{31}$**	18.7	5.9	-29.5
KI$_{11}$	19.7	8.7	-28.7	**KI$_{28}$**	18.9	8.9	-28.6	**KI$_{32}$**	20.0	8.9	-28.1
KI$_{12}$	20.6	13.8	-30.0	**KI$_{29}$**	20.5	12.6	-30.1	**KI$_{33}$**	22.2	14.1	-27.6
KI$_{13}$	21.7	12.6	-26.0	**KI$_{30}$**	20.4	10.9	-27.4	**KI$_{34}$**	22.0	12.4	-26.6

APPENDIX C: N_1-SUBSTITUENT EFFECT

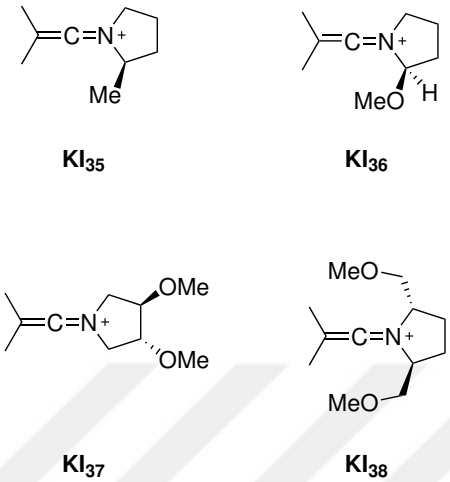

Figure C.1. KIs bearing chiral auxiliaries as N_1-substituent.

Table C.1. Free energy of activation ($\Delta G^{\ddagger}$) and reaction (ΔG_{rxn}) for KIs bearing chiral auxiliaries, M06-2X/6-31+G(d,p) with IEFPCM in $CHCl_3$ (ϵ=4.7113); energies in kcal/mol.

KI	$\Delta G^{\ddagger}_1$	$\Delta G^{\ddagger}_2$	ΔG_{rxn}
KI$_{35}$	21.6	12.3	-26.5
KI$_{36}$	19.4	9.3	-28.1
KI$_{37}$	19.4	10.1	-29.0
KI$_{38}$	22.9	14.9	-22.6

APPENDIX D: COPY-RIGHT LIST

D.1. The License for Figure 3.2

JOHN WILEY AND SONS LICENSE
TERMS AND CONDITIONS

Jul 11, 2021

This Agreement between Bogazici University -- Beyza Horoz ("You") and John Wiley and Sons ("John Wiley and Sons") consists of your license details and the terms and conditions provided by John Wiley and Sons and Copyright Clearance Center.

License Number	5102530597916
License date	Jul 05, 2021
Licensed Content Publisher	John Wiley and Sons
Licensed Content Publication	Angewandte Chemie International Edition
Licensed Content Title	Cyclobutanone and Cyclobutenone Derivatives by Reaction of Tertiary Amides with Alkenes or Alkynes
Licensed Content Author	Léon Ghosez, Sofia Taleb-Sahraoui, José Escudero, et al
Licensed Content Date	Dec 22, 2003
Licensed Content Volume	20
Licensed Content Issue	10
Licensed Content Pages	2
Type of use	Dissertation/Thesis
Requestor type	University/Academic
Format	Print and electronic

Portion	Figure/table
Number of figures/tables	1
Will you be translating?	No
Title	Mechanistic Investigation of [2+2] Cycloaddition Reactions of Keteniminium Salts: Probing Their Applications in Synthesis
Institution name	Bogazici University
Expected presentation date	Jul 2021
Portions	Figure on page 880
Requestor Location	Bogazici University Bogazici University Depermant of Chemistry Bebek istanbul, 34342 Turkey Attn: Bogazici University
Publisher Tax ID	EU826007151
Total	0.00 USD

Terms and Conditions

TERMS AND CONDITIONS

This copyrighted material is owned by or exclusively licensed to John Wiley & Sons, Inc. or one of its group companies (each a"Wiley Company") or handled on behalf of a society with which a Wiley Company has exclusive publishing rights in relation to a particular work (collectively "WILEY"). By clicking "accept" in connection with completing this licensing transaction, you agree that the following terms and conditions apply to this transaction (along with the billing and payment terms and conditions established by the Copyright Clearance Center Inc., ("CCC's Billing and Payment terms and conditions"), at the time that you opened your RightsLink account (these are available at any time at http://myaccount.copyright.com).

Terms and Conditions

- The materials you have requested permission to reproduce or reuse (the "Wiley Materials") are protected by copyright.
- You are hereby granted a personal, non-exclusive, non-sub licensable (on a stand-alone basis), non-transferable, worldwide, limited license to reproduce the Wiley Materials for the purpose specified in the licensing process. This license, **and any**

CONTENT (PDF or image file) purchased as part of your order, is for a one-time use only and limited to any maximum distribution number specified in the license. The first instance of republication or reuse granted by this license must be completed within two years of the date of the grant of this license (although copies prepared before the end date may be distributed thereafter). The Wiley Materials shall not be used in any other manner or for any other purpose, beyond what is granted in the license. Permission is granted subject to an appropriate acknowledgement given to the author, title of the material/book/journal and the publisher. You shall also duplicate the copyright notice that appears in the Wiley publication in your use of the Wiley Material. Permission is also granted on the understanding that nowhere in the text is a previously published source acknowledged for all or part of this Wiley Material. Any third party content is expressly excluded from this permission.

- With respect to the Wiley Materials, all rights are reserved. Except as expressly granted by the terms of the license, no part of the Wiley Materials may be copied, modified, adapted (except for minor reformatting required by the new Publication), translated, reproduced, transferred or distributed, in any form or by any means, and no derivative works may be made based on the Wiley Materials without the prior permission of the respective copyright owner.**For STM Signatory Publishers clearing permission under the terms of the STM Permissions Guidelines only, the terms of the license are extended to include subsequent editions and for editions in other languages, provided such editions are for the work as a whole in situ and does not involve the separate exploitation of the permitted figures or extracts,** You may not alter, remove or suppress in any manner any copyright, trademark or other notices displayed by the Wiley Materials. You may not license, rent, sell, loan, lease, pledge, offer as security, transfer or assign the Wiley Materials on a stand-alone basis, or any of the rights granted to you hereunder to any other person.

- The Wiley Materials and all of the intellectual property rights therein shall at all times remain the exclusive property of John Wiley & Sons Inc, the Wiley Companies, or their respective licensors, and your interest therein is only that of having possession of and the right to reproduce the Wiley Materials pursuant to Section 2 herein during the continuance of this Agreement. You agree that you own no right, title or interest in or to the Wiley Materials or any of the intellectual property rights therein. You shall have no rights hereunder other than the license as provided for above in Section 2. No right, license or interest to any trademark, trade name, service mark or other branding ("Marks") of WILEY or its licensors is granted hereunder, and you agree that you shall not assert any such right, license or interest with respect thereto

- NEITHER WILEY NOR ITS LICENSORS MAKES ANY WARRANTY OR REPRESENTATION OF ANY KIND TO YOU OR ANY THIRD PARTY, EXPRESS, IMPLIED OR STATUTORY, WITH RESPECT TO THE MATERIALS OR THE ACCURACY OF ANY INFORMATION CONTAINED IN THE MATERIALS, INCLUDING, WITHOUT LIMITATION, ANY IMPLIED WARRANTY OF MERCHANTABILITY, ACCURACY, SATISFACTORY QUALITY, FITNESS FOR A PARTICULAR PURPOSE, USABILITY, INTEGRATION OR NON-INFRINGEMENT AND ALL SUCH WARRANTIES ARE HEREBY EXCLUDED BY WILEY AND ITS LICENSORS AND WAIVED BY YOU.

- WILEY shall have the right to terminate this Agreement immediately upon breach of this Agreement by you.

- You shall indemnify, defend and hold harmless WILEY, its Licensors and their respective directors, officers, agents and employees, from and against any actual or threatened claims, demands, causes of action or proceedings arising from any breach of this Agreement by you.

- IN NO EVENT SHALL WILEY OR ITS LICENSORS BE LIABLE TO YOU OR ANY OTHER PARTY OR ANY OTHER PERSON OR ENTITY FOR ANY SPECIAL, CONSEQUENTIAL, INCIDENTAL, INDIRECT, EXEMPLARY OR PUNITIVE DAMAGES, HOWEVER CAUSED, ARISING OUT OF OR IN CONNECTION WITH THE DOWNLOADING, PROVISIONING, VIEWING OR USE OF THE MATERIALS REGARDLESS OF THE FORM OF ACTION,

WHETHER FOR BREACH OF CONTRACT, BREACH OF WARRANTY, TORT, NEGLIGENCE, INFRINGEMENT OR OTHERWISE (INCLUDING, WITHOUT LIMITATION, DAMAGES BASED ON LOSS OF PROFITS, DATA, FILES, USE, BUSINESS OPPORTUNITY OR CLAIMS OF THIRD PARTIES), AND WHETHER OR NOT THE PARTY HAS BEEN ADVISED OF THE POSSIBILITY OF SUCH DAMAGES. THIS LIMITATION SHALL APPLY NOTWITHSTANDING ANY FAILURE OF ESSENTIAL PURPOSE OF ANY LIMITED REMEDY PROVIDED HEREIN.

- Should any provision of this Agreement be held by a court of competent jurisdiction to be illegal, invalid, or unenforceable, that provision shall be deemed amended to achieve as nearly as possible the same economic effect as the original provision, and the legality, validity and enforceability of the remaining provisions of this Agreement shall not be affected or impaired thereby.
- The failure of either party to enforce any term or condition of this Agreement shall not constitute a waiver of either party's right to enforce each and every term and condition of this Agreement. No breach under this agreement shall be deemed waived or excused by either party unless such waiver or consent is in writing signed by the party granting such waiver or consent. The waiver by or consent of a party to a breach of any provision of this Agreement shall not operate or be construed as a waiver of or consent to any other or subsequent breach by such other party.
- This Agreement may not be assigned (including by operation of law or otherwise) by you without WILEY's prior written consent.
- Any fee required for this permission shall be non-refundable after thirty (30) days from receipt by the CCC.
- These terms and conditions together with CCC's Billing and Payment terms and conditions (which are incorporated herein) form the entire agreement between you and WILEY concerning this licensing transaction and (in the absence of fraud) supersedes all prior agreements and representations of the parties, oral or written. This Agreement may not be amended except in writing signed by both parties. This Agreement shall be binding upon and inure to the benefit of the parties' successors, legal representatives, and authorized assigns.
- In the event of any conflict between your obligations established by these terms and conditions and those established by CCC's Billing and Payment terms and conditions, these terms and conditions shall prevail.
- WILEY expressly reserves all rights not specifically granted in the combination of (i) the license details provided by you and accepted in the course of this licensing transaction, (ii) these terms and conditions and (iii) CCC's Billing and Payment terms and conditions.
- This Agreement will be void if the Type of Use, Format, Circulation, or Requestor Type was misrepresented during the licensing process.
- This Agreement shall be governed by and construed in accordance with the laws of the State of New York, USA, without regards to such state's conflict of law rules. Any legal action, suit or proceeding arising out of or relating to these Terms and Conditions or the breach thereof shall be instituted in a court of competent jurisdiction in New York County in the State of New York in the United States of America and each party hereby consents and submits to the personal jurisdiction of such court, waives any objection to venue in such court and consents to service of process by registered or certified mail, return receipt requested, at the last known address of such party.

WILEY OPEN ACCESS TERMS AND CONDITIONS

Wiley Publishes Open Access Articles in fully Open Access Journals and in Subscription journals offering Online Open. Although most of the fully Open Access journals publish open access articles under the terms of the Creative Commons Attribution (CC BY) License

only, the subscription journals and a few of the Open Access Journals offer a choice of Creative Commons Licenses. The license type is clearly identified on the article.

The Creative Commons Attribution License

The Creative Commons Attribution License (CC-BY) allows users to copy, distribute and transmit an article, adapt the article and make commercial use of the article. The CC-BY license permits commercial and non-

Creative Commons Attribution Non-Commercial License

The Creative Commons Attribution Non-Commercial (CC-BY-NC)License permits use, distribution and reproduction in any medium, provided the original work is properly cited and is not used for commercial purposes.(see below)

Creative Commons Attribution-Non-Commercial-NoDerivs License

The Creative Commons Attribution Non-Commercial-NoDerivs License (CC-BY-NC-ND) permits use, distribution and reproduction in any medium, provided the original work is properly cited, is not used for commercial purposes and no modifications or adaptations are made. (see below)

Use by commercial "for-profit" organizations

Use of Wiley Open Access articles for commercial, promotional, or marketing purposes requires further explicit permission from Wiley and will be subject to a fee.

Further details can be found on Wiley Online Library
http://olabout.wiley.com/WileyCDA/Section/id-410895.html

Other Terms and Conditions:

v1.10 Last updated September 2015

Questions? customercare@copyright.com or +1-855-239-3415 (toll free in the US) or +1-978-646-2777.

D.2. The License for Figure 3.3

ELSEVIER LICENSE
TERMS AND CONDITIONS

Jul 11, 2021

This Agreement between Bogazici University -- Beyza Horoz ("You") and Elsevier ("Elsevier") consists of your license details and the terms and conditions provided by Elsevier and Copyright Clearance Center.

License Number	5102551310114
License date	Jul 05, 2021
Licensed Content Publisher	Elsevier
Licensed Content Publication	Tetrahedron Letters
Licensed Content Title	Nonstereospecificity in the cycloadditions of keteneiminium salts to olefins. Evidence for a stepwise mechanism.
Licensed Content Author	Hiroyuki Saimoto,Catherine Houge,Anne-Marie Hesbain-Frisque,Anne Mockel,Léon Ghosez
Licensed Content Date	Jan 1, 1983
Licensed Content Volume	24
Licensed Content Issue	22
Licensed Content Pages	4
Start Page	2251
End Page	2254
Type of Use	reuse in a thesis/dissertation
Portion	figures/tables/illustrations
Number of figures/tables/illustrations	1

Format	both print and electronic
Are you the author of this Elsevier article?	No
Will you be translating?	No
Title	Mechanistic Investigation of [2+2] Cycloaddition Reactions of Keteniminium Salts: Probing Their Applications in Synthesis
Institution name	Bogazici University
Expected presentation date	Jul 2021
Portions	Scheme 3 on page 2254
Requestor Location	Bogazici University Bogazici University Depermant of Chemistry Bebek istanbul, 34342 Turkey Attn: Bogazici University
Publisher Tax ID	GB 494 6272 12
Total	0.00 USD

Terms and Conditions

INTRODUCTION

1. The publisher for this copyrighted material is Elsevier. By clicking "accept" in connection with completing this licensing transaction, you agree that the following terms and conditions apply to this transaction (along with the Billing and Payment terms and conditions established by Copyright Clearance Center, Inc. ("CCC"), at the time that you opened your Rightslink account and that are available at any time at http://myaccount.copyright.com).

GENERAL TERMS

2. Elsevier hereby grants you permission to reproduce the aforementioned material subject to the terms and conditions indicated.

3. Acknowledgement: If any part of the material to be used (for example, figures) has appeared in our publication with credit or acknowledgement to another source, permission must also be sought from that source. If such permission is not obtained then that material may not be included in your publication/copies. Suitable acknowledgement to the source must be made, either as a footnote or in a reference list at the end of your publication, as follows:

"Reprinted from Publication title, Vol /edition number, Author(s), Title of article / title of chapter, Pages No., Copyright (Year), with permission from Elsevier [OR APPLICABLE

SOCIETY COPYRIGHT OWNER]." Also Lancet special credit - "Reprinted from The Lancet, Vol. number, Author(s), Title of article, Pages No., Copyright (Year), with permission from Elsevier."

4. Reproduction of this material is confined to the purpose and/or media for which permission is hereby given.

5. Altering/Modifying Material: Not Permitted. However figures and illustrations may be altered/adapted minimally to serve your work. Any other abbreviations, additions, deletions and/or any other alterations shall be made only with prior written authorization of Elsevier Ltd. (Please contact Elsevier's permissions helpdesk here). No modifications can be made to any Lancet figures/tables and they must be reproduced in full.

6. If the permission fee for the requested use of our material is waived in this instance, please be advised that your future requests for Elsevier materials may attract a fee.

7. Reservation of Rights: Publisher reserves all rights not specifically granted in the combination of (i) the license details provided by you and accepted in the course of this licensing transaction, (ii) these terms and conditions and (iii) CCC's Billing and Payment terms and conditions.

8. License Contingent Upon Payment: While you may exercise the rights licensed immediately upon issuance of the license at the end of the licensing process for the transaction, provided that you have disclosed complete and accurate details of your proposed use, no license is finally effective unless and until full payment is received from you (either by publisher or by CCC) as provided in CCC's Billing and Payment terms and conditions. If full payment is not received on a timely basis, then any license preliminarily granted shall be deemed automatically revoked and shall be void as if never granted. Further, in the event that you breach any of these terms and conditions or any of CCC's Billing and Payment terms and conditions, the license is automatically revoked and shall be void as if never granted. Use of materials as described in a revoked license, as well as any use of the materials beyond the scope of an unrevoked license, may constitute copyright infringement and publisher reserves the right to take any and all action to protect its copyright in the materials.

9. Warranties: Publisher makes no representations or warranties with respect to the licensed material.

10. Indemnity: You hereby indemnify and agree to hold harmless publisher and CCC, and their respective officers, directors, employees and agents, from and against any and all claims arising out of your use of the licensed material other than as specifically authorized pursuant to this license.

11. No Transfer of License: This license is personal to you and may not be sublicensed, assigned, or transferred by you to any other person without publisher's written permission.

12. No Amendment Except in Writing: This license may not be amended except in a writing signed by both parties (or, in the case of publisher, by CCC on publisher's behalf).

13. Objection to Contrary Terms: Publisher hereby objects to any terms contained in any purchase order, acknowledgment, check endorsement or other writing prepared by you, which terms are inconsistent with these terms and conditions or CCC's Billing and Payment terms and conditions. These terms and conditions, together with CCC's Billing and Payment terms and conditions (which are incorporated herein), comprise the entire agreement between you and publisher (and CCC) concerning this licensing transaction. In the event of any conflict between your obligations established by these terms and conditions and those established by CCC's Billing and Payment terms and conditions, these terms and conditions shall control.

14. Revocation: Elsevier or Copyright Clearance Center may deny the permissions described in this License at their sole discretion, for any reason or no reason, with a full refund payable to you. Notice of such denial will be made using the contact information provided by you. Failure to receive such notice will not alter or invalidate the denial. In no event will Elsevier or Copyright Clearance Center be responsible or liable for any costs, expenses or damage incurred by you as a result of a denial of your permission request, other than a refund of the

amount(s) paid by you to Elsevier and/or Copyright Clearance Center for denied permissions.

LIMITED LICENSE

The following terms and conditions apply only to specific license types:

15. **Translation**: This permission is granted for non-exclusive world **English** rights only unless your license was granted for translation rights. If you licensed translation rights you may only translate this content into the languages you requested. A professional translator must perform all translations and reproduce the content word for word preserving the integrity of the article.

16. **Posting licensed content on any Website**: The following terms and conditions apply as follows: Licensing material from an Elsevier journal: All content posted to the web site must maintain the copyright information line on the bottom of each image; A hyper-text must be included to the Homepage of the journal from which you are licensing at http://www.sciencedirect.com/science/journal/xxxxx or the Elsevier homepage for books at http://www.elsevier.com; Central Storage: This license does not include permission for a scanned version of the material to be stored in a central repository such as that provided by Heron/XanEdu.

Licensing material from an Elsevier book: A hyper-text link must be included to the Elsevier homepage at http://www.elsevier.com . All content posted to the web site must maintain the copyright information line on the bottom of each image.

Posting licensed content on Electronic reserve: In addition to the above the following clauses are applicable: The web site must be password-protected and made available only to bona fide students registered on a relevant course. This permission is granted for 1 year only. You may obtain a new license for future website posting.

17. **For journal authors:** the following clauses are applicable in addition to the above:

Preprints:

A preprint is an author's own write-up of research results and analysis, it has not been peer-reviewed, nor has it had any other value added to it by a publisher (such as formatting, copyright, technical enhancement etc.).

Authors can share their preprints anywhere at any time. Preprints should not be added to or enhanced in any way in order to appear more like, or to substitute for, the final versions of articles however authors can update their preprints on arXiv or RePEc with their Accepted Author Manuscript (see below).

If accepted for publication, we encourage authors to link from the preprint to their formal publication via its DOI. Millions of researchers have access to the formal publications on ScienceDirect, and so links will help users to find, access, cite and use the best available version. Please note that Cell Press, The Lancet and some society-owned have different preprint policies. Information on these policies is available on the journal homepage.

Accepted Author Manuscripts: An accepted author manuscript is the manuscript of an article that has been accepted for publication and which typically includes author-incorporated changes suggested during submission, peer review and editor-author communications.

Authors can share their accepted author manuscript:

- immediately
  - via their non-commercial person homepage or blog
  - by updating a preprint in arXiv or RePEc with the accepted manuscript
  - via their research institute or institutional repository for internal institutional uses or as part of an invitation-only research collaboration work-group
  - directly by providing copies to their students or to research collaborators for their personal use

- for private scholarly sharing as part of an invitation-only work group on commercial sites with which Elsevier has an agreement
- After the embargo period
  - via non-commercial hosting platforms such as their institutional repository
  - via commercial sites with which Elsevier has an agreement

In all cases accepted manuscripts should:

- link to the formal publication via its DOI
- bear a CC-BY-NC-ND license - this is easy to do
- if aggregated with other manuscripts, for example in a repository or other site, be shared in alignment with our hosting policy not be added to or enhanced in any way to appear more like, or to substitute for, the published journal article.

Published journal article (JPA): A published journal article (PJA) is the definitive final record of published research that appears or will appear in the journal and embodies all value-adding publishing activities including peer review co-ordination, copy-editing, formatting, (if relevant) pagination and online enrichment.

Policies for sharing publishing journal articles differ for subscription and gold open access articles:

Subscription Articles: If you are an author, please share a link to your article rather than the full-text. Millions of researchers have access to the formal publications on ScienceDirect, and so links will help your users to find, access, cite, and use the best available version.

Theses and dissertations which contain embedded PJAs as part of the formal submission can be posted publicly by the awarding institution with DOI links back to the formal publications on ScienceDirect.

If you are affiliated with a library that subscribes to ScienceDirect you have additional private sharing rights for others' research accessed under that agreement. This includes use for classroom teaching and internal training at the institution (including use in course packs and courseware programs), and inclusion of the article for grant funding purposes.

Gold Open Access Articles: May be shared according to the author-selected end-user license and should contain a CrossMark logo, the end user license, and a DOI link to the formal publication on ScienceDirect.

Please refer to Elsevier's posting policy for further information.

18. **For book authors** the following clauses are applicable in addition to the above: Authors are permitted to place a brief summary of their work online only. You are not allowed to download and post the published electronic version of your chapter, nor may you scan the printed edition to create an electronic version. **Posting to a repository:** Authors are permitted to post a summary of their chapter only in their institution's repository.

19. **Thesis/Dissertation**: If your license is for use in a thesis/dissertation your thesis may be submitted to your institution in either print or electronic form. Should your thesis be published commercially, please reapply for permission. These requirements include permission for the Library and Archives of Canada to supply single copies, on demand, of the complete thesis and include permission for Proquest/UMI to supply single copies, on demand, of the complete thesis. Should your thesis be published commercially, please reapply for permission. Theses and dissertations which contain embedded PJAs as part of the formal submission can be posted publicly by the awarding institution with DOI links back to the formal publications on ScienceDirect.

Elsevier Open Access Terms and Conditions

You can publish open access with Elsevier in hundreds of open access journals or in nearly 2000 established subscription journals that support open access publishing. Permitted third party re-use of these open access articles is defined by the author's choice of Creative Commons user license. See our open access license policy for more information.

Terms & Conditions applicable to all Open Access articles published with Elsevier:

Any reuse of the article must not represent the author as endorsing the adaptation of the article nor should the article be modified in such a way as to damage the author's honour or reputation. If any changes have been made, such changes must be clearly indicated.

The author(s) must be appropriately credited and we ask that you include the end user license and a DOI link to the formal publication on ScienceDirect.

If any part of the material to be used (for example, figures) has appeared in our publication with credit or acknowledgement to another source it is the responsibility of the user to ensure their reuse complies with the terms and conditions determined by the rights holder.

Additional Terms & Conditions applicable to each Creative Commons user license:

CC BY: The CC-BY license allows users to copy, to create extracts, abstracts and new works from the Article, to alter and revise the Article and to make commercial use of the Article (including reuse and/or resale of the Article by commercial entities), provided the user gives appropriate credit (with a link to the formal publication through the relevant DOI), provides a link to the license, indicates if changes were made and the licensor is not represented as endorsing the use made of the work. The full details of the license are available at http://creativecommons.org/licenses/by/4.0.

CC BY NC SA: The CC BY-NC-SA license allows users to copy, to create extracts, abstracts and new works from the Article, to alter and revise the Article, provided this is not done for commercial purposes, and that the user gives appropriate credit (with a link to the formal publication through the relevant DOI), provides a link to the license, indicates if changes were made and the licensor is not represented as endorsing the use made of the work. Further, any new works must be made available on the same conditions. The full details of the license are available at http://creativecommons.org/licenses/by-nc-sa/4.0.

CC BY NC ND: The CC BY-NC-ND license allows users to copy and distribute the Article, provided this is not done for commercial purposes and further does not permit distribution of the Article if it is changed or edited in any way, and provided the user gives appropriate credit (with a link to the formal publication through the relevant DOI), provides a link to the license, and that the licensor is not represented as endorsing the use made of the work. The full details of the license are available at http://creativecommons.org/licenses/by-nc-nd/4.0. Any commercial reuse of Open Access articles published with a CC BY NC SA or CC BY NC ND license requires permission from Elsevier and will be subject to a fee.

Commercial reuse includes:

- Associating advertising with the full text of the Article
- Charging fees for document delivery or access
- Article aggregation
- Systematic distribution via e-mail lists or share buttons

Posting or linking by commercial companies for use by customers of those companies.

20. **Other Conditions**:

v1.10

Questions? customercare@copyright.com or +1-855-239-3415 (toll free in the US) or +1-978-646-2777.

D.3. The License for Figure 3.4

ELSEVIER LICENSE
TERMS AND CONDITIONS

Jul 11, 2021

This Agreement between Bogazici University -- Beyza Horoz ("You") and Elsevier ("Elsevier") consists of your license details and the terms and conditions provided by Elsevier and Copyright Clearance Center.

License Number	5102550620733
License date	Jul 05, 2021
Licensed Content Publisher	Elsevier
Licensed Content Publication	Tetrahedron
Licensed Content Title	A DFT study of the ionic [2+2] cycloaddition reactions of keteniminium cations with terminal acetylenes
Licensed Content Author	Luis R. Domingo,Mar Ríos-Gutiérrez,Patricia Pérez
Licensed Content Date	Apr 22, 2015
Licensed Content Volume	71
Licensed Content Issue	16
Licensed Content Pages	7
Start Page	2421
End Page	2427
Type of Use	reuse in a thesis/dissertation
Portion	figures/tables/illustrations
Number of figures/tables/illustrations	1

Format	both print and electronic
Are you the author of this Elsevier article?	No
Will you be translating?	No
Title	Mechanistic Investigation of [2+2] Cycloaddition Reactions of Keteniminium Salts: Probing Their Applications in Synthesis
Institution name	Bogazici University
Expected presentation date	Jul 2021
Portions	Scheme 3 on page 2423
Requestor Location	Bogazici University Bogazici University Depermant of Chemistry Bebek istanbul, 34342 Turkey Attn: Bogazici University
Publisher Tax ID	GB 494 6272 12
Total	0.00 USD
Terms and Conditions	

INTRODUCTION

1. The publisher for this copyrighted material is Elsevier. By clicking "accept" in connection with completing this licensing transaction, you agree that the following terms and conditions apply to this transaction (along with the Billing and Payment terms and conditions established by Copyright Clearance Center, Inc. ("CCC"), at the time that you opened your Rightslink account and that are available at any time at http://myaccount.copyright.com).

GENERAL TERMS

2. Elsevier hereby grants you permission to reproduce the aforementioned material subject to the terms and conditions indicated.

3. Acknowledgement: If any part of the material to be used (for example, figures) has appeared in our publication with credit or acknowledgement to another source, permission must also be sought from that source. If such permission is not obtained then that material may not be included in your publication/copies. Suitable acknowledgement to the source must be made, either as a footnote or in a reference list at the end of your publication, as follows:

"Reprinted from Publication title, Vol /edition number, Author(s), Title of article / title of chapter, Pages No., Copyright (Year), with permission from Elsevier [OR APPLICABLE SOCIETY COPYRIGHT OWNER]." Also Lancet special credit - "Reprinted from The

Lancet, Vol. number, Author(s), Title of article, Pages No., Copyright (Year), with permission from Elsevier."

4. Reproduction of this material is confined to the purpose and/or media for which permission is hereby given.

5. Altering/Modifying Material: Not Permitted. However figures and illustrations may be altered/adapted minimally to serve your work. Any other abbreviations, additions, deletions and/or any other alterations shall be made only with prior written authorization of Elsevier Ltd. (Please contact Elsevier's permissions helpdesk here). No modifications can be made to any Lancet figures/tables and they must be reproduced in full.

6. If the permission fee for the requested use of our material is waived in this instance, please be advised that your future requests for Elsevier materials may attract a fee.

7. Reservation of Rights: Publisher reserves all rights not specifically granted in the combination of (i) the license details provided by you and accepted in the course of this licensing transaction, (ii) these terms and conditions and (iii) CCC's Billing and Payment terms and conditions.

8. License Contingent Upon Payment: While you may exercise the rights licensed immediately upon issuance of the license at the end of the licensing process for the transaction, provided that you have disclosed complete and accurate details of your proposed use, no license is finally effective unless and until full payment is received from you (either by publisher or by CCC) as provided in CCC's Billing and Payment terms and conditions. If full payment is not received on a timely basis, then any license preliminarily granted shall be deemed automatically revoked and shall be void as if never granted. Further, in the event that you breach any of these terms and conditions or any of CCC's Billing and Payment terms and conditions, the license is automatically revoked and shall be void as if never granted. Use of materials as described in a revoked license, as well as any use of the materials beyond the scope of an unrevoked license, may constitute copyright infringement and publisher reserves the right to take any and all action to protect its copyright in the materials.

9. Warranties: Publisher makes no representations or warranties with respect to the licensed material.

10. Indemnity: You hereby indemnify and agree to hold harmless publisher and CCC, and their respective officers, directors, employees and agents, from and against any and all claims arising out of your use of the licensed material other than as specifically authorized pursuant to this license.

11. No Transfer of License: This license is personal to you and may not be sublicensed, assigned, or transferred by you to any other person without publisher's written permission.

12. No Amendment Except in Writing: This license may not be amended except in a writing signed by both parties (or, in the case of publisher, by CCC on publisher's behalf).

13. Objection to Contrary Terms: Publisher hereby objects to any terms contained in any purchase order, acknowledgment, check endorsement or other writing prepared by you, which terms are inconsistent with these terms and conditions or CCC's Billing and Payment terms and conditions. These terms and conditions, together with CCC's Billing and Payment terms and conditions (which are incorporated herein), comprise the entire agreement between you and publisher (and CCC) concerning this licensing transaction. In the event of any conflict between your obligations established by these terms and conditions and those established by CCC's Billing and Payment terms and conditions, these terms and conditions shall control.

14. Revocation: Elsevier or Copyright Clearance Center may deny the permissions described in this License at their sole discretion, for any reason or no reason, with a full refund payable to you. Notice of such denial will be made using the contact information provided by you. Failure to receive such notice will not alter or invalidate the denial. In no event will Elsevier or Copyright Clearance Center be responsible or liable for any costs, expenses or damage incurred by you as a result of a denial of your permission request, other than a refund of the

amount(s) paid by you to Elsevier and/or Copyright Clearance Center for denied permissions.

LIMITED LICENSE

The following terms and conditions apply only to specific license types:

15. **Translation**: This permission is granted for non-exclusive world **English** rights only unless your license was granted for translation rights. If you licensed translation rights you may only translate this content into the languages you requested. A professional translator must perform all translations and reproduce the content word for word preserving the integrity of the article.

16. **Posting licensed content on any Website**: The following terms and conditions apply as follows: Licensing material from an Elsevier journal: All content posted to the web site must maintain the copyright information line on the bottom of each image; A hyper-text must be included to the Homepage of the journal from which you are licensing at http://www.sciencedirect.com/science/journal/xxxxx or the Elsevier homepage for books at http://www.elsevier.com; Central Storage: This license does not include permission for a scanned version of the material to be stored in a central repository such as that provided by Heron/XanEdu.

Licensing material from an Elsevier book: A hyper-text link must be included to the Elsevier homepage at http://www.elsevier.com . All content posted to the web site must maintain the copyright information line on the bottom of each image.

Posting licensed content on Electronic reserve: In addition to the above the following clauses are applicable: The web site must be password-protected and made available only to bona fide students registered on a relevant course. This permission is granted for 1 year only. You may obtain a new license for future website posting.

17. **For journal authors:** the following clauses are applicable in addition to the above:

Preprints:

A preprint is an author's own write-up of research results and analysis, it has not been peer-reviewed, nor has it had any other value added to it by a publisher (such as formatting, copyright, technical enhancement etc.).

Authors can share their preprints anywhere at any time. Preprints should not be added to or enhanced in any way in order to appear more like, or to substitute for, the final versions of articles however authors can update their preprints on arXiv or RePEc with their Accepted Author Manuscript (see below).

If accepted for publication, we encourage authors to link from the preprint to their formal publication via its DOI. Millions of researchers have access to the formal publications on ScienceDirect, and so links will help users to find, access, cite and use the best available version. Please note that Cell Press, The Lancet and some society-owned have different preprint policies. Information on these policies is available on the journal homepage.

Accepted Author Manuscripts: An accepted author manuscript is the manuscript of an article that has been accepted for publication and which typically includes author-incorporated changes suggested during submission, peer review and editor-author communications.

Authors can share their accepted author manuscript:

- immediately
  - via their non-commercial person homepage or blog
  - by updating a preprint in arXiv or RePEc with the accepted manuscript
  - via their research institute or institutional repository for internal institutional uses or as part of an invitation-only research collaboration work-group
  - directly by providing copies to their students or to research collaborators for their personal use

- for private scholarly sharing as part of an invitation-only work group on commercial sites with which Elsevier has an agreement
- After the embargo period
  - via non-commercial hosting platforms such as their institutional repository
  - via commercial sites with which Elsevier has an agreement

In all cases accepted manuscripts should:

- link to the formal publication via its DOI
- bear a CC-BY-NC-ND license - this is easy to do
- if aggregated with other manuscripts, for example in a repository or other site, be shared in alignment with our hosting policy not be added to or enhanced in any way to appear more like, or to substitute for, the published journal article.

Published journal article (JPA): A published journal article (PJA) is the definitive final record of published research that appears or will appear in the journal and embodies all value-adding publishing activities including peer review co-ordination, copy-editing, formatting, (if relevant) pagination and online enrichment.

Policies for sharing publishing journal articles differ for subscription and gold open access articles:

Subscription Articles: If you are an author, please share a link to your article rather than the full-text. Millions of researchers have access to the formal publications on ScienceDirect, and so links will help your users to find, access, cite, and use the best available version.

Theses and dissertations which contain embedded PJAs as part of the formal submission can be posted publicly by the awarding institution with DOI links back to the formal publications on ScienceDirect.

If you are affiliated with a library that subscribes to ScienceDirect you have additional private sharing rights for others' research accessed under that agreement. This includes use for classroom teaching and internal training at the institution (including use in course packs and courseware programs), and inclusion of the article for grant funding purposes.

Gold Open Access Articles: May be shared according to the author-selected end-user license and should contain a CrossMark logo, the end user license, and a DOI link to the formal publication on ScienceDirect.

Please refer to Elsevier's posting policy for further information.

18. **For book authors** the following clauses are applicable in addition to the above: Authors are permitted to place a brief summary of their work online only. You are not allowed to download and post the published electronic version of your chapter, nor may you scan the printed edition to create an electronic version. **Posting to a repository:** Authors are permitted to post a summary of their chapter only in their institution's repository.

19. **Thesis/Dissertation**: If your license is for use in a thesis/dissertation your thesis may be submitted to your institution in either print or electronic form. Should your thesis be published commercially, please reapply for permission. These requirements include permission for the Library and Archives of Canada to supply single copies, on demand, of the complete thesis and include permission for Proquest/UMI to supply single copies, on demand, of the complete thesis. Should your thesis be published commercially, please reapply for permission. Theses and dissertations which contain embedded PJAs as part of the formal submission can be posted publicly by the awarding institution with DOI links back to the formal publications on ScienceDirect.

Elsevier Open Access Terms and Conditions

You can publish open access with Elsevier in hundreds of open access journals or in nearly 2000 established subscription journals that support open access publishing. Permitted third party re-use of these open access articles is defined by the author's choice of Creative Commons user license. See our open access license policy for more information.

Terms & Conditions applicable to all Open Access articles published with Elsevier:

Any reuse of the article must not represent the author as endorsing the adaptation of the article nor should the article be modified in such a way as to damage the author's honour or reputation. If any changes have been made, such changes must be clearly indicated.

The author(s) must be appropriately credited and we ask that you include the end user license and a DOI link to the formal publication on ScienceDirect.

If any part of the material to be used (for example, figures) has appeared in our publication with credit or acknowledgement to another source it is the responsibility of the user to ensure their reuse complies with the terms and conditions determined by the rights holder.

Additional Terms & Conditions applicable to each Creative Commons user license:

CC BY: The CC-BY license allows users to copy, to create extracts, abstracts and new works from the Article, to alter and revise the Article and to make commercial use of the Article (including reuse and/or resale of the Article by commercial entities), provided the user gives appropriate credit (with a link to the formal publication through the relevant DOI), provides a link to the license, indicates if changes were made and the licensor is not represented as endorsing the use made of the work. The full details of the license are available at http://creativecommons.org/licenses/by/4.0.

CC BY NC SA: The CC BY-NC-SA license allows users to copy, to create extracts, abstracts and new works from the Article, to alter and revise the Article, provided this is not done for commercial purposes, and that the user gives appropriate credit (with a link to the formal publication through the relevant DOI), provides a link to the license, indicates if changes were made and the licensor is not represented as endorsing the use made of the work. Further, any new works must be made available on the same conditions. The full details of the license are available at http://creativecommons.org/licenses/by-nc-sa/4.0.

CC BY NC ND: The CC BY-NC-ND license allows users to copy and distribute the Article, provided this is not done for commercial purposes and further does not permit distribution of the Article if it is changed or edited in any way, and provided the user gives appropriate credit (with a link to the formal publication through the relevant DOI), provides a link to the license, and that the licensor is not represented as endorsing the use made of the work. The full details of the license are available at http://creativecommons.org/licenses/by-nc-nd/4.0. Any commercial reuse of Open Access articles published with a CC BY NC SA or CC BY NC ND license requires permission from Elsevier and will be subject to a fee.

Commercial reuse includes:

- Associating advertising with the full text of the Article
- Charging fees for document delivery or access
- Article aggregation
- Systematic distribution via e-mail lists or share buttons

Posting or linking by commercial companies for use by customers of those companies.

20. **Other Conditions**:

v1.10

Questions? customercare@copyright.com or +1-855-239-3415 (toll free in the US) or +1-978-646-2777.

D.4. The License for Figure 1.3, Figure 4.1, Figure 4.2, Figure 4.3, Figure 4.4 and Figure 4.5

JOHN WILEY AND SONS LICENSE
TERMS AND CONDITIONS

Jun 30, 2021

This Agreement between Bogazici University -- Beyza Horoz ("You") and John Wiley and Sons ("John Wiley and Sons") consists of your license details and the terms and conditions provided by John Wiley and Sons and Copyright Clearance Center.

License Number	5098681054757
License date	Jun 30, 2021
Licensed Content Publisher	John Wiley and Sons
Licensed Content Publication	Helvetica Chimica Acta
Licensed Content Title	Total Synthesis and Biological Evaluation of Zealactone 1a/b
Licensed Content Author	Alain De Mesmaeker, Saron Catak, Beyza Horoz, et al
Licensed Content Date	Mar 23, 2020
Licensed Content Volume	103
Licensed Content Issue	4
Licensed Content Pages	26
Type of use	Dissertation/Thesis
Requestor type	Author of this Wiley article
Format	Print and electronic

Portion	Full article
Will you be translating?	No
Title	Mechanistic Investigation of [2+2] Cycloaddition Reactions of Keteniminium Salts: Probing Their Applications in Synthesis
Institution name	Bogazici University
Expected presentation date	Jun 2021
Requestor Location	Bogazici University Bogazici University Depermant of Chemistry Bebek istanbul, 34342 Turkey Attn: Bogazici University
Publisher Tax ID	EU826007151
Total	0.00 USD

Terms and Conditions

TERMS AND CONDITIONS

This copyrighted material is owned by or exclusively licensed to John Wiley & Sons, Inc. or one of its group companies (each a"Wiley Company") or handled on behalf of a society with which a Wiley Company has exclusive publishing rights in relation to a particular work (collectively "WILEY"). By clicking "accept" in connection with completing this licensing transaction, you agree that the following terms and conditions apply to this transaction (along with the billing and payment terms and conditions established by the Copyright Clearance Center Inc., ("CCC's Billing and Payment terms and conditions"), at the time that you opened your RightsLink account (these are available at any time at http://myaccount.copyright.com).

Terms and Conditions

- The materials you have requested permission to reproduce or reuse (the "Wiley Materials") are protected by copyright.
- You are hereby granted a personal, non-exclusive, non-sub licensable (on a stand-alone basis), non-transferable, worldwide, limited license to reproduce the Wiley Materials for the purpose specified in the licensing process. This license, **and any CONTENT (PDF or image file) purchased as part of your order,** is for a one-time use only and limited to any maximum distribution number specified in the license. The first instance of republication or reuse granted by this license must be completed within two years of the date of the grant of this license (although copies prepared before the end date may be distributed thereafter). The Wiley Materials shall not be used in any other manner or for any other purpose, beyond what is granted in the license. Permission is granted subject to an appropriate acknowledgement given to the

author, title of the material/book/journal and the publisher. You shall also duplicate the copyright notice that appears in the Wiley publication in your use of the Wiley Material. Permission is also granted on the understanding that nowhere in the text is a previously published source acknowledged for all or part of this Wiley Material. Any third party content is expressly excluded from this permission.

- With respect to the Wiley Materials, all rights are reserved. Except as expressly granted by the terms of the license, no part of the Wiley Materials may be copied, modified, adapted (except for minor reformatting required by the new Publication), translated, reproduced, transferred or distributed, in any form or by any means, and no derivative works may be made based on the Wiley Materials without the prior permission of the respective copyright owner.**For STM Signatory Publishers clearing permission under the terms of the STM Permissions Guidelines only, the terms of the license are extended to include subsequent editions and for editions in other languages, provided such editions are for the work as a whole in situ and does not involve the separate exploitation of the permitted figures or extracts,** You may not alter, remove or suppress in any manner any copyright, trademark or other notices displayed by the Wiley Materials. You may not license, rent, sell, loan, lease, pledge, offer as security, transfer or assign the Wiley Materials on a stand-alone basis, or any of the rights granted to you hereunder to any other person.

- The Wiley Materials and all of the intellectual property rights therein shall at all times remain the exclusive property of John Wiley & Sons Inc, the Wiley Companies, or their respective licensors, and your interest therein is only that of having possession of and the right to reproduce the Wiley Materials pursuant to Section 2 herein during the continuance of this Agreement. You agree that you own no right, title or interest in or to the Wiley Materials or any of the intellectual property rights therein. You shall have no rights hereunder other than the license as provided for above in Section 2. No right, license or interest to any trademark, trade name, service mark or other branding ("Marks") of WILEY or its licensors is granted hereunder, and you agree that you shall not assert any such right, license or interest with respect thereto

- NEITHER WILEY NOR ITS LICENSORS MAKES ANY WARRANTY OR REPRESENTATION OF ANY KIND TO YOU OR ANY THIRD PARTY, EXPRESS, IMPLIED OR STATUTORY, WITH RESPECT TO THE MATERIALS OR THE ACCURACY OF ANY INFORMATION CONTAINED IN THE MATERIALS, INCLUDING, WITHOUT LIMITATION, ANY IMPLIED WARRANTY OF MERCHANTABILITY, ACCURACY, SATISFACTORY QUALITY, FITNESS FOR A PARTICULAR PURPOSE, USABILITY, INTEGRATION OR NON-INFRINGEMENT AND ALL SUCH WARRANTIES ARE HEREBY EXCLUDED BY WILEY AND ITS LICENSORS AND WAIVED BY YOU.

- WILEY shall have the right to terminate this Agreement immediately upon breach of this Agreement by you.

- You shall indemnify, defend and hold harmless WILEY, its Licensors and their respective directors, officers, agents and employees, from and against any actual or threatened claims, demands, causes of action or proceedings arising from any breach of this Agreement by you.

- IN NO EVENT SHALL WILEY OR ITS LICENSORS BE LIABLE TO YOU OR ANY OTHER PARTY OR ANY OTHER PERSON OR ENTITY FOR ANY SPECIAL, CONSEQUENTIAL, INCIDENTAL, INDIRECT, EXEMPLARY OR PUNITIVE DAMAGES, HOWEVER CAUSED, ARISING OUT OF OR IN CONNECTION WITH THE DOWNLOADING, PROVISIONING, VIEWING OR USE OF THE MATERIALS REGARDLESS OF THE FORM OF ACTION, WHETHER FOR BREACH OF CONTRACT, BREACH OF WARRANTY, TORT, NEGLIGENCE, INFRINGEMENT OR OTHERWISE (INCLUDING, WITHOUT LIMITATION, DAMAGES BASED ON LOSS OF PROFITS, DATA, FILES, USE, BUSINESS OPPORTUNITY OR CLAIMS OF THIRD PARTIES), AND WHETHER OR NOT THE PARTY HAS BEEN ADVISED OF THE POSSIBILITY OF SUCH DAMAGES. THIS LIMITATION SHALL APPLY NOTWITHSTANDING ANY FAILURE OF ESSENTIAL PURPOSE OF ANY LIMITED REMEDY PROVIDED

HEREIN.

- Should any provision of this Agreement be held by a court of competent jurisdiction to be illegal, invalid, or unenforceable, that provision shall be deemed amended to achieve as nearly as possible the same economic effect as the original provision, and the legality, validity and enforceability of the remaining provisions of this Agreement shall not be affected or impaired thereby.
- The failure of either party to enforce any term or condition of this Agreement shall not constitute a waiver of either party's right to enforce each and every term and condition of this Agreement. No breach under this agreement shall be deemed waived or excused by either party unless such waiver or consent is in writing signed by the party granting such waiver or consent. The waiver by or consent of a party to a breach of any provision of this Agreement shall not operate or be construed as a waiver of or consent to any other or subsequent breach by such other party.
- This Agreement may not be assigned (including by operation of law or otherwise) by you without WILEY's prior written consent.
- Any fee required for this permission shall be non-refundable after thirty (30) days from receipt by the CCC.
- These terms and conditions together with CCC's Billing and Payment terms and conditions (which are incorporated herein) form the entire agreement between you and WILEY concerning this licensing transaction and (in the absence of fraud) supersedes all prior agreements and representations of the parties, oral or written. This Agreement may not be amended except in writing signed by both parties. This Agreement shall be binding upon and inure to the benefit of the parties' successors, legal representatives, and authorized assigns.
- In the event of any conflict between your obligations established by these terms and conditions and those established by CCC's Billing and Payment terms and conditions, these terms and conditions shall prevail.
- WILEY expressly reserves all rights not specifically granted in the combination of (i) the license details provided by you and accepted in the course of this licensing transaction, (ii) these terms and conditions and (iii) CCC's Billing and Payment terms and conditions.
- This Agreement will be void if the Type of Use, Format, Circulation, or Requestor Type was misrepresented during the licensing process.
- This Agreement shall be governed by and construed in accordance with the laws of the State of New York, USA, without regards to such state's conflict of law rules. Any legal action, suit or proceeding arising out of or relating to these Terms and Conditions or the breach thereof shall be instituted in a court of competent jurisdiction in New York County in the State of New York in the United States of America and each party hereby consents and submits to the personal jurisdiction of such court, waives any objection to venue in such court and consents to service of process by registered or certified mail, return receipt requested, at the last known address of such party.

WILEY OPEN ACCESS TERMS AND CONDITIONS

Wiley Publishes Open Access Articles in fully Open Access Journals and in Subscription journals offering Online Open. Although most of the fully Open Access journals publish open access articles under the terms of the Creative Commons Attribution (CC BY) License only, the subscription journals and a few of the Open Access Journals offer a choice of Creative Commons Licenses. The license type is clearly identified on the article.

The Creative Commons Attribution License

The Creative Commons Attribution License (CC-BY) allows users to copy, distribute and transmit an article, adapt the article and make commercial use of the article. The CC-BY license permits commercial and non-

Creative Commons Attribution Non-Commercial License

The Creative Commons Attribution Non-Commercial (CC-BY-NC)License permits use, distribution and reproduction in any medium, provided the original work is properly cited and is not used for commercial purposes.(see below)

Creative Commons Attribution-Non-Commercial-NoDerivs License

The Creative Commons Attribution Non-Commercial-NoDerivs License (CC-BY-NC-ND) permits use, distribution and reproduction in any medium, provided the original work is properly cited, is not used for commercial purposes and no modifications or adaptations are made. (see below)

Use by commercial "for-profit" organizations

Use of Wiley Open Access articles for commercial, promotional, or marketing purposes requires further explicit permission from Wiley and will be subject to a fee.

Further details can be found on Wiley Online Library
http://olabout.wiley.com/WileyCDA/Section/id-410895.html

Other Terms and Conditions:

v1.10 Last updated September 2015

Questions? customercare@copyright.com or +1-855-239-3415 (toll free in the US) or +1-978-646-2777.

D.5. The License for Figure 1.4, Figure 4.6, Figure 4.7, Figure 4.8, Figure 4.9, Figure 4.10 and Figure 4.11

JOHN WILEY AND SONS LICENSE
TERMS AND CONDITIONS

Jul 05, 2021

This Agreement between Bogazici University -- Beyza Horoz ("You") and John Wiley and Sons ("John Wiley and Sons") consists of your license details and the terms and conditions provided by John Wiley and Sons and Copyright Clearance Center.

License Number	5102440609047
License date	Jul 05, 2021
Licensed Content Publisher	John Wiley and Sons
Licensed Content Publication	Helvetica Chimica Acta
Licensed Content Title	Synthesis of Highly Substituted Cyclobutanones by a One-Pot Keteniminium-Enamine Process
Licensed Content Author	Dylan Dagoneau, Amandine Kolleth, Pierre Quinodoz, et al
Licensed Content Date	Apr 16, 2021
Licensed Content Volume	104
Licensed Content Issue	5
Licensed Content Pages	11
Type of use	Dissertation/Thesis
Requestor type	Author of this Wiley article
Format	Print and electronic

Portion	Full article
Will you be translating?	No
Title	Mechanistic Investigation of [2+2] Cycloaddition Reactions of Keteniminium Salts: Probing Their Applications in Synthesis
Institution name	Bogazici University
Expected presentation date	Jul 2021
Requestor Location	Bogazici University Bogazici University Depermant of Chemistry Bebek istanbul, 34342 Turkey Attn: Bogazici University
Publisher Tax ID	EU826007151
Total	0.00 USD

Terms and Conditions

TERMS AND CONDITIONS

This copyrighted material is owned by or exclusively licensed to John Wiley & Sons, Inc. or one of its group companies (each a"Wiley Company") or handled on behalf of a society with which a Wiley Company has exclusive publishing rights in relation to a particular work (collectively "WILEY"). By clicking "accept" in connection with completing this licensing transaction, you agree that the following terms and conditions apply to this transaction (along with the billing and payment terms and conditions established by the Copyright Clearance Center Inc., ("CCC's Billing and Payment terms and conditions"), at the time that you opened your RightsLink account (these are available at any time at http://myaccount.copyright.com).

Terms and Conditions

- The materials you have requested permission to reproduce or reuse (the "Wiley Materials") are protected by copyright.
- You are hereby granted a personal, non-exclusive, non-sub licensable (on a stand-alone basis), non-transferable, worldwide, limited license to reproduce the Wiley Materials for the purpose specified in the licensing process. This license, **and any CONTENT (PDF or image file) purchased as part of your order,** is for a one-time use only and limited to any maximum distribution number specified in the license. The first instance of republication or reuse granted by this license must be completed within two years of the date of the grant of this license (although copies prepared before the end date may be distributed thereafter). The Wiley Materials shall not be used in any other manner or for any other purpose, beyond what is granted in the license. Permission is granted subject to an appropriate acknowledgement given to the

author, title of the material/book/journal and the publisher. You shall also duplicate the copyright notice that appears in the Wiley publication in your use of the Wiley Material. Permission is also granted on the understanding that nowhere in the text is a previously published source acknowledged for all or part of this Wiley Material. Any third party content is expressly excluded from this permission.

- With respect to the Wiley Materials, all rights are reserved. Except as expressly granted by the terms of the license, no part of the Wiley Materials may be copied, modified, adapted (except for minor reformatting required by the new Publication), translated, reproduced, transferred or distributed, in any form or by any means, and no derivative works may be made based on the Wiley Materials without the prior permission of the respective copyright owner.**For STM Signatory Publishers clearing permission under the terms of the STM Permissions Guidelines only, the terms of the license are extended to include subsequent editions and for editions in other languages, provided such editions are for the work as a whole in situ and does not involve the separate exploitation of the permitted figures or extracts,** You may not alter, remove or suppress in any manner any copyright, trademark or other notices displayed by the Wiley Materials. You may not license, rent, sell, loan, lease, pledge, offer as security, transfer or assign the Wiley Materials on a stand-alone basis, or any of the rights granted to you hereunder to any other person.

- The Wiley Materials and all of the intellectual property rights therein shall at all times remain the exclusive property of John Wiley & Sons Inc, the Wiley Companies, or their respective licensors, and your interest therein is only that of having possession of and the right to reproduce the Wiley Materials pursuant to Section 2 herein during the continuance of this Agreement. You agree that you own no right, title or interest in or to the Wiley Materials or any of the intellectual property rights therein. You shall have no rights hereunder other than the license as provided for above in Section 2. No right, license or interest to any trademark, trade name, service mark or other branding ("Marks") of WILEY or its licensors is granted hereunder, and you agree that you shall not assert any such right, license or interest with respect thereto

- NEITHER WILEY NOR ITS LICENSORS MAKES ANY WARRANTY OR REPRESENTATION OF ANY KIND TO YOU OR ANY THIRD PARTY, EXPRESS, IMPLIED OR STATUTORY, WITH RESPECT TO THE MATERIALS OR THE ACCURACY OF ANY INFORMATION CONTAINED IN THE MATERIALS, INCLUDING, WITHOUT LIMITATION, ANY IMPLIED WARRANTY OF MERCHANTABILITY, ACCURACY, SATISFACTORY QUALITY, FITNESS FOR A PARTICULAR PURPOSE, USABILITY, INTEGRATION OR NON-INFRINGEMENT AND ALL SUCH WARRANTIES ARE HEREBY EXCLUDED BY WILEY AND ITS LICENSORS AND WAIVED BY YOU.

- WILEY shall have the right to terminate this Agreement immediately upon breach of this Agreement by you.

- You shall indemnify, defend and hold harmless WILEY, its Licensors and their respective directors, officers, agents and employees, from and against any actual or threatened claims, demands, causes of action or proceedings arising from any breach of this Agreement by you.

- IN NO EVENT SHALL WILEY OR ITS LICENSORS BE LIABLE TO YOU OR ANY OTHER PARTY OR ANY OTHER PERSON OR ENTITY FOR ANY SPECIAL, CONSEQUENTIAL, INCIDENTAL, INDIRECT, EXEMPLARY OR PUNITIVE DAMAGES, HOWEVER CAUSED, ARISING OUT OF OR IN CONNECTION WITH THE DOWNLOADING, PROVISIONING, VIEWING OR USE OF THE MATERIALS REGARDLESS OF THE FORM OF ACTION, WHETHER FOR BREACH OF CONTRACT, BREACH OF WARRANTY, TORT, NEGLIGENCE, INFRINGEMENT OR OTHERWISE (INCLUDING, WITHOUT LIMITATION, DAMAGES BASED ON LOSS OF PROFITS, DATA, FILES, USE, BUSINESS OPPORTUNITY OR CLAIMS OF THIRD PARTIES), AND WHETHER OR NOT THE PARTY HAS BEEN ADVISED OF THE POSSIBILITY OF SUCH DAMAGES. THIS LIMITATION SHALL APPLY NOTWITHSTANDING ANY FAILURE OF ESSENTIAL PURPOSE OF ANY LIMITED REMEDY PROVIDED

HEREIN.

- Should any provision of this Agreement be held by a court of competent jurisdiction to be illegal, invalid, or unenforceable, that provision shall be deemed amended to achieve as nearly as possible the same economic effect as the original provision, and the legality, validity and enforceability of the remaining provisions of this Agreement shall not be affected or impaired thereby.
- The failure of either party to enforce any term or condition of this Agreement shall not constitute a waiver of either party's right to enforce each and every term and condition of this Agreement. No breach under this agreement shall be deemed waived or excused by either party unless such waiver or consent is in writing signed by the party granting such waiver or consent. The waiver by or consent of a party to a breach of any provision of this Agreement shall not operate or be construed as a waiver of or consent to any other or subsequent breach by such other party.
- This Agreement may not be assigned (including by operation of law or otherwise) by you without WILEY's prior written consent.
- Any fee required for this permission shall be non-refundable after thirty (30) days from receipt by the CCC.
- These terms and conditions together with CCC's Billing and Payment terms and conditions (which are incorporated herein) form the entire agreement between you and WILEY concerning this licensing transaction and (in the absence of fraud) supersedes all prior agreements and representations of the parties, oral or written. This Agreement may not be amended except in writing signed by both parties. This Agreement shall be binding upon and inure to the benefit of the parties' successors, legal representatives, and authorized assigns.
- In the event of any conflict between your obligations established by these terms and conditions and those established by CCC's Billing and Payment terms and conditions, these terms and conditions shall prevail.
- WILEY expressly reserves all rights not specifically granted in the combination of (i) the license details provided by you and accepted in the course of this licensing transaction, (ii) these terms and conditions and (iii) CCC's Billing and Payment terms and conditions.
- This Agreement will be void if the Type of Use, Format, Circulation, or Requestor Type was misrepresented during the licensing process.
- This Agreement shall be governed by and construed in accordance with the laws of the State of New York, USA, without regards to such state's conflict of law rules. Any legal action, suit or proceeding arising out of or relating to these Terms and Conditions or the breach thereof shall be instituted in a court of competent jurisdiction in New York County in the State of New York in the United States of America and each party hereby consents and submits to the personal jurisdiction of such court, waives any objection to venue in such court and consents to service of process by registered or certified mail, return receipt requested, at the last known address of such party.

WILEY OPEN ACCESS TERMS AND CONDITIONS

Wiley Publishes Open Access Articles in fully Open Access Journals and in Subscription journals offering Online Open. Although most of the fully Open Access journals publish open access articles under the terms of the Creative Commons Attribution (CC BY) License only, the subscription journals and a few of the Open Access Journals offer a choice of Creative Commons Licenses. The license type is clearly identified on the article.

The Creative Commons Attribution License

The Creative Commons Attribution License (CC-BY) allows users to copy, distribute and transmit an article, adapt the article and make commercial use of the article. The CC-BY license permits commercial and non-

Creative Commons Attribution Non-Commercial License

The Creative Commons Attribution Non-Commercial (CC-BY-NC)License permits use, distribution and reproduction in any medium, provided the original work is properly cited and is not used for commercial purposes.(see below)

Creative Commons Attribution-Non-Commercial-NoDerivs License

The Creative Commons Attribution Non-Commercial-NoDerivs License (CC-BY-NC-ND) permits use, distribution and reproduction in any medium, provided the original work is properly cited, is not used for commercial purposes and no modifications or adaptations are made. (see below)

Use by commercial "for-profit" organizations

Use of Wiley Open Access articles for commercial, promotional, or marketing purposes requires further explicit permission from Wiley and will be subject to a fee.

Further details can be found on Wiley Online Library
http://olabout.wiley.com/WileyCDA/Section/id-410895.html

Other Terms and Conditions:

v1.10 Last updated September 2015

Questions? customercare@copyright.com or +1-855-239-3415 (toll free in the US) or +1-978-646-2777.